

Editors

Prof. Dr. Gaston Berthier
Université de Paris
Institut de Biologie
Physico-Chimique
Fondation Edmond de Rothschild
13, rue Pierre et Marie Curie
F-75005 Paris

Prof. Dr. Michael J. S. Dewar
Department of Chemistry
The University of Texas
Austin, Texas 78712/USA

Prof. Dr. Hanns Fischer
Physikalisch-Chemisches Institut
der Universität Zürich
Rämistr. 76
CH-8001 Zürich

Prof. Kenichi Fukui
Kyoto University
Dept. of Hydrocarbon Chemistry
Kyoto/Japan

Prof. Dr. George G. Hall
Department of Mathematics
The University of Nottingham
University Park
Nottingham NG7 2RD/Great Britain

Prof. Dr. Jürgen Hinze
Fakultät für Chemie
Universität Bielefeld
Postfach 8640
D-4800 Bielefeld

Prof. Dr. Hans H. Jaffé
Department of Chemistry
University of Cincinnati
Cincinnati, Ohio 45221/USA

Prof. Joshua Jortner
Institute of Chemistry
Tel-Aviv University
61390 Ramat-Aviv
Tel-Aviv/Israel

Prof. Dr. Werner Kutzelnigg
Lehrstuhl für Theoretische Chemie
der Universität Bochum
Postfach 102148
D-4630 Bochum 1

Prof. Dr. Klaus Ruedenberg
Department of Chemistry
Iowa State University
Ames, Iowa 50010/USA

Prof. Jacopo Tomasi
Dipartimento di Chimica e
Chimica Industriale
Università di Pisa
Via Risorgimento, 35
I-Pisa

Lecture Notes in Chemistry

Edited by G. Berthier M.J.S. Dewar H. Fischer
K. Fukui G.G. Hall J. Hinze H.H. Jaffé J. Jortner
W. Kutzelnigg K. Ruedenberg J. Tomasi

42

W. Duch

GRMS or Graphical Representation of Model Spaces

Vol. 1 Basics



Springer-Verlag

Berlin Heidelberg New York London Paris Tokyo

Author

W. Duch*

Max-Planck-Institut für Physik und Astrophysik
Karl-Schwarzschild-Straße 1, D-8046 Garching bei München

*Alexander-von-Humboldt Fellow 1985/86. Permanent address:
Instytut Fizyki UMK, ul. Grudziądzka 5, 87-100 Toruń, Poland

ISBN-13: 978-3-540-17169-0 e-ISBN-13: 978-3-642-93347-9
DOI: 10.1007/978-3-642-93347-9

This work is subject to copyright. All rights are reserved, whether the whole or part of the material is concerned, specifically those of translation, reprinting, re-use of illustrations, broadcasting, reproduction by photocopying machine or similar means, and storage in data banks. Under § 54 of the German Copyright Law where copies are made for other than private use, a fee is payable to "Verwertungsgesellschaft Wort", Munich.

© Springer-Verlag Berlin Heidelberg 1986

2152/3140-543210

TABLE OF CONTENTS

| | | |
|----|------------------------|---|
| | Acknowledgements | |
| 1. | Preface | 1 |
| 2. | Introduction | 4 |

PART I: ARCHITECTURE OF MODEL SPACES

| | | |
|------|--|----|
| 1.1 | Introducing graphical representation | 11 |
| 1.2 | Labeling and ordering the paths | 14 |
| 1.3 | \hat{S}_z -adapted graphs in different forms | 18 |
| 1.4 | \hat{L}_z -adapted graphs | 29 |
| 1.5 | (\hat{L}_z, \hat{S}_z) -adapted graphs | 37 |
| 1.6 | \hat{S}^2 -adapted graphs | 44 |
| 1.7 | (\hat{L}_z, \hat{S}^2) -adapted graphs | 52 |
| 1.8 | (\hat{L}^2, \hat{S}^2) -adapted graphs | 57 |
| 1.9 | (\hat{J}^2, \hat{T}^2) -adapted graphs | 64 |
| 1.10 | Spatial symmetry in the graph | 67 |
| 1.11 | Visualization of restricted model spaces | 74 |
| 1.12 | Physical intuitions and graphs | 80 |
| 1.13 | Mathematical remarks | 90 |
| 1.14 | Graphs and computers | 96 |
| 1.15 | Summary and open problems | 98 |

PART II: QUANTUM MECHANICS IN FINITE DIMENSIONAL SPACES

| | | |
|-----|---|-----|
| 2 | Matrix elements in model spaces | 102 |
| 2.1 | The shift operators | 103 |
| A. | Definitions | 104 |
| B. | Properties of the shift operators | 105 |
| C. | Examples of operators in \hat{E}_{ij} basis | 108 |
| 2.2 | General formulas for matrix elements | 111 |

| | | |
|-----|---|-----|
| 2.3 | Matrix elements in the \hat{S}_z and \hat{L}_z -adapted spaces | 117 |
| A. | The three-slope graphs | 117 |
| B. | Classification of loops in the three-slope graphs | 119 |
| C. | Graphical rules for matrix elements | 121 |
| D. | Example | 130 |
| E. | Four-slope graphs | 131 |
| F. | Other non-fagot graphs | 134 |
| G. | Matrix elements in the \hat{L}_z and (\hat{L}_z, \hat{S}_z) -adapted spaces | 135 |
| 2.4 | Reduction from \hat{S}_z to \hat{S}^2 eigenspace | 136 |
| 2.5 | Matrix elements in the \hat{S}^2 -adapted space | 140 |
| A. | Permutations in the spin space | 141 |
| B. | Spin function transformation (SFT) graph and table | 143 |
| C. | Manipulations with permutations | 148 |
| D. | Presence of the singlet-coupled pairs | 149 |
| E. | Products of shift operators | 153 |
| F. | Evaluation of matrix elements in the (\hat{L}_z, \hat{S}^2) eigenspace | 159 |
| 2.6 | Non-fagot graphs and the \hat{S}^2 -adapted space | 161 |
| A. | One-body segments | 162 |
| B. | Two-body segments | 168 |
| C. | Summary | 178 |
| | References | 179 |
| | Index | 190 |

Preliminary contents of Volume II.

Part III: Degenerate representations of point groups

Degenerate point groups/ Complete system of commuting operators approach/
The use of Young skew representations/ Graphical approach/ Reduction from
 (\hat{L}_z, \hat{S}^2) to (\hat{L}^2, \hat{S}^2) / (\hat{J}^2, \hat{T}^2) eigenfunction/ Elements in $GL(n)$ carrier space.

Part IV: Matrix representation of operators acting in model spaces

Understanding the structure of one and two-particle operators/ Complete analysis of formulas for the three-slope graph's loops/ Complete analysis of segment values for the four-slope graph's loops/ Structure of the Hamiltonian: explicit separation of some parts of the graph/ Applications to methods of quantum chemistry: conventional, direct, complete active space configuration interaction, approximations to CI/ Perturbation theories/ Other methods/ Extension of orbital basis/ Applications to nuclear shell-model calculations/ Summary

ACKNOWLEDGEMENTS

Over the years I have been blessed with a friendship of and collaboration with Jacek Karwowski. Although our opinions on virtually every subject differ diametrically we understand each other very well. Parts of the material on matrix element calculation and applications to the configuration interaction method presented in this book are related to the work we have done together when I was his graduate student. However, Jacek has declined the responsibility of being the co-author of these notes, despite the suggestion of a referee. The discussions with him were certainly of invaluable help.

Many people have influenced me through their books – I feel compelled here to name just a few titles but, being unable to do justice to all of them, I shall refrain from doing that. Many good books are quoted among the references.

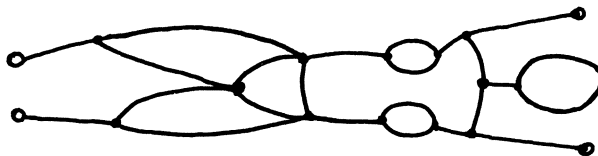
This work was started in Toruń, Poland, and finished far from home worries in Garching bei München. Hospitality of my host, Geerd H.F. Diercksen, who told me “have fun and get useful work done” (that suited very much to my taste), is gratefully acknowledged. My stay was financed by the Alexander von Humboldt Foundation that has been invaluable to so many foreign scientists working in Germany, providing us, i.e. the Humboldt fellows, not only with the money but also with advice and a cultural program. I would like to dedicate this volume to Dr. Heinrich Pfeiffer on the occasion of his 60th birthday and 30 years of work as Secretary General of the Alexander von Humboldt Foundation.

Excellent facilities of the Max-Planck Institutes in Garching have allowed me to acquire a new profession, namely that of a typesetter. It is much harder than I ever expected when I started this work. This manuscript was designed and prepared entirely by myself using a \TeX system and a laser printer. Murphy’s laws certainly apply to computerized typesetting: if you can loose a long text file you will and you will have to retype it. Ben Jeffreys is responsible for british spelling in some parts of this volume. In the rest errors abound.

1

Preface

The purpose of these notes is to give some simple tools and pictures to physicists and chemists working on the many-body problem. Abstract thinking and seeing have much in common – we say “I see” meaning “I understand”, for example. Most of us prefer to have a picture of an abstract object. The remarkable popularity of the Feynman diagrams, and other diagrammatic approaches to many-body problem derived thereof, may be partially due to this preference. Yet, paradoxically, the concept of a linear space, as fundamental to quantum physics as it is, has never been cast in a graphical form. We know that



is a high-order contribution to a two-particle scattering process (this one invented by Cvitanović(1984)) corresponding to a complicated matrix element. The lines in such diagrams are labeled by indices of single-particle states. When things get complicated at this level it should be good to take a global view from the perspective of the whole many-particle space. But how to visualize the space of all many-particle states? Methods of such visualization or graphical representation of the spaces of interest to physicists and chemists are the main topic of this work.

Notes on this subject have now been piling up on my desk for a couple of years and, although I have already managed to publish a few things about graphical representations, I have gradually realized that the scope of such a work is much broader

than my humble abilities allow. I received a formal training in physics and made my PhD in quantum chemistry. Working on applications of the symmetric group theory to the configuration interaction method I stumbled, motivated by Shavitt's work (1977), upon a graphical description of the configuration space. The physical meaning of Shavitt's graph was at that time unclear to most of the scientists who used it, the reason being a detoured way of approaching the problem via the unitary group theory. Years later I began to understand how useful the concept of a graphical representation of a space really is and how rich are its connections with the well-established branches of mathematics, like group theory, the theory of partitions, graph theory, integer programming, operations research or the theory of natural numbers. Thus, leaving the safe waters of my own speciality I have ventured into the unknown oceans of knowledge, discovering a number of fascinating books besides quite a few journals the existence of which I had never suspected. I have looked through shelves of books on mathematical subjects related to quantum mechanics, but even those books that refer directly to the bases of Hilbert or Banach tensor spaces (cf Singer 1970) fail to provide any geometrical pictures or to make connections with the graph theory or the group theory, while the number theory fits there as well as a third leg to trousers. Yet many examples may be found where Diophantine problems and graphical methods are related in a natural way, as with Dynkin diagrams in group-theoretical methods applied to unified models (cf Gilmore 1974; Slansky 1981). As Primas (1981) writes: "*The most important task of contemporary theoretical chemistry is to stimulate the mutual understanding of the various branches of chemistry and its neighboring sciences.*"

On a piece of paper glued to the wall of an office in the Max-Planck-Institute for Astrophysics in Garching b. München I have found this quotation from T.S. Eliot's poem "The Rock"

*All man are ready to invest their money
But most expect dividends
I say to you: Make perfect your will
I say: take no thought of the harvest,
But only of proper sowing.*

Being a physicist of a saturation time (read: having no one to work for me) I have thus decided to limit the scope of the present work and leave some things for others, more mathematically gifted than myself, if they would find the subject interesting. In these notes I present simple tools, giving both the language and the methods of calculation, i.e. graphical representation of certain model spaces useful in many-body problem, plus the methods of matrix element calculation. This in itself took about 200 pages, so I decided to publish it separately as the first volume, leaving the mathematically more complicated Part III, as well as Part IV dealing with applications, for the second volume. My intention was to keep the whole work self-contained, in the sense that only a basic knowledge of mathematics is assumed and, although the list of references

is rather long, the reader should still be able to understand the text without digging through this literature.

Finally, if the reader, used to the impersonal style of most scientific papers, finds the personal tone of these notes rather distasteful, I should say that I have looked into my family tree searching in vain for any Polish king that would justify the use of a plural form “we”.

2

Introduction

In which I am trying to explain why have I done it, what have I done, and what it is for.

Many-body experts like to start from the one-particle approximation. Even when geminals or group functions are used they are ultimately expanded in the one-particle basis (Wilson 1984). Computational difficulties with the explicitly correlated wavefunctions prevented the use of these methods for all but a few-electron systems (Handy 1978), although there are still some, who have not buried all their hopes, and whose results are promising (cf Jankowski and Malinowski 1980; Jeziorski *et al* 1984). Notwithstanding their hopes the majority votes for one-particle approximation, because it is fundamental to our intuitions and capable of high accuracy (cf Handy 1978).

Many-body equations, whatever is our choice, take place in the many-particle Hilbert space \mathcal{H} . The experts are usually so eager to solve their equations that they tend to forget that. This space is created from n -dimensional one-particle space $\mathcal{V}_n = \{|\phi_i\rangle\}_{i=1}^n$ called the orbital space and two-dimensional one-particle spin space $\mathcal{V}_2 = \{|\alpha\rangle, |\beta\rangle\}$. To be a little more general let's assume that we have a set of primitive objects (like orbital or geminal states) that are used in construction of many-particle states. It is convenient to formulate equations in a formalism that does not depend on the number of particles in the system nor on the size of the orbital space, i.e. to work in the Fock space (Kutzelnigg 1984). Finally however both the number of particles N and the number of orbitals n have to be specified, no matter what method we use. The full Hilbert space \mathcal{H}_n^N has a very large dimension $\dim \mathcal{H}_n^N = \binom{2n}{N}$. In practice we are forced to truncate this space severely; manageable dimensions for the present-day computers are of the order of 10^6 basis states. This truncated space $\tilde{\mathcal{H}}_n^N \subseteq \mathcal{H}_n^N$ is a part of the

physical model of our system, therefore it is called a model space.* The model space, as any other mathematical structure build from simpler objects, has a particular architecture. Primitive objects like orbital and spin states correspond here to building blocks or bricks that come only in a few sizes, while the space itself corresponds to a building. The architecture of a model Hilbert space may be visualized using simple graphs. We certainly do not want to inspect individual basis states if there are thousands of them, but we would like to see the relations between these states, recognize certain useful classes of states and develop some intuitions to tell the solid constructions (spaces giving good approximations) from the rickety ones (spaces giving poor approximations). The concept of a space structure is here implicit and I will use the word 'structure' in the same sense as it is used in any architectural context. In case of architectural objects we can also talk about shape. The concept of shape may not be precisely defined for a space, because there usually exist many different graphical representations that are topologically equivalent and thus preserve the structure of the space. However, if we fix the rules of a graphical representation and decide how to picture the primitive states we may talk about different shapes of spaces, and the shape will obviously depend on what kind of model spaces we are using and what kind of symmetries the basis states posses.

It is undoubtedly nice to see the structure of a space, but is it useful? Summarizing the prospects of molecular quantum mechanics McWeeny and Pickup (1980) write: "*ab initio* molecular calculations of 'chemical' accuracy, are going to be dominated more and more by the development of computers and highly efficient algorithms". The same is true in other branches of many-body theory (cf Wilson 1982), therefore computational aspects should not be ignored. Graphical representation should allow us to see the structure of a space and to teach the computer how to make use of this structure. Moreover the graphs should be constructed in such a way that would allow all required matrix elements to be obtained directly from the graphs, without recourse to the algebraic manipulations with the many-particle functions. Thus we come to the next concept – of a proper label for a state. Designation like $|^2P, M_S = \frac{1}{2}, M_L = 1\rangle$ is not a proper label because it doesn't say anything about the construction of this state from primitives or one-particle states. Weyl tableaux or Gelfand patterns may serve as an example of the proper labels. A properly constructed graph \mathcal{G} should contain enough information about the basis states of many-particle space to facilitate the mapping:

$$\mathcal{G} : \hat{A}(\mathcal{H}) \rightarrow \mathbf{A}(\tilde{\mathcal{H}}_n^N)$$

of a differential or integral operator \hat{A} acting in the infinite-dimensional space \mathcal{H} to its matrix representative \mathbf{A} in the model space $\tilde{\mathcal{H}}_n^N$. Biedenharn and Van Dam (1965) write "One of the basic problems, if not the basic problem in spectroscopy, both atomic

*In many-body perturbation theory the space of zeroth-order functions is sometimes called the model space; this is obviously not what is meant here.

and nuclear, is the construction of antisymmetric N -particle wave functions from the (degenerate) states of a given energy shell." The construction of such a wave functions is precisely what I hope to avoid, replacing it by graphical labels and graphical rules of matrix element evaluation. The theory should be simple, basically no more than an exercise in labeling of the many-particle states by a graphical means.

What kind of spaces can one visualize graphically? Any kind of tensor spaces, i.e. all those with the bases being combinations of products of primitive states. Such states are well represented by Young tableaux or Gelfand patterns (cf Barut and Rączka 1980; Hammermesh 1962). One could say that any carrier space of $GL(n)$ can be represented in such way, but throughout this work I will try to avoid explicit use of a complicated mathematics, in particular the use of symmetric or unitary group theory. In those passages, where group-theoretical explanations are so natural that other seem clumsy, I have placed a warning sign **GT** to let the uninitiated skip them – material included there is by no means necessary to understand the rest of the text. I am very well aware that one can almost always dress the methodological developments in a now distinguished language of group theory. Condon and Shortley (1935) relate the following story:

When Dirac visited Princeton in 1928 he gave a seminar report on his paper showing the connection of the exchange energy with the spin variables of the electrons. In discussion following the report, Weyl protested that Dirac has said that he would derive the results without the use of group theory but, as Weyl said, all of Dirac's arguments were really applications of group theory. Dirac replied, "I said I would obtain the results without any previous knowledge of group theory".

This anecdote* illustrates very well the sense in which group theory is not used here. Personally I like group theory, especially when it is presented in the not-so-formal way (cf Lipkin 1965; Cvitanović 1984), and I do not manage to get along completely without it. But, as Condon and Shortley (1935) write in their book: "Hence, if we can minimize the amount of new mathematics he (i.e. the physicist) must learn in order to penetrate a new field we do him a real service". I am in favour of new mathematics; Wormer (1975) has rightly pointed that there always was a resistance to accept new mathematical ideas, even such 'obvious' (for us now) concepts like negative numbers or the use of letters in equations. There are cases where we certainly need powerful mathematical techniques (cf Primas 1980). Condon himself turned to group theory in his last book (Condon and Odabaşı 1980). But, to quote from his first book again "the new developments bring with them so many new things to be learned that it seems inadvisable to add this additional burden to the load". In some respects, because of this additional burden, we seem to fall back in our understanding of fundamental concepts,

*I am indebted to Prof. R. McWeeny for telling me this anecdote.

as a quick comparison between say Condon and Shortley's book and some of the latest quantum chemistry textbooks, will immediately show.

Symmetries, existing in the physical system we want to describe, are usually reflected in the construction and properties of the states of this system. Eigenstates of an operator \hat{O} are called \hat{O} -adapted states and the space of these states \hat{O} -adapted space. Frequently construction of such states is too complicated to be worth the trouble; simpler basis sets are used instead and the space enlarged to ensure that the subspace of desired symmetry is included in it. For example, we may easily construct \hat{L}_z -adapted states but the construction of \hat{L}^2 -adapted states is much more complicated. The states included in model space $\tilde{\mathcal{H}}_n^N$ are thus selected first on the basis of their symmetry. Further selection of basis states is based on their importance, frequently estimated by the perturbation theory; contrary to the selection by symmetry this does not complicate the construction of many-particle states. Estimates of importance are either used globally (this is sometimes called preselection, cf Shavitt 1977) or locally. Taking all two-particle, two-hole states relative to some Fermi vacuum is a global selection. Local selections demand checking individual states and admitting to $\tilde{\mathcal{H}}_n^N$ only those that give a contribution larger than certain threshold. Global selection leads to spaces with certain regular structure while local selection in general destroys it. As I will show in Part IV of this work the structure of a model space $\tilde{\mathcal{H}}_n^N$ is reflected in the structure of the matrices corresponding to the operators acting in this space. Although graphical representation is very useful for calculation of matrix elements no matter how the selection is done it is with the global selection and the regular structure of the corresponding matrices where the biggest gains should be expected.

Techniques of a graphical representation of many-particle basis states adapted to different symmetry operators should be helpful in case of a complicated fermion and boson systems, although here such ambitious applications are not presented. The formulas of many-body perturbation theory are very compact when many-particle states are used, and get very complicated when spin-adapted formalism is coupled with diagrammatic reduction to one-particle level (El Baz and Castel 1972). Why do I hope that graphical representation of model spaces (or GRMS for short) will be effective as a computational method? GRMS may be used just for visualization, i.e. the classification and labeling of many-particle states used in traditional many-body methods, but such a representation fosters a new way of thinking about the organization of computations. To some degree this is already evident from the success of the unitary group approach. In applied quantum mechanics the unitary group approach (UGA) to the many-electron correlation problem is certainly one of the more popular subjects of research in recent years (cf Paldus 1976; Harter and Patterson 1976; Drake and Schlesinger 1977; Downward and Robb 1977; Shavitt 1977-1983; Paldus and Boyle 1980; Hinze 1981; Kent *et al* 1981; Payne 1982; Robb and Niazi 1984; Paldus and Wormer 1986). There are good reasons for this: the programs, based on UGA ideas, proved to be much more effective than the conventional ones (Siegbahn 1979,1980; Brooks *et al* 1979,1980; Lischka *et al*

1981; Saunders and van Lenthe 1983). Configuration interaction (CI) calculations with over one million terms (Saxe *et al* 1982; Diamond *et al* 1984) or potential curves for molecules like Cr_2 in $^{11}\Sigma_g^+$ state (Roos *et al* 1982) calculated with 220000 functions are without doubt remarkable achievements, but the applications did not stop with CI. The unitary group approach was successfully applied to the MCSCF method (Brooks *et al* 1980b; Shephard *et al* 1980,1982) complete active space SCF (Roos 1980; Roos *et al* 1980; Siegbahn *et al* 1980,1981), coupled electron pair approximation (CEPA) (Lischka 1982), open-shell electron propagator method (Born and Shavitt 1982), energy gradient calculations (Brooks *et al* 1980c) and crystal field theory (Zhenyi 1983). There are hopes for many other applications as well (Shavitt 1983b).

The theory that lies behind all these applications does not look simple to a profane eye. Pages and pages of coefficients and complicated diagrams are reported in all papers containing derivations of UGA based formulas (cf Payne 1982 or Robb and Niazi 1984). One has to admire the amount of work that Paldus had to perform writing his monumental paper (Paldus 1976) that has turned the attention of many scientists to the unitary group theory. However, despite the beauty of its mathematics one is tempted to ask – is it possible to find some shortcuts that lead to the same results in a more direct and simple way ?

I would like to argue here that the real power of this new computational methods lies not so much in the efficiency of matrix element calculations, as claimed by Paldus (1981), but rather in the new organisation of computations, fostered by the graphical representation of the \hat{S}^2 -adapted basis, due to Shavitt (1977). The pre-graphical applications of UGA were not successful (Robb and Hegarty 1978); however, once the insight from the graphical representation was gained it was possible to avoid the explicit use of graphs in some cases (Saunders and van Lenthe 1983). Thus in the graphical unitary group approach (GUGA) the emphasis should be placed rather on 'G' for 'graphical' than 'U' for 'unitary'. UGA results concerning matrix elements are easily obtained by simpler and at the same time more general means. Group theory need not to be mentioned in the derivation, except for comparison with the previous approaches. Shavitt's graph, introduced at first as a representation of a table of distinct rows in Paldus tableaux (Shavitt 1977) is now being slowly recognized as a representation of a many-electron model space (Shavitt 1983a), although the Gelfand basis (Gelfand and Tsetlin 1950; Barut and Rączka 1980) and A,B,C tableaux (Paldus 1976) are still presented as a prerequisite for understanding of the graph (cf Esser 1984).

Shavitt's graph has inspired us to develop the symmetric group graphical approach (SGGA) (Duch and Karwowski 1981–1985). Both GUGA and SGGA may be treated as a special cases of the graphical representation of model spaces. It should be emphasized that the graphs used in these approaches are rather different from other types of graphs used in physics. They do not represent chemical structures, interactions or formulae, but give a global description of many-particle model spaces. They are successors of the branching diagram (van Vleck 1932) describing the structure of a spin

space in a similar way as the SGA graph describes the structure of the space of orbital configurations. The graphs used in UGA and SGA are in fact different projections of the same three-dimensional graph describing \hat{S}^2 -adapted states. I shall explore other graphical representations of these states as well as states adapted to \hat{S}_z , \hat{L}_z , \hat{L}^2 , \hat{J}^2 and spatial symmetry point group operators, and point out some connections of this theory to well-established branches of mathematics.

First part of this book deals with the architecture of many-particle model spaces, i.e. with the labeling and classification of their basis states. In the second part operators acting in the model space are introduced and techniques of deriving matrix elements straight from the graph are elaborated. In the finite-dimensional spaces of states built from primitive objects every operator is equivalent to a polynomial in the shift operators, i.e. operators that replace one primitive object by another. An elegant theory of matrix element calculations that fits very well to a graphical representation of model spaces is based on the use of these operators, called in the context of UGA 'generators of the unitary group'. The celebrated result of UGA (Paldus 1981) – segmentation of the two-generator product matrix elements – is obtained as an example of this approach. In the second volume matrix elements between states belonging to the degenerate representations of the point groups and matrix elements between (\hat{L}^2, \hat{S}^2) eigenstates are considered. The structure of matrices representing operators acting in model spaces is elucidated in the last part. The insight, gained from understanding of this structure, is applied to various methods of solution of the Schrödinger equation. Experience gathered with computer programs dealing with graphs is also presented in the second volume. So far applications of group-theoretical approaches have influenced the techniques of computations rather than bringing with them new developments in the methods. It is my hope that investigation of the structure of matrix representations of operators may lead not only to computational efficiency but also to new methods. The effect of an extension of orbital basis, for some operators and some types of graphs, should have a predictable influence on the eigenvalues of matrices corresponding to these operators. Is it possible to obtain the eigenvalues in an infinite orbital basis set in this way, i.e. to solve the problem exactly? Or to formulate the perturbation theory to account for an extension of the orbital basis? These are new types of questions that can be stated in the context of GRMS and that conclude this work.

PART I

**ARCHITECTURE
OF MODEL SPACES**

1.1

Introducing graphical representation

What does it mean to represent a many-particle model space graphically? It means, that we should be able to identify and label each basis state of that space. For fermionic systems these basis states should be antisymmetric – a very strong requirement, immediately invoking the Pauli principle. Adding spin states $|\alpha\rangle$ and $|\beta\rangle$ to each orbital state that belongs to \mathcal{V}_n we obtain $2n$ spin-orbital states. These spin-orbital states are ordered and identified in some way, for example

$$|\phi_1\rangle = |\phi_1\rangle|\alpha\rangle, |\bar{\phi}_1\rangle = |\phi_1\rangle|\beta\rangle, \dots |\phi_n\rangle, |\bar{\phi}_n\rangle$$

In the construction of an antisymmetric N -particle state each spin orbital appears at most once, therefore $\binom{2n}{N}$ spin-orbital configurations or different states are possible, provided that no other restriction than antisymmetry is imposed. Description of a non-symmetric molecule in Born-Oppenheimer approximation requires such states when a strong spin-orbit interaction is present. Graphical representation of the states that do not possess any symmetry other than being antisymmetric (corresponding to determinants) is particularly simple.

Each N -particle state has a label which is specified in a convenient way by writing $2n$ occupation numbers (equal to 0 or 1) of spin orbital states $|\phi_1\rangle, |\bar{\phi}_1\rangle, \dots, |\bar{\phi}_n\rangle$. Every $2n$ -digit binary string containing N times 1 and $2n - N$ times 0 corresponds to a basis state of the full $\binom{2n}{N}$ - dimensional space. A model space is called full when it contains all states that may be formed from a given set of primitive objects or orbital states. Let us represent a binary string in a coordinate system e, o (Fig 1), where $e = 0, 1, \dots, N$ is a horizontal axis and $o = 1, 2, \dots, 2n$ vertical axis division. Each point (e, o) , called a vertex or a node, in this coordinate system corresponds to one of $\binom{o}{e}$ partial binary strings of o digits containing e times 1 and $(o - e)$ times 0. Adding 0 does not increase

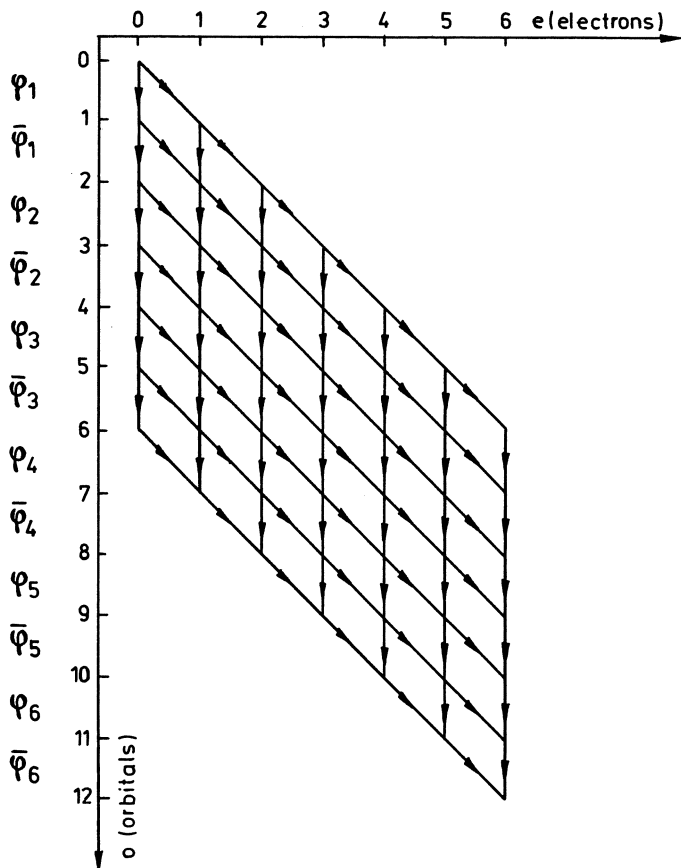


Fig 1. An example of a graph representing binary strings or spin-orbital configurations.

e , only o , so 0 is represented by a short vertical line (arc) joining two vertices. Adding 1 increases both e and o , so 1 corresponds to a skew arc. Moving from the highest point $(0,0)$, called the head of the graph, to the lowest vertex $(N, 2n)$, called the tail of the graph, through one of the $\binom{2n}{N}$ possible routes we get a binary label of the N -particle basis state. The set of vertices joined by directed arcs forms a graph. Each path in the graph corresponds to a configuration or a basis function – in this case to a spin-orbital configuration or to a determinantal function. The graph contains all labels of the basis functions, therefore it represents the many-particle model space, in this case the space of all determinants. From a mathematical point of view it represents all strings of digits $b_1 b_2 \dots b_{2n} = \{b_i\}_{i=1}^{2n}$ with the restriction

$$\sum_{i=1}^{2n} b_i = N; \quad b_i = 0, 1 \quad (1.1)$$

The graph of Fig 1, as well as other graphs described later, although formally a directed graph (digraph) according to the definition of the theory of graphs (cf Harray

1969; Deo 1974), is used here in a rather special way. For example, representing the spin-orbital configurations it is natural to have a coordinate system, and although one could transform the graph to any other isomorphic form (examples are presented in section 1.13) it is good to preserve the two fixed arc slopes to identify the occupied and unoccupied spin-orbital states easily. Therefore it is appropriate to call this graph “the two-slope graph” and designate it $\mathcal{G}_2(2n : N)$. It is a planar graph, which means that it is possible to draw it in such a way that the arcs intersect only in the vertices. As we will soon see basis states adapted to some operators lead to model spaces that are represented by a more complicated, non-planar graphs.

The two-slope graph, although so simple, allows me to introduce some concepts useful for other types of graphs. Vertical arc is referred to as the empty or unoccupied arc; skew arc as the singly occupied arc. The shape of a full graph (corresponding to a full space) does not depend in this case on the ordering of its levels or spin orbitals. The full space has a high symmetry, reflected in the geometrical symmetry of a graph (the symmetry of a space should not be confused with the symmetries of its basis states). Unfortunately the full space is unmanagably large even for a modest number of orbitals and a rather small number of particles. Although a graph describing millions of states could easily be fitted on one page, the computers used to analyze such a graph would protest. Smaller spaces are made by removing some vertices and arcs from a graph, however the shape of such a restricted graph depends on the ordering of its levels. I will elaborate on this point later. First let us introduce an ordering among the paths of a graph.

1.2

Labeling and ordering the paths

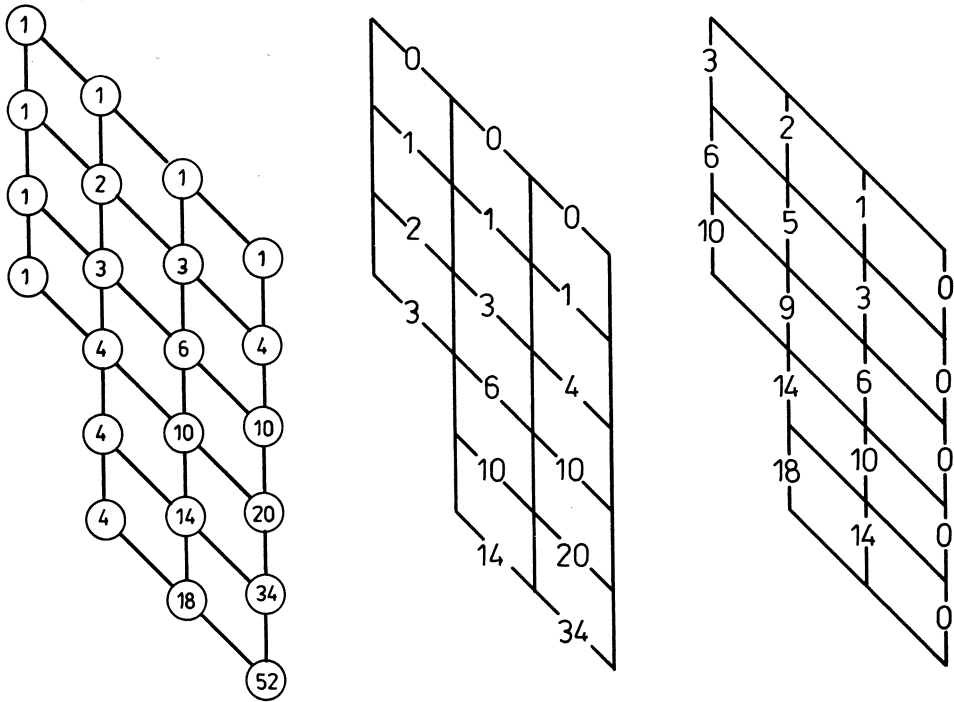
Smaller model spaces, i.e spaces of a smaller number of orbitals $n' \leq n$ or particles, $N' \leq N$, are represented by subgraphs embedded in a natural way in $\mathcal{G}_2(2n : N)$, with $(N', 2n')$ vertex as their tail. Similarly one can imagine larger graphs in which $\mathcal{G}_2(2n : N)$ is embedded. Description of the borders of a graph is simpler if we regard vertices and arcs of these larger graphs as ‘virtually present’: existing, but giving a null contribution to the real graph. The fixed-slope graphs, by virtue of this embedding property, admit a natural ordering of paths.

To characterize the embedding property better let’s assign to each vertex (e, o) a number $\overline{W}(e, o)$, called the weight of a vertex, equal to the number of paths contained in a subgraph that has (e, o) vertex as its head. In Fig 2a we see a graph, describing a restricted model space for 3 particles and 8 spin orbitals, with the weights inscribed in the vertices. The head of the graph has an arbitrarily fixed weight $\overline{W}(0, 0) = 1$. The embedding property is now translated into algebraic terms as:

$$\overline{W}(e, o) = \overline{W}(e, o - 1) + \overline{W}(e - 1, o - 1) \quad (1.2)$$

i.e. each graph with (e, o) as its tail is a sum of two subgraphs. To facilitate ordering of the paths let’s assign to each path L a unique number $I(L) = 1, 2, .. \overline{W}(N, 2n)$, and call it an index of the path in a graph.

Paths in a subgraph $\mathcal{G}_2(o, e)$ should have indices $I(L) = 1, 2, .. \overline{W}(o, e)$. Let’s consider the two subgraphs $\mathcal{G}_2(o, e)$ is composed of, $\mathcal{G}_2(o - 1, e)$ and $\mathcal{G}_2(o - 1, e - 1)$. In the $\mathcal{G}_2(o, e)$ graph $\overline{W}(e, o - 1)$ paths of the first subgraph may have either $I(L) = 1, 2, .. \overline{W}(e, o - 1)$ indices or may follow $\overline{W}(e - 1, o - 1)$ paths of the second subgraph, i.e. $I(L) = \overline{W}(e - 1, o - 1) + 1, .. \overline{W}(e, o)$. Choosing the first possibility means that



$$\bar{Y}_1(e, o) = \bar{W}(e, o - 1)$$

Fig 2. Reversed lexical ordering: a) weights of vertices only, b) with unoccupied arc weights set to zero, c) with occupied arc weights set to zero.

the paths reaching (e, o) vertex through the unoccupied arc precede all those reaching it through the singly occupied arc. In consequence the rightmost path has the index $I(L) = 1$. To assure that the paths reaching (e, o) vertex through the singly occupied arc have indices $I(L) = \bar{W}(e, o - 1) + 1, \bar{W}(e, o - 1) + 2, \dots, \bar{W}(e, o - 1) + \bar{W}(e - 1, o - 1)$ we will assign a weight $\bar{Y}_1(e, o) = \bar{W}(e, o - 1)$ to the singly occupied arc joining vertex $(e - 1, o - 1)$ with (e, o) and a weight $\bar{Y}_0(e, o) = 0$ to the unoccupied arc (Fig 2b). Thus the index $I(L)$ is calculated as a sum of the arc weights of the path L

$$I(L) = 1 + \sum_{i=1}^{2n} \bar{Y}_{L_i}(N_i, i) \tag{1.3}$$

where L_i is the occupation of the i -th arc, (N_i, i) are the coordinates of vertices crossed by path L , and $+1$ is added to avoid counting from zero. The ordering of the paths described above corresponds to the ‘reverse lexical ordering’ (cf Robb and Niazi 1984). Let’s fix a vertex (e, o) and a lower path connecting this vertex with the tail of a graph. Reverse lexical ordering is characterized by the fact that all upper paths crossing (e, o)

$W(e + 1, o + 1)$, where the unoccupied arc joins the (e, o) and $(e, o + 1)$ vertex. This time it is more convenient to assign the weights $Y_k(e, o)$ to the arcs leaving a vertex (i.e. joining it with the vertex below) rather than coming to it (i.e. joining it with the vertex above). Paths with a fixed upper part and an arbitrary lower part have now contiguous indices. This ordering corresponds to the ‘lexical ordering’ introduced for four – slope graphs used in UGA by Shavitt (1977). The lexical ordering of the paths is the same as that of binary numbers B_L where the arcs near the top of a graph correspond to the more important digits of B_L . One may also call it ‘the first letter sequence’ ordering. Alternative arc weights, with $Y_1 = 0$, are shown in Fig 3c. Different arc weights in the lexical and the reverse lexical orderings should be assigned if we assume, that the leftmost path L_m has an index $I(L_m) = 1$ and the rightmost path R_m an index $I(R_m) = W(0, 0)$ or $I(R_m) = \overline{W}(N, 2n)$. In this way we have eight ordering schemes, of which four are particularly simple. Remember that $Y_k(e, o)$ refers to the $(e, o), (e + k, o + k)$ arc, and $\overline{Y}_k(e, o)$ to the $(e - k, o - 1), (e, o)$ arc, and that $Y_k(e, o) = \overline{Y}_k(e, o) + 0$ for all vertices (e, o) that do not belong to the graph. The four simple ordering schemes may be summarized as follows:

$$\begin{aligned}
 I(L_m) = 0; \quad Y_0(e, o) = 0; \quad Y_1(e, o) = W(e, o + 1) \\
 I(R_m) = 0; \quad Y_1(e, o) = 0; \quad Y_0(e, o) = W(e + 1, o + 1) \\
 I(R_m) = 0; \quad \overline{Y}_0(e, o) = 0; \quad \overline{Y}_1(e, o) = \overline{W}(e, o - 1) \\
 I(L_m) = 0; \quad \overline{Y}_1(e, o) = 0; \quad \overline{Y}_0(e, o) = \overline{W}(e - 1, o - 1)
 \end{aligned}
 \tag{1.5}$$

The first of these ordering schemes was originally described by Shavitt (1977,1981). The lexical and the reverse lexical orderings with weights of unoccupied or of occupied arcs set to zero are easily generalized for the case of a more complicated graphs. For example, assigning $I(R_m) = 0, \overline{Y}_0(e, o) = 0$ for the k -slope graph the arc weights should be defined as

$$\begin{aligned}
 \overline{Y}_1(e, o) &= \overline{W}(e, o - 1) \\
 \overline{Y}_2(e, o) &= \overline{Y}_1(e, o) + \overline{W}(e - 1, o - 1) \\
 &\dots\dots\dots \\
 \overline{Y}_k(e, o) &= \overline{Y}_{k-1}(e, o) + \overline{W}(e - k + 1, o - 1)
 \end{aligned}
 \tag{1.6}$$

Although more sophisticated orderings may be useful in special cases the ordering schemes described above seem to be quite sufficient for my purposes.

1.3

\hat{S}_z -adapted graphs in different forms

In this section the full $\binom{2n}{N}$ dimensional space visualized using $\mathcal{G}_2(2n : N)$ graph is decomposed into the subspaces labeled by M_S values of \hat{S}_z operator. To reflect this decomposition the graph has to change its shape. In the \hat{S}_z -adapted space each spin-orbital configuration should have a fixed number s_α of α -type spin orbitals and a fixed number s_β of β -type spin orbitals. In general the number of primitive states $|\phi_k\rangle$ and $|\bar{\phi}_k\rangle$ should be fixed. The simplest way to achieve it in a graph is to separate the two groups of one-particle states $|\phi_k\rangle$ and $|\bar{\phi}_k\rangle$, placing the first group at the top levels and the second group at the bottom levels of a graph. In this way two subgraphs, the first describing the space of s_α particles in $|\phi_k\rangle$ basis and the second representing the space of s_β particles in $|\bar{\phi}_k\rangle$ basis, are obtained (Fig 4). The two subgraphs are joined by one vertex.

This approach was used in a general CI program by J. Wasilewski (1986) and was found to be quite effective. For full \hat{S}_z - adapted spaces it does not present any problems, but in such a case, as shown in context of the full CI method by Handy and Knowles (1984), one may as well avoid graphical representation exploiting the high symmetry of the full space. The trouble starts when we want to select some states using such a graph because standard criteria like a selection by the excitation level can not be implemented. It is worth noting that as long ago as 1937 Shudeman in his work on the orbital angular momentum coupling made similar division of the spin spaces and this idea seems still to be useful in atomic calculations (cf Armstrong and Judd 1970).

To avoid the drawbacks of the separated spin spaces a more complicated graph is needed, with each arc specifying not only the occupation of an orbital state but also its type. To the axis numbering orbitals o and numbering electrons e we should therefore add a perpendicular axis to measure M_S values, or the difference between the

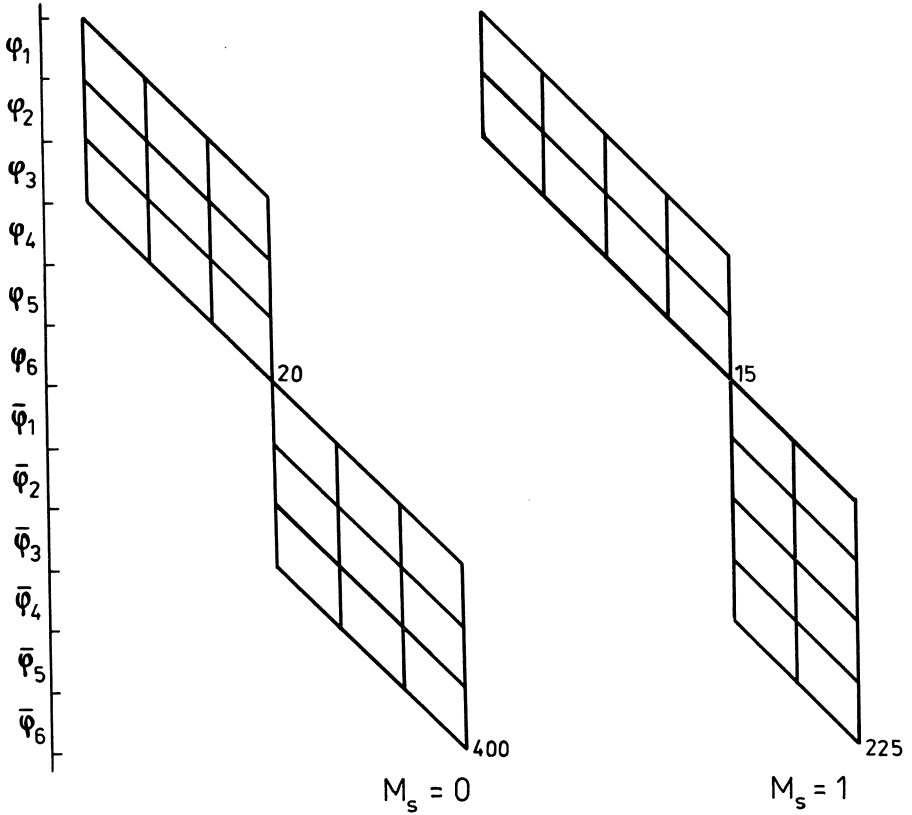


Fig 4. \hat{S}_z -adapted two-slope graphs with $|\alpha\rangle$ -type spin orbitals at the top, for $M_S = 0, 1$.

number of $|\phi_k\rangle$ and $|\bar{\phi}_k\rangle$ states. The two types of primitive states are assigned now to consecutive levels. In this way a rather complicated three-dimensional graph is created. Because it is hard to draw and interpret multidimensional graphs (in fact its impossible if more than three dimensions are needed) we will use their projections, either on the plane perpendicular to one of the axis (Fig 5a,b and Fig 6 a,b) or out of this plane (Fig 5c and Fig 6c). In the example shown in Fig 5 and 6 the full space of $N = 6$ particles distributed among $2n = 12$ spin orbitals is represented for $M_S = 0$ (Fig 5) and $M_S = 1$ (Fig 6). The dimensions $d(n, N, M_S)$ of the corresponding subspaces are easily calculated

$$\begin{aligned} s_\alpha + s_\beta &= N \\ s_\alpha - s_\beta &= 2M_S \end{aligned} \implies d(n, N, M_S) = \binom{n}{s_\alpha} \binom{n}{s_\beta} = \binom{n}{\frac{1}{2}N + M_S} \binom{n}{\frac{1}{2}N - M_S} \quad (1.7)$$

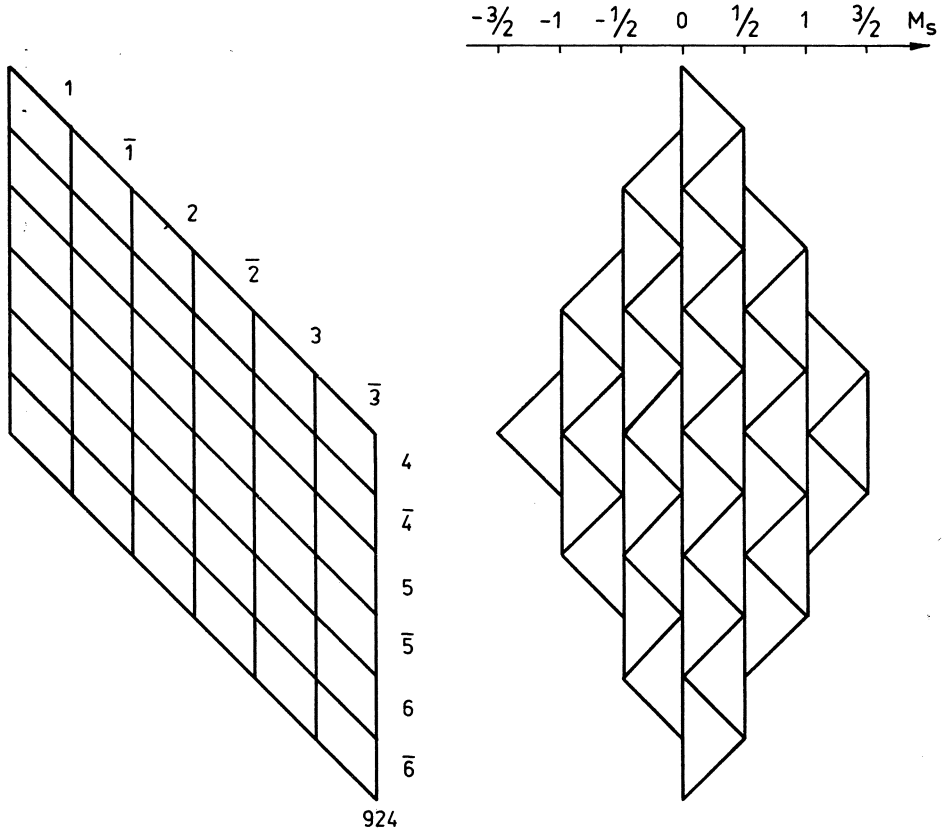


Fig 5. Projections of three-dimensional \hat{S}_z -adapted graph, $M_S = 0$
 a) on the (o, N) plane, b) on the (o, M_S) plane.

therefore instead of $\binom{12}{6} = 924$ basis states $\binom{6}{3} \binom{6}{3} = 400$ for $M_S = 0$ and $\binom{6}{4} \binom{6}{2} = 225$ for $M_S = 1$ are needed.

The projection on the (o, N) plane shown in Fig 5a and Fig 6a does not contain any information about M_S values. Its usefulness is doubtful because it shows too many paths. Projections on the (o, M_S) plane on the other hand do not contain any information about the number of particles and therefore also show too many paths. Choosing the skew projection we can see the whole graph (Fig 5c, Fig 6c). The horizontal axis corresponds now to a mixture of e and M values. Each vertex in the graph has o , e , and M as coordinates. The values of the intermediate number of particles e and the intermediate projection values M are marked separately above the graph. The skew projection graphs have only two slopes at each level, but the slopes at the α and β -type levels differ. In referring to these graphs a designation $\mathcal{G}_{2,2}(2n : N, M_S)$ will be used.

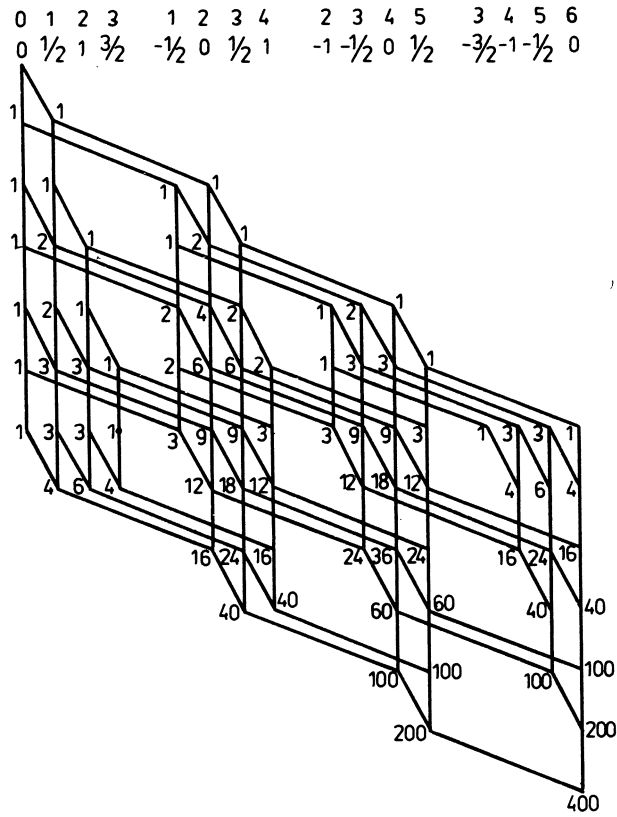


Fig 5c. Projections of three-dimensional \hat{S}_z -adapted graph, $M_S = 0$.
 Skew projection showing the whole graph.

The head of the $\mathcal{G}_{2,2}(2n : N, M_S)$ graph obviously corresponds to $e = M = 0$. At the second level, $o = 2$, there are 2 vertices corresponding to $e = 1$ (for $M = +\frac{1}{2}$ and for $M = -\frac{1}{2}$) but only one vertex for $e = 0$ or 2 and $M = 0$. In general all $M = 0$ vertices correspond to a unique, even number of particles. Fixing such a vertex for $M = 0$ and e' particles the number of particles corresponding to the neighbouring vertices is $e = e' + 2M$.

Occupied arcs of α type followed by β type correspond to a $|\phi\bar{\phi}\rangle$ spin-orbital pair, i.e. to a doubly occupied orbital. It is clear that adding to the three types of arcs (empty plus two kinds of singly occupied arcs) the doubly occupied arcs we may draw the same graphs as in Fig 5 and 6 using orbital instead of spin-orbital states as our primitive objects. In this way Fig 7 and 8 is obtained. The three-dimensional graph has now n levels and its projections have the following meaning: (o, N) projection is a three-slope graph $\mathcal{G}_3(n : N)$ representing orbital configurations. In this projection the singly occupied arc corresponds to α or β -type singly occupied orbital state ($|\phi_k\rangle$ or $|\bar{\phi}_k\rangle$)

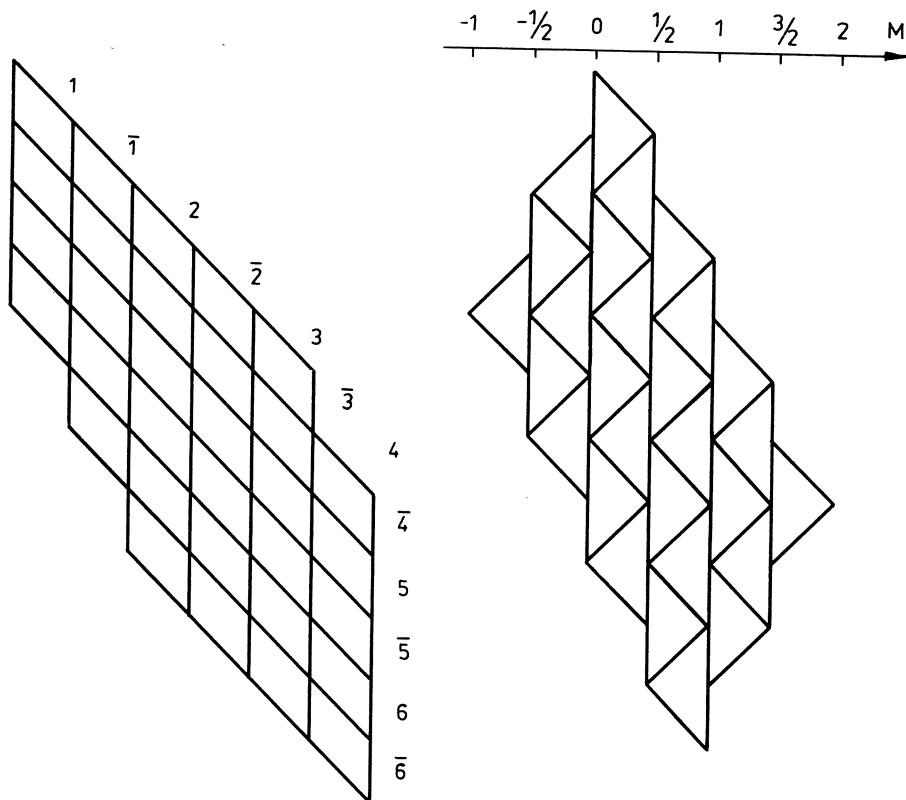


Fig 6. Projections of three-dimensional \hat{S}_z -adapted graph, $M_S = 1$
 a) on the (o, N) plane, b) on the (o, M_S) plane.

primitive state). The information about spin states is contained in the projection on the (o, M) plane, with the empty and the doubly occupied orbitals represented by the same vertical arcs. Finally the skew projection shows the whole information contained in the graph, with the singly occupied arcs in (o, e) projection splitted into two types. The graph has now four slopes and will be designated $\mathcal{G}_4(n : N, M_S)$. The skew projection drawn here (Fig 7c, 8c) is close to the projection on the (o, N) plane. Notice that I am free to choose my point of view closer to (o, M) projection; then I should rather write the M values at the top and the e values below them – it would not affect the structure of the projected graph.

The difference between $\mathcal{G}_{2,2}(2n : N, M_S)$ graph and $\mathcal{G}_4(n : N, M_S)$ graph is not very big. At each even level $2k$ of $\mathcal{G}_{2,2}(2n : N, M_S)$ the same vertices as at the k -th level of $\mathcal{G}_4(n : N, M_S)$ appear, with the same weights. However, the (o, e) projections are quite

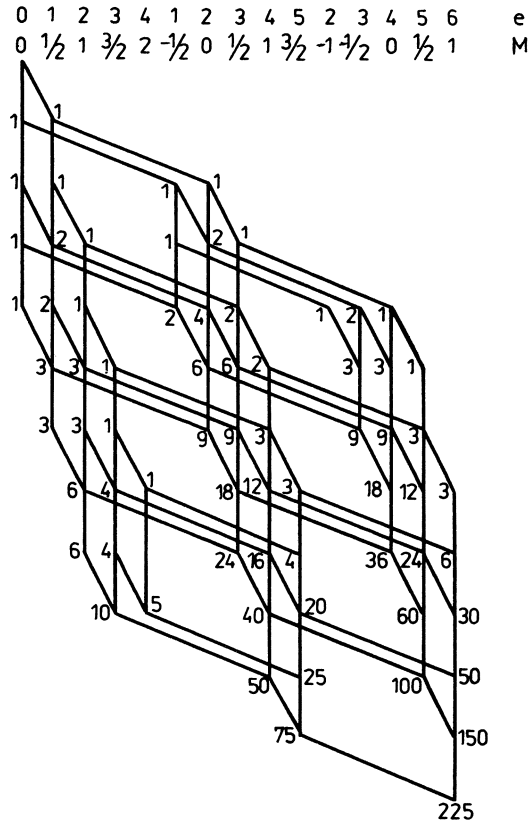


Fig 6c. Projections of three-dimensional \hat{S}_z -adapted graph, $M_S = 1$.
Skew projection showing whole graph.

different. In the spin orbital case the (o, e) projection has the form of $\mathcal{G}_2(2n : N)$ graph and contains more paths than needed, while in the orbital case the $\mathcal{G}_3(n : N)$ graph contains less paths than the original three-dimensional one. Moreover, although one can not easily delete the irrelevant information from $\mathcal{G}_2(2n : N)$ adding the information about spin functions to $\mathcal{G}_3(n : N)$ presents no problems. How many paths should be connected with one orbital configuration of $\mathcal{G}_3(n : N)$? Only the singly occupied orbitals should be considered. Changing our plane of projection a little we see that each orbital configuration containing s singles, that is $s_\alpha = \frac{1}{2}s + M_S$ of α -type and $s_\beta = \frac{1}{2}s - M_S$ of β -type, correspond to $s! / s_\alpha! s_\beta!$ paths in the original three-dimensional graph. Instead of using the oblique projection (Fig 7c, 8c) we may therefore use the three-slope configuration graph and a simplification of (o, M) projections. Let's remove all information about unoccupied and singly occupied arcs from the graph projected on the (o, M) plane. A kind of the two-slope graph is left (Fig 9), called further the M -diagram or $\mathcal{G}_2(s : M_S)$ graph. Combining the graph of orbital configurations $\mathcal{G}_3(n :$

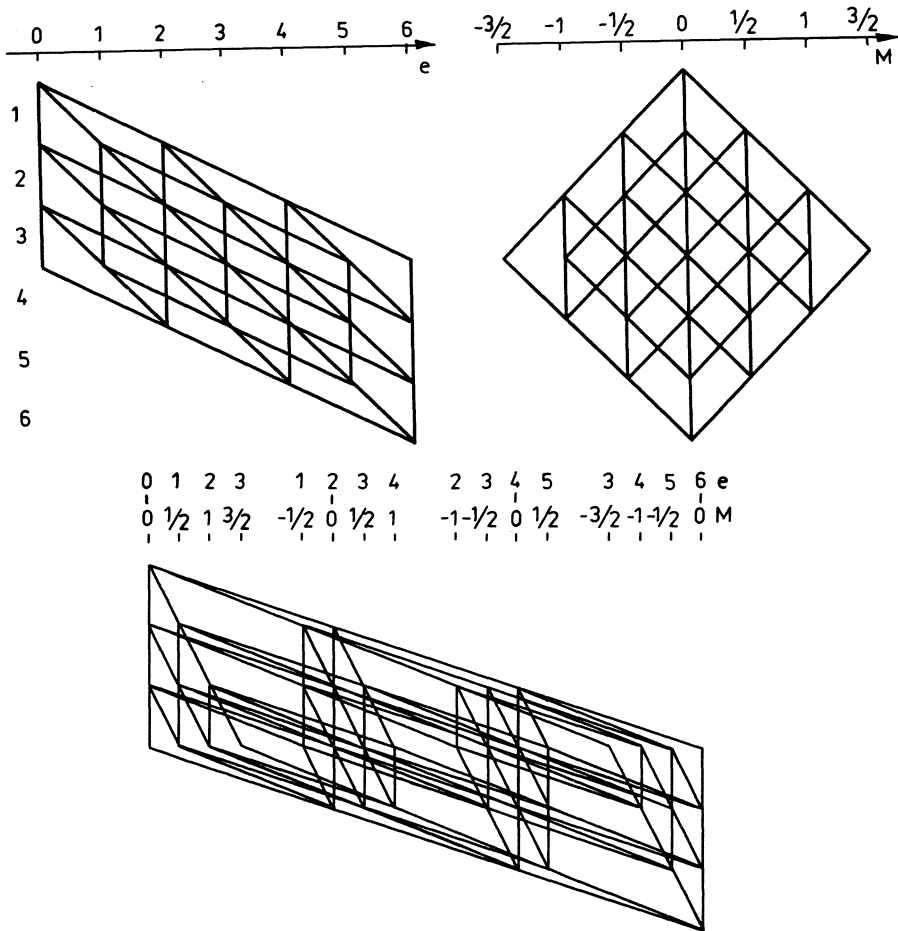


Fig 7. Projections of the n -level three-dimensional \hat{S}_z -adapted graph, $M_S = 0$
 a) on the (o, N) plane, b) on the (o, M_S) plane
 c) skew projection showing the whole graph.

N) with M -diagram $\mathcal{G}_2(s : M_S)$, an operation that may be symbolically designated $\mathcal{G}_3(n : N) \odot \mathcal{G}_2(s : M_S)$, one may recreate all the complexity of the four-slope graph. The three-slope graph is hiding one dimension that, for a given number of singles in a path, is described by the M -diagram. In fact the M -diagram simply classifies the distribution of $|\alpha\rangle$ and $|\beta\rangle$ spin states in the orbital configurations.

So far the graphs I have introduced were describing basis states of spaces. Here we have qualitatively different situation: $\mathcal{G}_3(n : N)$ describes only some aspects of our space, giving a 'rough' description, i.e. dividing our spaces into small subspaces. Complete description is obtained when M -diagram paths are connected to the three-slope graph's paths. We can imagine more complicated cases when several such 'layers' of graphs are used, each resolving the subspaces connected with the paths of a previous

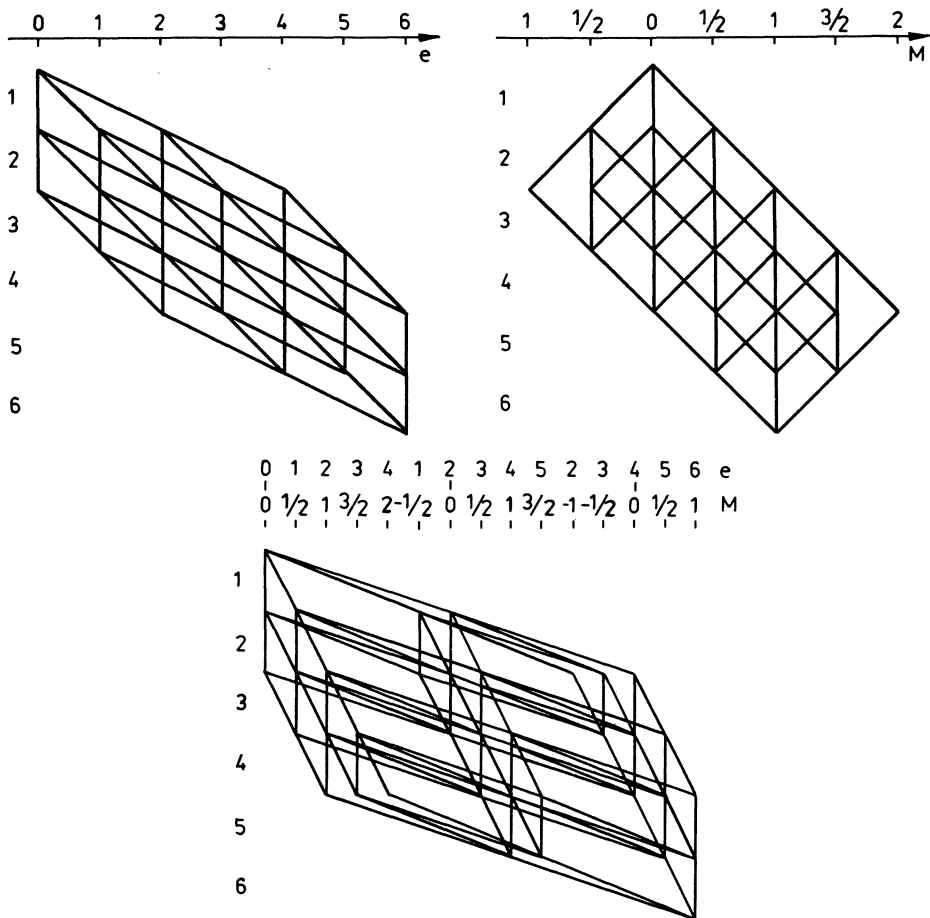


Fig 8. Projections of the n -level, three-dimensional \hat{S}_z -adapted graph, $M_S = 1$
 a) on the (o, N) plane, b) on the (o, M_S) plane,
 c) skew projection showing the whole graph.

one, thus avoiding the complexity of multi-dimensional graphs. Because such a situation is not uncommon I will introduce a new term: 'fagot graph'. It is a graph that describes not individual states but only groups or fagots of these states, i.e. aspects of the model space. The paths of the fagot graph are called 'fagot paths' and this should simply remind us that they refer to subspaces rather than single states. Both the three-slope graph and the M-diagram may be regarded as fagot graphs: the paths of the configuration graph branch into different spin-orbital configurations, the paths of the M-diagram may be connected with the subgraphs of $\mathcal{G}_3(n : N)$ like those of Fig 10, with a fixed number of singles (for $M = 0$ the head of the graph is connected with the subgraph containing only empty and doubly occupied orbitals). M-diagrams may also be regarded as non-fagot graphs, giving the final classification of many-particle

states. On the other hand the four-slope graph $\mathcal{G}_4(n : N, M_S)$ and the two-slope graph $\mathcal{G}_{2,2}(2n : N, M_S)$, each containing a detailed description of the basis of a model space, are always non-fagot graphs.

There is a price to be paid for a simplification resulting from the use of fagot graphs. For example some unwanted paths may be left in the fagot graph. In Fig 8a we see such a case: there are paths that do not contain any singly occupied arcs, while at least two singly occupied arcs are necessary to get the paths with $M_S = 1$. To avoid complication of the $\mathcal{G}_3(n : N)$ graphs we will ignore these unwanted paths now and use techniques described in one of the later sections to remove them while representing the graphs in a computer.

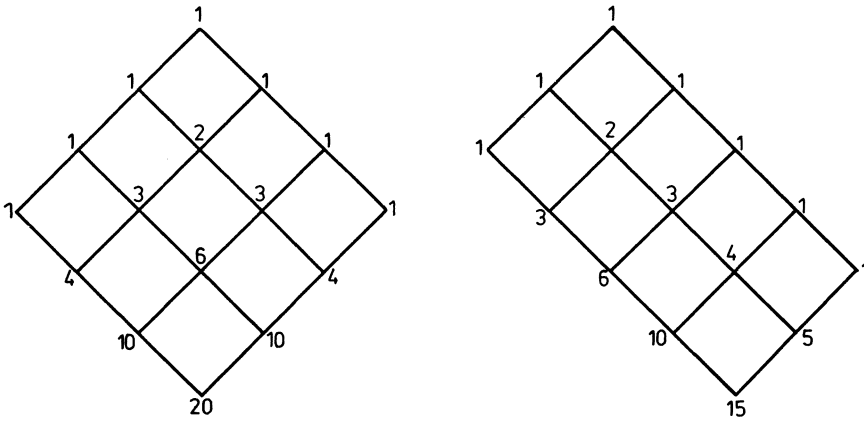


Fig 9. M -diagrams for $M_S = 0$ and $M_S = 1$.

Another possibility to remove the unwanted paths of this type is to use a different representation of the three-slope graph, with a few tails, each corresponding to a fixed number of singles. As an example Fig 10a shows the graph of Fig 8a with different terminal vertices (tails) for $s = 2, 4$ and 6 singles, and Fig 10b,c represents graphically the states with exactly two and exactly four singles. The three-dimensional structure of these graphs is evident; they are certainly non-planar. Their interpretation and drawing in the general case is not so straightforward as that of the three-slope configuration graphs, therefore I will not elaborate on this type of graphs further.

The weights in the M -diagram (Fig 9), as well as other two-slope full graphs, form a subset of Pascal-triangle numbers. The paths of the configuration graph with different number of singles s are classified according to a different subgraphs of the M -diagram, where the head is always fixed and the tail vertex is (s, M_S) . The weight $W(s, M_S)$ gives

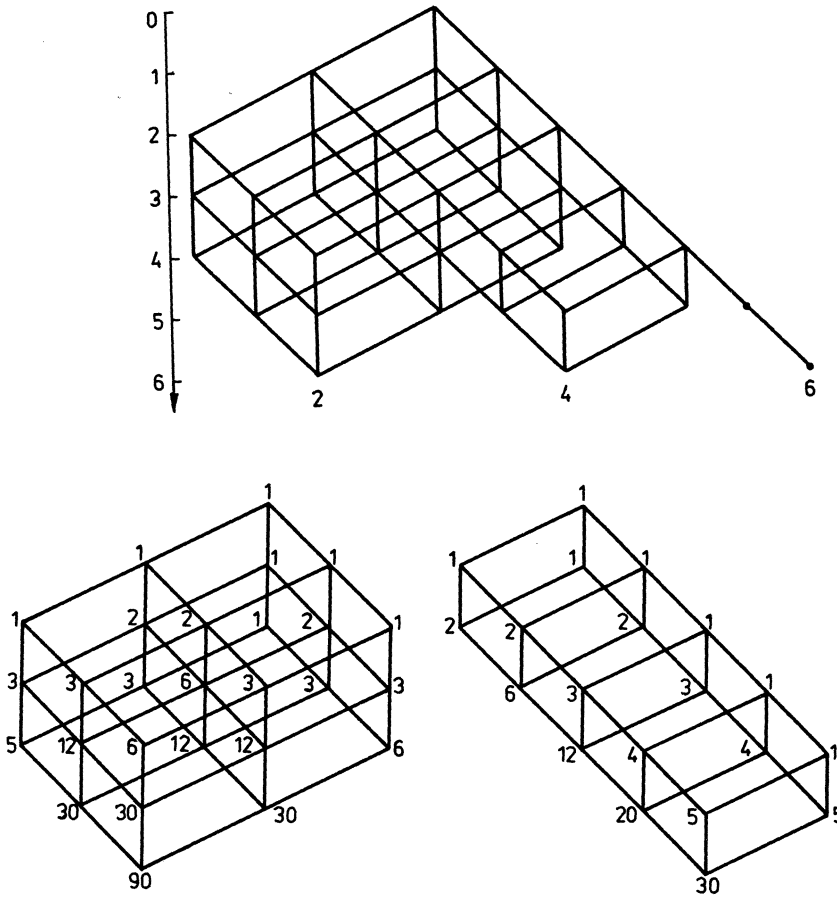


Fig 10. a) Graph of Fig 8 with separate tails for 2, 4 and 6 singles, b) subgraph for 2 singles, c) subgraph for 4 singles.

the number of basis states associated with the configuration of s singles, i.e. dimension of this configuration subspace. Of course it is equal to

$$d(s, M_S) = \frac{s!}{(\frac{1}{2}s + M_S)! (\frac{1}{2}s - M_S)!} \tag{1.8}$$

The dimension of the space of orbital configurations, or the number of paths in the $\mathcal{G}_3(n : N)$ graph, is also easy to calculate. For n orbitals with s singles, $d = \frac{1}{2}(N - s)$ doubles and $v = n - s - d$ empty orbitals there are $\frac{n!}{s!d!v!}$ configurations. Summing over all values of s we obtain

$$d_3(n, N) = \sum_{l=0}^{N/2} \binom{n}{l} \binom{n-l}{N-2l} \tag{1.9}$$

For $M_s \neq 0$ the number of paths in $\mathcal{G}_3(n : N)$ graph may be slightly lower if some vertices are removed (cf Fig 8a). To find the number of configurations with $s \geq |2M_S|$

we should sum to $l = \frac{1}{2}N - |M_S|$. It is interesting to note that this sum seems to have no simpler form. The dimension of the space of spin-orbital states or the number of paths in $\mathcal{G}_{2,2}(2n : N, M_S)$ or $\mathcal{G}_4(n : N, M_S)$ graphs is equal to the same sum of the number of configurations weighted by $d(s, M_S)$. This last sum is easily reduced to a single term, Eq (1.7).

Summing up, I have introduced different graphical representations of \hat{S}_z -adapted model spaces in the form of $2n$ -level (spin orbital) and of n -level (orbital) graphs that either describe (label) individual basis states of the model space or label fagots of such states. I could go back now and use the three and four-slope graphs to represent the spaces that are not adapted to any operators, improving the $\mathcal{G}_2(2n : N)$ graph. The new graphs, useful for relativistic problems, are even simpler than the ones described in this section. Let us move to the more complicated cases; the \hat{S}_z -operator leads to the relatively simple shapes and architectures of the graphs.

1.4

\hat{L}_z -adapted graphs

Let us consider now a more complicated case of the \hat{L}_z -adapted space. Complications arise from the fact that the orbital momentum projection quantum numbers m_l of a single particle take many values $m_l = 0, \pm 1, \pm 2, \dots$ while for the spin only two values $m_s = \pm \frac{1}{2}$ were possible. Orbitals (primitive states) with different m_l values should be represented by arcs of different slopes. There are two parameters demanding careful choice in order to make legible graphs. First, the absolute value of an arc's slope has to be chosen for the orbital state with a fixed m_l value. Second, slopes for the orbitals with $m_l \pm 1$ have to be specified. The slope of an arc may be measured by the horizontal distance h_m of the two vertices connected by this arc. The slope of an empty arc is most frequently set to zero making the arc vertical. The difference $h_m - h_{m-1}$ should be chosen in such a way that h_m is always different from the slope of an empty arc and that each vertex is uniquely labeled by (o, M_L) values.

Let us take an example: 5 electrons distributed among $2s$, $2p$ and $3p$ orbitals. The full space for these 14 spin orbitals is composed of $\binom{14}{5} = 2002$ determinants. We have $2s$, $2p_0$, $3p_0$ orbitals with $m_l = 0$; $2p_+$, $3p_+$ with $m_l = 1$ and $2p_-$, $3p_-$ with $m_l = -1$. The subspace with $M_L = 1$ contains 444 functions and is represented in Fig 11. Two different orderings of orbitals were used, the first corresponding to the increasing orbital energies (Fig 11a), the second with separated $m_l = 0$, $m_l = -1$ and $m_l = 1$ spin orbitals (Fig 11b). As we see clearly in Fig 11 ordering of orbitals has a great effect on the legibility of graphs. In this case, since the two-slope per level representation was used, the graph of Fig 11b, designated in compliance with the previous designations as $\mathcal{G}_{2,2}(2n : N, M_L)$, became planar, besides reduction in the number of vertices by one half. If more than two slopes per level are allowed planar representation is not possible but the reordering of orbitals still has a great influence on the complexity of the graph. In general finding the ordering of levels and choosing the slopes of orbitals to achieve

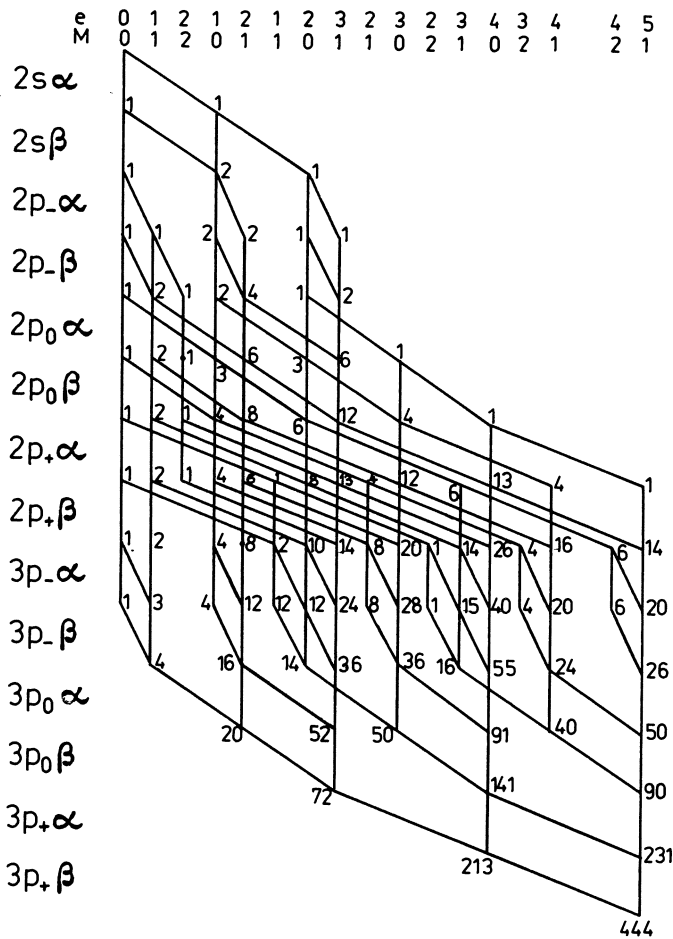


Fig 11a. Representation of \hat{L}_z -adapted space for $(2s + 2p + 3p)^5$ basis, $M_L = 1$: orbitals ordered according to the increasing energies.

the minimal graph, i.e. graph with the minimum number of vertices and arcs, is not a trivial task.

The formula for the dimension of the \hat{L}_z -adapted space is also much more complicated comparing to the \hat{S}_z -adapted space. Designating by n_m the number of orbitals with quantum number $m = m_l$ we may write

$$d(n_0, n_{+1}, n_{-1}, \dots; N, M_L) = \sum_{[k]} \left\{ \binom{2n_0}{k_0} \binom{2n_{-1}}{k_{-1}} \binom{2n_{+1}}{k_{+1}} \dots \right\} \quad (1.10)$$

where the sum runs over all partitions $[k] = [k_0 k_{-1} k_{+1} \dots]$ of the number N subject to

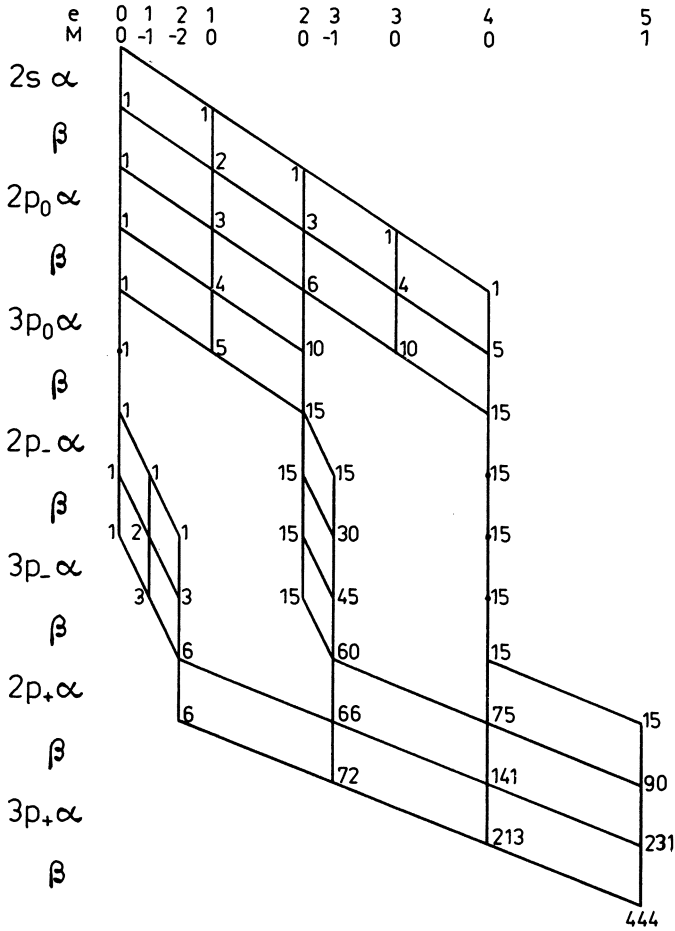


Fig 11b. Representation of \hat{L}_z -adapted space for $(2s + 2p + 3p)^5$ basis, $M_L = 1$: orbitals ordered according to their m_l values.

conditions

$$N = \sum_{m=-m_l}^{m_l} k_m; \quad M_L = \sum_m m k_m; \quad k_m \leq 2n_m \quad (1.11)$$

We can check now if the number of paths in Fig 11 is correct: three partitions of $N = 5$, $M_L = 1$ are possible in this basis, $n_0 = 6$, $n_{-1} = n_{+1} = 4$. The partitions $[k_{-1} \ k_0 \ k_{+1}]$ are $[2 \ 0 \ 3]$, $[1 \ 2 \ 2]$, and $[0 \ 4 \ 1]$. Summing the contribution from each partition $d = 444$ is obtained.

Let us turn now to a more complicated example of $n = 3$ shell, involving d -orbitals. $3s$, $3p$ and $3d$ functions give together 18 spin orbitals, so that the total space for 5 electrons has $\binom{18}{5} = 8568$ dimensions. In Fig 12 the subspaces for $M_L = 0$ (Fig 12a)

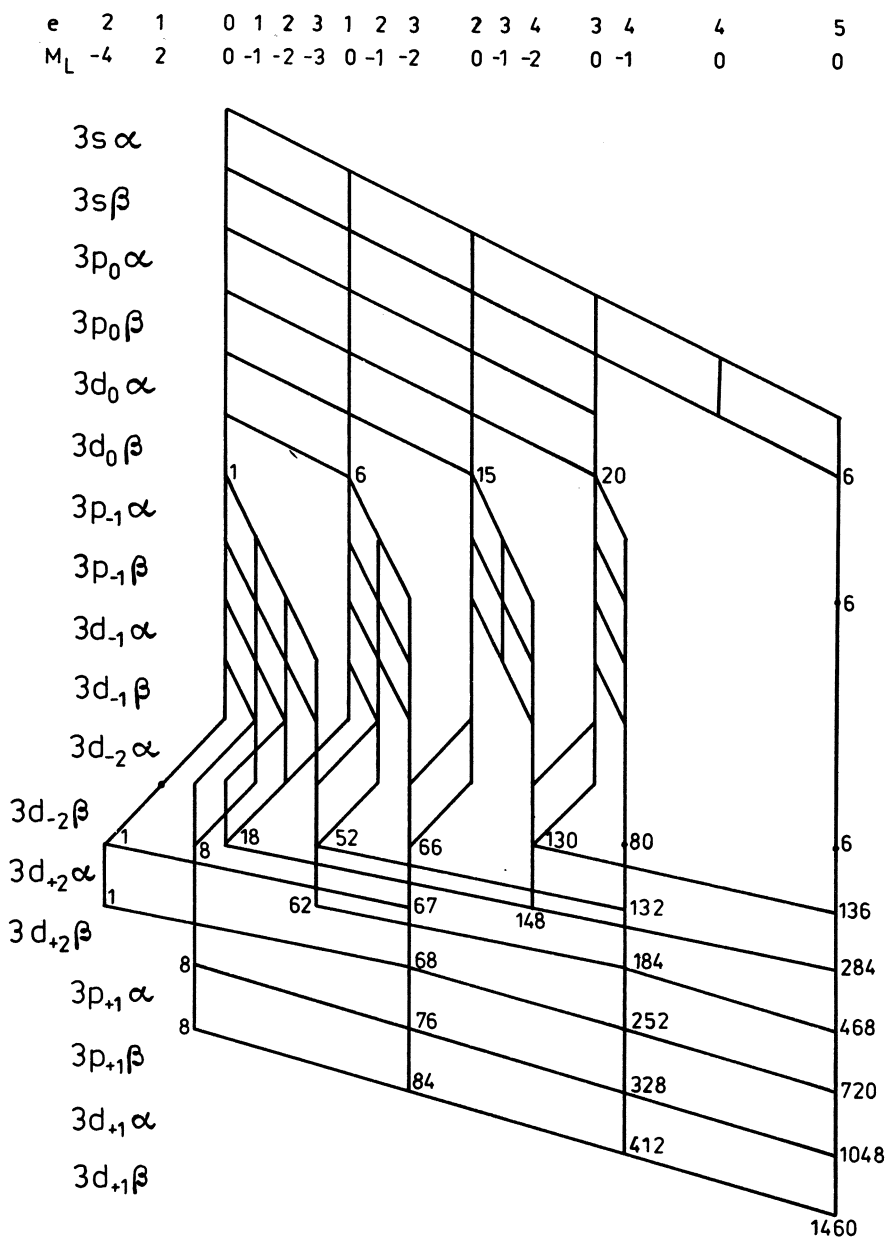


Fig 12a. Representation of \hat{L}_z -adapted $(3s + 3p + 3d)^5$ space, $M_L = 0$: orbitals ordered according to their energies.

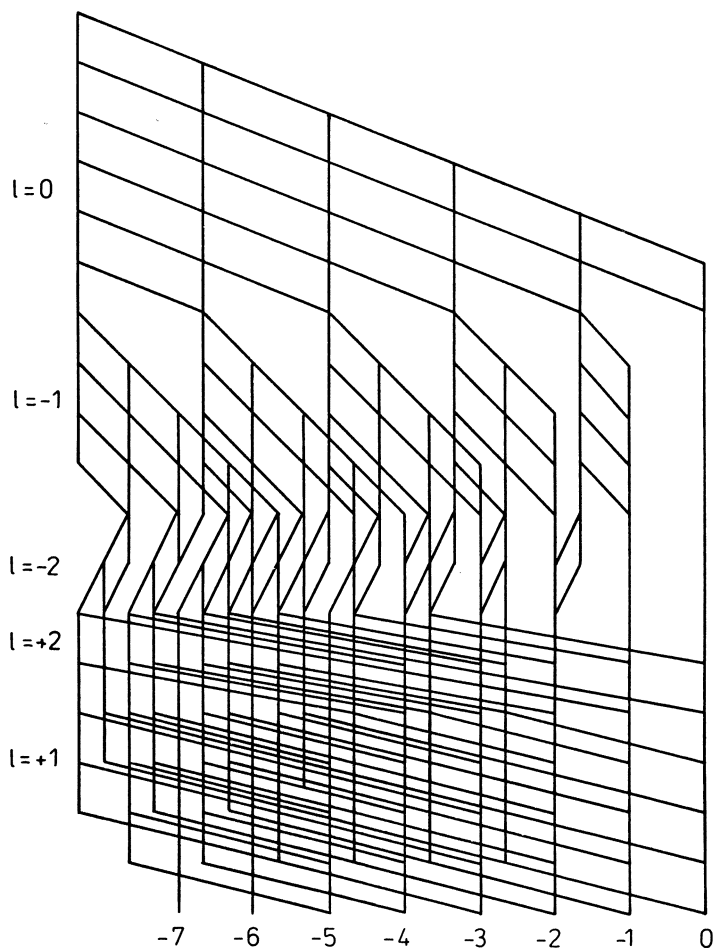


Fig 13. Representation of \hat{L}_z -adapted $(3s + 3p + 3d)^5$ space: all states with $M_L \leq 0$ are presented.

and for $M_L = 1$ (Fig 12b) are represented. Although the graphs are not planar there are only a few arc crossings between the levels. In this case the graphs are complicated enough to justify a comment on their construction. From each vertex we may draw two new arcs leading to two vertices: if it is possible to join the new vertices with the tail vertex, i.e. the $(2n; N, M_L)$ vertex, the arc is drawn. For example, the vertex $(6; 4, 0)$ does not belong to the graph of Fig 12a, and the corresponding arc was not drawn, because it can not be connected with the $(18; 5, 0)$ vertex. A set of simple rules may be formulated for each type of a graphical representation allowing for computer generation of graphs. Drawing of multiple tail graphs is even simpler: in Fig 13 we see a graph representing all many-particle states with $M_L \leq 0$. The graph of Fig 12a is embedded in Fig 13. The part with p_+ and d_+ orbitals is now very 'crowded' with lines.

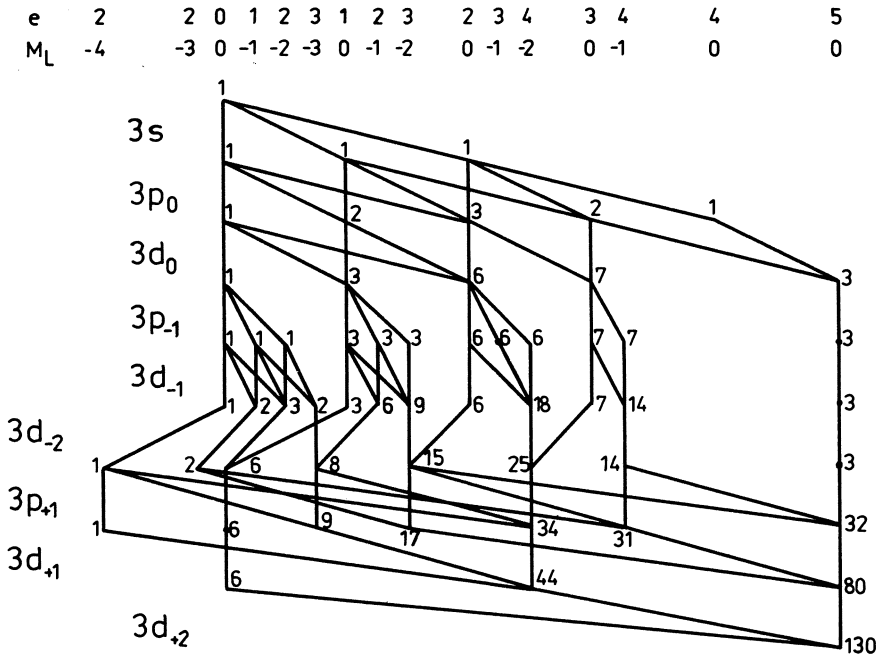


Fig 14a. Configurations of $(3s + 3p + 3d)^5$ space represented by \hat{L}_z - adapted fagot graph.

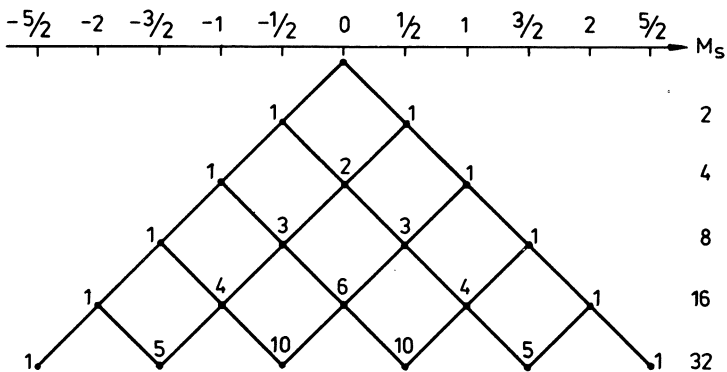


Fig 14b. Diagram assigning spin functions to singly occupied orbitals of the fagot graph.

The graphs described so far are spin orbital, i.e. $2n$ -level graphs. Similarly as in the previous section I will introduce also representation by the orbital, i.e. n -level graphs. However, the four-slope per level graph (cf Fig 7c, Fig 8c) is in this case very complicated and has 7 tails, automatically leading to separation of $M_S = 0, \pm\frac{1}{2}, \pm\frac{3}{2}, \pm\frac{5}{2}$ states. The orbital description becomes relatively simple if we use the fagot graph. The simplest fagot graph is obtained by removing the distinction between α and β -type spin orbitals from Fig 12. In this way the graph of Fig 14a was obtained. Instead of 1460 it contains only 130 paths, but each paths represents now a subspace of states. This fagot graph may represent \hat{L}_z -adapted space or (\hat{L}_z, \hat{S}_z) -adapted space. In the first case, useful in relativistic atomic physics and in nuclear physics, the final identification of many-particle states is done by assigning spin functions to the singly occupied orbitals in all possible ways, i.e. for s singles in 2^s ways. This is represented in Fig 14b by the paths reaching all nodes on level s , the leftmost path always representing pure $\beta\beta\beta\dots$ functions and the rightmost path pure $\alpha\alpha\alpha\dots$ functions. Thus a path with 5 singles represents 32 determinants differing only by their spin parts. Leaving only one node at the level s in diagram of Fig 14b we automatically obtain classification of (\hat{L}_z, \hat{S}_z) states. A fagot path represents here an orbital configuration: this coarse description of the space is the same for \hat{L}_z and (\hat{L}_z, \hat{S}_z) -adapted spaces, as well as for (\hat{L}_z, \hat{S}^2) -adapted space, as we will see shortly.

1.5

$(\hat{\mathbf{L}}_z, \hat{\mathbf{S}}_z)$ -adapted graphs

In many applications there is more than one operator that commutes with the Hamiltonian of a system. Eigenstates of angular momentum usually have also some spin symmetry. In the simplest case the states should be adapted to $(\hat{\mathbf{L}}_z, \hat{\mathbf{S}}_z)$ operators. One way of representing the space of such states is to use a fagot graph describing $\hat{\mathbf{L}}_z$ -adapted configurations, as in Fig 14a, and classify the final states for each fagot function (subspace) according to a subgraph of Fig 14b, as already mentioned in the previous section. Several other representations may also be useful. The simplest non-fagot representation is obtained when α and β -type orbitals are separated, with $\frac{1}{2}N + M_S$ orbitals of the α -type at top and $\frac{1}{2}N - M_S$ orbitals of the β -type at bottom of a graph. In Fig 15 full space for states with $M_L = 1$ and $M_S = \frac{1}{2}$ of $N = 5$ electrons distributed among $2s$, $2p$, and $3p$ orbitals, is represented for two orbital orderings. Although it is not possible to find a planar graph representing this space the graph of Fig 15b, with orbitals grouped according to their m_l values, is more legible than the graphs corresponding to other orbital orderings. In Fig 16 more complicated case, with $3s$, $3p$ and $3d$ orbital basis, is represented. The graph is almost planar, with only a few arc lines that cross off vertices. Each vertex in the $(\hat{\mathbf{L}}_z, \hat{\mathbf{S}}_z)$ -adapted graphs is uniquely labeled by: the number of electrons e , the intermediate projection of angular momentum m_l , the spin projection m_s and the level o corresponding to some orbital, i.e. it may be designated $v(o : e, m_l, m_s)$.

The graphs with α and β parts separated are legible relatively well and give convenient representation of the full spaces as well as of some types of restricted spaces. However, they are not as flexible in the choice of physically justified restrictions on the space shape as are the graphs without such separation. In Fig 17 we see the graph of Fig 16 with the orbitals placed in $\phi_1\alpha, \phi_1\beta\dots$ order. The graph is now considerably more complicated. To assure the correct value of the spin projection M_S different arc

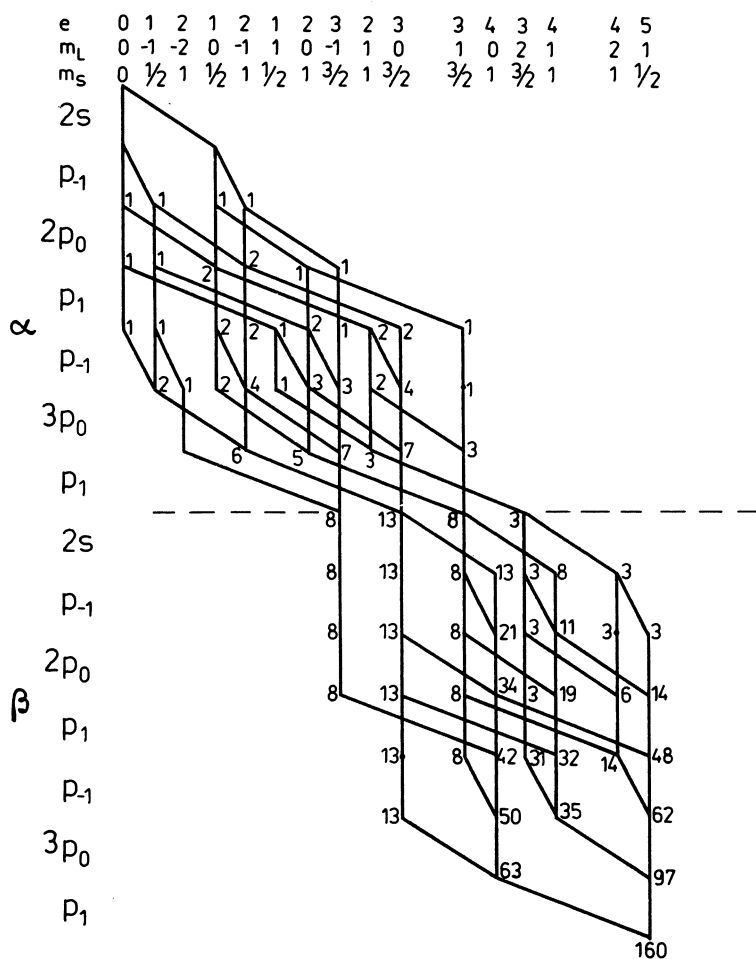


Fig 15a. Representation of (\hat{L}_z, \hat{S}_z) -adapted $(2s + 2p + 3p)^5$ space with α and β -type spin orbitals separated: orbitals in energetical order.

slopes are used to represent ϕ_α and ϕ_β spin orbitals. Combined with the slopes used to distinguish among different m_l values the number of arc slopes that we have to use is rather high. Situation becomes even worse if we want to use the n -level orbital graph, with the four slopes appearing at each level (Fig 18). Such graphs are highly non-planar and their interpretation is tedious. Therefore fagot graphs should be preferred for restricted (\hat{L}_z, \hat{S}_z) -adapted spaces, with the α and β -separated non-fagot graphs being a convenient alternative in a description of full spaces.

The formula for the dimension of the full (\hat{L}_z, \hat{S}_z) -adapted space is similar to that of \hat{L}_z eigenspace

$$d(n_0, n_{+1}, n_{-1}, \dots; N, M_L, M_S) = \sum_{|k|} \left\{ \binom{n_0}{k_0^\alpha} \binom{n_0}{k_0^\beta} \binom{n_{-1}}{k_{-1}^\alpha} \binom{n_{-1}}{k_{-1}^\beta} \binom{n_{+1}}{k_{+1}^\alpha} \dots \right\} \quad (1.12)$$

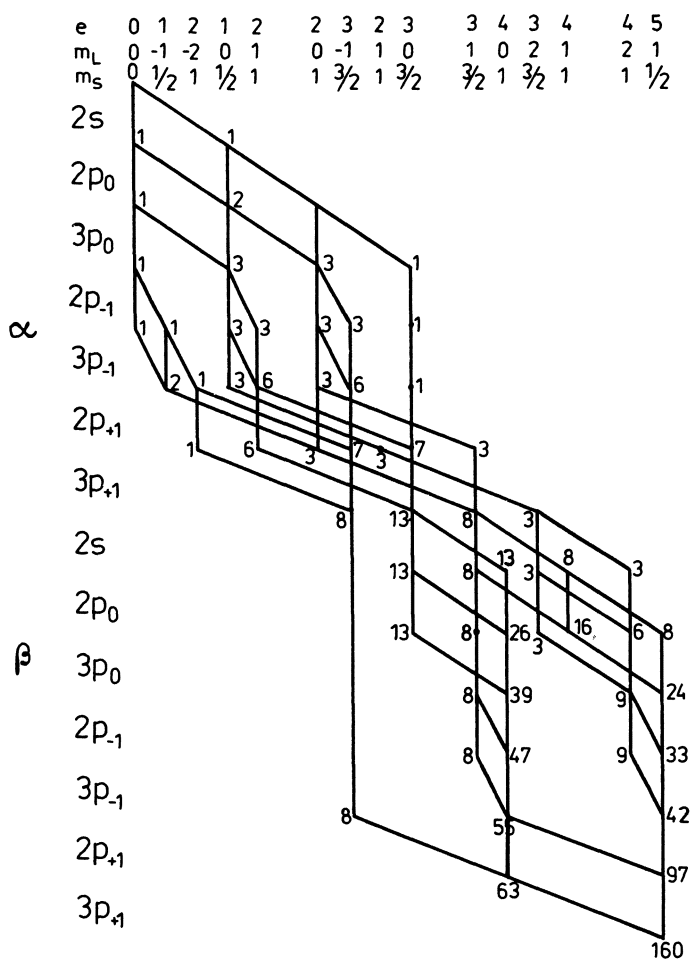


Fig 15b. Representation of (\hat{L}_z, \hat{S}_z) -adapted $(2s + 2p + 3p)^5$ space with α and β -type spin orbitals separated: orbitals ordered according to their m_l values.

where the partitions $[k]$ are now more complicated because each k_m is now further partitioned to k_m^α and k_m^β

$$[k] = [k_0 \ k_{-1} \ k_{+1} \dots] = [k_0^\alpha \ k_0^\beta \ k_{-1}^\alpha \ k_{-1}^\beta \ k_{+1}^\alpha \ k_{+1}^\beta \dots] \quad (1.13)$$

subject to conditions

$$N = \sum_{m=-m_l}^{m_l} (k_m^\alpha + k_m^\beta); \quad M_L = \sum_{m,\sigma} m k_m^\sigma; \quad k_m^\sigma \leq n_m \quad (1.14)$$

$$\sum_m k_m^\alpha = \frac{1}{2}N + M_S; \quad \sum_m k_m^\beta = \frac{1}{2}N - M_S;$$

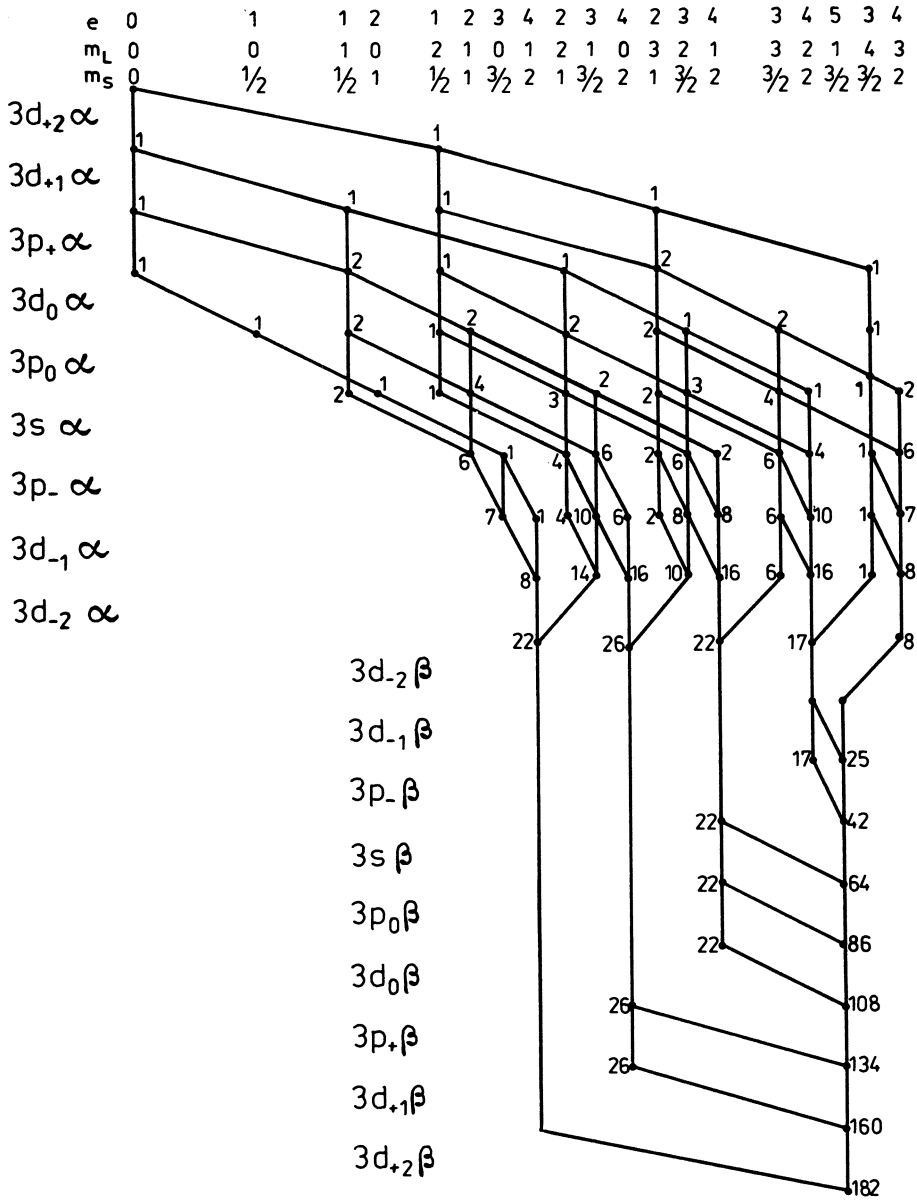


Fig 16. Representation of (\hat{L}_z, \hat{S}_z) -adapted $(3s + 3p + 3d)^5$ space for $M_L = 1, M_S = \frac{3}{2}$, with separation of α and β parts.

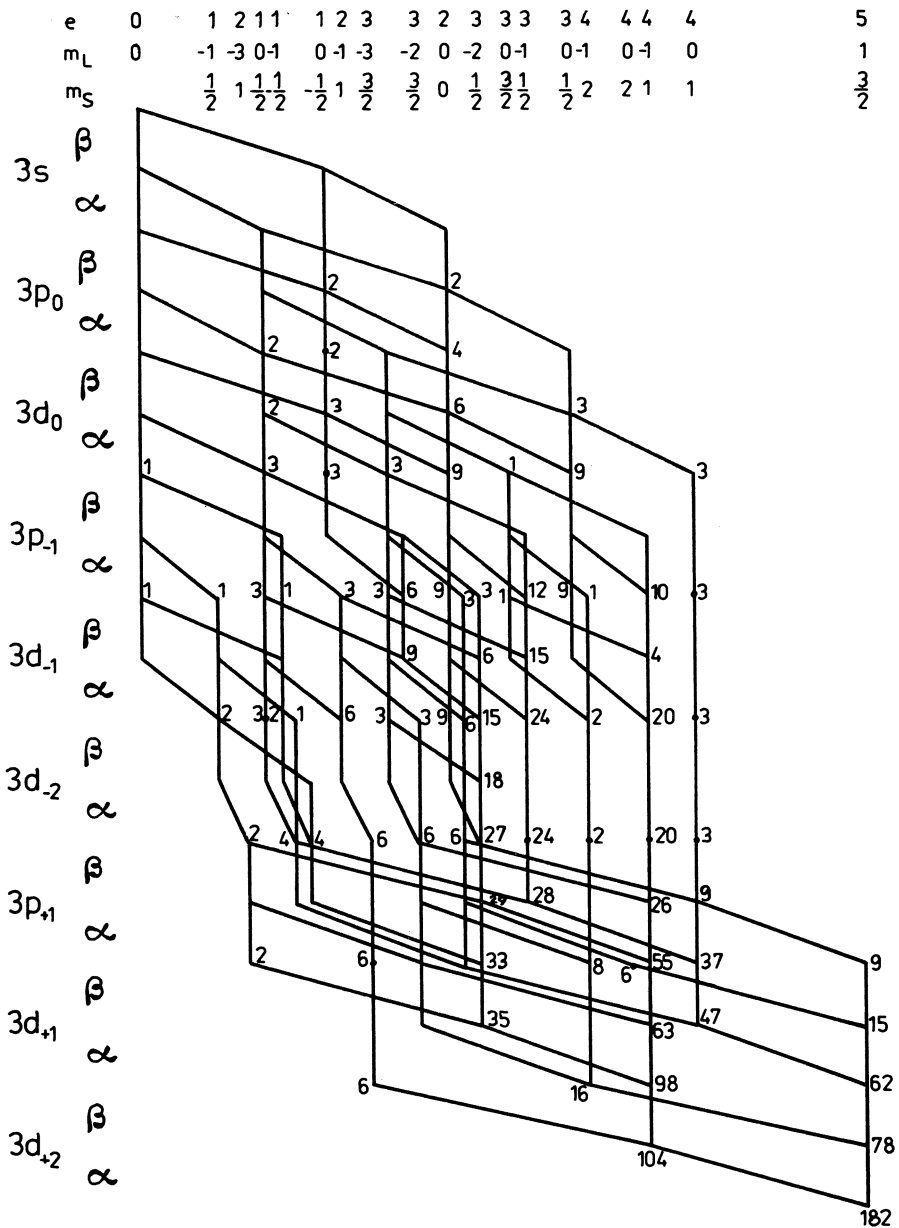


Fig 17. Representation of (\hat{L}_z, \hat{S}_z) -adapted $(3s+3p+3d)^5$ space for $M_L = 1, M_S = \frac{3}{2}$: orbitals ordered according to their m_l values.

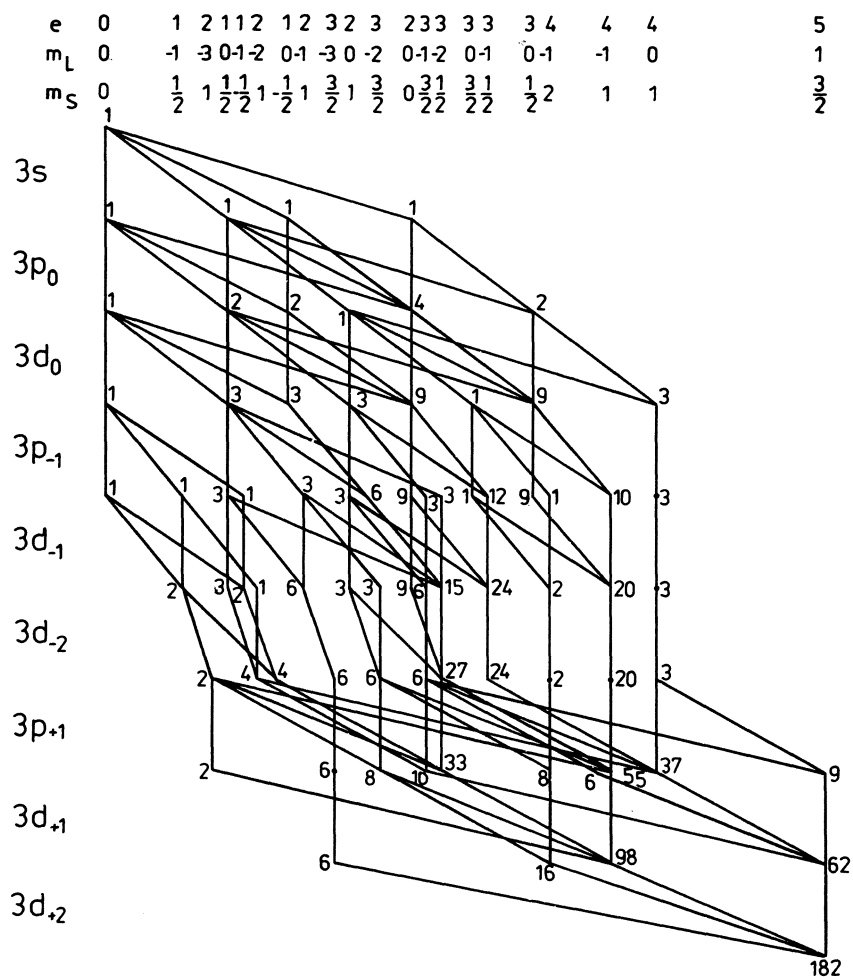


Fig 18. The space of Fig 16, 17 represented by a four-slope graph.

It may seem that the dimension formulas are hard to use in practice. To convince the reader that such is not the case let me calculate the dimension of $(2s + 2p + 3p)^5$ space shown in Fig 15. Here $N = 5$, $M_L = 1$, $M_S = \frac{1}{2}$; the last two conditions mean that the sum of partition numbers in α part should be 3 and in β part 2. The condition for partition of N is always automatically satisfied; $n_0 = 3$, $n_{+1} = 2$, $n_{-1} = 2$. There are 9 partitions possible and the sum of the number of states for all partitions gives 160 as it should. Similar table for the space shown in Fig 16 contains 22 partitions.

| 0 | α type | | 0 | β type | | Number of states |
|---|---------------|----|---|--------------|----|------------------|
| | -1 | +1 | | -1 | +1 | |
| 3 | | | 1 | | 1 | 6 |
| 2 | 1 | | | | 2 | 6 |
| 2 | | 1 | 2 | | | 18 |
| 2 | | 1 | | 1 | 1 | 24 |
| 1 | 1 | 1 | 1 | | 1 | 72 |
| 1 | | 2 | 1 | 1 | | 18 |
| | 2 | 1 | | | 2 | 2 |
| | 1 | 2 | 2 | | | 6 |
| | 1 | 2 | | 1 | 1 | 8 |

The graphs discussed so far have a simple correspondence between the paths and the basis states. Antisymmetric function adapted to \hat{L}_z and \hat{S}_z operators is usually taken as determinant, with a fixed total M_S and M_L values resulting from restrictions on the type of orbitals or spin orbitals involved in the determinant. Such simple correspondence is unfortunately no longer possible when we move to \hat{S}^2 or \hat{L}^2 -adapted spaces.

1.6

\hat{S}^2 -adapted graphs

The total spin operator \hat{S}^2 operator commutes with all spin free Hamiltonians. Apart from the spatial point group symmetry the spin symmetry is frequently the only useful symmetry of a physical system (this is true in particular for molecular systems). Moreover, the isospin operator \hat{T} of nucleons has the same formal properties as the total spin operator \hat{S}^2 . Construction and use of the spin eigenfunctions is therefore particularly important and whole monographs are devoted to this subject (cf Pauncz 1979). From the point of view that I have adopted here, namely GRMS, the thing that is important is not how to construct spin eigenfunctions, but how to find proper graphical labels for them. In the second part of this work I will show how the information contained in the labels or in the structure of graphs may be used to calculate arbitrary matrix elements.

Let us concentrate for a moment on the spin functions. One of the oldest methods to illustrate how one can build spin eigenfunctions in a systematic, genealogical way, is by means of the branching diagram (van Vleck and Sherman 1935). Traditional interpretation of the branching diagram (Fig 19) is the following: a spin function for N spins and the eigenvalue of \hat{S}^2 equal S is obtained from the two functions corresponding to $N - 1$ spins coupled to $S' = S - \frac{1}{2}$ and $S' = S + \frac{1}{2}$.

The number of spin functions $d(N, S)$ for N spins $\frac{1}{2}$ coupled to S is therefore a sum of $d(N - 1, S - \frac{1}{2}) + d(N - 1, S + \frac{1}{2})$ and is equal to the number of paths in the branching diagram that reach (N, S) node. However, if only one final node is left (solid lines in Fig 19) it is clear that the branching diagram represents graphically the space of all spin functions. Each path in the diagram corresponds to certain pure spin eigenfunction. We can introduce arc weights and lexical order among the paths. Thus branching diagram should be considered as a precursor of the graphs that represent model spaces. M-diagrams shown in Fig 9 differ from branching diagrams only because they contain

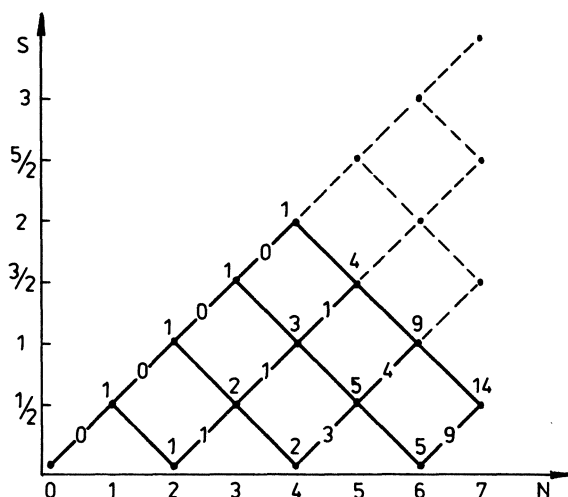


Fig 19. Branching diagram for seven spins $\frac{1}{2}$.

vertices corresponding to $M < 0$. By analogy to M-diagrams I will also use the name S-diagram for branching diagram.

The theory of groups gives two other ways of labeling the spin functions: $U(n)$ group theory using Gelfand tableaux, and S_N group theory using Young tableaux. Both methods are completely equivalent to the branching diagram representation. Although they are always presented in the context of group theory I will show now how one can introduce the Gelfand and Young tableaux starting from physical rather than mathematical point of view. This will be done with the help of an example.

Let us consider a case of 5 electrons in a doublet state, each electron occupying different orbital. There are 5 states, classified easily with the help of branching diagram paths (Fig 19). Let us now assign to a vertex (N,S) a row of N digits 0, 1 or 2, called a Gelfand row, in such a way that the number of 1's, designated by b , is equal $b = 2S$, the number of 2's, designated by a , is taken as $2a = n - b$, and the rest, i.e. $c = N - a - b$, are zeros. Thus the vertices in our example are associated with the following Gelfand rows:

| (N,S) | Gelfand row |
|------------------|-------------|
| $5, \frac{1}{2}$ | 2 2 1 0 0 |
| $4, 0$ | 2 2 0 0 |
| $4, 1$ | 2 1 1 0 |
| $3, \frac{1}{2}$ | 2 1 0 |
| $3, \frac{3}{2}$ | 1 1 1 |
| $2, 0$ | 2 0 |
| $2, 1$ | 1 1 |
| $1, \frac{1}{2}$ | 1 |

It is obvious that a path may be represented by listing the vertices, starting from (N,S) vertex defining the case, to the last vertex $(1, \frac{1}{2})$. Replacing the list of vertices by the list of Gelfand rows we obtain spin path label of a general form:

$$\begin{array}{c}
 m_{1n}m_{2n}\dots\dots\dots m_{nn} \\
 \dots\dots\dots \\
 m_{13}m_{23}m_{33} \\
 m_{12}m_{22} \\
 m_{11}
 \end{array}$$

Such triangular-shaped collections of integers are called Gelfand tableaux (Gelfand and Tsetlin 1950) and arise naturally in the unitary group theory (see for example Paldus 1976, Barut and Rączka 1980). Here we shall simply treat a tableau as a label, equivalent to the branching diagram path, without any deeper significance. Please note that a number of other unique ways of labeling the vertices of the branching diagram paths exist and therefore inventing different ‘representations’ of the spin eigenfunctions in form of a special tableaux is rather simple.

Another way of labeling spin functions frequently encountered in the literature (cf Pauncz 1979 and references therein) arise in the context of the symmetric group theory. Spin paths have $m_\alpha = (\frac{1}{2}N + S)$ segments going up and $m_\beta = (\frac{1}{2}N + S)$ segments going down, when we draw the path from left to right. Let us write the position of the segments in two rows of boxes, those going up in the upper row, those going down in the lower row. The two-row tableaux, with increasing natural numbers in the upper row, are known as Young tableaux (Rutherford 1948). In the example below (Example 1) spin paths for $N = 5, S = \frac{1}{2}$ are represented by the Gelfand and by Young tableaux.

It is easy to note that the natural ordering of the spin paths is expressed in case of Gelfand tableaux in the following way: Gelfand tableau $[m]$ precedes $[m']$ if the number $M = m_{1n}m_{1n-1}\dots m_{11}m_{2n}m_{2n-1}\dots m_{22}\dots m_{nn}$ formed from digits m_{ij} of $[m]$ is lower than the number M' formed from digits m'_{ij} of $[m']$. Ordering of the Young tableaux is established in an even simpler way: it is enough to compare the numbers formed from the digits of the first row.

So far we have considered only the labeling of spin functions, equivalent to the classification of functions corresponding to a configuration of singly occupied orbitals only. An obvious way of adding information about the orbital part of \hat{S}^2 -adapted functions is by drawing the three-slope fagot graph describing the orbital configurations (Fig 5a, 6a). The graph for the case of 5 electrons distributed among 5 orbitals is shown in Fig 20a. There are 266 configurations in this case, 21 with 5 singles, 140 with 3 singles and 105 with one single only ($266 = 21_5 + 140_3 + 105_1$; it is easy to keep track of the number of singles separating the weights into components with different number of singles). Complemented with the branching diagram to classify the states in the subspaces corresponding to each configuration, the operation that may be symbolically

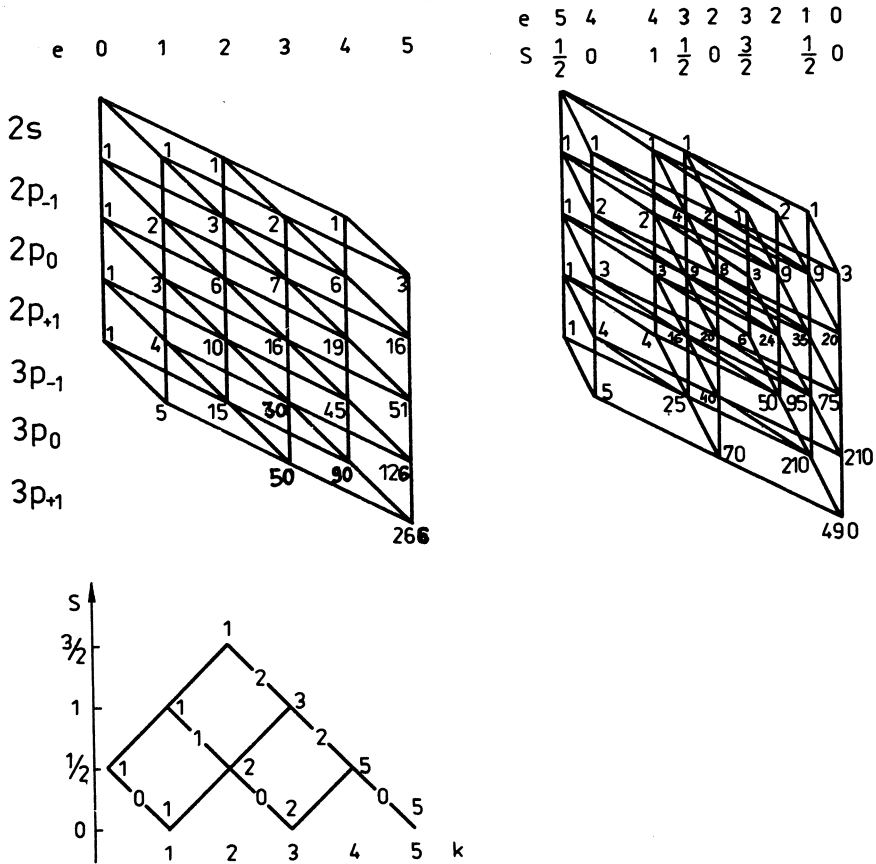


Fig 20. Representation of \hat{S}^2 -adapted $(2s + 2p + 3p)^5$ space by: a) three-slope graph combined with a branching diagram, and b) by a four-slope graph.

Combining $\mathcal{G}_3(n : N)$ graph with S-diagram $\mathcal{G}_2(s : S)$ we should use $d(s, S)$ as weights in Eq (1.9) giving the number of paths in the three-slope graph. The sum of binomial coefficient is then reduced to one term

$$d(n, N, S) = \frac{2S + 1}{n + 1} \binom{n + 1}{\frac{1}{2}N - S} \binom{n + 1}{\frac{1}{2}N + S + 1} \tag{1.16}$$

giving the dimension of a full N -particle space of spin eigenfunctions coupled to S in the basis of n orbitals.

It is quite easy to specify full information about \hat{S}^2 -adapted states using Gelfand tableaux. In fact these tableaux may contain much more information that we need, information relevant to classification of general $U(n)$ representations, but redundant here. The simplest approach is to assign to each vertex of a four-slope graph a Gelfand row, as was done previously for branching diagram, i.e. writing a times 2, b times 1 and c times 0, where a, b, c are calculated from coordinates $(k; N_k, S_k)$ of a vertex using:

$$b = 2S_k; \quad 2a + b = N_k; \quad a + b + c = k; \tag{1.17}$$

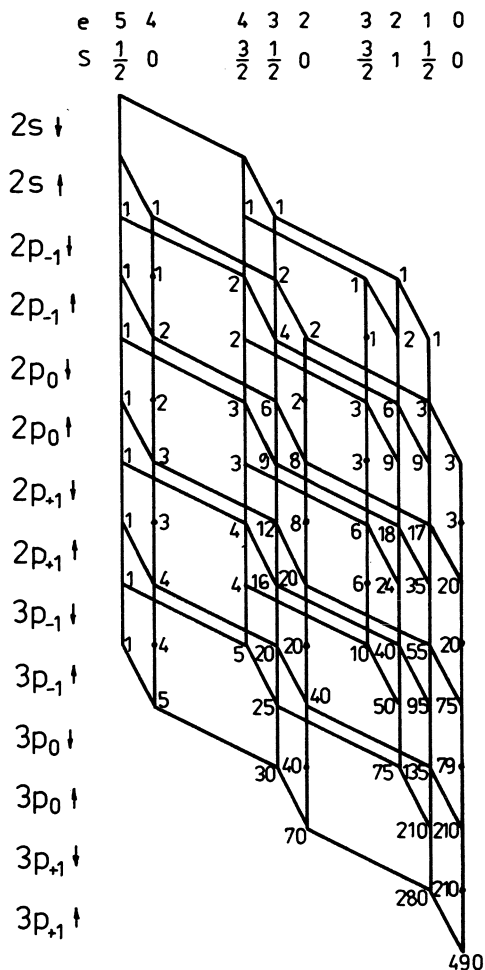


Fig 20c. Representation of \hat{S}^2 -adapted $(2s + 2p + 3p)^5$ by a two-slope graph.

i.e. vertices belonging to the row k of a four-slope graph have Gelfand rows with k numbers, 1 appears b times, and the sum of all 2's and 1's in a given row is equal to N_k . It is interesting to note that different functions belonging to the same configuration are characterized by the Gelfand tableaux that differ only by replacing pairs 1 1 by 2 0 (compare Example 1).

It is equally easy to modify Young tableaux to label \hat{S}^2 -adapted states. To be in harmony with the tradition we will use two-column rather than two-row tableaux. These tableaux are usually called Weyl tableaux and may contain the same number in two boxes, while all numbers in the Young tableaux have to be different. Weyl tableaux have m_α boxes in the first column and m_β in the second, i.e. their shape is conjugate to that of the Young tableaux. While Gelfand rows refer to the vertices of the graph, i.e. describe N_k, S_k values as a function of orbital level, the numbers in Weyl tableaux

refer to the graph's arcs, i.e. describe types of orbitals: doubly occupied appear in both columns while singly occupied increasing S_k value in the branching diagram appear in the first column, and those decreasing S_k value only in the second column. In the Example 2 the first 5 configurations of Fig 20a are labeled in a few different ways for comparison. In this example full spin paths are also presented: doubly occupied orbitals represented by the short horizontal lines correspond to a singlet-coupled pairs. Full spin path are formed by adding singlet-coupled pair symbols to the branching diagram paths. Together with the orbital designations they give yet another method of labeling.

Example 2

| Lex No | 1 | 2 | 3 | 4 | 5 | |
|-----------------------|---|---|---|---|---|---|
| Orbital configuration | 2 2 1 0 0 | 2 1 2 0 0 | 1 2 2 0 0 | 2 2 0 1 0 | 2 1 1 1 0 | |
| Spin path | | | | | | |
| Full spin path | | | | | | |
| Gelfand tableaux | $\begin{matrix} 2 & 2 & 1 & 0 & 0 \\ & 2 & 2 & 1 & 0 \\ & & 2 & 2 & 1 \\ & & & 2 & 2 \\ & & & & 2 \end{matrix}$ | $\begin{matrix} 2 & 2 & 1 & 0 & 0 \\ & 2 & 2 & 1 & 0 \\ & & 2 & 2 & 1 \\ & & & 2 & 1 \\ & & & & 2 \end{matrix}$ | $\begin{matrix} 2 & 2 & 1 & 0 & 0 \\ & 2 & 2 & 1 & 0 \\ & & 2 & 2 & 1 \\ & & & 2 & 1 \\ & & & & 1 \end{matrix}$ | $\begin{matrix} 2 & 2 & 1 & 0 & 0 \\ & 2 & 2 & 1 & 0 \\ & & 2 & 2 & 0 \\ & & & 2 & 2 \\ & & & & 2 \end{matrix}$ | $\begin{matrix} 2 & 2 & 1 & 0 & 0 \\ & 2 & 2 & 1 & 0 \\ & & 2 & 2 & 0 \\ & & & 2 & 1 \\ & & & & 2 \end{matrix}$ | |
| Weyl tableaux | $\begin{matrix} 1 & 1 \\ 2 & 2 \\ 3 \end{matrix}$ | $\begin{matrix} 1 & 1 \\ 2 & 3 \\ 3 \end{matrix}$ | $\begin{matrix} 1 & 2 \\ 2 & 3 \\ 3 \end{matrix}$ | $\begin{matrix} 1 & 1 \\ 2 & 2 \\ 4 \end{matrix}$ | $\begin{matrix} 1 & 1 \\ 2 & 4 \\ 3 \end{matrix}$ | $\begin{matrix} 1 & 1 \\ 2 & 3 \\ 4 \end{matrix}$ |

The advantages of a graphical representation should be clear already at this point. Instead of storing the labels in a form of Gelfand tableaux or Weyl tableaux information about the whole graph is stored. The information necessary for calculation of matrix elements is embedded in the graph's structure. Using the tableaux-type of labels on the other hand not only takes a lot of memory, but also does not allow us to see the global structure of the model space. Other ways of labeling the states may be devised (cf Sahasrabudhe *et al* 1980) but graphical labeling is the simplest and the most convenient. It is therefore surprising that historically Paldus work (1976) on adaptation of the unitary group theory to the solutions of the Schrödinger equation started with Gelfand tableaux, and subsequently, via simplifications arising from representation of Gelfand rows by a, b, c numbers (ABC tableaux), led to the representation of 'distinct

rows' in ABC tableaux in a graphical form (Shavitt 1977), topologically equivalent to the four-slope representation of Fig 20b. When the problem is seen as a labeling exercise this historical route represents a great detour. As I will show in the second part also from the point of view of matrix element calculations it is a detour. However, it is doubtful whether the present research would have been started had that detour not been made.

1.7

$(\hat{\mathbf{L}}_z, \hat{\mathbf{S}}^2)$ -adapted graphs

Representation of $(\hat{\mathbf{L}}_z, \hat{\mathbf{S}}^2)$ -adapted spaces does not differ much from the representation of $(\hat{\mathbf{L}}_z, \hat{\mathbf{S}}_z)$ -adapted spaces, as the reader has probably guessed by now. S-diagram is made from M-diagram by removing vertices corresponding to negative M values. The graph with $\alpha, \beta, \alpha\dots$ order of spin orbitals as well as four-slope graphs are a kind of extended M-diagrams: their paths, after doubly occupied orbitals are removed and dependence of arc slopes on m_i values ignored, are indeed reduced to the paths of M-diagram. Therefore restricting in Fig 17,18 values of S_k to the positive ones we obtain description of $(\hat{\mathbf{L}}_z, \hat{\mathbf{S}}^2)$ -adapted space. However, the simpler $(\hat{\mathbf{L}}_z, \hat{\mathbf{S}}_z)$ -adapted graphs with α and β -type orbitals separated (Fig 15,16) can not be easily modified to represent spin eigenfunctions. These graphs, if α -type levels are placed at the top, have for all vertices $M_S \geq 0$. In this section previously unexplored possibility of representing the $(\hat{\mathbf{L}}_z, \hat{\mathbf{S}}_z)$ and $(\hat{\mathbf{L}}_z, \hat{\mathbf{S}}^2)$ -adapted spaces with the help of a fagot graph is presented. The $(\hat{\mathbf{L}}_z, \hat{\mathbf{S}}^2)$ -adapted graphs are very convenient in calculations of atomic properties and in nuclear shell model calculations; bearing in mind the complexity of $\hat{\mathbf{L}}^2$ -adapted states it is better to use larger but simpler bases of $(\hat{\mathbf{L}}_z, \hat{\mathbf{S}}^2)$ -adapted spaces, especially that we may transform whole blocks of matrix elements instead of individual functions from spaces in which matrix elements are easy to calculate to spaces where calculation is more complicated (cf Duch 1986a and Section 2.4 of this volume). In some cases, important for practical calculations, when the space of the highest S value is desired description of $(\hat{\mathbf{L}}_z, \hat{\mathbf{S}}^2)$ and $(\hat{\mathbf{L}}_z, \hat{\mathbf{S}}_z)$ -adapted spaces is equivalent. Such a case is presented in Fig 21, where $(1s + 2s + 2p + 3s + 3p + 3d)^5$ one-particle space is used to form a five-particle space of states for $M_L = 1$ and $S = \frac{5}{2}$. The 357 states that belong to this space are associated with 86 atomic configurations, as shown in Fig 22. In this case $S = \frac{1}{2}N$, therefore all orbitals are singly occupied and the configurations contain at most half-filled shells (i.e. s^1, p^3, d^5). For $M_L = 1$ the configurations d^5 and $ss'p^3$ must

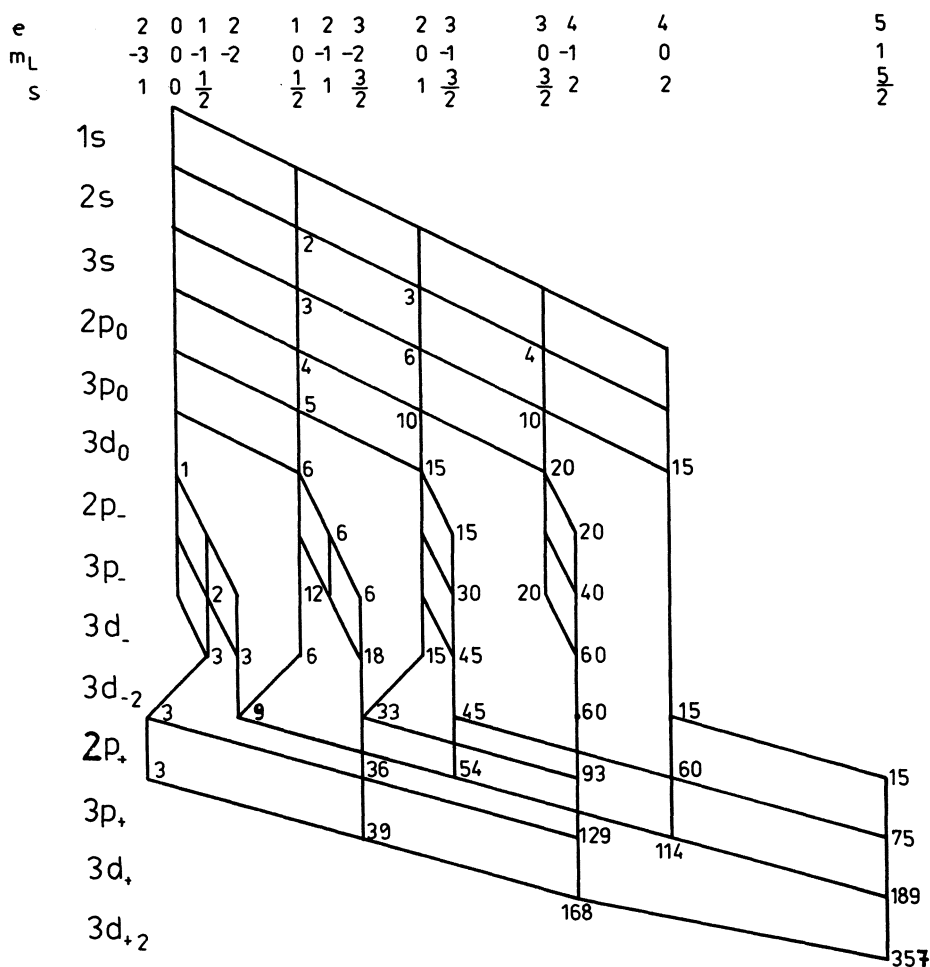


Fig 21. Representation of (\hat{L}_z, \hat{S}^2) -adapted space for $M_L = 1$ and $S = \frac{5}{2}$.

not appear and two arcs are removed from the graph. However, only the $2p^3$ arc for $ss'p^3$ type of configuration is removed, $3p^3$ arc being necessary for other configurations. Even in this simple case graph of configurations contains thus some spurious paths.

We can easily write down all different configuration types by splitting the vertices of the fagot graph, Fig 22, as is illustrated in Example 3 (one could as well draw a graph with multiple tails to show all different configuration types). Classification of configuration types is necessary if we intend to transform blocks of matrix elements to the \hat{L}^2 eigenspaces. At each level (or for each orbital added) partial configurations are listed, splitting the weight of the vertex into the sum of the weights for different configuration types. Each new type of configuration is obtained from the configurations of the upper level by adding orbitals with appropriate l values. In this way 25 types of atomic configurations are found. The total number of configurations calculated in

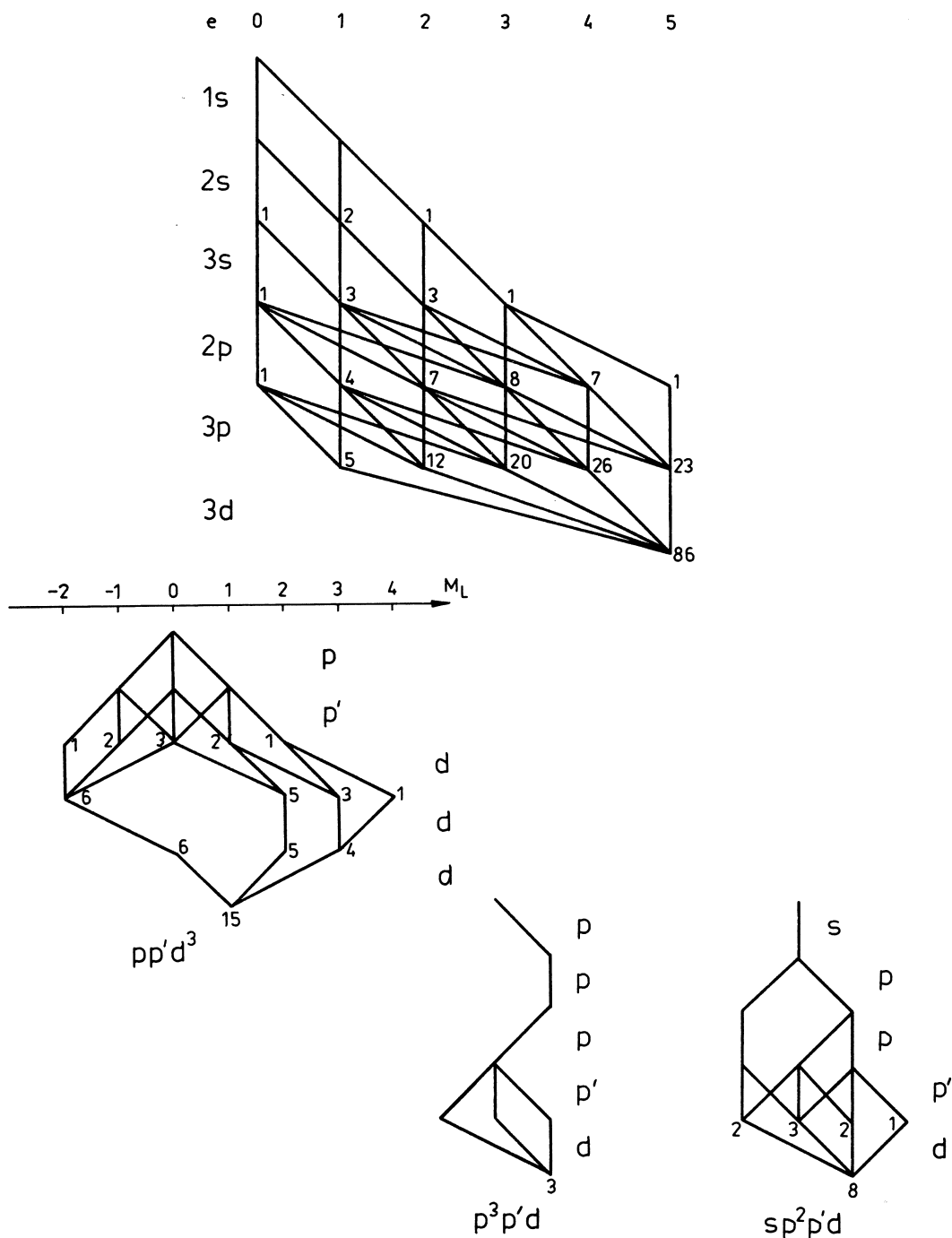


Fig 22. Representation of atomic configurations and a few examples of M_L -diagrams for classification of \hat{L}_z eigenstates associated with these configurations.

Example 3 is 83. The 3 configurations of the type $ss'3p^3$, included in the graph of Fig 22, are spurious for $M_L = 1$. In parenthesis the number of configurations belonging to each configuration type is given, and the number of states belonging to each configuration is given as a subscript, i.e. $sp^2d^2(6_5)$ means that 6 configurations of this type appear in Fig 22, each corresponding to 5 paths (functions) in Fig 21.

Example 3

| Orbital | N | Conf | Configuration types(number _{dimension}) |
|---------|-----|----------------|--|
| 1 s | 0 | 1 | – |
| | 1 | 1 | $s(1)$ |
| 2 s | 0 | 1 | – |
| | 1 | 2 | $s(2)$ |
| | 2 | 1 | $ss'(1)$ |
| 3 s | 0 | 1 | – |
| | 1 | 3 | $s(3)$ |
| | 2 | 3 | $ss'(3)$ |
| | 3 | 1 | $ss's''(1)$ |
| 2 p | 0 | 1 | – |
| | 1 | 4 | $s(3), p(1)$ |
| | 2 | 7 | $ss'(3), sp(3), p^2(1)$ |
| | 3 | 8 | $ss's''(1), ss'p(3), sp^2(3), p^3(1)$ |
| | 4 | 7 | $ss's''p(1), ss'p^2(3), sp^3(3)$ |
| 5 | 1 | $ss's''p^2(1)$ | |
| 3 p | 1 | 5 | $s(3), p(2)$ |
| | 2 | 12 | $ss'(3), sp(6), p^2(2), pp'(1)$ |
| | 3 | 20 | $ss's''(1), ss'p(6), sp^2(6), p^3(2), spp'(3), p^2p'(2)$ |
| | 4 | 26 | $ss's''p(2), ss'p^2(6), sp^3(6), ss'pp'(3), sp'p^2(6), p'p^3(2), p'^2p^2(1)$ |
| | 5 | 23 | $ss's''p^2(2), ss's''pp'(1), ss'p'p^2(6), sp'p^3(6), sp'^2p^2(3), p'^2p^3(2)$ |
| 3 d | 5 | 83 | $ss's''p^2(2_1), ss's''pp'(1_2), ss'p'p^2(6_2), sp'p^3(6_1), sp'^2p^2(3_2), p'^2p^3(2_1),$ $ss's''pd(2_3), ss'p^2d(6_3), sp^3d(6_1), ss'pp'd(3_8),$ $sp'p^2d(6_8), p'p^3d(2_3), p'^2p^2d(1_8),$ $ss's''d^2(1_2), ss'pd^2(6_5), sp^2d^2(6_5), p^3d^2(2_2), spp'd^2(3_{15}), p^2p'd^2(2_{15}),$ $ss'd^3(3_2), spd^3(6_5), p^2d^3(2_5), pp'd^3(1_{15}), sd^4(3_1), pd^4(2_3)$ |

The ordering of the states for each configuration type is obtained using small M_L -diagrams; although each type of configuration corresponds to a different M_L -diagram most of them are very simple, with one or two paths only (Example 3). Diagrams shown in Fig 22 as an example belong to the more complicated ones. It is important to note that they differ from the M-diagrams in Fig 9 because here equivalent electrons appear and spin $S = \frac{1}{2}N$ requires all orbitals inside l^r shell to be different. Therefore many paths are eliminated from these diagrams and the pictures should be drawn carefully to avoid false connections. For example, in a d^3 shell we may draw the lines in d_+, d_0, d_- , or d_0, d_-, d_+ or any other ordering, but they should contribute only once.

The paths of the M_L diagrams represent subspaces or fagots of functions differing by their spin components. The final classification is done with the help of a S–diagram (or M–diagram, if $(\hat{\mathbf{L}}_z, \hat{\mathbf{S}}_z)$ eigenspace is represented) and is straightforward. In the example considered here only one spin path is of course possible. We could reverse the order in which we split the subspaces into smaller subspaces by first connecting S–diagram with the fagot graph describing configurations and then treat S–diagram itself as a fagot graph. This multi–level fagot graph approach allows us to look at these aspects of the space structure description we are interested in. In particular it helps to circumvent some problems with the $\hat{\mathbf{L}}^2$ –adapted spaces.

As we see from section 1.5 and from this section $(\hat{\mathbf{L}}_z, \hat{\mathbf{S}}^2)$ eigenspaces may be represented in a variety of ways. Let us proceed now to the ambitious task of visualization of $(\hat{\mathbf{L}}^2, \hat{\mathbf{S}}^2)$ –adapted spaces.

1.8

$(\hat{\mathbf{L}}^2, \hat{\mathbf{S}}^2)$ -adapted graphs

Despite the great progress in application of group-theoretical methods to atomic spectroscopy (cf Biedenharn and Louck 1981) even such simple case like d^3 configuration structure is not fully understood (Judd 1979). The problem of atomic states classification, although clear from the point of view of group theory (Wybourne 1970), is not solved satisfactorily. The celebrated methods of Racah (1949) are not well-suited for large scale computations, especially when g or higher orbitals are used (Judd 1979). The unitary calculus of Harter and Petterson (1976) has also not solved the problem; although the authors claim that they have "a perfect labeling system", it is true only for $\hat{\mathbf{S}}^2$ eigenfunctions, where their favorite description using Weyl tableaux is sufficient, as we have seen in the previous sections. The problem is indeed that of labeling: to obtain a proper label ('proper' in the sense of carrying sufficient information about the construction of the labeled function to calculate arbitrary matrix elements) one should know genealogy of the function and derive a term of l^r configuration from those of l^{r-1} . Coefficients of fractional parentage, allowing for such a procedure, have unfortunately no closed form formulas, and the recursive relations (Redmond 1954) are complicated.

Let us take $p^r, r = 0, 1, \dots, 6$ configuration as the simplest example. There are $2(2l + 1) = 6$ spin orbitals; the space of r -particle functions build from these spin orbitals, designated $\mathcal{V}(p^r)$, has $\binom{2(2l+1)}{r} = \binom{6}{r}$ dimensions. In each $\mathcal{V}(p^r)$ space we may introduce a basis of $\hat{\mathbf{L}}^2$ and $\hat{\mathbf{S}}^2$ states, obtaining decomposition of $\mathcal{V}(p^r)$ into $\mathcal{V}(p^r, {}^{2S+1}L)$ subspaces. Thus $\mathcal{V}(p^1) = \mathcal{V}(p^1, {}^2P)$,

$$\text{for } r = 2: \mathcal{V}(p^2) = \mathcal{V}(p^2, {}^1S) \oplus \mathcal{V}(p^2, {}^3P) \oplus \mathcal{V}(p^2, {}^1D)$$

$$\text{for } r = 3: \mathcal{V}(p^3) = \mathcal{V}(p^3, {}^4S) \oplus \mathcal{V}(p^3, {}^2P) \oplus \mathcal{V}(p^3, {}^2D)$$

and the decomposition for p^4 and p^5 is like that for p^2 and p^1 . The important thing is that there is no simple relation between the decomposition of $\mathcal{V}(p^r)$ and $\mathcal{V}(p^{r-1})$.

The full burden of antisymmetrization in a pure l^r shell is absorbed by the angular and the spin momentum variables, making the whole situation so complicated. The number of subspaces a given $\mathcal{V}(l^r)$ space is decomposed to, or the number of terms ^{2S+1}L allowed, is equal to the number of paths in the (\hat{L}_z, \hat{S}_z) -adapted graph for $M_L = 0$ and $M_S = 0$ (if r is even) or $M_S = \frac{1}{2}$ (if r is odd). Figure 23 shows an example of a graph for $d^r, r \leq 5$, configurations. We may formally establish a one-to-one correspondence between each path in this graph and a subspace of $(2S + 1)(2L + 1)$ functions belonging to a given term ^{2S+1}L , but such a path does not give us a proper (i.e. useful) label.

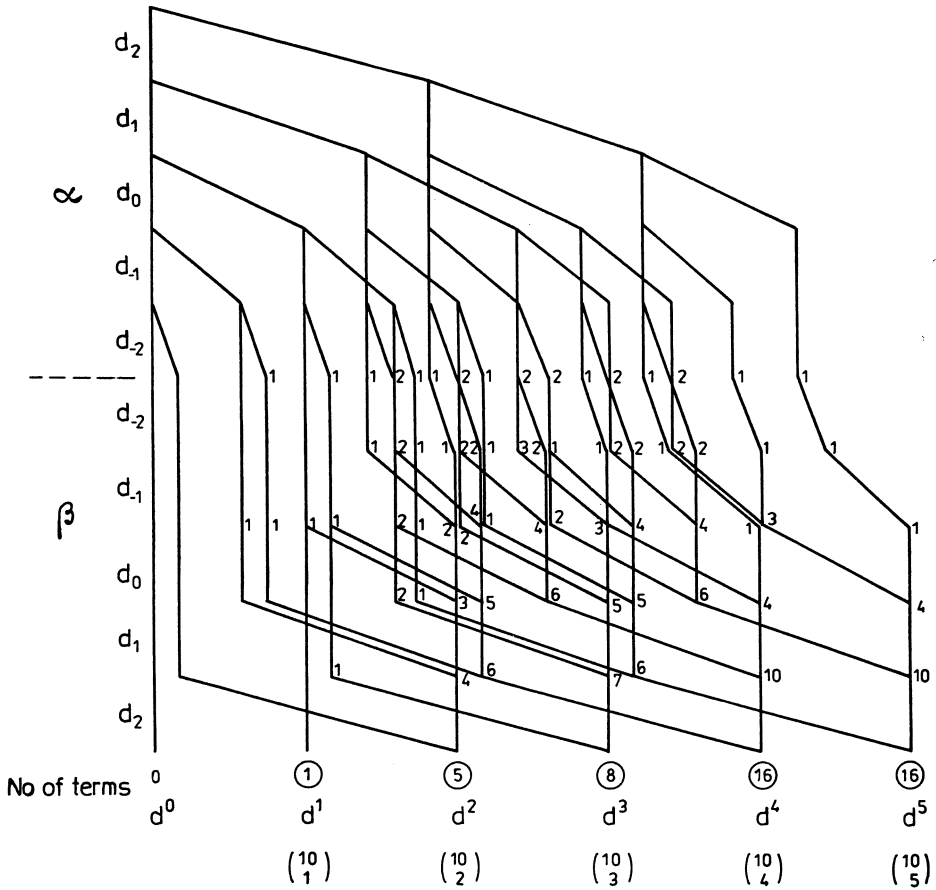


Fig 23. Representation of all $M_L = 0$ and $M_S = \frac{1}{2}$ states for d^r configurations, giving the number of different terms.

We may further split each tail vertex in Fig 23, drawing (\hat{L}_z, \hat{S}^2) -adapted graphs for $S = \frac{r}{2}, \frac{r}{2} - 1, \dots$ and even find the terms drawing a multiple-tail graph to find the number of states with $M_L \geq 0, M_S \geq 0$, and from these numbers derive the terms in a standard way (cf Weissbluth 1978). However, this does not solve the problem of labeling the individual eigenfunctions of (\hat{L}^2, \hat{S}^2) operators. While this problem remains open

I do hope that, if more convenient labels exist at all, it should be easier to find them using graphical techniques than using the algebraic ones.

Let us assume now that the terms of a pure configurations are known (as indeed is the case) and concentrate on the description of mixed configurations. As an example consider a manifold of terms coming from $(5d + 6s + 7s)^3$ configuration of *La I*, an example used by Wybourne (1980).

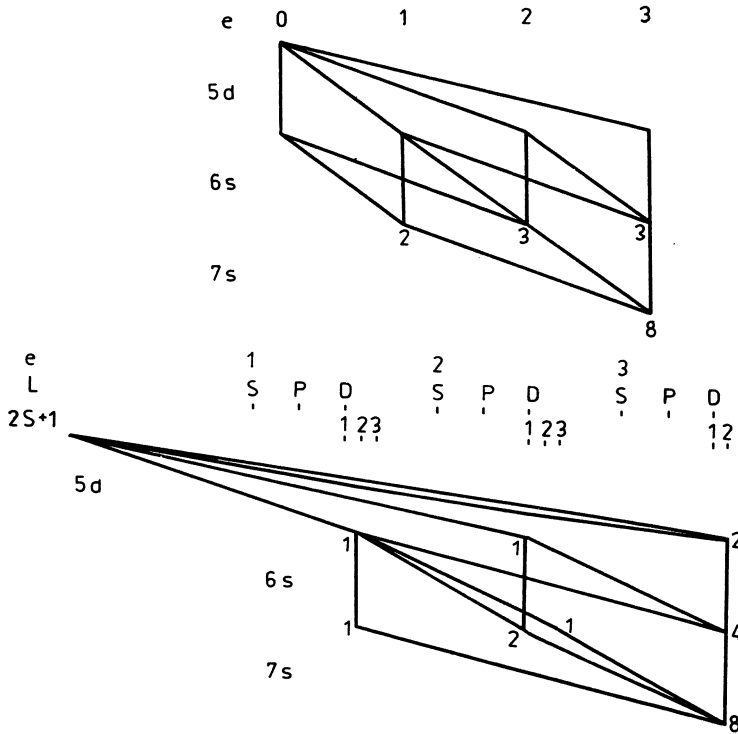


Fig 24. Configurations of the $(5d + 6s + 7s)^3$ space and 2D terms of this space.

Once we know d^1, d^2, d^3 terms we can immediately find all 29 terms belonging to this manifold. First, using configuration graph, Fig 24a, we identify 8 possible configurations, starting from $5d^3$, to $6s7s^2$, and then we couple spins and angular momenta for each configuration. In lexical order they are:

| Configuration | 5d | 6s | 7s | No. | Terms |
|---------------|----|----|----|-----|---------------------|
| 1 | 3 | 0 | 0 | 8 | ${}^2PD_2FGH {}^4P$ |
| 2 | 2 | 1 | 0 | 7 | ${}^2SPDFG {}^4PF$ |
| 3 | 1 | 2 | 0 | 1 | 2D |
| 4 | 2 | 0 | 1 | 7 | ${}^2SPDFG {}^4PF$ |
| 5 | 1 | 1 | 1 | 3 | ${}^2D_2, {}^4D$ |
| 6 | 2 | 2 | 1 | 1 | 2S |
| 7 | 1 | 0 | 2 | 1 | 2D |
| 8 | 0 | 1 | 2 | 1 | 2S |

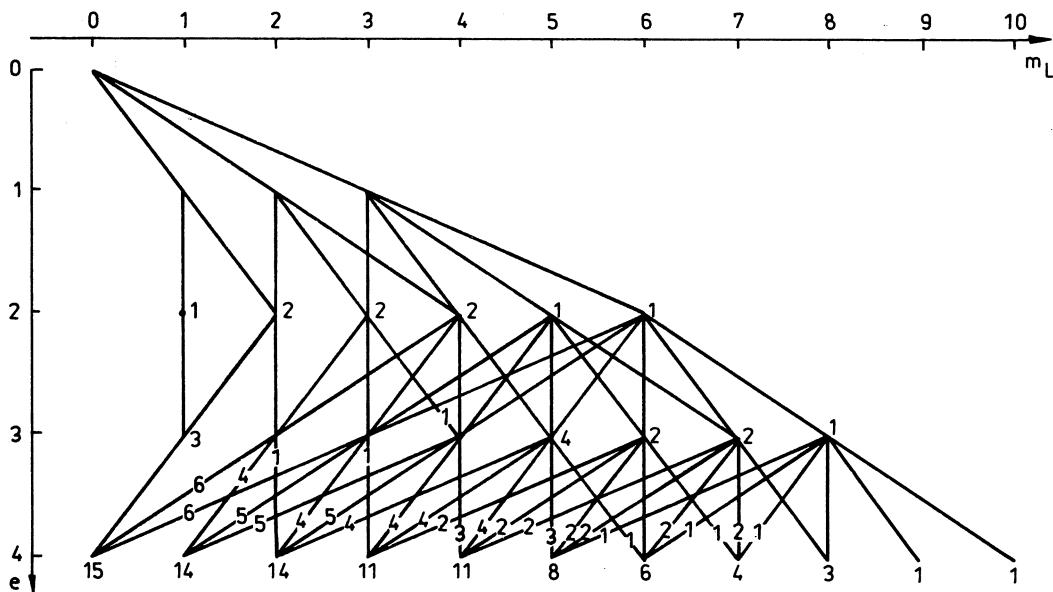


Fig 25. The tree of partitions for configuration f^4 .

Genealogy of the states also does not present any problems; Fig 24b shows for example 2D state that appears 8 times among the terms of $(5d + 6s + 7s)^3$ manifold. The first two 2D terms come from $5d^3$ configuration and differ only by seniority; they are represented by splitting the arc in the graph.

GT Full classification, giving different genealogy for the repeated terms, has to be based in this case on a chain of groups:

$$U(14) \supset Sp(14) \supset SU_2 \otimes (R_7 \rightarrow R_6 \rightarrow R_5 \rightarrow R_3)$$

as described by Wybourne (1970). The graphical approach presented here is much simpler and, for a description of large (\hat{L}^2, \hat{S}^2) -adapted spaces, more efficient. **GT**

Let us consider a more complicated example: 3 electrons in the space of $(4s + 4p + 4d + 4f + 5s + 5p + 5d)$ orbitals. In this space of 50 spin orbitals there are $\binom{50}{3} = 19\,600$ determinants. Introducing M_S as a good quantum number we have $\binom{25}{3} = 2300$ determinants with $M_S = \frac{3}{2}$ or $\binom{25}{2} \binom{25}{1} = 7500$ determinants with $M_S = \frac{1}{2}$. Each of the M_S labeled subspaces is further decomposed into the S -labeled subspaces: $S = \frac{3}{2}, M_S = \frac{3}{2}$ has 2300 (\hat{S}^2, \hat{S}_z) -adapted basis states, while $S = \frac{1}{2}, M_S = \frac{1}{2}$ has $7500 - 2300 = 5200$ states. Calculation of the dimensions of M_L -labeled subspaces is not so simple and requires summation over all partitions of M_L , as described in the previous sections. In Fig 25 a 'partition tree' is presented for the case of f^4 configuration, a diagram that enables systematic derivation of all partitions. Each valid partition corresponds to a convex path in this diagram, i.e. a path $[k_1 k_2 k_3]$ for which $k_1 \geq k_2 \geq k_3$. Using the partition tree it is easy to decompose complicated l^r configurations into all possible terms, as shown in Fig 25.

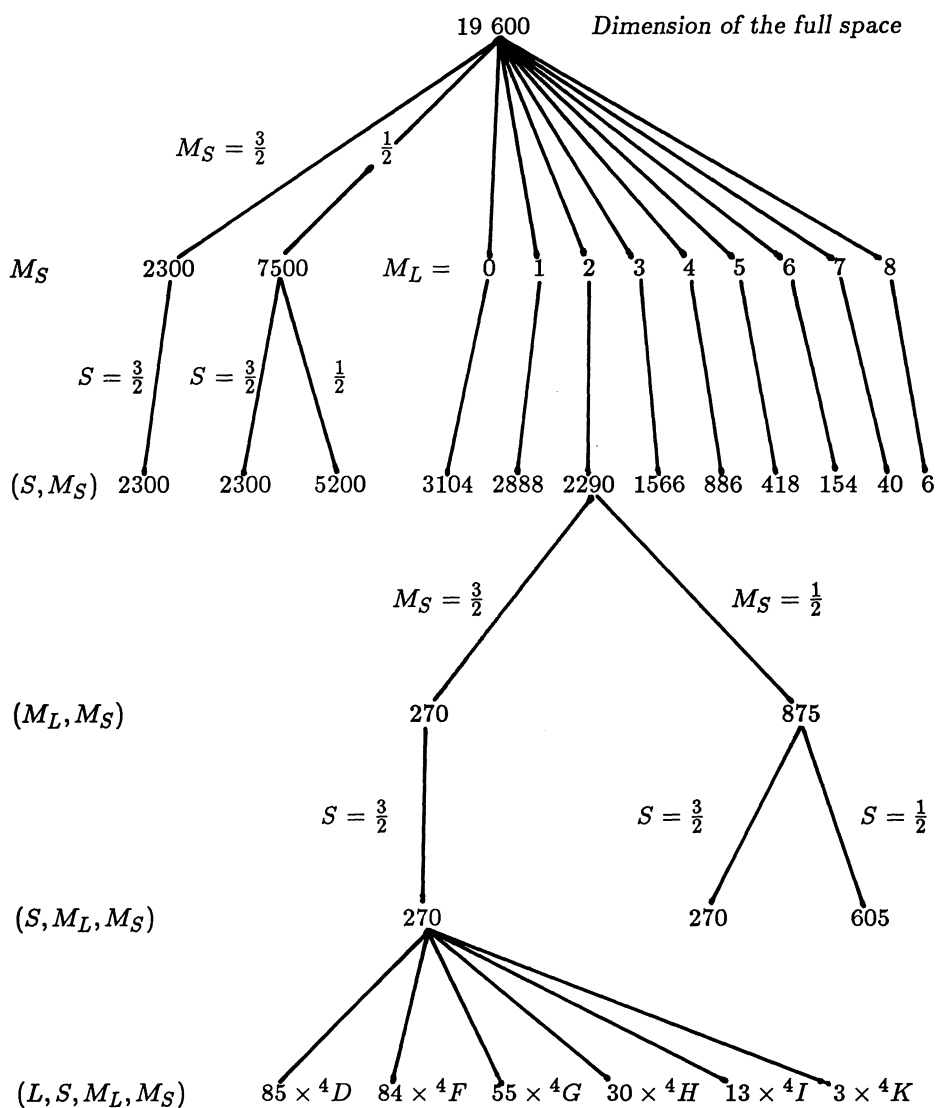
First we have to count the number of paths reaching (r, M_L) node. Because only convex paths are of interest it is not possible to assign unique weights to vertices but one can assign the number of convex paths that pass through a given arc as its weight. Assigning these weights we should also remember that at most 2 arcs of the same type may appear in one path. Among the paths reaching a given final node there are some with all arcs different, some with one pair of arcs of the same type (the arcs must come one after another), some with two pairs of arcs of the same type, ect. Let us denote by N_p the number of paths reaching the (r, M_L) node, so $N_0 + N_1 + N_2 \dots$ is the total number of path reaching this node. For example, in Fig 25 node $(4, 0)$ has $N_0 = 5$, $N_1 = 7$, $N_2 = 3$, as may be verified in the tree of partitions. These numbers are all that is needed to find the terms allowed for an arbitrary configuration.

The number of terms for a given L and $S = \frac{1}{2}r$, i.e terms $r^{+1}L$ of maximal multiplicity, must be equal to the number of paths N_0 (paths with all arcs or functions with all orbitals different) for $M_L = L$ minus the number N_0 for $M_L = L + 1$, because N_0 is the number of functions (determinants) with M_L and $M_S = r/2$. Total number of functions for $M_S = \frac{1}{2}r - 1$ is $N_1 + N_0 \binom{r}{1}$ but N_0 of these belong to $r^{+1}L$ terms, so there is $N_1 + N_0(r - 1)$ functions for $r^{-1}L$ terms. Because $L \geq M_L$ for which the N_k numbers are calculated to get the number of terms for a given L we have to subtract the total number of terms for $M_L = L$ and $M_L = L + 1$. Similarly for $M_S = \frac{1}{2}r - 2$ there are $N_2 + N_1 \binom{r-2}{1} + N_0 \binom{r}{2}$ functions with $N_1 + N_0 \binom{r}{1}$ functions belonging to higher multiplicities, i.e. $N_2 + N_1 \left[\binom{r-2}{1} - 1 \right] + N_0 \left[\binom{r}{2} - \binom{r}{1} \right]$ belonging to $r^{-3}L$ terms. Thus using Fig 25 the number of times the terms 5L are included in f^4 configuration is obtained calculating ΔN_0 , terms 3L calculating ΔQ_3 , $Q_3 = N_1 + 3N_0$ and terms 1L calculating ΔQ_1 , $Q_1 = N_2 + N_1 + 2N_0$. In practice the following table is set up:

| M_L | 0 | 1 | 2 | 3 | 4 | 5 | 6 | 7 | 8 | 9 | 10 |
|----------------------|-----|-----|-----|-----|-----|-----|-----|-----|-----|-----|-----|
| L | S | P | D | F | G | H | I | K | L | M | N |
| Total | 15 | 14 | 14 | 11 | 11 | 8 | 6 | 4 | 3 | 1 | 1 |
| N_0 | 5 | 4 | 4 | 3 | 2 | 1 | 1 | 0 | 0 | 0 | 0 |
| N_1 | 7 | 10 | 7 | 8 | 7 | 7 | 3 | 4 | 2 | 1 | 0 |
| N_2 | 3 | 0 | 3 | 0 | 2 | 0 | 2 | 0 | 1 | 0 | 1 |
| Q_3 | 22 | 22 | 19 | 17 | 13 | 10 | 6 | 4 | 2 | 1 | 0 |
| Q_1 | 20 | 18 | 18 | 14 | 13 | 9 | 7 | 4 | 3 | 1 | 1 |
| ${}^5L = \Delta N_0$ | 1 | 0 | 1 | 1 | 1 | 0 | 1 | 0 | 0 | 0 | 0 |
| ${}^3L = \Delta Q_3$ | 0 | 3 | 2 | 4 | 3 | 4 | 2 | 2 | 1 | 1 | 0 |
| ${}^1L = \Delta Q_1$ | 2 | 0 | 4 | 1 | 4 | 2 | 3 | 1 | 2 | 0 | 1 |

giving in the last three lines the terms for f^4 : 5SDFGI , 3P_3D_2F_4G_3H_4I_2K_2LM , and 1S_2D_4FG_4H_2I_3KL_2N . The same partition tree may be used for f^3 configuration. When the terms for pure configurations are known it is then easy to decompose spaces for complicated mixed configurations into different subspaces labeled by L, S, M_L, M_S quantum numbers. To see how rapidly the dimensions of various subspaces are reduced decomposition of $(4s + 4p + 4d + 4f + 5s + 5p + 5d)^3$ space is made as an example (Example 4). Let us take now one of the (\hat{L}^2, \hat{S}^2) -adapted subspaces, for example the 4D space, and represent the 85 terms of this space by (\hat{L}^2, \hat{S}^2) -adapted graph.

Example 4: Decomposition of $(4s + 4p + 4d + 4f + 5s + 5p + 5d)^3$ space into (L, S, M_L, M_S) -labeled subspaces.



One may understand the graph in Fig 26 as a fagot graph, each path representing all $(2S+1)(2L+1)$ functions differing by M_L and M_S , or as a non-fagot graph, representing paths with fixed M_L, M_S . In Fig 26 the levels corresponding to orbitals other than s -type are doubled. This leaves enough space to represent the splitting of pure l^r shells: an artificial vertex, lying off the level, is introduced in this case to represent intermediate couplings in pure configurations. For example, $4f4d^2$ configuration gives rise to 2 terms

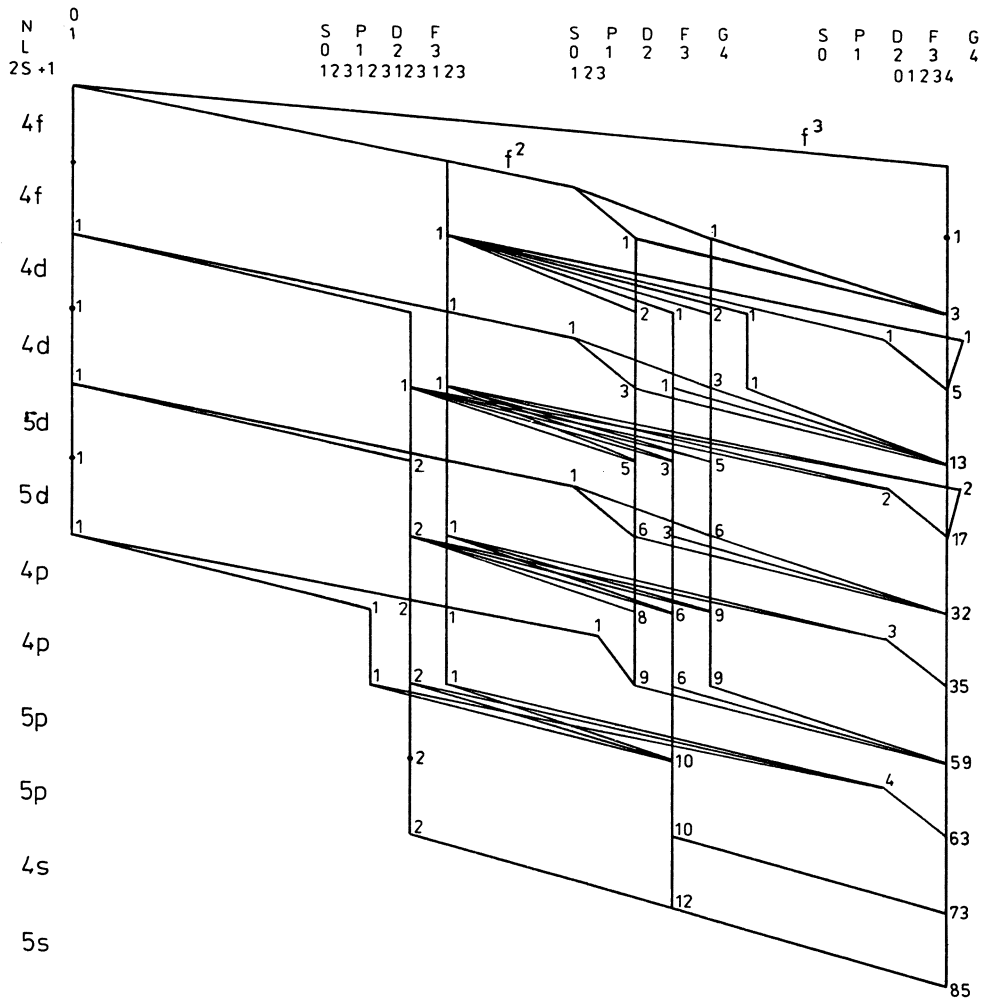


Fig 26. (\hat{L}^2, \hat{S}^2) -adapted space for 4D terms of $(4s + 4p + 4d + 4f + 5s + 5p + 5d)^3$ manifold.

4D , differing only by d^2 coupling.

Although the problem of atomic states representation can not be considered completely solved due to the troubles with equivalent electrons, it is clear that the graphical representation should be useful also in this case. I will discuss one more type of angular momentum coupling here because of its importance in nuclear shell-model calculations.

1.9

(\hat{J}^2, \hat{T}^2) -adapted graphs

The eigenspace of the total angular and spin momentum operator \hat{J}^2 in the $j - j$ coupling and of the isospin operator \hat{T}^2 is the most appropriate for calculation of the nuclear properties. Due to the nature of nuclear forces solutions of nuclear equations are sought in full many-particle spaces built from primitive functions, called in context of nuclear shell-model calculations 'orbits', that are almost always taken as harmonic oscillator functions (cf Wong 1981; Brussaard and Glaudemans 1977). The full spaces have very high dimensions and therefore shell-model calculations in nuclear physics are concentrated mainly in the sd shell, with only a modest studies of other shells (McGrory and Wildenthal 1980). A program determining the dimensionalities of such model spaces has recently been published (Draayer and Valdes 1985). Calculation of matrix elements in (\hat{J}^2, \hat{T}^2) -adapted space is not simple, therefore computer programs performing calculations of nuclear structure work frequently in the 'M-scheme' or determinantal spaces where calculation of matrix elements is simpler but the dimension of the space is much bigger (Duch 1986b).

The isospin operator \hat{T}^2 for a fermion doublet may be treated in the same way as the total spin operator \hat{S}^2 . The problems arising with visualization of \hat{J}^2 eigenfunctions are similar to those of the previous section: couplings in the pure shells do not give a simple genealogy. Provided that the states arising from pure shells are known (for example from tables given in Hammermesh 1962) the graphs are still useful, showing genealogy of the states of mixed configurations.

As an example Fig 27 shows the often used basis $(d_{\frac{5}{2}} + s_{\frac{1}{2}} + d_{\frac{3}{2}})$ for the case of 2 neutrons and 2 protons, with the four-particle states coupled to $J = 2$, $T = 0$. The graph is complicated because each vertex is characterized by the number of particles plus intermediate J and T values. To make the graph more legible the T values are

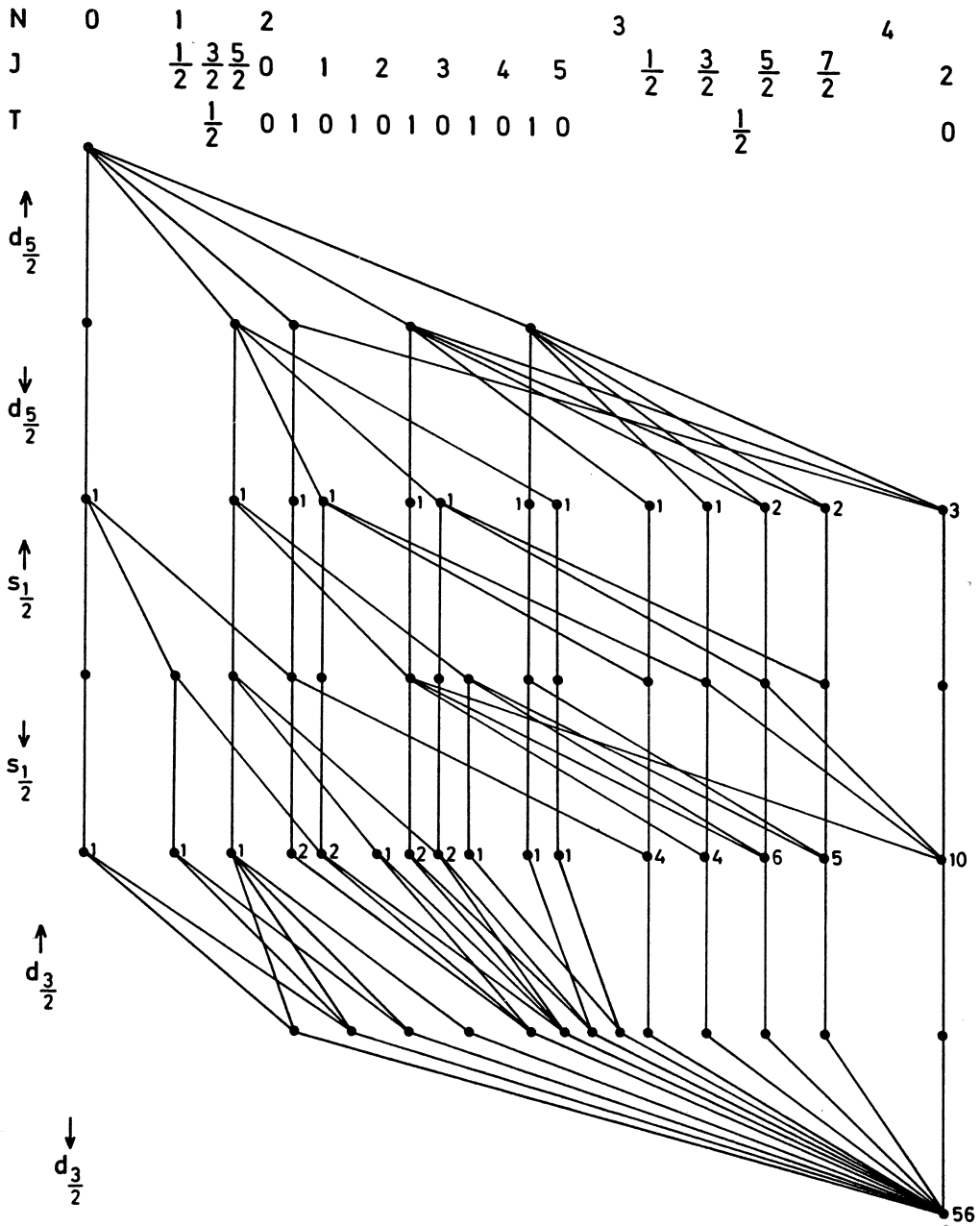


Fig 27. (\hat{J}^2, \hat{T}^2) -adapted space of $J = 2, T = 0$ states of two neutrons and two protons in $(d_{5/2} + s_{1/2} + d_{3/2})$ basis.

shown only for $N = 2$, because T for $N = 1$ and $N = 3$ has only one value ($T = \frac{1}{2}$). The labeling of the $\hat{\mathbf{J}}^2$ eigenfunctions always presents a problem in traditional schemes; graphical labeling, showing the whole genealogy, could make all redundancy labels spurious. Unfortunately it would also make the graph much more complicated.

The paths in Fig 27 do not give proper labels of the states they represent because no attempt has been made to present the parentage within the equivalent groups of particles, therefore only the mixed groups have proper genealogy. In case when ambiguity could arise different intermediate couplings, arising for mixed configurations, are shown in the middle of a level to give genealogy of the states. To obtain proper labels a supplementary graphs showing the couplings within equivalent configurations ($s_{\frac{1}{2}}^r, d_{\frac{3}{2}}^r, d_{\frac{5}{2}}^r$, $r = 2, 3, 4$ in this case) are needed. Because these type of graphs are quite complicated, to simplify the analysis of the corresponding spaces we can use a fagot graph approach: draw a graph of configurations (there are only 14 in this case) and then resolve separately each subspace corresponding to a configuration into $(\hat{\mathbf{J}}^2, \hat{\mathbf{T}}^2)$ -eigenstate graphs, similarly as it was done in the previous section.

The $(\hat{\mathbf{J}}^2, \hat{\mathbf{T}}^2)$ -adapted graph is the most complicated structure presented in this book. Let us turn now to a slightly simpler problems.

1.10

Spatial symmetry in the graph

So far the spaces we have described were invariant under the action of one or two operators. Description of molecules or crystals requires the adaptation of many-electron functions to a certain representation Γ of a point group G (cf Hammermesh 1962; Hochstrasser 1966; Bunker 1980). In this case we do not have a single operator but a whole set of group operators to deal with. The situation is simplified very much if the 'basic building bricks', i.e. one-electron states, are symmetrized orbitals. The problem of choosing the Γ -adapted subspace is then reduced to the selection of orbital products, such that the desired representation Γ is included in the product of representations for each symmetry orbital, i.e.

$$\Gamma \subset \gamma_1 \times \gamma_2 \times \dots \times \gamma_N$$

where γ_i characterizes the symmetry of ϕ_i orbital. This problem will be solved now using graphical techniques. Elementary group theory used in this section does not deserve the use of my **GT** sign.

Representations of the point groups are either non-degenerate (designated A and B), doubly degenerate (designated E) or triply degenerated (designated F or T). As a first step we must know the multiplication rules of these representations. The rules can be found in a standard way (cf Hammermesh 1962 or tables in Herzberg 1966); it is possible to determine the result of multiplication of the representation symbols A, B, E, F , of the subscripts $1, 2, g, u$, and superscripts $^1, ^2$ separately:

| | |
|---------------|--|
| subscripts: | $1 \times 1 = 2 \times 2 = 1; 1 \times 2$ |
| superscript: | $g \times g = u \times u = 1; g \times u = u$ |
| main symbols: | $A \times \Gamma = \Gamma; \Gamma = A, B, E, F$ |
| | $B \times B = A; B \times E = E, B \times F = F$ |

in D_{2d} and $C_4, D_4, S_4, C_{4h}, C_{4v}, D_{4h}$:

$$E \times E = A_1 + A_2 + B_1 + B_2$$

in other groups: $E_1 \times E_1 = E_2 \times E_2 = A_1 + A_2 + E_2$

$$E_1 \times E_2 = B_1 + B_2 + E_1 \quad (1.18)$$

$$E \times F_1 = E \times F_2 = F_1 + F_2$$

$$F_1 \times F_1 = F_2 \times F_2 = A_1 + E + F_1 + F_2$$

$$F_1 \times F_2 = A_2 + E + F_1 + F_2$$

In case of degenerate representations we have to distinguish two cases: multiplication of two different orbitals corresponding to the same degenerate representation or multiplication of one degenerate orbital by itself. In the first case the corresponding spin function for the two orbitals is either singlet or triplet; thus resolving $E \times E$ product we have to include:

$$E \times E \longrightarrow {}^1A_1, {}^1A_2, {}^1E, {}^3A_1, {}^3A_2, {}^3E \quad (1.19)$$

However, if the two functions are identical the situation is not so simple: it is analogous to the case of equivalent electrons in atoms. We can not separate the problem of spin and space functions inside the equivalent group of electrons. The states allowed are found in an elegant way using the concept of a symmetric and antisymmetric product of representations (cf Landau and Lifshitz 1974). Because in many standard books this subject is not mentioned (for example, it is well hidden in such monographs like Watanabe 1966) an example should be helpful.

Let us consider the 24 element T_d group. Its character table is:

| | \mathcal{E} | $8C_3$ | $3C_2$ | $6\sigma_d$ | $6S_4$ |
|-------|---------------|--------|--------|-------------|--------|
| A_1 | 1 | 1 | 1 | 1 | 1 |
| A_2 | 1 | 1 | 1 | -1 | -1 |
| E | 2 | -1 | 2 | 0 | 0 |
| F_1 | 3 | 0 | -1 | -1 | 1 |
| F_2 | 3 | 0 | -1 | 1 | -1 |

Multiplication rules give in this case:

$$A_1 \times \Gamma = \Gamma; A_2 \times A_2 = A_1; A_2 \times E = E; A_2 \times F_1 = F_2; A_2 \times F_2 = F_1$$

$$E \times E = A_1 + A_2 + E; E \times F_1 = E \times F_2 = F_1 + F_2 \quad (1.20)$$

$$F_1 \times F_1 = F_2 \times F_2 = A_1 + E + F_1 + F_2; F_1 \times F_2 = A_2 + E + F_1 + F_2$$

To find E^2 , F^2 and F^3 let us write the characters of the antisymmetric representation. For the antisymmetric product $\{E^2\}$ and $\{F^2\}$ the character formula is:

$$\chi_2(R) = \frac{1}{2}\{\chi(R)^2 - \chi(R^2)\} \quad (1.21)$$

and for $\{F^3\}$

$$\chi_3(R) = \frac{1}{6}\{\chi(R)^3 + 2\chi(R^3) - 3\chi(R)\chi(R^2)\} \quad (1.22)$$

Writing down the characters for $\chi_\Gamma(R)$ we obtain a table:

| $\Gamma \setminus R$ | \mathcal{E} | $8C_3$ | $3C_2$ | $6\sigma_d$ | $6S_4$ |
|----------------------|---------------|--------|--------|-------------|--------|
| $\{E^2\}$ | 1 | 1 | 1 | -1 | -1 |
| $\{F_1^2\}$ | 3 | 0 | -1 | -1 | 1 |
| $\{F_2^2\}$ | 3 | 0 | -1 | -1 | 1 |
| $\{F_1^3\}$ | 1 | 1 | 1 | 1 | 1 |
| $\{F_2^3\}$ | 1 | 1 | 1 | -1 | -1 |

Using character tables and the formula for the multiplicity $a(\Gamma_i)$ of representation Γ_i in the (reducible) product representation,

$$a(\Gamma_i) = \frac{1}{24} \sum_R \chi_\Gamma(R) \chi_{\Gamma_i}(R) \quad (1.23)$$

we obtain

$$\{E^2\} = {}^3A_2; \{F_1^2\} = \{F_2^2\} = {}^3F_1; \{F_1^3\} = {}^4A_1; \{F_2^3\} = {}^4A_2 \quad (1.24)$$

and hence

$$E^2 = {}^3A_2 + {}^1A_1 + {}^1E; F_1^2 = F_2^2 = {}^3F_1 + {}^1A_1 + {}^1E + {}^1F_2 \quad (1.25)$$

The decomposition of F_k^3 is slightly more complicated and may be taken from Herzberg (1966, p 333) or computed using character formulas given by Goscinsky and Öhrn (1968)

$$F_1^3 = {}^4A_1 + {}^2E + {}^2F_1 + {}^2F_2; F_2^3 = {}^4A_2 + {}^2E + {}^2F_1 + {}^2F_2 \quad (1.26)$$

Now we are ready to draw graphs. Let us take a very small basis set $(e + f_1)$, i.e. the one-particle space has 5 orbitals. For 4 electrons the total number of determinants is $\binom{10}{4} = 210$. These determinants are immediately divided into sets differing by M_S values and one-dimensional representation labels. The group T_d has C_{2v} as its subgroup

slightly and work with a subgroup instead of a full group. In our case we will simply split each vertex in the two, three or four-slope graphs into different symmetry species. Fig 27a represents all $M_S = 0$ determinants for A_1, A_2, B_1, B_2 symmetries, while Fig 28b shows configurations only. The space of 15 configurations corresponding to 28 determinants of A_1 symmetry is decomposed further into $2^5 A_1, 9^3 A_1$ and $17^1 A_1$ eigenfunctions of \hat{S}^2 operator.

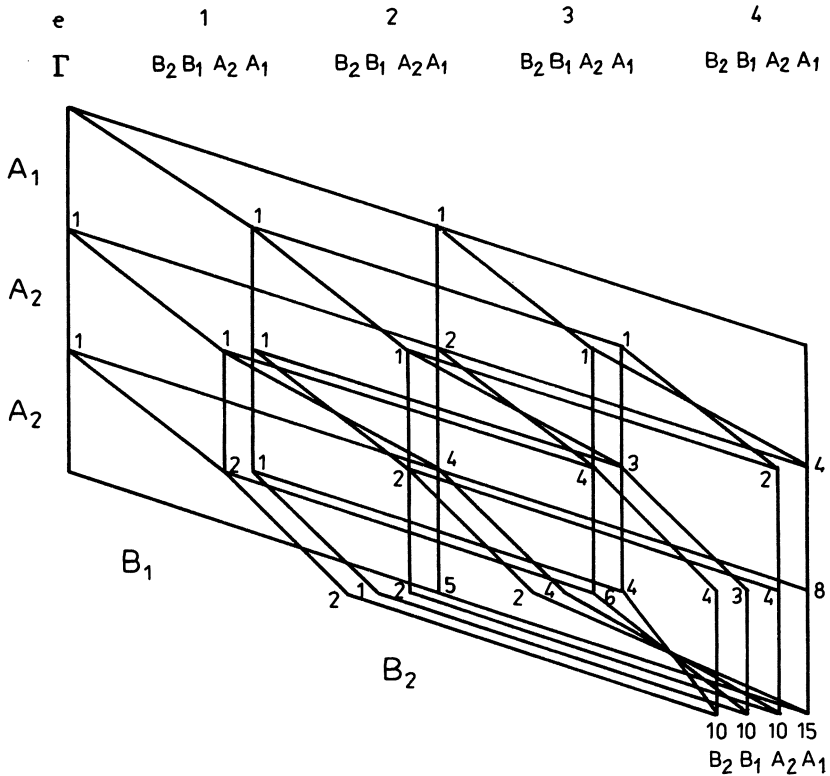


Fig 28b. Configurations adapted to the four representations of C_{2v} group.

In the full T_d group we have only 5 possible configurations in $(e + f_1)$ basis: $e^4, e^3 f_1, e^2 f_1^2, e f_1^3$ and f_1^4 . Each configuration represents a linear subspace invariant in respect to symmetry operators of the point group and of the \hat{S}^2 operator. Using the multiplication rules Eq (1.20) we obtain the following states:

$$\begin{aligned}
 (e + f_1)^4 \rightarrow & \quad {}^5 E + {}^5 F_2 + {}^3 A_1 + 2^3 A_2 + 3^3 E + 7^3 F_1 + 5^3 F_2 + \\
 & \quad 5^1 A_1 + 2^1 A_2 + 5^1 E + 4^1 F_1 + 7^1 F_2
 \end{aligned}
 \tag{1.28}$$

To see genealogy let us represent all the states arising from $e^2 f_1^2$ configuration; decomposition of the other configurations is much simpler. Formally this means that we use

a fagot graph approach, but we may skip the drawing of the graph for 5 configurations. In C_{2v} this configuration gives rise to the following states:

$$e^2 f_1^2 \xrightarrow{C_{2v}} {}^5A_1 + {}^5B_1 + {}^5B_2 + 3{}^3A_1 + 5{}^3A_2 + 5{}^3B_1 + 5{}^3B_2 + \\ 8{}^1A_1 + 5{}^1A_2 + 4{}^1B_1 + 4{}^1B_2 \quad (1.29)$$

while in T_d it gives rise to the states shown in Fig 29a. The same example was discussed by Buenker and Peyerimhoff (1968), but diagonalization of \hat{C}_3 rotation operator in the basis of (\hat{S}_z, C_{2v}) -adapted determinants, advocated in their paper, does not give us genealogy of the states. In Fig 29b the 11^1A_1 states arising from $e^2 f_1^2 f_2^2$ configurations are presented. These states are listed explicitly, using Gelfand symbols, in a paper by Rettrup, Sarma and Dahl (1982), but their method does not give genealogy of the states either. Therefore graphical representation is a useful complement to the above mentioned methods, besides being interesting in its own rights.

The example described above shows how much the original space of 210 determinants is reduced when the symmetry is used. While for the groups with one-dimensional representations only the situation is satisfactory (compare also the graphs in Section 1.12), degenerate representations create similar problems as the equivalent electrons in atomic shells. Graphical representation of such states (Fig 29) does not give us the information about the genealogy inside partially filled degenerate orbitals, and thus is not a satisfactory labeling scheme. The problem of equivalent electrons has not found so far elegant algebraic solution; again, it is my hope that further work on the graphical labeling will eventually help if not to solve then at least to circumvent the problem.

1.11

Visualization of restricted model spaces

In the previous sections I have discussed how to visualize spaces adapted to various operators and spatial point group symmetries. All eigenfunctions of the desired operators and of the desired symmetry that can be built from a set of given one-particle states were taken as the bases of model spaces. Symmetry was thus the only selection criterium employed so far. For practical purposes this is usually not sufficient: full symmetry-adapted many-particle space grows very rapidly with the number of primitive states and although the graphs can always be drawn and their general properties analyzed for practical calculations the dimension of the full space becomes quickly too large to handle even for the best computers. The traditional way of reducing the size of a model space is based on the concept of reference states. Coulomb forces are rather weak, therefore in atomic and molecular problems the independent-particle approximation works rather well and it is possible to choose the one-particle states in such a way, that among all many-particle symmetry-adapted states there is one state or a combination of a few states clearly dominating the exact solution. In such cases one may argue that the model space with a basis composed of these few states (called 'the reference states' or simply 'references') plus the states that are 'not far' from them allow to form a very good approximation to the exact state (wave function) of our system. 'Not far' usually means configurations built from almost the same orbitals as the references are, with at most one or two orbitals changed. Matrix elements of a two-particle operator between the reference and the singly or doubly substituted states are in general different from zero, justifying the choice of these states to our model space by their contributions in the second-order perturbation theory.

The reference states form a basis of a zeroth-order space. We can systematically enlarge this space by taking single, double, ... up to N -tuple excited states that together cover the whole space. Further restrictions would involve selection of individual

states from, say MRSD (multi-reference + singly and doubly excited configurations) space using one of the general perturbation-theory based selection schemes (cf Shavitt 1977b), or more global selection, for example taking the MRSD subspace of \hat{S}^2 -adapted states interacting through the Hamiltonian with the reference functions, the subspace called the first-order interaction space (FOIS) by McLean and Liu (1973). Graphical visualization of such restricted subspaces is very important for practical applications. In this and in the next section I will use the three-slope $\mathcal{G}_3(n : N)$ graphs in the examples. These graphs are relatively simple and have a wide range of applications; the reader may try to draw other kinds of restricted graphs in an analogous way.

Let us start from the single-reference cases. In Fig 30 we see 3 graphs describing spaces created by excitations from one reference configuration of the closed-shell type, i.e. involving no singles. The first of these graphs shows a singly excited space. The reference configuration is drawn with a solid line; the simple shape is achieved thanks to reordering of the orbitals that are doubly occupied in the reference so that they appear at the top of the graph. This graph has two distinct parts: the upper part, at the levels of doubly occupied orbitals in the reference, called the \mathcal{D} -part and the lower part, at the levels of unoccupied or external orbitals, called the \mathcal{E} -part. Adding more electrons makes the \mathcal{D} -part longer, more orbitals increases the \mathcal{E} -part, but the simple structure of the graph is not changed. If the states corresponding to the reference configurations are dominant in the exact solution (e.g. if Hartree-Fock configuration is taken as the reference) the intuitive notion of important configurations as lying near the reference is well reflected in the graph, because all singly and doubly excited configurations are near the reference one. At each level of the \mathcal{D} -part the separation between a given path and the reference path, i.e. the difference between the total occupations (at this level) of the two paths, gives the excitation level of that path. The vertices at the lowest level of the \mathcal{D} -part (or highest level of the \mathcal{E} -part) are named V for references (zero excited), S for singly excited, D for doubly excited, ect.

In the second graph of Fig 30 we see visualization of SD , or singly and doubly excited, space of configurations, and in the next graph also quadruply excited, but not triply excited, configurations are included. The structure of SD one reference spaces is so simple that explicit description of this space without graphical representation is rather easy. The SDQ graph has more complicated structure. We can draw this graph in two ways: by expanding the SD graph, or by reducing the full graph, in this case by removing $v(3,0)$, $v(3,1)$ and $v(3,3)$ vertices of the third level. In general one may achieve quite flexible choice of the basis states by removing individual vertices or removing individual arcs from the graph (in the next section I will try to show how to couple this with physical intuitions). For example, we may allow only pair excitations from specific orbitals by removing singly occupied arcs at the corresponding levels. In some ways the graphical methods of description may be more convenient than the strict excitation level criteria. However, in multi-reference or open-shell cases the natural restrictions from graphical point of view do not correspond exactly to the selection by

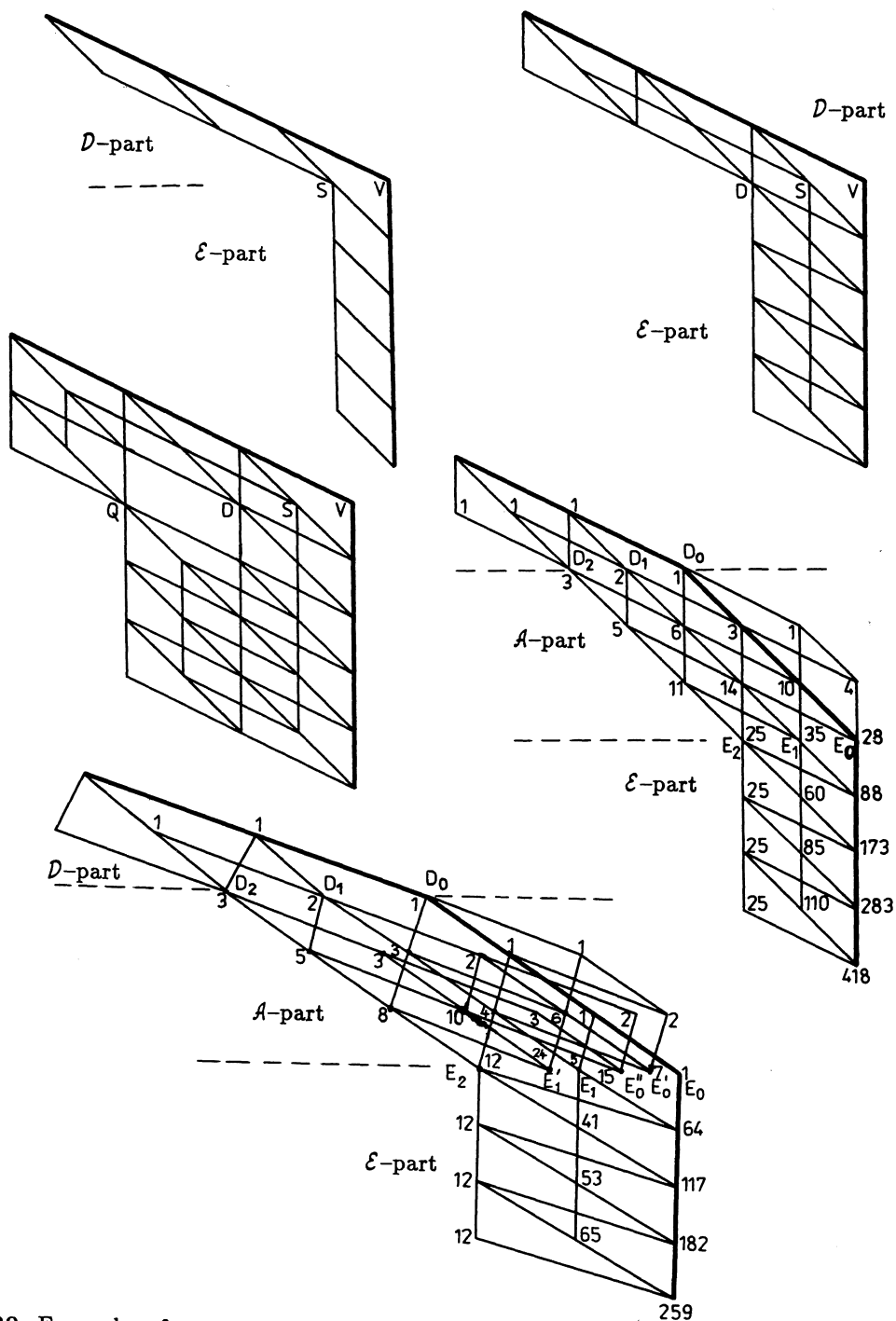


Fig 30. Examples of restricted model spaces: closed-shell reference states and S , SD , SDQ spaces, open shell reference and SD plus some higher excited configurations, and the exact SD space for open shell reference state.

the excitation level. In Fig 30 we see a graph representing single and double excitations out of a reference configuration containing 3 open shells. The levels corresponding to these singly occupied orbitals, or more generally, the levels corresponding to orbitals that are less than doubly occupied in the references, define a more complex part of the graph called the \mathcal{A} -part or the active part. The \mathcal{D} -part plus the \mathcal{A} -part is called the \mathcal{I} -part or the internal part. These names are adopted from the unitary group approach (cf Shavitt 1983) terminology, where they are used in connection with the Shavitt's graph. The \mathcal{D} -part and \mathcal{E} -part have still their simple structure: the \mathcal{D} -part has 3 vertices at the lowest level, called here (Fig 30) D_2, D_1, D_0 for doubly, singly and zero-excited configurations, and the \mathcal{E} -part at the highest level has also 3 vertices, called E_2, E_1 and E_0 for 2, 1, 0 electrons in the external part.

The \mathcal{A} -part contains some paths that are more than doubly excited, for example D_2 and E_2 vertices should be joined only by one path, parallel to the reference one, other paths corresponding to triply excited configurations. One may remove the unwanted paths introducing the excitation level as the additional classification number, i.e. a vertex in the three-slope graph would have the level, number of particles and excitation level as its coordinates. If the vertices differing only on the excitation level are near each other the slopes of arcs are only slightly changed and the vertices are 'splitted'. An example of such graph with splitted vertices is given in Fig 30 (last graph). Configurations that are more than doubly excited were removed from the \mathcal{A} -part. Instead of 28 path reaching E_0 vertex 1 reference path (zero-excited, E_0), 7 singly excited paths (E'_0 vertex) and 15 doubly excited paths (E''_0 vertex) are left; 5 paths were removed. Similarly E_1 vertex is also splitted into singly (E_1) and doubly excited version (E'_1) with 6 higher-excited paths removed. Of course 5 paths reaching E_1 vertex and 24 paths reaching E'_1 vertex should be complemented by the same external part. The E_2 vertex has not been splitted because all paths reaching it are doubly excited. Limitation of the excitation level strictly to single and double excitations has reduced the number of paths for the graph with 3 open shells in the reference path from 418 to 259. This large difference is caused primarily by the 13 triply excited paths reaching the E_2 vertex that were removed in the last graph. One may argue that these triply excited configurations are next in importance to the doubly excited ones, but if the \mathcal{E} -part is large practical limitations may force us to remove them from the model space. However, the large number of vertices and arcs appearing in the graphs with splitted vertices make these graphs considerably less legible; moreover they are hard to draw in the multi-reference cases. Therefore it is better to leave the graph unchanged and remove the unwanted paths from the \mathcal{A} -part when the graph is represented in a computer. A simple way of such selection is described in section 1.14.

The active part may also be placed at the top of the graph, as shown in Fig 31, where a 3-reference SD graphs are presented. It is clear that the number of paths in such a graph is greater than the number of paths in a graph with the \mathcal{A} -part in the middle, but, as was first shown in the context of Shavitt's graph (Brooks and Schaefer

1979) and is also true for the three-slope graphs (Duch 1985a), the number of interacting states may actually become lower. This special case occurs in \hat{S}^2 -adapted spaces when only the functions belonging to FOIS are required (Shavitt 1981; Duch and Karwowski 1985). Because the \mathcal{D} -part and the \mathcal{E} -part have always the same structure one can concentrate on the complexity of the \mathcal{A} -part. With the active part at the top the \mathcal{D} -part is broader but can be still conveniently analysed when it comes to calculation of matrix elements. Controlling the level of excitation is also easy: for example, in Fig 31 all paths reaching A_2 vertex are doubly excited and, if single and double excitations only are allowed, these paths must continue to the E_0 vertex.

In the next section I will show some more ways of restricting the full model spaces and introducing abelian symmetry into the graphs.

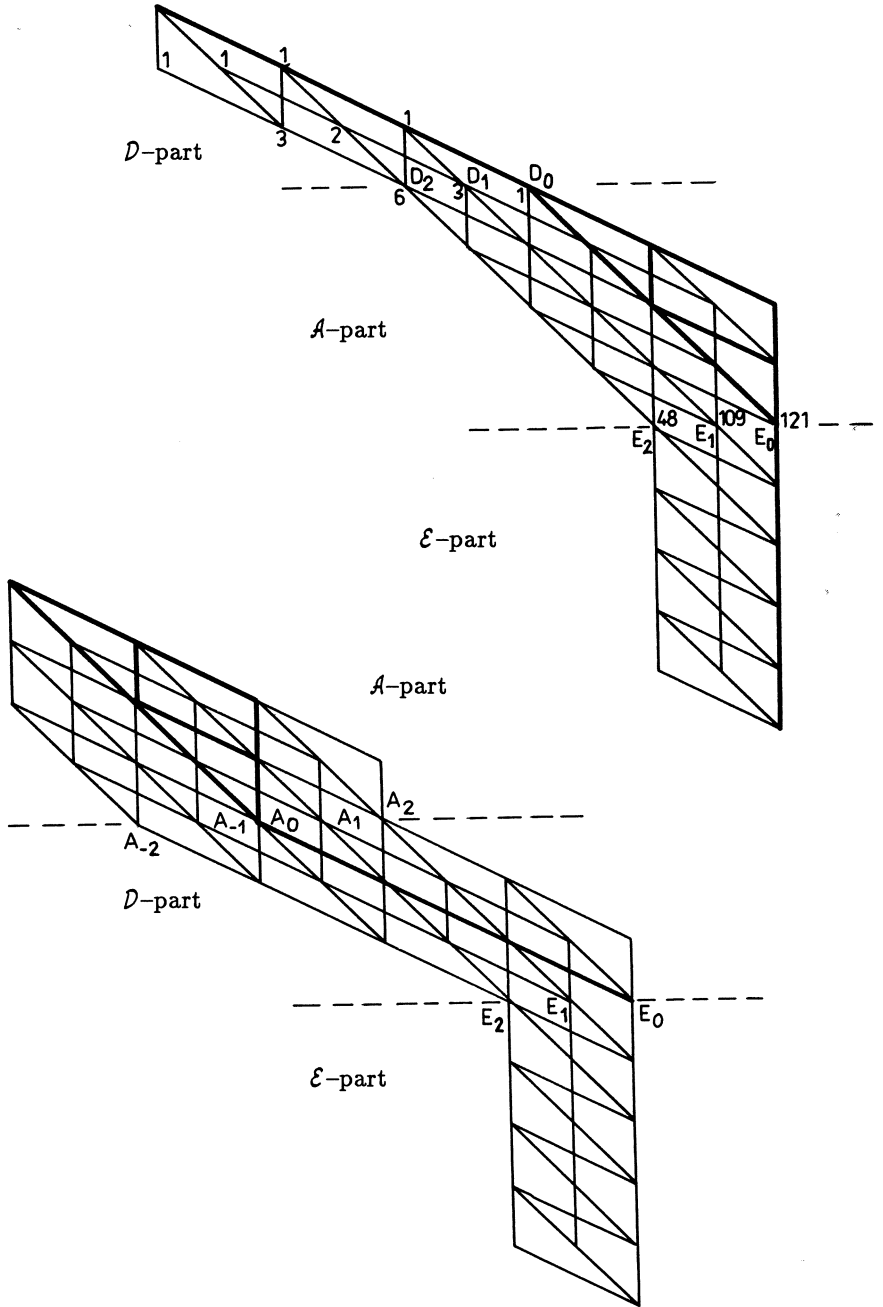


Fig 31. Representation of the singly and doubly excited configurations out of 3 references: active part in the middle or in the top.

1.12

Physical intuitions and graphs

The shape of the graph is not uniquely defined, depending on the ordering of graph's levels. Nevertheless one may try to visualize and compare different approximations using corresponding graphs. In recent years development of computer programs and computer hardware has allowed to solve Schrödinger equation exactly for several molecules in rather large full model spaces. I will discuss here benchmark calculations on water in double-zeta basis (Saxe *et al* 1981; Harrison and Handy 1983). The 10 electrons of water distributed among 14 orbitals of double zeta basis give rise to 270 270 orbital configurations, as shown in Fig 32, corresponding to 1 002 001 singlet states of the full space. Taking into account spatial symmetry leaves 256 473 A_1 symmetry singlet states. Abelian symmetry is for the graphs representing full spaces in this orbital basis easily taken into account if the orbitals are ordered according to their symmetry species and certain vertices at the lowest levels of a given symmetry removed. Following Fig 32 graphs showing A_1 , A_2 , B_1 , B_2 symmetry configurations for water are presented (these graphs were produced on a normal line printer and are a part of output of a computer program). The full graph is decomposed into its four symmetry versions. Such a simple symmetry adaptation is possible because there are no a_2 symmetry orbitals in the one-particle space. The graphs that easily fit on one page describe hundreds of thousands of functions. Calculations in such a large space are very expensive (4 hours of CRAY 1S time, as quoted by Harrison and Handy 1983) but allow us to study the influence of various approximations to the full space on the errors. I will represent the approximate spaces in terms of the three-slope configuration graphs without build-in symmetry, obtaining thus rather simple pictures and trying to find whether it is possible to develop some intuitions how 'good' the space is depending on the graph's shape. To simplify things further percent of the correlation energy obtained in the full space is used as the only parameter to measure how 'good' the approximations are.

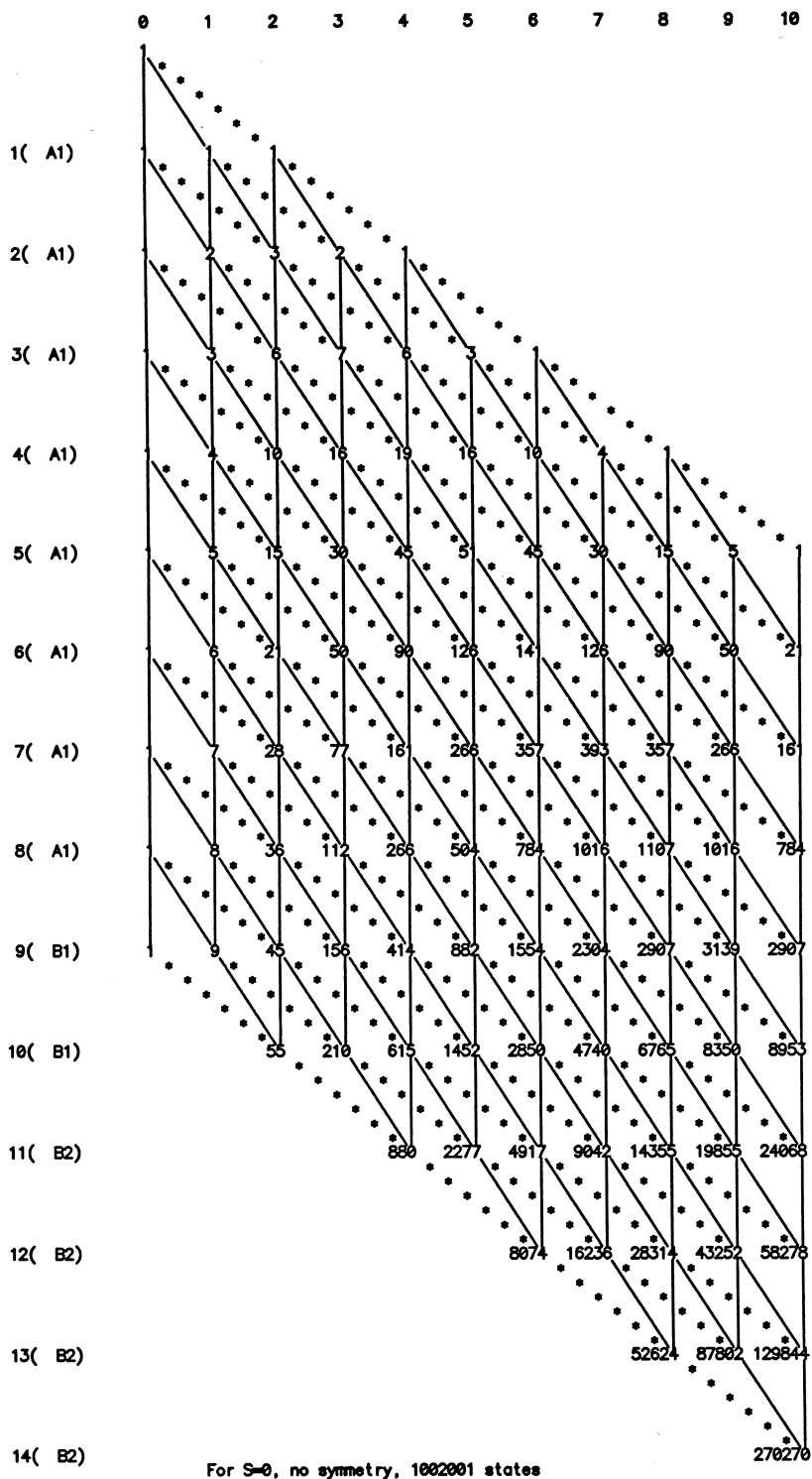
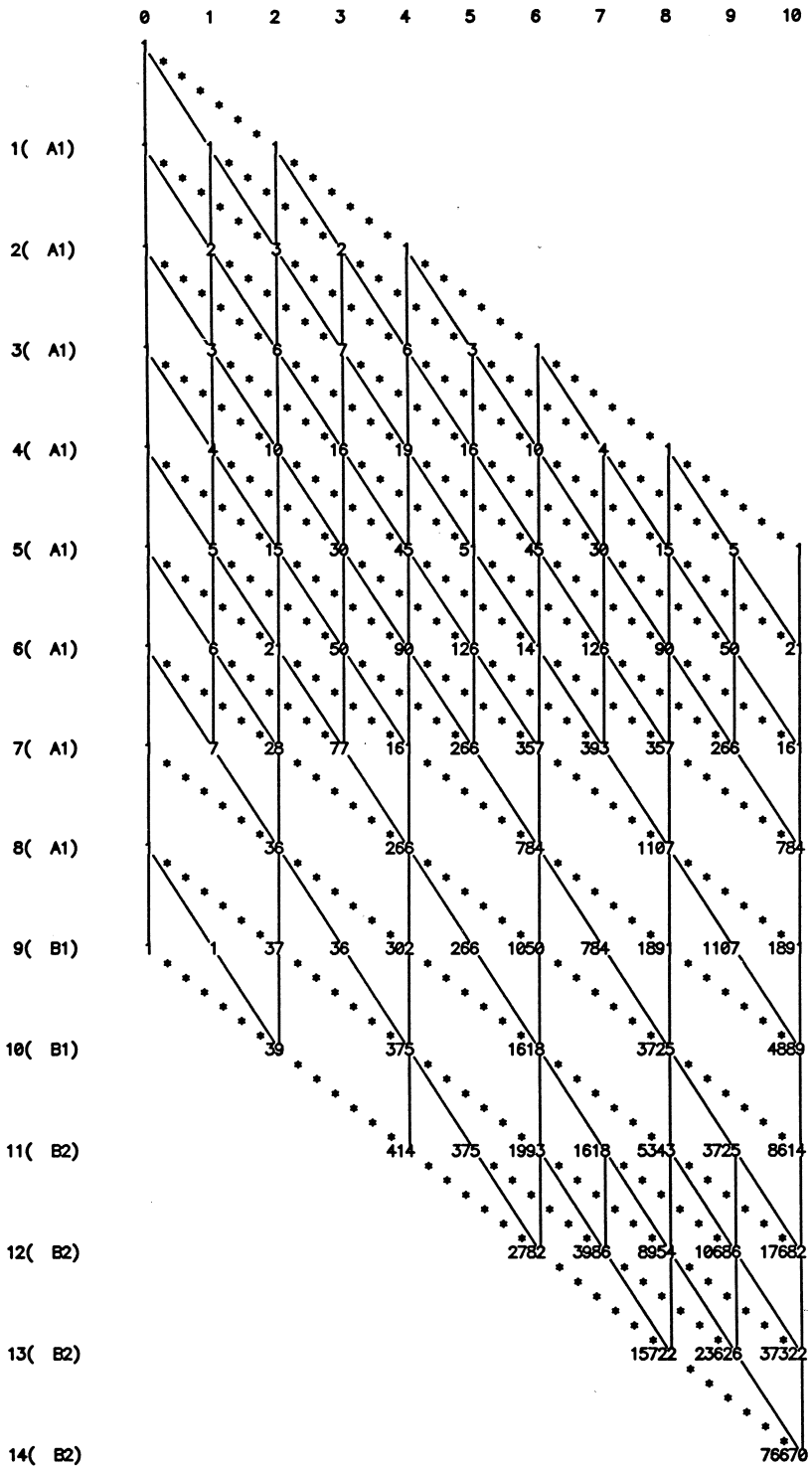
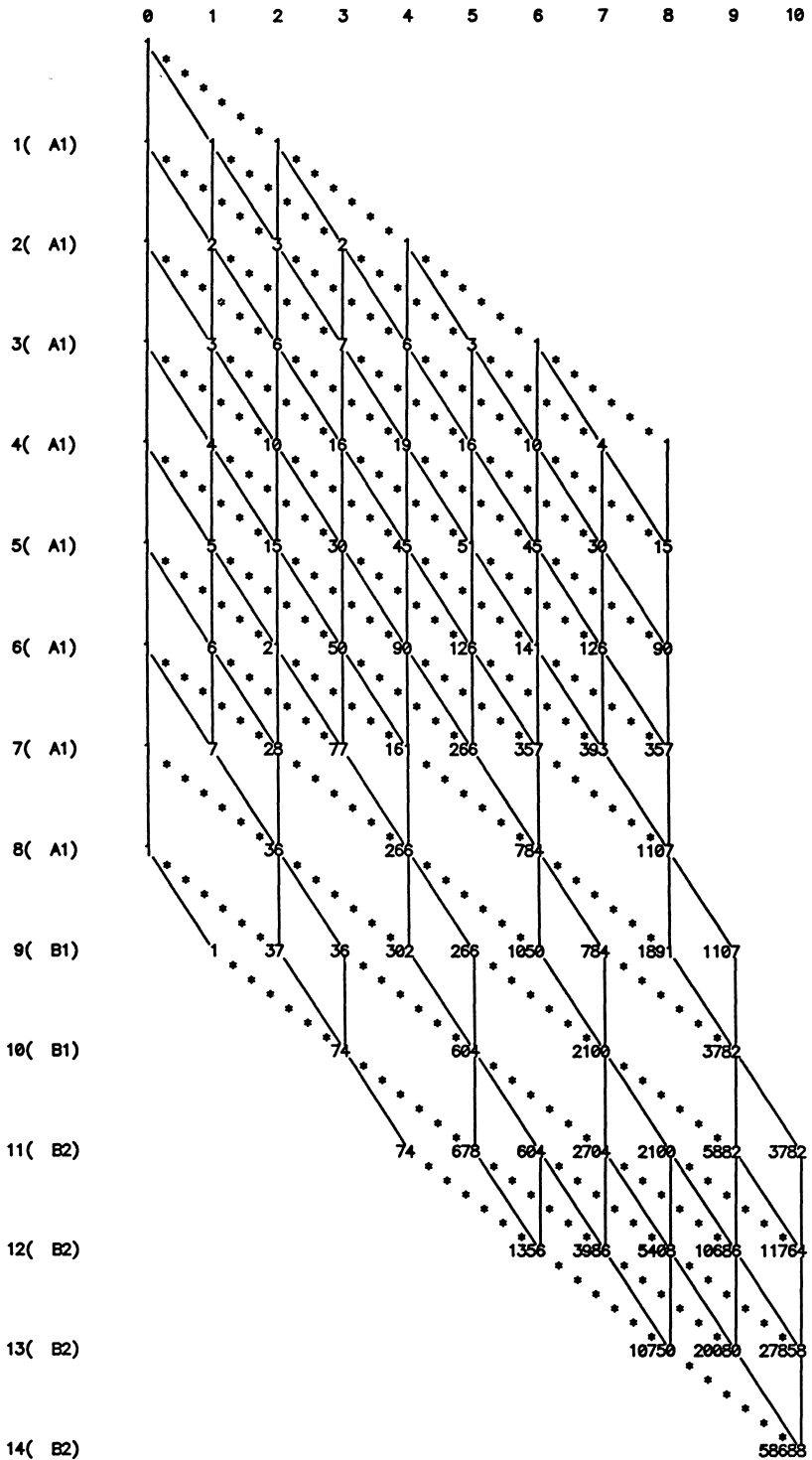
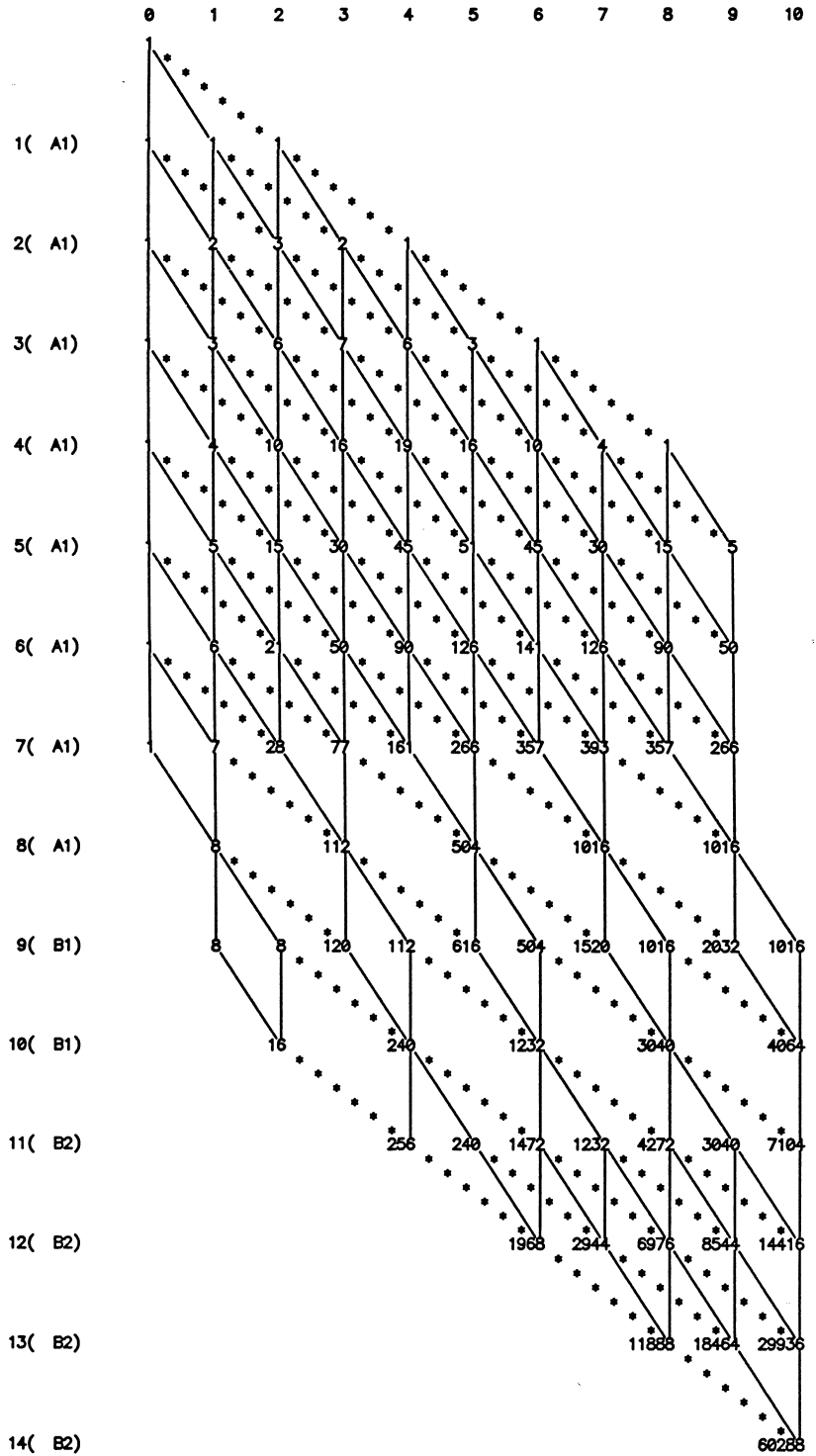


Fig 32. Configurations of water in a full space generated from double zeta basis and (next pages) the same space decomposed into four symmetry species (output from a computer program).

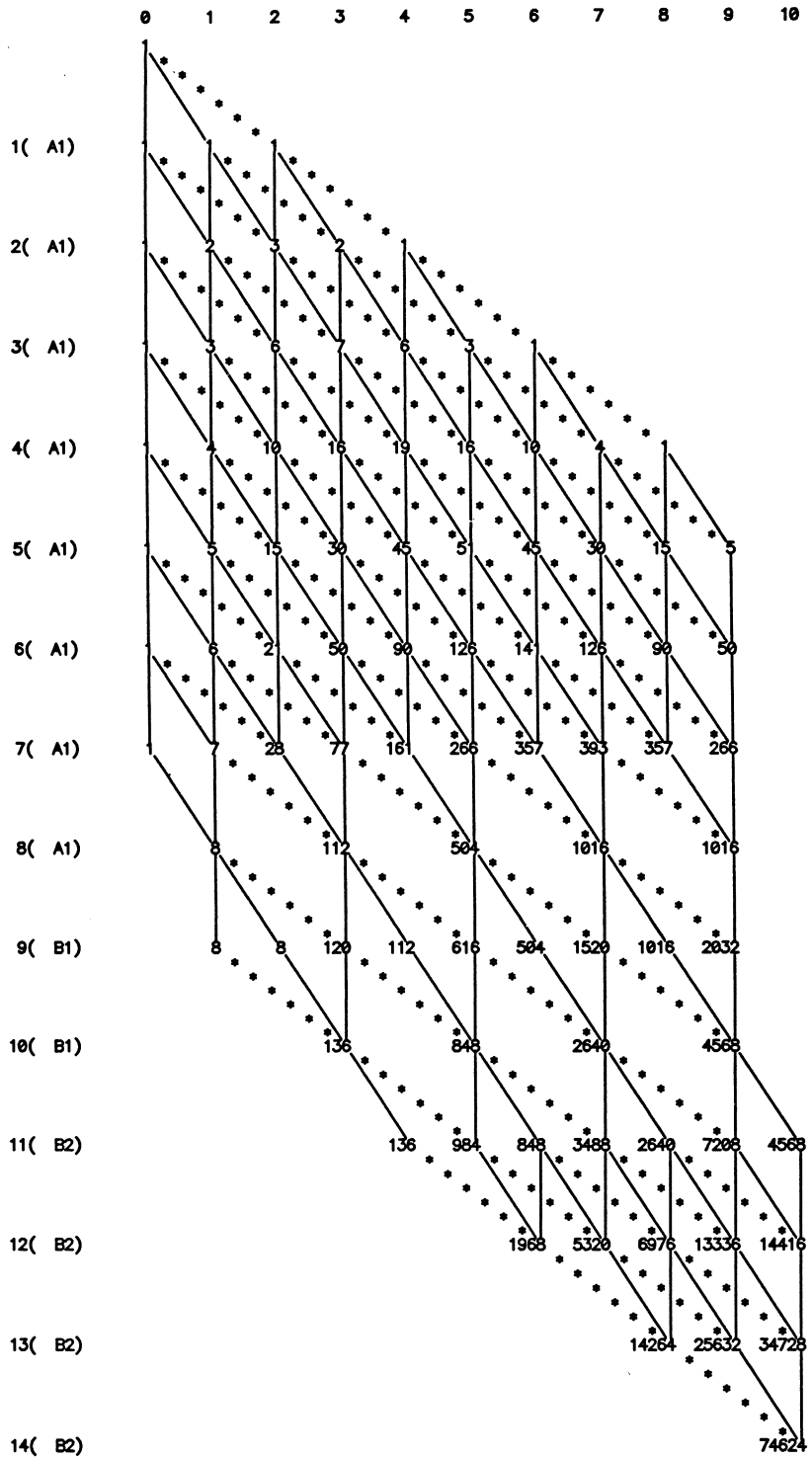




For $S=0$, A_2 symmetry, 245000 states



For $S=0$, B1 symmetry, 245776 states



For $S=0$, B2 symmetry, 254752 states

The most common approximation in calculations on water involves single and double excitations from the SCF configuration $1a_1^2 2a_1^2 1b_2^2 3a_1^2 1b_1^2$, as the first graph in Fig 33 shows. The SCF reference configuration is represented by the uppermost path. It should be noted that while the full graph of Fig 32 is invariant in respect to the orbital order the graphs of Fig 33 are invariant only to the reordering of orbitals inside the \mathcal{D} -part and inside the \mathcal{E} -part, but not in the \mathcal{A} -part. The one-reference case (1R) gives 371-dimensional space of A_1 symmetry singlet states. It is a very small subspace of the full 256 473 dimensional space (around 0.14% of all states) but it already allows to recover 94.7% of the correlation energy. Which paths in the graph correspond to the states next in importance ?

I will present first the traditional approach based on the reference configurations: Burton and Gray (1983) have calculated the correlation energy in a few spaces represented by the graphs in Fig 33. To be more precise we should represent these spaces as in Fig 29 to remove higher than double excited configurations from the picture, but to keep it simple I will use three-slope graphs all the time. The references were selected using second-order perturbation theory to estimate the energy contribution of individual states; a better procedure would be to estimate the coefficients in the final CI expansion (Shavitt 1977b). The same orbital ordering as for the 1R graph is assumed for all graphs of Fig 33. The 3R case, involving 1989 spin adapted states, gives 96.87% of correlation energy. Please note that Burton and Gray (1983) do not use spin-adapted configuration state functions but rather spin complemented determinants (Gray PD, private communication) and therefore the dimensions of the spaces quoted here are smaller than the one they use. It should be interesting to get the results in a full 2745-dimensional space described by the 3R graph, because one may expect that the major portion of the remaining correlation effects is accounted for by a few more than doubly excited configurations out of these 3 important references (for the list of references see Burton and Gray 1983). The perturbation procedure showed its weakness selecting $(1a_1^2 \rightarrow 8a_1^2)$ configuration as the 4-th reference, although in the final state the corresponding function proved to be rather unimportant (Gray PD, private information). Thus 6R graph has no \mathcal{D} -part because $1a_1$ orbital which is at the top is already in the active part. Adding more references, up to a total of 26, the percent of correlation energy obtained grows to 99.61% and the shape of the graph goes to that of a one-reference quadruply excited case, i.e. *SDTQ* graph. This shape is preserved when the number of references is increased to 35 (giving 99.70% of correlation energy) and 45 (99.76% of E_{corr}). Full *SDTQ* space is slightly larger, with 17 678 states, and gives 99.82% of correlation energy (Harrison and Handy 1983).

Clearly there are some parts of the full space contributing very little to the energy and the wavefunction. From the analysis of CI coefficients given by Harrison and Handy (1983) we see that there are some important sextuples which should be included in our space. The importance of $4a_1$ and $2b_2$ valence orbitals for correlation in water is well known (Schaefer and Bender 1971); also the $4a_1$ and $2b_2$ lowest-lying virtual orbitals

are very important. Therefore we should allow highly excited configurations involving primarily these 4 orbitals to be included in our space. Let us place them right after the occupied orbitals. We will add these 4 orbitals, one at a time, to our internal space, accepting all configurations that can be build from the internal orbitals with no more than two external orbitals allowed. Thus we will make a full space of $k=6, 7, 8$ or 9 orbitals and include all singly and doubly excited configurations relatively to this space. Such reference spaces are called "complete active spaces" or CAS (Roos *et al* 1980); examples are shown in Fig 34.

Brown, Shavitt and Shephard (1984) made calculations using CAS spaces and obtained excellent results. The errors in correlation energy are not only very small but are almost independent of geometry. With 9 orbital CAS and 52 452 states 99.95% of correlation energy was achieved. However, the 8 orbital CAS with 22 644 states gives 99.75% of correlation energy which is not as good as 99.82% obtained from calculations including 17 678 states in the *SDTQ* case, although the former space was larger. It is clear that the choice of the configuration space of CAS type is not optimal: one can remove vertices like $v(0,3)$, $v(1,4)$ and $v(2,4)$, Fig 34, without noticable loss of accuracy (to reach these vertices at least 4 electrons have to be removed from bonding orbitals). Instead vertices $v(7,4)$, $v(7,5)$ and $v(8,6)$ are more important, leading to the shape of the graph as shown as the last in Fig 34. It is similar to the 9 orbital CAS but the irrelevant parts are removed. The results of the 8 orbital CAS should be improved and one can still expect the energy errors to be almost independent from geometry, because the removed configurations are unlikely to be of any importance at any geometry. In this case we end up with extremely good approximation but also with a large fraction of the full space. However, one may expected that our restricted space (last graph in Fig 32) remains still a very good approximation to the full space even if the orbital basis set is extended, adding more external orbitals. The fraction of the full space of configurations will then be much lower.

It is clear that more experience with programs using graphical description of model spaces is needed, although some general conclusions may be drawn on the basis of limited data presented above. The highest occupied orbitals and the lowest unoccupied orbitals should correspond to a rather broad, active part of the graph. The lowest-lying occupied orbitals may either be frozen or one can allow single excitations or pair excitations (removing points corresponding to odd numbers of electrons from the D -part) only. Situation is different for different classes of molecules. However, with some experience one should be able to guess the optimal shape of the graph.

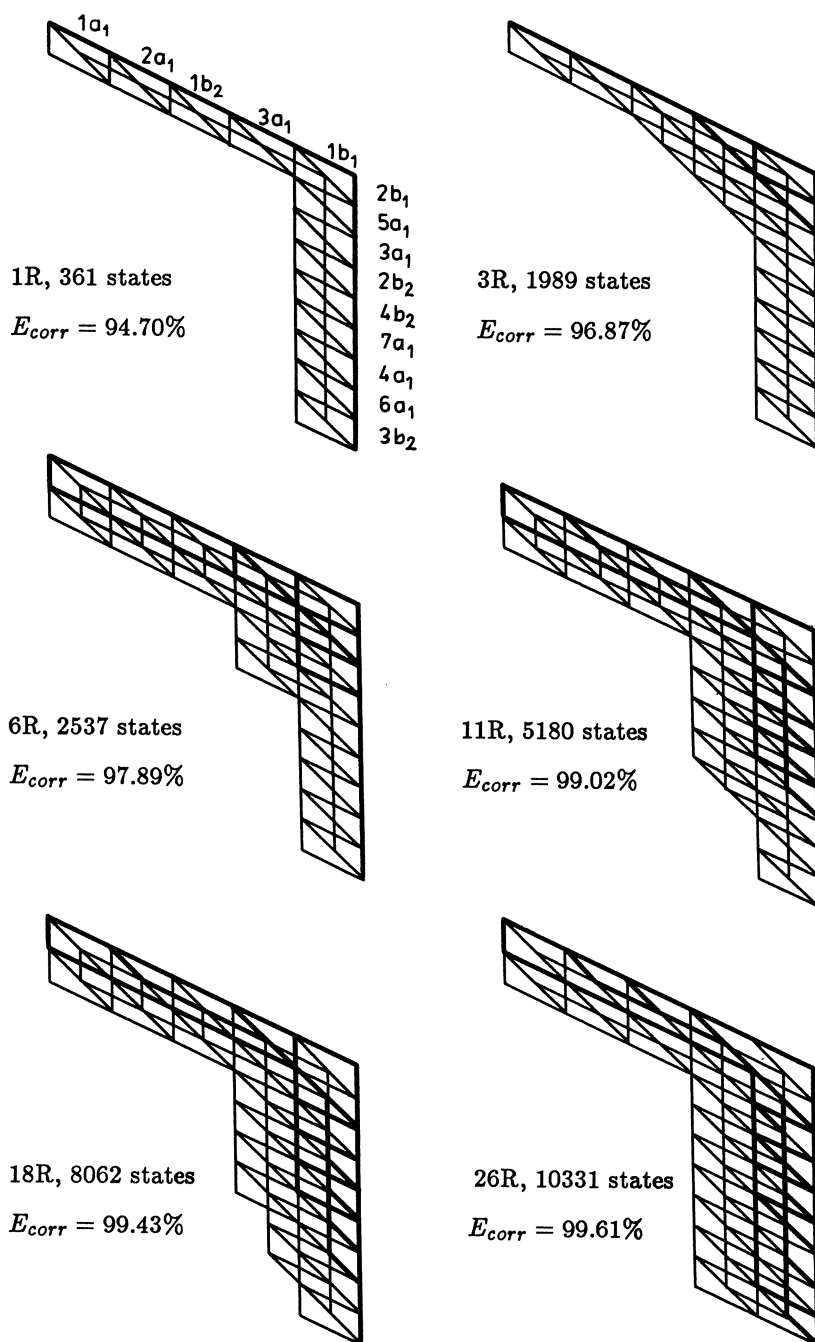


Fig 33. Calculations on water (Burton and Gray 1983) using double zeta basis, with 1 to 26 references. Number of singlet states and percent of E_{corr} is given in each case.

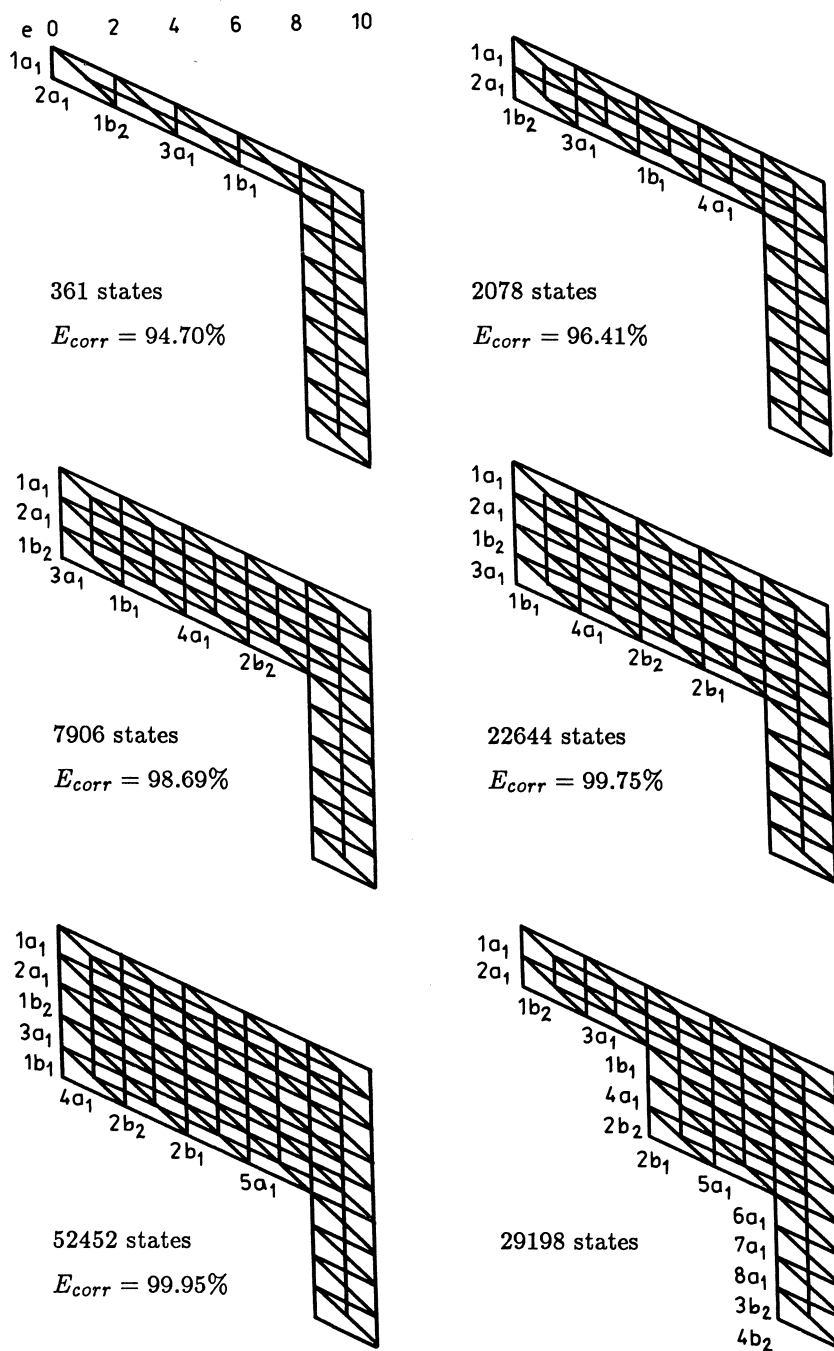


Fig 34. Calculations on water (Brown *et al* 1984) using double zeta basis; complete active spaces with up to 9 active orbitals were used. The last graph should lead to the best results.

1.13

Mathematical remarks

The preceding sections dealt with the graphical representations of model spaces, therefore it is quite natural to look for associations with the graph theory on one side, and group-theoretical methods to characterize these model spaces on the other. However, examining books on graph theory (cf Ore 1962; Harary 1969; Deo 1974; Beineke and Wilson 1978; Swamy and Thulasiraman 1981) I have found rather little relevant material. Although it is possible to fit some problems into “structural graph theory” of Nash-Williams (1973) it seems to me that the graph theory is at present not very useful in setting up and analyzing graphs representing model spaces. The graphs used here are real digraphs (directed graphs) in the sense of the theory of graphs but we are really interested in representations of model spaces rather than the graphs themselves. Therefore, although formally the three graphs of Fig 35 are equivalent the first is the most natural, because the contribution of each arc to the total N and M_G numbers is clearly visible and we may introduce a horizontal axis to measure N , M_G values. In the two other cases we have to label each arc with two weights, one for the number of electrons associated with it ($e_k = 0, 1, 2$) and one for \hat{S}_z projection numbers ($m_k = 0, \pm\frac{1}{2}$).

It is easy to notice that even the simple three-slope graphs are non-planar. However, we may use many equivalent graphs to represent our space, and some of these may be planar – a striking example was given in Fig 11a,b. There are results in the graph theory – Menger’s theorem for example (Harary 1969) – that may help to find a representation with a minimum number of intersecting arcs. In general a problem of finding the minimal graph – i.e. a graph with the minimal number of vertices and arcs – is a rather difficult one, especially when the restricted graphs are considered.

GT Let us look now at the graphical representation of model spaces from quite different point of view. The problems discussed so far are connected with the graphs and graphical representation, but we would like to use this representation to map differential

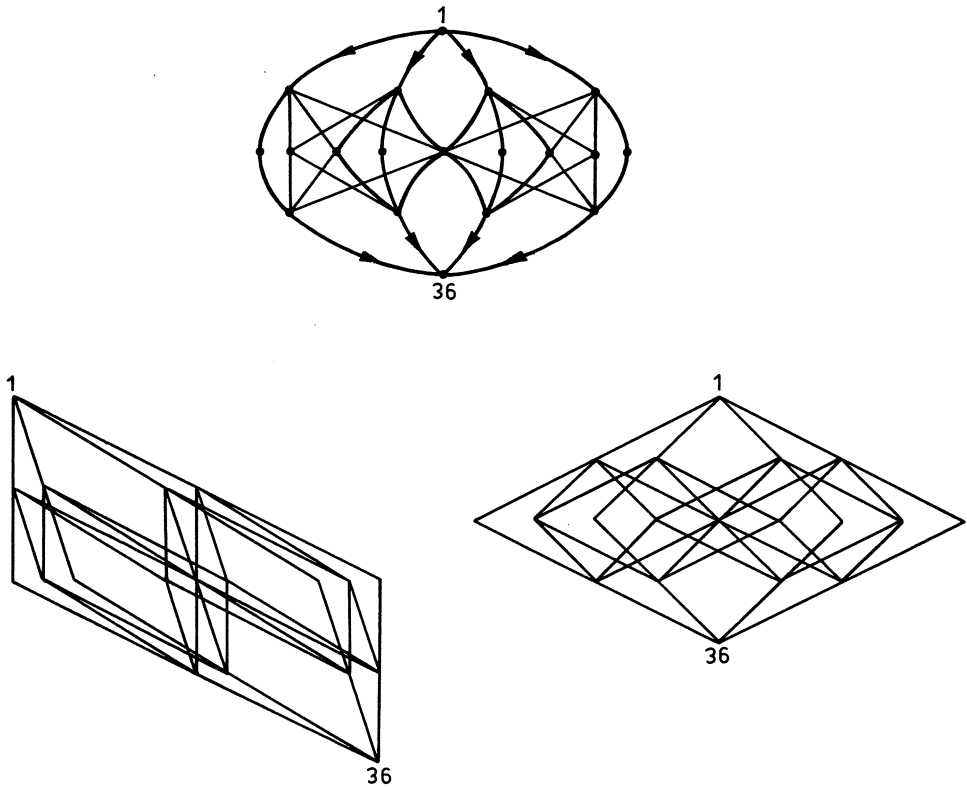


Fig 35. Topologically equivalent representations of 4 orbital, 4 particle \hat{S}_z -adapted space.

operators into matrices, i.e. to calculate some matrix elements. Therefore we should ask: what can we really represent? In most general sense we can represent graphically any basis of a tensor space $\mathcal{V}_n \otimes^N$. This space is a carrier space for the representations of S_N and $GL(n)$ groups (cf Wormer 1975; Barut and Rączka 1980). Although the two groups are so different their representations are closely connected. The importance of this fact for physics was pointed out already by Weyl (1928); all the physically important spaces may be approximated by carrier spaces of S_N and $GL(n)$ groups. The operators acting in these spaces are thus equivalent to linear combinations of permutation operators or generators of the linear group. It is natural to assume that the carrier space of a particular $GL(n)$ or S_N representation is adapted to a nested chain of subgroups $GL(n) \supset GL(n-1) \supset \dots GL(1)$ or $S_N \supset S_{N-1} \supset \dots S_1$. This adaptation is reflected in the embedding of the subgraphs in the graph representing such a carrier space. In Fig 36 we see graphical visualization of a carrier space for the $[3,2]$ representation of the general linear group $GL(7)$ or a special unitary group $SU(7)$. Regular structure of this graph reflects the genealogical chaining. Alternative representation by Gelfand tableaux (cf Moshinsky 1968) would take many pages without giving much insight into

| | | | | | | | | |
|---|---|---|---|---|---|---|---|---|
| 0 | 1 | 2 | 3 | 1 | 2 | 3 | 2 | 3 |
| 0 | 0 | 0 | 0 | 1 | 1 | 1 | 2 | 2 |

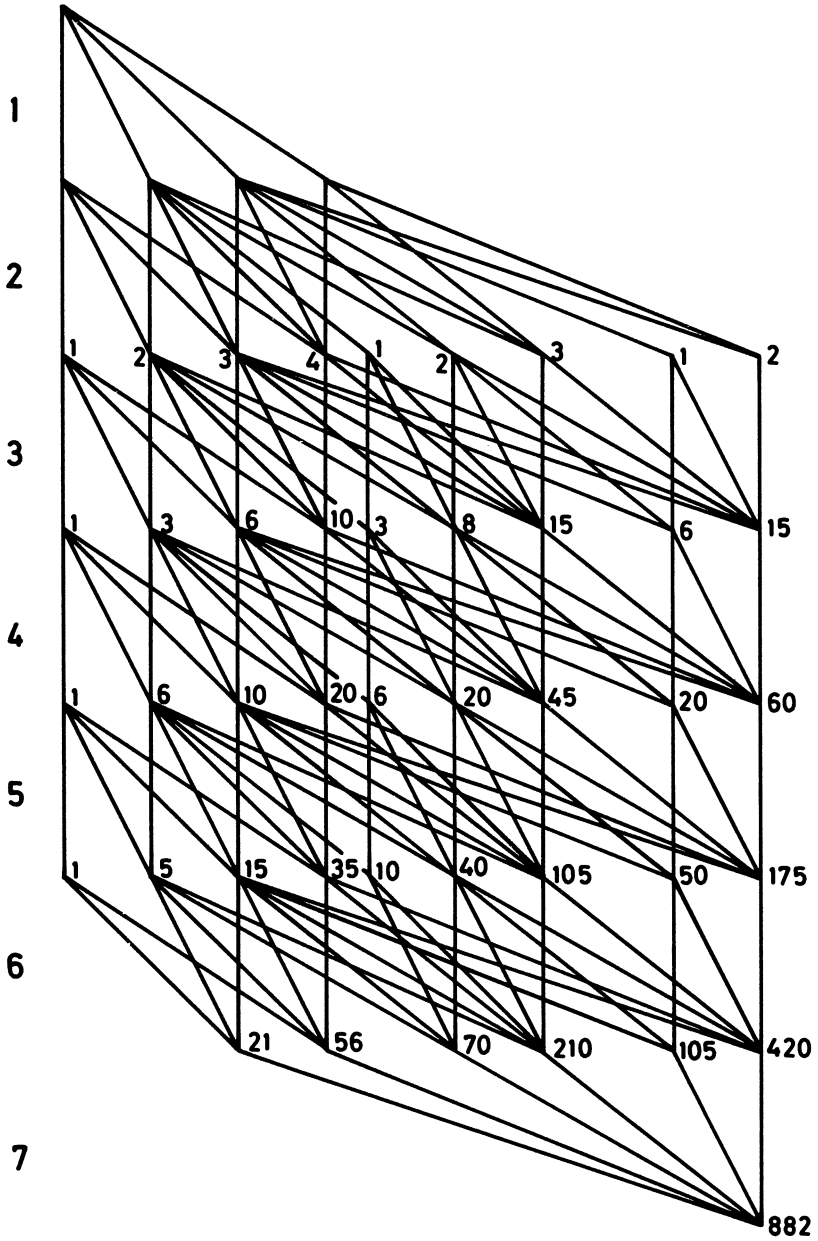


Fig 36. Visualization of the carrier space for $[3, 2]$ representation of $SU(7)$ or $GL(7)$ group.

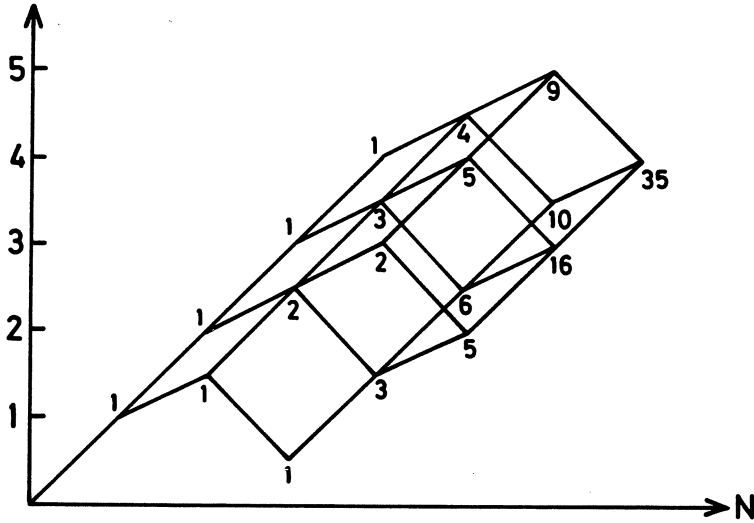


Fig 37. Visualization of the carrier space for $[4, 2, 1]$ representation of the symmetric group S_7 .

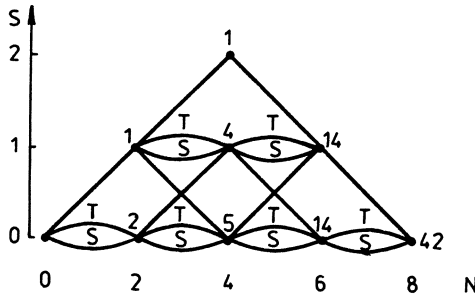


Fig 38. Serber, or geminal, spin branching diagram.

the structure of the representation space. In Fig 37 the carrier space of representation $[4, 2, 1]$ of the symmetric group S_7 is presented. These type of graphs should find wide applications in many physical problems (cf Hammermesh 1962).

The genealogical chaining of subgroups is not the only possible choice, other chains of subgroups are worth to explore. The genealogical embedding corresponds to the use of the one-particle states as the building blocks in \mathcal{V}_n space. Using two-particle states (geminals) corresponds to $GL(n) \supset GL(n - 2) \supset \dots$ or $S_N \supset S_{N-2} \dots$ chain. The best known example of this chaining is the spin space, where the genealogical embedding is used in the Yamanouchi-Kotani branching diagram, Fig 19, while the two-particle embedding is used in the geminal spin function (known also as the Serber spin function) diagram (Serber 1934), represented graphically in Fig 38. To finish group-theoretical

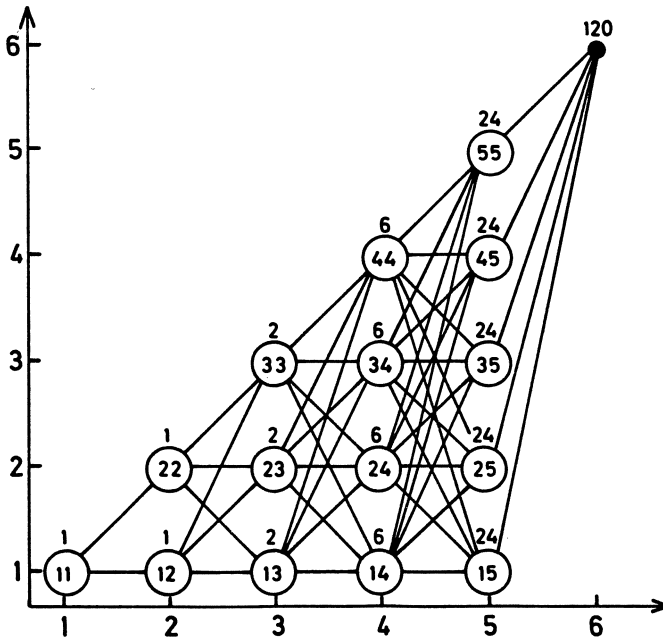


Fig 39. Classification of $5! = 120$ permutations belonging to S_5 group.

part let me mention that not only the carrier spaces but also elements of groups may be represented by graphs. For example, permutations belonging to the S_5 group are classified in a natural way in Fig 39. Each permutation has its lexical number that is easily read from this graph (Rettrup 1986).

Each path in the orbital graph contains exactly n arcs. A graph gives in fact all solutions to a set of Diophantine equations, for example, graphs in Fig 35 solve

$$\sum_{k=1}^n e_k = 4; \quad e_k = 0, 1, 2 \quad \sum_{k=1}^n 2m_k = 0; \quad 2m_k = \begin{cases} 0 & \text{for } e_k = 0, 2 \\ \pm 1 & \text{for } e_k = 1 \end{cases} \quad (1.30)$$

each path giving one particular solution $\{(e_k, m_k)\}_{k=1}^4$ of these equations. Adaptation of the basis states to additional operators is equivalent to adding more equations to this set, with more complicated restrictions on the values of arc weights (compare Eq (1.10-1.14)). We should consider all graphs that provide a solution to this set of diophantine equations as equivalent. In particular, when the full space of the solutions is represented, the ordering of graph's levels is unimportant. The theory of Diophantine equations, forming one of the oldest branches of mathematics (Mordell 1969), is thus connected to the theory of graphs, the relation being somehow overlooked by mathematicians. The reason is rather simple – linear systems of Diophantine equations have never attracted much interest, although, as Mordell writes in his monographic book on Diophantine equations: “It is well known that for many centuries no other topic has engaged the attention of so many mathematicians, both professional and amateur, or has resulted

in so many published papers". However, to linear equations he devotes only 4 pages of his book.

Another well-established branches of mathematics that are relevant here are the combinatorial theory (cf Hall 1967) and the theory of partitions (Andrews 1976). Powerful methods of group theory together with the combinatorial theory and partitions theory are necessary to solve even such a relatively simple problem like determining the number of times a given term appears in an atomic configuration (Karayiamis 1965). Methods of graph theory should be simpler in attacking such problems, especially the more complicated problems of mixed atomic and molecular configurations, as described in sections 1.8–1.10. Another branch of mathematics relevant here is operations research, and especially the integer programming (Garfinkel and Nemhauser 1972). Graph theory and Diophantine equations are used in the linear programming problems quite frequently. So far fixed-slope graphs were not used in these problems, although it is evident that the 'tree-type' graphs may easily be folded into the fixed-slope graphs containing only the required solutions: numerous blind paths in the trees and the whole "fathoming procedure" may then be avoided (Garfinkel and Nemhauser 1972).

It is clear that GRMS stands on the crossroads of different branches of mathematics, helping to solve some problems and posing some new ones.

1.14

Graphs and computers

The last subject that I want to cover briefly is of more technical nature. For more information the reader is referred to the literature quoted in this section.

How does one deal with a graph when it comes to programming? Computer scientists certainly know how to do it, as graphs and trees are their favorite tools. There are many general methods to represent arbitrary graphs (cf Deo 1974) and powerful techniques to retrieve information from the graph (cf Knuth 1973). The trouble with general methods is that they are too general and therefore not very efficient when one deals with the graphs that have such a simple structure as two, three, or four-slope graphs. The fixed-slope graphs are represented in a most economic and convenient way by describing the weights of their arcs and vertices. If the graph has L vertices and p slopes than p vectors, each of the length L , plus 3 small auxiliary arrays suffice to represent it in a computer. The auxiliary arrays are needed to obtain the consecutive number of a vertex from its position in a graph (i.e. knowing the level, number of electrons and other numbers specified for vertices). An example of representation by three weight vectors is given in Duch and Karwowski (1985) and in Duch (1985c). Representation using weight vectors is very economical: the A_1 symmetry graph of Fig 32 for example is represented using only 330 numbers. Another method of computer representation for a fixed-slope graph is described by Shavitt (1977a) and in more details by Robb and Niazi (1984) in context of the four-slope graphs used in GUGA. The information about the graph is collected in a 'distinct row table' (DRT): for each level and each vertex at that level the weights of the vertex and the arcs off this vertex, the position of the vertex in the graph (in form of a,b,c numbers) and the 4 'chaining indices' are stored. Representation of a graph by DRT is not so economical as by the weight vectors, but still does not take much space. One can easily devise many variations of these two methods of computer representation of graphs and find a method best suited to a particular type of graph.

The problem of searching a graph, for example finding all paths (i.e. their lexical numbers) that connect two given vertices, is not described here in details because the depths search and the breadth search algorithms specialized for the p -slope graphs are already described (Duch and Karwowski 1985; Duch 1985c) and the reader is referred to the extensive book of Knuth (1973) for more general algorithms. Using the three-slope graphs of Fig 32 as an example different search algorithms were tested (Duch and Karwowski 1986) including several versions of depth search (DS) algorithms: a simple DS algorithm, DS modified to take advantage of the simple structure of the graph near its borders (when $(k, N - 1)$ vertex is reached the remaining arc is on one of $n - k$ levels and these $n - k$ paths form a kind of 'ladder' in the graph that is easily analysed explicitly; similarly for $(k, N - 2)$ vertex), and DS with fixed number of singly occupied arcs (Duch 1985). We have also tested a global algorithm (cf Duch 1986), and breadth search algorithm (as described in Duch and Karwowski 1985). For full spaces with a rather small number of orbitals all these algorithms are about equally efficient, except that the breadth search and the global algorithms become impractical for large spaces, requiring too much memory. For spaces with large number of orbitals and only few particles the modified depth search algorithm is preferable. However, the best approach seems to be the cutting of a graph at a level where the total number of paths coming from the top is roughly equal to the number of paths coming from the bottom. For each of the vertices at such level the analysis is done separately in the upper part and in the lower part and the results are combined. Using this approach on a scalar computer, Siemens 7880, the lexical indices of the 270270 paths corresponding to the graph without symmetry (Fig 32) were found in 0.34 sec, while on a Cray XMP (single processor) machine it took 0.06 sec. The corresponding times for other algorithms were at least an order of magnitude longer. Although the searching algorithms are hard to vectorize because of non-linear indexing and recursive nature of searching, cutting the graph into two parts leaves most of the work for the loops connecting the two parts and makes vectorization possible. With this approach (it may be pictured as taking the square root of a graph) the logical part of the large scale calculations should take a rather insignificant part of the total time.

In some applications we would like to have the paths in a special order, divided into classes, some paths should be deleted from the graph, in case of fagot graphs each path corresponds to a number of states. It is possible to use a very specialized representation of a graph, such as was used by Gołębiewski and Broclawik (1985) in the three-slope graph case, to obtain consecutive numeration of all configurations sharing the same doubly occupied orbitals. The double-level indexing scheme allows for easy reordering and deleting of paths in an arbitrary way. Instead of taking the lexical number l_L as the number pointing to a function corresponding to the path L we define a vector $I(l_L)$ that points to that function. The use of the double-indexing scheme was described in detail by Duch and Karwowski (1985) in context of a three-slope graph and its use for other graphs is analogous. This type of indexing is very convenient when we want to remove some paths from a graph without complicating the graph itself.

General methods and a few specialized ones are thus available for computer representation of graphs in practical calculations.

1.15

Summary and open problems

In the preceding sections hitchhiker's guide to the architecture of Hilbert spaces was presented. Although the analysis of various graphical representations was restricted to a minimum – as if pictures of buildings were presented without really entering into details of engineering problems – the multitude of spaces used in physics is responsible for this rather long presentation. I realize that many kinds of spaces were omitted and thus description of the architecture of Hilbert spaces given here is far from being complete. The representation of spinor and tensor spaces used in relativistic methods for example was not mentioned. On the other hand spaces most important for molecular, atomic and nuclear physics were all covered. One may draw graphs representing the spaces of a very high dimension, too high to list all paths explicitly, and still find interesting information about the structure of such spaces. Spaces built from a large number of primitive states of the same type have particularly simple structures. The techniques of graphical evaluation of matrix elements are developed in Part II (abelian symmetries) and Part III (non-abelian symmetries). The insight that the graphs give into the structure of model spaces and the graphical methods of matrix element calculation may than be applied to construction of matrix representations of differential operators.

It should be useful to summarize different graphical representations of various spaces in a table. The first column contains operators the space is adapted to, in the second column number of levels (n for orbital and $2n$ for spin-orbital graphs) is given, third column gives the number of slopes in the graph, with $k(m)$ meaning that there are k slopes and each depends on values of m . The fourth column gives reference to figures in the previous sections, and the last column contains graph designations and remarks.

| Operators | Lev | Slopes | Figures | Remarks, designations |
|--------------------------|------|---------------|----------------|--|
| - | $2n$ | 2 | 1 | $\mathcal{G}_2(2n : N)$ |
| | n | 3 | 7a+14b | configurations + all spin products |
| \hat{S}_z | s | 2 | 9 | M-diagram $\mathcal{G}_2(s : M_S)$ |
| | $2n$ | 2 | 4 | α, β -parts separated |
| | $2n$ | 2+2 | 5c,6c | $\mathcal{G}_{2,2}(2n : N, M_S)$ |
| | n | 3 | 7a,8a+9 | $\mathcal{G}_3(n : N) \odot \mathcal{G}_2(s : M_S)$, conf+M-diagram |
| | n | 4 | 7c,8c | $\mathcal{G}_4(n : N, M_S)$ |
| \hat{S}^2 | s | 2 | 19 | $\mathcal{G}_2(s : S)$ Yamanouchi-Kotani diagram |
| | s | 4 | 38 | Serber diagram |
| | $2n$ | 2+2 | 20c | $\mathcal{G}_{2,2}(2n : N, S)$ |
| | n | 3 | 20a | $\mathcal{G}_3(n : N) \odot \mathcal{G}_2(s : S)$ |
| | n | 4 | 20b | $\mathcal{G}_4(n : N, S)$ (Shavitt's graph) |
| \hat{L}_z | $2n$ | $2(m_l)$ | 11,12 | levels $\alpha\beta\alpha\beta\dots$ |
| | n | $3(m_l)$ | 14 | fagot graph |
| (\hat{L}_z, \hat{S}_z) | $2n$ | $2(m_l)$ | 15,16 | α, β -parts separated |
| | $2n$ | $2(m_l, m_s)$ | 17 | levels $\alpha\beta\alpha\beta\dots$ |
| | n | $4(m_l, m_s)$ | 18 | too many slopes |
| | n | $2l + 2$ | 22 | Fagot graph+M-diagram |
| (\hat{L}_z, \hat{S}^2) | $2n$ | $2(m_l, S)$ | 21 | Fig 21 shows case with $S = \frac{1}{2}N$ |
| | n | $2l + 2$ | 22 | Fagot graph+S-diagram |
| | $2n$ | $2(m_l, m_s)$ | 17 | with $M_S < 0$ vertices removed |
| | n | $4(m_l, m_s)$ | 18 | with $M_S < 0$ vertices removed |
| (\hat{L}^2, \hat{S}^2) | n | $2l + 2$ | 24 | atomic configurations+terms |
| | n | variable | 26 | atomic terms |
| (\hat{J}^2, \hat{T}^2) | $2n$ | variable | 27 | nuclear states |
| Γ | $2n$ | 2 | 28a | with symmetry vertices |
| | n | 3 | 28b | configurations, as above |
| | n | 3 | 32 | configurations, vertices removed |
| | n | variable | 29 | non-abelian symmetry groups |
| $GL(n)$ | n | variable | 36 | carrier space for $GL(n)$ or $SU(n)$ rep. |
| S_N | N | variable | 37 | carrier space for S_N representations. |

* * *

Open problems were mentioned already a few times in the text. I am not quite satisfied with the graphical visualization of non-abelian symmetry spaces. Drawing the graphs is in this case not straightforward and depends on previous analysis of pure shells. Improvements here are very important for atomic and nuclear applications. Is it possible to enforce graphically strict excitation limits in a more elegant way than

shown in Fig 30? Flexibility of such restrictions is of great importance in molecular physics applications. The particle-hole formulation of Boyle and Paldus (1980) does not seem to be a good solution for open-shell or many reference states.

When is it possible to find representation of a model space by a planar graph? If it is not possible then how to find the most legible non-planar graph?

I did not give the dimension formulae for the (\hat{L}_z, \hat{S}^2) , (\hat{L}^2, \hat{S}^2) , (\hat{J}^2, \hat{T}^2) and the spaces adapted to point groups because the dimension formula for (\hat{L}_z, \hat{S}_z) -adapted space is already cumbersome. Can one simplify it?

S-diagrams for elementary spins $> \frac{1}{2}$ are worth discussing (cf Kartiel *et al* 1985) but were not mentioned here. Spinor and tensor spaces were completely neglected.

The connection with traditional graph theory, theory of group representations, Diophantine equations and integer programming should prove particularly fruitful. The architectural part of GRMS should find wider applications than only those mentioned above. Architectural features are of fundamental importance to the whole GRMS approach.

PART II

MATRIX ELEMENTS

AND GRAPHS

Matrix elements in model spaces

So far we have solved kinematical part of our problem, that is we have a convenient graphical description of the many-particle state spaces. Now comes the dynamical part: we want to solve some equations in these spaces. The first step in this direction is to project the operators defined in the infinite dimensional Hilbert space to the finite-dimensional model space (cf Kemble 1958). Thus an operator $\hat{A} = \mathbf{1}_\infty \hat{A} \mathbf{1}_\infty$ in M -dimensional space becomes:

$$\hat{A}_M = \mathbf{1}_M \hat{A} \mathbf{1}_M = \sum_{L=1}^M |L\rangle\langle L| \hat{A} \sum_{R=1}^M |R\rangle\langle R| = \sum_{L,R=1}^M |L\rangle\langle L| \hat{A} |R\rangle\langle R|$$

The elements $\langle L|\hat{A}|R\rangle$ form a matrix representative of the operator \hat{A} in a model space. The structure of this matrix reflects the structure of the model space as depicted by a graph. Understanding of this structure is the main task of this work. To accomplish this we must first learn how to calculate matrix elements with the help of graphs.

In this part I will restrict myself to the many-electron states transforming according to the one-dimensional representations of a point group, leaving the case of degenerate representations for Part III. In the most common case the model space is taken as a subspace of a tensor product $\mathcal{V}_n^N = \mathcal{V}_n \otimes^N$ of the n -dimensional space of orthonormal one-particle states, i.e. the states $|R\rangle$, represented by paths of a graph, are linear combinations of orbital products. These multiconfigurational spaces, as they are sometimes called (Wormer 1975), are the only ones that I will consider. Although the extension to the geminal and to more complicated cases may not be straightforward, the orbital spaces should at least give some guidance how to proceed.

The first two sections are rather pedagogic, introducing a complete set of operators, called here the shift operators, allowing to express an arbitrary operator acting in a model space as a polynomial in these operators and deriving the well-known general formula for matrix elements of these operators. This formula is then used to derive graphical rules of matrix element calculation for various \hat{S}_z , \hat{L}_z , and \hat{S}^2 -adapted graphs. In particular Shavitt's results (1981) are rederived as an example.

2.1

The shift operators.

The interactions we deal with in physics involve one or two particles and therefore are represented by one and two-particle operators. Some formalisms introduce more than two-particle operators. In general calculating matrix elements we would like to separate the physical information, the part that depends on the p -particle operator \hat{A} and thus is expressed by the p -dimensional integrals

$$\int \phi_{a_1}^*(1) \dots \phi_{a_p}^*(p) \hat{A}(1 \dots p) \phi_{b_1}(1) \dots \phi_{b_p}(p) dx_1 \dots dx_p$$

that carry information about the interactions i.e. about physics, from the structural information that depends only on the construction of the bases of many-particle model spaces. We have to define the complete set of operators that act in the model space and that carry purely structural information. In context of a graphical description the most obvious choice seems to be the replacement or level-shifting operators \hat{E}_{ij} . Acting on a given path they should simply decrease the occupation or the slope of j -th arc (or give zero if the arc's slope can not be decreased further) and increase the occupation (slope) of the i -th arc (or give zero if the arc has already maximal occupation). However, such a definition of the replacement operators is not natural from the algebraical point of view. The p -particle operator \hat{A} , acting on a state (path) gives a combination of states (paths) differing at most by p orbitals, i.e. paths differing at most by p arcs. Thus it should be possible to express the p -particle operator in a natural way as a p -th order polynomial in the operators replacing orbitals. Expressing an arbitrary operator with the help of such replacement operators is easy if a projector on a whole one-particle space, i.e. one-particle unit operator is first defined. The projector may be written as:

$$\mathbf{1} = \sum_{k=1}^{2n} |k\rangle \langle k| = \sum_{i=1}^{n_i} \sum_{\Gamma_i} |i_{\Gamma_i}\rangle \langle i_{\Gamma_i}| \quad (2.1)$$

The second summation runs over all n_l levels of the graph, i.e. the projector

$$|i\rangle\langle i| = \sum_{\Gamma_i} |i_{\Gamma_i}\rangle\langle i_{\Gamma_i}|$$

corresponding to a degenerate one-particle state, projects on the whole degenerate subspace.

A. Definitions.

Using the unit operator we can express an arbitrary one-particle operator acting in the tensor product space \mathcal{V}_n^N in the following way:

$$\begin{aligned} \hat{A}|\gamma_n^N\rangle &= \sum_{q=1}^N \hat{a}(r_q) = \sum_{q=1}^N (\mathbf{1}\hat{a}(q)\mathbf{1}) \\ &= \sum_{ij} \sum_{\Gamma_i\Gamma_j} \sum_{q=1}^N |i_{\Gamma_i}(q)\rangle\langle i_{\Gamma_i}(q)|\hat{a}(q)|j_{\Gamma_j}(q)\rangle\langle j_{\Gamma_j}(q)| \\ &= \sum_{ij} \sum_{\Gamma_i\Gamma_j} \langle i_{\Gamma_i}|\hat{a}|j_{\Gamma_j}\rangle \hat{E}(i_{\Gamma_i}, j_{\Gamma_j}) \end{aligned} \quad (2.2)$$

where

$$\hat{E}(i_{\Gamma_i}, j_{\Gamma_j}) = \sum_{q=1}^N |i_{\Gamma_i}(q)\rangle\langle j_{\Gamma_j}(q)| \quad (2.3)$$

is the replacement operator. Acting on a many-particle state this operator replaces all kets $|j_{\Gamma_j}\rangle$ with $|i_{\Gamma_i}\rangle$. Operators of such kind were used first in nuclear physics and called 'the shift operators' (cf Moshinsky 1968 or Bohr and Mottelson 1969). Later they appeared also in molecular and atomic physics under different names: Matsen (1974) and Koutecký and Laforgue (1977) calls them 'the basic symmetry operators', Hinze and Broad (1981) 'the spin free reduced density operators of the first order', Paldus (1976) and Harter and Patterson (1976) use the name 'the unitary group generators'. The name 'generator' is now the most common, having the advantage of using one word instead of two words as in the 'shift operator' or the 'replacement operator'. The name 'generator' seems however to be completely out of context in most papers where no unitary group theory is invoked, therefore I prefer to use the older name 'shift operators' (perhaps 'shifters' would be the most convenient).

A few equivalent definitions of the shift operators are possible:

$$\hat{E}(i_{\Gamma_i}, j_{\Gamma_j}) = \sum_{q=1}^N \hat{E}_{j_{\Gamma_j}}^{i_{\Gamma_i}}(q); \quad \langle k_{\Gamma_k}|\hat{E}_{j_{\Gamma_j}}^{i_{\Gamma_i}}|l_{\Gamma_l}\rangle = \delta(i_{\Gamma_i}, k_{\Gamma_k})\delta(j_{\Gamma_j}, l_{\Gamma_l}) \quad (2.4)$$

or using creation and annihilation operators:

$$\hat{E}(i_{\Gamma_i}, j_{\Gamma_j}) = a_{i_{\Gamma_i}}^\dagger a_{j_{\Gamma_j}} \quad (2.5)$$

where we see even better that the $\hat{E}(i_{\Gamma_i}, j_{\Gamma_j})$ operator simply replaces one-particle state $|j_{\Gamma_j}\rangle$ by one-particle state $|i_{\Gamma_i}\rangle$. If

$$\langle i_{\Gamma_i} | \hat{a} | j_{\Gamma_j} \rangle = \delta_{\Gamma_i \Gamma_j} \langle i | \hat{a} | j \rangle = \delta_{\Gamma_i \Gamma_j} \{i|j\} \quad (2.6)$$

as it happens when the labels Γ_i, Γ_j designate spin functions α, β or when the operator \hat{a} is invariant in respect to the symmetries giving rise to Γ labels, we may introduce symmetry contracted replacement operators

$$\hat{E}_{ij} = \sum_{\Gamma \in \{\Gamma_i\} \cap \{\Gamma_j\}} \hat{E}(i_{\Gamma}, j_{\Gamma}) = \sum_{\Gamma} \sum_{q=1}^N |i_{\Gamma}(q)\rangle \langle j_{\Gamma}(q)| \quad (2.7)$$

and

$$\hat{A} = \sum_{i,j=1}^{n_l} \{i|j\} \hat{E}_{ij} \quad (2.8)$$

is expressed as a sum over i, j corresponding directly to the n_l graph levels. In particular, if the orbital graph is used, i.e. $n_l = n$,

$$\hat{E}_{ij} = \sum_{\Gamma} (|i_{\Gamma}\alpha\rangle \langle j_{\Gamma}\alpha| + |i_{\Gamma}\beta\rangle \langle j_{\Gamma}\beta|) \quad (2.9)$$

B. Properties of the shift operators.

Although $\hat{E}_{ij}^\dagger = \hat{E}_{ji}$ is not Hermitian the symmetric combination $\hat{F}_{ij} = \frac{1}{2}(\hat{E}_{ij} + \hat{E}_{ji})$ is Hermitian. Treating the integrals $\{i|j\} = \langle i | \hat{a} | j \rangle$ as a matrix \mathbf{a} and the operators \hat{E}_{ij} and \hat{F}_{ij} as elements of the operator matrices \mathbf{E} and \mathbf{F} introduces a compact notation

$$\hat{A} = \text{Tr}(\mathbf{a} \cdot \mathbf{E}) = \text{Tr}(\mathbf{a} \cdot \mathbf{F}) \quad (2.10)$$

Hence $\text{Tr}(\mathbf{E}) = \mathbf{I}$. For convenience in dealing with the many-particle operators let us assume that i and j indices include symmetry labels Γ and that symmetry Γ_i may be different than Γ_j , so that $\hat{E}_{ij}|R\rangle$ may have different symmetry than $|R\rangle$. The \hat{E}_{ij} operators are classified as raising ($i < j$), weight ($i = j$) and lowering ($i > j$) operators. From the definitions of \hat{E}_{ij} given above it is quite obvious that the weight operator \hat{E}_{ii} is the occupation number operator and thus the particle number operator is

$$\hat{n}_i = \hat{E}_{ii}; \quad \hat{N} = \sum_i \hat{E}_{ii} \quad (2.11)$$

The commutation relations of the shift operators are interesting:

$$\begin{aligned} [\hat{E}_{ij}, \hat{E}_{kl}] &= \sum_q \{ |i(q)\rangle \langle j(q)| |k(q)\rangle \langle l(q)| - |k(q)\rangle \langle l(q)| |i(q)\rangle \langle j(q)| \} \\ &= \sum_q \{ \delta_{jk} |i(q)\rangle \langle l(q)| - \delta_{li} |k(q)\rangle \langle j(q)| \} = \delta_{jk} \hat{E}_{il} - \delta_{li} \hat{E}_{kj} \end{aligned} \quad (2.12)$$

These commutation relations are the same as those of the generators of the general linear group $GL(n)$ and of the generators of the unitary group $U(n)$ (Wormer 1975, Paldus 1976). The symmetry contracted shift operators \hat{E}_{ij} are used here in a slightly more general way than in UGA because the indices i, j refer either to spin orbitals or to orbitals (as in UGA), or to a degenerate subspaces of orbitals, whatever we use to designate the levels of our graph. Introducing a two-particle shift operator

$$\hat{E}_{ijkl} = \sum_{p \neq q} |i(p)\rangle \langle j(p)| |i(q)\rangle \langle l(q)| = a_i^\dagger a_k^\dagger a_l a_j = \hat{E}_{ij} \hat{E}_{kl} - \delta_{jk} \hat{E}_{il} \quad (2.13)$$

commutation relations become equivalent to the symmetry of the indices of this operator, $\hat{E}_{ijkl} = \hat{E}_{klij}$. In the spin orbital space additional relations are possible:

$$\hat{E}_{ijkl} = a_i^\dagger a_k^\dagger a_l a_j = -a_k^\dagger a_i^\dagger a_l a_j = -\hat{E}_{kjil}$$

Hence

$$\begin{aligned} \hat{E}_{ij} \hat{E}_{kl} + \hat{E}_{kj} \hat{E}_{il} &= \delta_{jk} \hat{E}_{il} + \delta_{ij} \hat{E}_{kl} \\ \hat{E}_{ij} \hat{E}_{kl} + \hat{E}_{il} \hat{E}_{kj} &= \delta_{jk} \hat{E}_{il} + \delta_{kl} \hat{E}_{ij} \end{aligned} \quad (2.14)$$

These relations can not be valid in the orbital space because for $i = j = k = l$ it follows that $\hat{n}_i^2 = \hat{n}_i$ and the occupations must be 0,1.

Let us consider now a two-particle operator

$$\hat{\mathbf{B}} = \frac{1}{2} \sum_{p \neq q} \hat{\mathbf{b}}(r_p, r_q) = \frac{1}{2} \sum_{p \neq q} \hat{\mathbf{b}}(p, q) \quad (2.15)$$

Using the identity resolutions we obtain

$$\begin{aligned} \hat{\mathbf{B}} &= \frac{1}{2} \sum_{p \neq q} \mathbf{1}(r_p) \mathbf{1}(r_q) \hat{\mathbf{b}}(r_p, r_q) \mathbf{1}(r_q) \mathbf{1}(r_p) \\ &= \frac{1}{2} \sum_{p \neq q} \sum_{ijkl} |i(p)\rangle \langle k(q)| \langle i(p)| \langle k(q)| \hat{\mathbf{b}}(p, q) |j(p)\rangle |l(q)\rangle \langle j(p)| \langle l(q)| \\ &= \frac{1}{2} \sum_{ijkl} \{ij|kl\} \sum_{p \neq q} |i(p)\rangle \langle j(p)| |k(q)\rangle \langle l(q)| \\ &= \frac{1}{2} \sum_{ijkl} \{ij|kl\} \hat{E}_{ijkl} \\ &= \frac{1}{2} \sum_{ijkl} \{ij|kl\} (\hat{E}_{ij} \hat{E}_{kl} - \delta_{jk} \hat{E}_{il}) \end{aligned} \quad (2.16)$$

With the two-particle integrals

$$\{ij|kl\} = \langle i(r_1)|\langle k(r_2)|\hat{\mathbf{b}}(r_1, r_2)|j(r_1)\rangle|l(r_2)\rangle \quad (2.17)$$

The two-particle Hermitian operator $\hat{F}_{ijkl} = \hat{F}_{ij}\hat{F}_{kl} - \delta_{jk}\hat{F}_{il}$ may be used instead of \hat{E}_{ijkl}

$$\hat{\mathbf{B}} = \frac{1}{2} \sum_{ijkl} \{ij|kl\} \hat{E}_{ijkl} = \frac{1}{2} \sum_{ijkl} \{ij|kl\} \hat{F}_{ijkl} \quad (2.18)$$

One may introduce also higher-order shift operators; they will appear in the perturbation theory expansions and other formalisms. For example three-particle spin independent shift operator is:

$$\begin{aligned} \hat{E}_{ijklmn} &= \sum_{p \neq q \neq t} |i(p)\rangle \langle j(p)||k(q)\rangle \langle l(q)||m(t)\rangle \langle n(t)| \\ &= \sum_{\sigma\tau\rho} a_{i\sigma}^\dagger a_{k\tau}^\dagger a_{m\rho}^\dagger a_{n\rho} a_{l\tau} a_{j\sigma} = \hat{E}_{ij}\hat{E}_{klmn} - \delta_{jk}\hat{E}_{ilmn} + \delta_{jm}\hat{E}_{ilkn} \end{aligned} \quad (2.19)$$

Calculation of matrix elements via Wick's theorem requires the shift operators \hat{E}_{ijji} , \hat{E}_{ijkkji} and similar higher-order operators. Such 'circular' shift operators are also useful in calculation of spin-adapted reduced Hamiltonians (Karwowski *et al* 1986). Operator $\hat{T}_{ij} = \hat{E}_{ijji}$ acting on a state $|L\rangle$ is equivalent to a transposition of i and j orbitals if both i and j are singly occupied in $|L\rangle$. Connection of the shift operators with the reduced density matrices is especially interesting. Expanding one-particle transition density matrix in the orbital basis

$$\begin{aligned} \rho(x|x') &= \langle x|\hat{\rho}|x'\rangle = \sum_{ij} D_{ij} \phi_i(x) \phi_j^*(x') = \sum_{ij} D_{ij} \langle x|i\rangle \langle j|x'\rangle \\ \hat{\rho} &= \sum_{ij} D_{ij} |i\rangle \langle j| = \sum_{ij} D_{ij} \hat{E}_{ij} \end{aligned} \quad (2.20)$$

we find an expansion of the density operator in the \hat{E}_{ij} operator basis. To find the elements of the density matrix D_{ij} let us use Eq (2.8) and Eq (2.20)

$$\langle \Psi|\hat{\mathbf{A}}|\Psi\rangle = \int_{x'=x} \hat{\mathbf{a}}\rho(x|x') dx = \sum_{ij} \{i|j\} D_{ij} = \sum_{ij} \{i|j\} \langle \Psi|\hat{E}_{ij}|\Psi\rangle \quad (2.21)$$

Elements D_{ij} of a density matrix in a state $|\Psi\rangle = \sum_R C_R |R\rangle$ are therefore equal to the expectation value of the \hat{E}_{ij} operator

$$D_{ij} = \langle \Psi|\hat{E}_{ij}|\Psi\rangle = \sum_{R,L} C_R C_L^* \langle L|\hat{E}_{ij}|R\rangle \quad (2.22)$$

$$\text{Tr } \mathbf{D} = \text{Tr} \langle \Psi|\mathbf{E}|\Psi\rangle = \text{Tr} \langle \Psi|\mathbf{F}|\Psi\rangle = 1$$

Let us note that for localized states $|R\rangle$ the matrix $\langle\Psi|\mathbf{F}|\Psi\rangle$ may be interpreted as the “bond order and atomic charges” matrix (cf McWeeny and Sutcliffe 1969). For two-particle density matrix we obtain

$$P_{ijkl} = \langle\Psi|\hat{E}_{ijkl}|\Psi\rangle = \sum_{L,R} C_L^* C_R \langle L|\hat{E}_{ijkl}|R\rangle \quad (2.23)$$

This intimate connection between the shift operators and the reduced density matrix operators justifies the name ‘spin free reduced density operators’ used by Hinze and Broad (1981).

C. Examples of operators in \hat{E}_{ij} basis.

Before the action of the shift operators on states symbolized by the paths of a graph will be considered let us look at some well-known operators expressed in the \hat{E}_{ij} basis. In atomic physics Racah (1949) has introduced an operator basis $\{V_\lambda^a : \lambda = a, \dots -a; a = 0, 1, \dots, 2l\}$ that is very convenient and natural for calculation of matrix elements of tensor operators, especially for $l \leq 3$ (Judd 1979). While the theory of tensor operators became a standard part of more advanced textbooks on quantum mechanics (cf Weissbluth 1978) the simpler basis of the shift operators $\{\hat{E}_{jk} : j, k = 1, 2, \dots, 2l+1\}$, called sometimes the Weyl basis (Biedenharn and Louck 1981), was rediscovered in atomic physics by Harter (Harter 1973; Harter and Patterson 1976). The orthogonal transformation matrix between V_λ^a and \hat{E}_{ij} basis is given in terms of Clebsch–Gordan coefficients

$$\begin{aligned} V_\lambda^a &= \sqrt{\frac{2a+1}{2l+1}} \sum_{mm'} C_{m\lambda m'}^{l a l} \hat{E}_{l-m'+1, l-m+1} \\ \hat{E}_{l-m'+1, l-m+1} &= \sum_{a\lambda} \sqrt{\frac{2a+1}{2l+1}} C_{m\lambda m'}^{l a l} V_\lambda^a \end{aligned} \quad (2.24)$$

Therefore it is quite easy to express angular momentum operators in the Weyl basis (Biedenharn and Louck 1981)

$$\begin{aligned} \hat{L}_{+1} &= \sum_{m_i=-l}^l \sqrt{(l-m)(l+m+1)} \hat{E}_{l-m, l-m+1} \\ \hat{L}_{-1} &= \sum_{m_i=-l}^l \sqrt{(l-m)(l+m+1)} \hat{E}_{l-m+1, l-m} \\ \hat{L}_0 &= \sum_{m_i=-l}^l m \hat{E}_{l-m+1, l-m+1} \\ \hat{L}^2 &= \sum_{q=-1}^{+1} (-1)^q \hat{L}_q \hat{L}_{-q} \end{aligned} \quad (2.25)$$

Harter and Patterson (1976) give explicit expressions for various tensor operators and also discuss mixed atomic configurations (Patterson and Harter 1977). Atomic configurations are also discussed in a series of papers by Kent and Schlessinger (1981,1982). Moshinsky (1966) gives expressions for angular momentum operators and for the pairing interaction operator important in nuclear physics. The \hat{E}_{ij} operators do not depend on the number of particles and thus appear naturally in the Fock space formalism (Kutzelnigg 1984).

The full electronic Hamiltonian is simply a sum of one and two-electron terms:

$$\hat{H} = \sum_{i=1}^N h_1(i) + \frac{1}{2} \sum_{i \neq j} h_2(i, j) = \sum_{ij} \{i|j\} \hat{E}_{ij} + \frac{1}{2} \sum_{ijkl} \{ij|kl\} \hat{E}_{ijkl} \quad (2.26)$$

Approximations to this Hamiltonian assuming zero differential overlap (such as PPP or CNDO models), are of the following form (cf Parr 1964; Pople and Beveridge 1970; Paldus 1976):

$$\hat{H}_a = \sum_i \left(\alpha_i \hat{E}_{ii} + \frac{1}{2} \gamma_{ii} \hat{E}_{ii} (\hat{E}_{ii} - 1) \right) + \sum_{i \neq j} \left(\beta_{ij} \hat{E}_{ij} + \frac{1}{2} \gamma_{ij} (\hat{E}_{ii} - Z_i) (\hat{E}_{jj} - Z_j) \right) \quad (2.27)$$

The Fock operator is particularly simple

$$\hat{F} = \sum_{ij} [\{i|j\} + \sum_h (2\{ij|kk\} - \{ik|jk\})] \hat{E}_{ij} \quad (2.28)$$

Formal structure of the relativistic Hamiltonian in the Pauli or the Dirac form is the same as in the non-relativistic case except that two or four-component spinors appear instead of orbitals and the spin-dependent terms have to be included in the one-particle part:

$$\hat{H}_s = \sum_{ij} \sum_{\sigma\tau} \langle i\sigma | \hat{H}_s | j\tau \rangle \hat{E}_{i\sigma, j\tau} \quad (2.29)$$

The point group operators $\hat{R} \in \mathcal{G}$ are expressed as

$$\begin{aligned} \hat{R} &= \sum_{i,j=1}^{n_l} \sum_{\Gamma_i}^{d(\Gamma^{(i)})} \sum_{\Gamma_j}^{d(\Gamma^{(j)})} \langle i_{\Gamma_i} | \hat{R} | j_{\Gamma_j} \rangle \hat{E}(i_{\Gamma_i}, j_{\Gamma_j}) \\ &= \sum_{i,j=1}^{n_l} \delta(\Gamma^{(i)}, \Gamma^{(j)}) \sum_{\Gamma_i, \Gamma_j=1}^{d(\Gamma^{(i)})} \Gamma^{(i)}(R)_{\Gamma_i \Gamma_j} \hat{E}(i_{\Gamma_i}, j_{\Gamma_j}) \end{aligned} \quad (2.30)$$

where $d(\Gamma^{(i)})$ is the dimension of $\Gamma^{(i)}$ representation. One can not express pure spin operators using the orbital shift operators. However, introducing operators replacing spin functions in a way analogous to the orbital case

$$\hat{E}_{ij} = \sum_{q=1}^N |\Theta_i(\sigma_q)\rangle \langle \Theta_j(\sigma_q)| \quad (2.31)$$

we may express spin operators as:

$$\begin{aligned}\hat{S}_z &= \frac{1}{2}(\hat{\mathcal{E}}_{11} - \hat{\mathcal{E}}_{22}); \quad \hat{S}_+ = \hat{\mathcal{E}}_{12}; \quad \hat{S}_- = \hat{\mathcal{E}}_{21} \\ \hat{S}^2 &= \hat{S}_- \hat{S}_+ + \hat{S}_z(\hat{S}_z + 1) = \hat{\mathcal{E}}_{21} \hat{\mathcal{E}}_{12} + \frac{1}{4}(\hat{\mathcal{E}}_{11} - \hat{\mathcal{E}}_{22})(\hat{\mathcal{E}}_{11} - \hat{\mathcal{E}}_{22} + 1)\end{aligned}\quad (2.32)$$

Let us go back to graphs now. We know the results of the shift operator's \hat{E}_{ij} action on the one-particle states, but graph's paths represents N -particle states. I will designate those states by $|R; \Lambda\rangle$ where R represents the arcs of path and Λ all quantum numbers; because Λ is usually specified for the whole graph in most cases it may be omitted without introducing ambiguities. We would like to know the states that appear when \hat{E}_{ij} acts on a given state:

$$\hat{E}_{ij}|R; \Lambda\rangle = \sum_L C_{LR}^\Lambda |L; \Lambda\rangle \quad (2.33)$$

The coefficients (or blocks of coefficients, if $|R; \Lambda\rangle$ represents more than one state) $C_{LR}^\Lambda = \langle L; \Lambda | \hat{E}_{ij} | R; \Lambda \rangle$ give a matrix representation of \hat{E}_{ij} in the model space. These coefficients depend only on the structure of states $|R; \Lambda\rangle$ and are therefore called structure constants. In the next sections I will calculate them explicitly in different spaces. In case of a $2n$ -level spin-orbital graph \hat{S}_z and/or \hat{L}_z -adapted, each path is equivalent to a determinant. Then $\hat{E}_{ij}|R\rangle$ is either zero or it corresponds to the $|R\rangle$ path with j -th and i -th arcs appropriately changed. When the four-slope n -level graph is used to describe the \hat{S}_z -adapted space $\hat{E}_{ij}|R\rangle$ may be a combination of at most 2 states, if $n_j = 2$ and $n_i = 0$, i.e. of determinants $|\dots i \bar{j} \dots| + |\dots \bar{j} i \dots|$. Much more interesting situations are encountered when a fagot graph such as the three-slope graph of configurations is used. There may be many states associated with a given orbital configuration; if we can obtain them by applying an operator to a product of one-particle states, i.e. if $|R; \Lambda, l\rangle = \hat{\omega}_l^\Lambda |R\rangle$ and $[\hat{\omega}_l^\Lambda, \hat{E}_{ij}] = 0$ then $\hat{E}_{ij}|R; \Lambda, l\rangle = \hat{\omega}_l^\Lambda(\hat{E}_{ij}|R\rangle)$ is represented by a path differing from $|R\rangle$ only in the i -th and j -th arc. In particular this is true for the \hat{S}^2 -adapted spaces and three-slope graphs. Introduction of spatial symmetry simply adds some selection rules if one-dimensional representations are the only allowed, i.e. the shift operators \hat{E}_{ij} should refer to the i and j of the same symmetry, $\delta(\Gamma^{(i)}, \Gamma^{(j)}) \hat{E}_{ij}$, unless they are a part of operator product. The case of atoms and of multidimensional representations will be discussed in Part III.

As already noted, the shift operators, acting in the antisymmetric spaces, are equivalent to products of creation and annihilation operators, i.e.

$$\hat{E}_{ij}^{\sigma\sigma} = a_{i\sigma}^\dagger a_{j\sigma}; \quad \hat{E}_{ij} = \sum_\sigma a_{i\sigma}^\dagger a_{j\sigma}$$

One could rewrite most of Avery's book "Creation and annihilation operators" using the shift operators. However, the creation and the annihilation operators through their anticommutation relations have the antisymmetry principle build into the spaces they act in. They are more natural in context of the Fock space where the number of particles is not preserved. On the other hand the shift operators always preserve the number of particles but do not enforce antisymmetry of the states. Therefore the two sets of operators are equivalent only in the antisymmetric space (restriction on a^\dagger, a) of a fixed particle number (restriction on \hat{E}_{ij}).

2.2

General formulas for matrix elements

In this section I am rederiving in a slightly generalized form a general formula given already by Corson(1951) and Kotani *et al* (1955) – nothing new under the sun. There are two pitfalls one should avoid: one is not being general enough to cover all the cases and the other being so general that the results become impractical (cf Seligman 1981). We are really not interested in any formulas, we would rather like to have graphical rules to calculate matrix elements, but one has to start from something. In the previous section the physical part of matrix element calculation has been separated from the structural one, therefore it is enough to calculate the elements of the shift operators, i.e. structure constants. However, the projection operator approach presented in the last section is clearly not the most general, for example it does not work for the two-slope, \hat{S}^2 -adapted graph of Fig 20c. Here we should use the $\hat{E}_{ij}^{\uparrow\uparrow}, \hat{E}_{ij}^{\downarrow\downarrow}$ shift operators (for typographical convenience $\hat{E}_{i\uparrow j\uparrow}$ is written as $\hat{E}_{ij}^{\uparrow\uparrow}$) but we can not define the one-particle states $|i\uparrow\rangle, |i\downarrow\rangle$. The arrows refer to the spin couplings and have meaning only in context of many-particle states. Although we may formally write:

$$|\Phi\rangle = |2p_0\uparrow\rangle|2p_{-1}\uparrow\rangle|2p_{-1}\downarrow\rangle|2s\downarrow\rangle|2s\uparrow\rangle$$

to designate the first state in Fig 20c, the projection $|2s\downarrow\rangle\langle 2s\downarrow|$ works only for the N -th particle. Fortunately in case of the spin-independent operators we may always use $\hat{E}_{ij} = \hat{E}_{ij}^{\uparrow\uparrow} + \hat{E}_{ij}^{\downarrow\downarrow}$. Because the paths of the two-slope graph are in the one-to-one correspondence with the paths of the four-slope graph (note the same number of states at each $|\uparrow\rangle$ level in Fig 20b and 20c) we may use the same formulas for the elements of \hat{E}_{ij} in both cases. In all \hat{S}^2 -adapted cases we may therefore use \hat{E}_{ij} operators. In \hat{S}_z -adapted graphs we have similarly $\hat{E}_{ij} = \hat{E}_{ij}^{\alpha\alpha} + \hat{E}_{ij}^{\beta\beta}$ and we may use \hat{E}_{ij} for n -level graphs and $\hat{E}_{ij}^{\sigma\sigma}$ for $2n$ -level graphs. When no adaptation to spin operators is

required we can formally have $\hat{E}_{ij}^{\alpha\beta}$ operators, but without spin-dependent terms in the Hamiltonian such operators never appear.

There are two kinds of variables, space and spin, and in the spin-independent case with abelian symmetry group one can separate the contributions from them. Let us designate a state corresponding to a path in some graph that we want to use by $|L, \Sigma\rangle$ with the label L identifying the orbitals appearing in this path and the label Σ giving information about the spin part: for \hat{S}_z -adapted graphs it may simply be a list of α, β functions, for \hat{S}^2 -eigenstates list of up and down segments in the S-diagram.

A state $|L, \Sigma\rangle$ is constructed from the orbital product $|L\rangle$ and the appropriate total spin eigenfunctions $|\Sigma\rangle$ by antisymmetrizing the two:

$$|L, \Sigma\rangle = N_L \hat{A}(|L\rangle|\Sigma\rangle) \quad (2.34)$$

where N_L is the normalization factor and

$$\hat{A} = \frac{1}{N!} \sum_P (-1)^P P$$

is the standard antisymmetrizer. Thus in contrast with many other approaches to \hat{S}^2 eigenfunctions (Pauncz 1979) we assume that the spin eigenstates $|\Sigma\rangle$ are constructed before antisymmetrization is performed. The permutation P in the antisymmetrizer acts on the space as well as on the spin coordinates, $P = P_r P_\sigma$. If a transposition $(i \ i + 1)$ leaves $|L\rangle$ invariant it must change the sign of $|\Sigma\rangle$ to preserve antisymmetry. Using relation $\hat{A}^\dagger \hat{A} = \hat{A}$ we easily find:

$$\begin{aligned} \langle L, \Sigma | \hat{E}_{ij} | R, \Theta \rangle &= N_L N_R \langle L | \langle \Sigma | \hat{E}_{ij} \hat{A} | R \rangle | \Theta \rangle = \\ &= \frac{N_L N_R}{N!} \sum_P (-1)^P \langle L | \langle \Sigma | \hat{E}_{ij} P_r P_\sigma | R \rangle | \Theta \rangle \end{aligned} \quad (2.35)$$

The permutations and the replacement operators commute; if \hat{E}_{ij} operators are used they do not act on the spin variables, if $\hat{E}_{ij}^{\alpha\alpha} + \hat{E}_{ij}^{\beta\beta}$ or $\hat{E}_{ij}^{\uparrow\uparrow} + \hat{E}_{ij}^{\downarrow\downarrow}$ are used they also leave spin functions unchanged. Therefore we may write:

$$\langle L, \Sigma | \hat{E}_{ij} | R, \Theta \rangle = \frac{N_L N_R}{N!} \sum_P (-1)^P \langle \Sigma | P | \Theta \rangle \langle L | \hat{E}_{ij} P | R \rangle$$

where subscripts σ and r are dropped because there is no ambiguity, each permutation being enclosed in separate brackets. The normalization coefficients are easily calculated taking instead of \hat{E}_{ij} a unit operator. For \hat{S}^2 eigenfunctions with D_R doubly occupied orbitals in $|R\rangle$ only 2^{D_R} 'inner' permutations of the doubles that do not change $|R\rangle$ are then left (for orthogonal orbitals) and for these permutations $P|\Theta\rangle = (-1)^P|\Theta\rangle$ to preserve antisymmetry of $|R, \Theta\rangle$. For \hat{S}_z eigenfunctions $D_R = 0$ because $P|\Theta\rangle$ gives for these permutations always another function, orthogonal to $|\Theta\rangle$. There is an obvious

graphical interpretation of this fact: if the M-diagram path with $+ -$ arcs belong to the diagram the path with $- +$ arcs also belongs to it, while in the S-diagram spins corresponding to doubly occupied orbital are always $+ -$. The concept of a doubly occupied orbital is applicable only to \hat{S}^2 eigenfunctions. The normalization coefficient is

$$\langle R, \Theta || R, \Theta \rangle = 1 = \frac{N_R^2}{N!} \sum_P \langle L | P | R \rangle = \frac{N_R^2}{N!} 2^{D_R}$$

and the final formula, with $D_L = D_R = 0$ for \hat{S}_z eigenfunctions is

$$\langle L, \Sigma | \hat{E}_{ij} | R, \Theta \rangle = 2^{-\frac{1}{2}(D_L + D_R)} \sum_P (-1)^P \langle \Sigma | P | \Theta \rangle \langle L | \hat{E}_{ij} | P | R \rangle \quad (2.36)$$

In context of \hat{S}^2 eigenfunctions this formula was rediscovered and rederived many times (cf Corson 1951; Kotani *et al* 1955; Harris 1967; Ruedenberg 1971; Ruedenberg and Poshusta 1972; Karwowski 1973; Sarma and Rettrup 1977; Wormer and Paldus 1979; Duch and Karwowski 1982). Because it contains a sum over all permutations it is a starting point of the symmetric group approach to the matrix element calculations (Duch and Karwowski 1981–1985). In particular matrices of spin integrals $\langle \Sigma | P | \Theta \rangle$ and the matrices $U(P)$ defined below form a representation of the symmetric group and it is convenient to call them ‘representation matrices’ similarly as it is convenient to call the shift operators ‘generators’. Here however no properties of the symmetric group will be invoked and the general formula we derive is only an intermediate step towards graphical rules.

There are two improvements that I will make in the last equation. First, for \hat{S}^2 eigenfunctions, all 2^{D_R} permutations P acting on $|R\rangle$ give the same result, as also do 2^{D_L} permutation acting on $|L\rangle$ (mathematicians call it “a double coset”). Choosing P_0 as one of these permutations giving non-zero element $\langle L | \hat{E}_{ij} | P | R \rangle$ in Eq (2.36) a factor 2^{D_L} is introduced and the sum is reduced to a single element. In front of the sum $\sqrt{2}^{n_i + n_j - 1}$ coefficient is left. To prove it consider 3 cases: first take $D_L = D_R$ and $n_i + n_j = 1$, i.e. $n_i = 0, n_j = 1$ for \hat{E}_{ij} operator. The normalization factor 2^{-D_L} cancels the number of identical terms 2^{D_L} from sum over permutations. Suppose now that $n_i + n_j = 2$, corresponding to $n_i = 0, n_j = 2$ (for $n_i = n_j = 1$ the same result is obtained) and $D_R = D_L + 1$. There are two classes of permutations giving non-zero overlaps in Eq (2.36), differing on a transposition ($j j'$) of the two orbitals belonging to the doubly occupied orbital j . Each class has 2^{D_L} elements, making the numerical factor equal to $2^{-\frac{1}{2}(2D_L + 1) + D_L + 1} = \sqrt{2}$. Finally for $n_i + n_j = 3$ we have $D_L = D_R$ and the same two classes of permutations make the coefficient equal 2. Collecting these cases together coefficient $\sqrt{2}^{n_i + n_j - 1}$ is taken. In \hat{S}_z case $n_i + n_j = 1$, i.e. the scalar coefficient is always one; the sum over all permutations is reduced to at most two terms. They appear when \hat{E}_{ij} acts on $|R\rangle$ with occupations $n_i = 0, n_j = 2$. If in $|R, \Theta\rangle$ we have

$|\dots j(k)j(k+1)\dots\rangle$ the two permutations are $P_0 - (k\ k+1)P_0$, where the minus sign has to remind that the two contributions are of opposite sign.

Second improvement, due to Karwowski (1973), is the following: instead of acting with P on the space variables of $|R\rangle$ we may act on the orbital indices of $|L\rangle$. Because in Eq (2.36) $\hat{E}_{ij}|R\rangle = |L'\rangle = P^{-1}|L\rangle = |PL\rangle$ the orbital factor is $\langle L|\hat{E}_{ij}P|R\rangle = \langle PL|\hat{E}_{ij}|R\rangle$. This is very convenient especially in the graphical context. The final form of the matrix element equation is:

$$\langle L, \Sigma|\hat{E}_{ij}|R, \Theta\rangle = \sqrt{2^{n_i+n_j-1}}(-1)^{P_0}\langle \Sigma|P_0|\Theta\rangle\langle P_0L|\hat{E}_{ij}|R\rangle \quad (2.37)$$

with P_0 replaced by $(I + \delta_{n_i,0}\delta_{n_j,2}(k\ k+1))P_0$ in \hat{S}_z eigenspaces. We could proceed now directly to applications, but let us fool for a while with the 'matrix build-up', that is let us convert this equation to an equation for the whole block of elements. If $|L\rangle$ is an orbital product all $\hat{O} = \mathbf{I}$, \hat{S}_z or \hat{S}^2 -adapted spin functions share the same $\langle PL|\hat{E}_{ij}|R\rangle$ factor, so designating the subspace of these states by $|R : \hat{O}\rangle$ we have a structure constants matrix

$$\langle L : \hat{O}|\hat{E}_{ij}|R : \hat{O}\rangle = \mathbf{U}(P_0)\langle PL|\hat{E}_{ij}|R\rangle \quad (2.38)$$

with $\mathbf{U}(P_0)$ matrix

$$\mathbf{U}(P_0)_{\Sigma,\Theta} = \begin{cases} \sqrt{2^{n_i+n_j-1}}(-1)^{P_0}\langle \Sigma|P_0|\Theta\rangle & \text{for } \hat{S}^2 \\ (-1)^{P_0}[\langle \Sigma|P_0|\Theta\rangle + \delta_{n_i,0}\delta_{n_j,2}\langle \Sigma|(k\ k+1)P_0|\Theta\rangle] & \text{for } \hat{S}_z \end{cases} \quad (2.39)$$

We could go a step further and introduce 'superstructures': for example, in the atomic case we may define:

$$\{p|d\}\hat{E}_{pd} = \sum_{k=-1,0,1} \{p_k|d_k\}\hat{E}_{p_k d_k} \quad (2.40)$$

and work with a graph of configurations (cf Fig 22), setting up matrix elements between all states belonging to the subspaces corresponding to the two configurations, i.e.

$$\langle \mathcal{M}_L : \hat{O}|\{i|j\}\hat{E}_{ij}|\mathcal{M}_R : \hat{O}\rangle = \mathbf{U}(P)\tilde{\otimes}\mathbf{W}(P : \hat{E}_{ij}) \quad (2.41)$$

where $\tilde{\otimes}$ means that each element of \mathbf{W} depending on the number of singles and the permutation P is multiplied by the matrix $\mathbf{U}(P)$ of appropriate dimensions. A simple example will illustrate this idea clearly. In Fig 24 the two uppermost paths designate $5d^3$ and $5d^26s$ configurations. Let us take (\hat{L}_z, \hat{S}^2) -adapted space and $\{6s|5d\}\hat{E}_{6s,5d} = \{6s|5d_0\}\hat{E}_{6s,5d_0}$ operator. The two configurations in \hat{L}_z space are resolved into:

$$\begin{aligned} 5d^3 &= \{d_{+2}d_{-1}^2; d_{+2}d_0d_{-2}; d_{+1}^2d_{-2}; d_1d_0d_{-1}\} \\ 5d^26s &= \{d_{+2}d_{-2}s; d_{+1}d_{-1}s; d_0^2s\} \end{aligned} \quad (2.42)$$

Therefore $\langle \mathcal{M}_{5d^2 6s} : \hat{S}^2 | \hat{E}_{6s,5d_0} | \mathcal{M}_{5d^3} : \hat{S}^2 \rangle$ element is a 3×4 matrix \mathbf{W} , with two non-zero submatrices:

$$\langle d_{+2}d_{-2}6s : \hat{S}^2 | \hat{E}_{6s,5d_0} | d_{+2}d_0d_{-2} : \hat{S}^2 \rangle; \quad \langle d_{+1}d_{-1}6s : \hat{S}^2 | \hat{E}_{6s,5d_0} | d_{+1}d_0d_{-1} : \hat{S}^2 \rangle$$

multiplied by the $\mathbf{U}((2,3))$ matrix. For doublet states \mathbf{U} is a 2×2 matrix and when we sum the dimensions of submatrices the element $\langle \mathcal{M}_{5d^2 6s} : \hat{S}^2 | \hat{E}_{6s,5d_0} | \mathcal{M}_{5d^3} : \hat{S}^2 \rangle$ is not a 3×4 but a 5×6 matrix. This element may now be transformed to the $\hat{\mathbf{L}}^2$ -adapted basis.

As we can see from this example in the formula Eq (2.37) orbital factors $\langle PL | \hat{E}_{ij} | R \rangle$ simply pick up a permutation P that gives non-zero overlap. In case of the two-particle operator $\hat{\mathbf{B}}$ one should extract from the four-fold sum Eq (2.16) the part that connect the two states on left and right side (Duch and Karwowski 1982). Diagonal part, connecting identical states is:

$$\hat{\mathbf{B}}_0 = \frac{1}{2} \sum_i \{ii|ii\} \hat{n}_i (\hat{n}_i - 1) + \sum_{i < j} [\{ii|jj\} \hat{n}_i \hat{n}_j + (\hat{E}_{ij} \hat{E}_{ji} - \hat{n}_i) \{ij|ij\}] \quad (2.43)$$

The part connecting two states differing on one orbital is:

$$\hat{\mathbf{B}}_1 = \sum_k \{ij|kk\} (\hat{n}_k - \delta_{jk}) \hat{E}_{ij} + \sum_{k \neq i,j} \{ik|jk\} \hat{E}_{kj} \hat{E}_{ik} \quad (2.44)$$

Configurations differing on two orbitals select the following part:

$$\hat{\mathbf{B}}_2 = 2^{-\delta_{ik}\delta_{jl}} \{ij|kl\} \hat{E}_{ij} \hat{E}_{kl} + (1 - \delta_{ik})(1 - \delta_{jl}) \{il|kj\} \hat{E}_{il} \hat{E}_{kj} \quad (2.45)$$

A useful form of the one-particle operator is:

$$\hat{\mathbf{A}} = \sum_{ij} \{i|j\} \hat{E}_{ij} = \sum_i \{i|i\} \hat{n}_i + 2 \sum_{i < j} \{i|j\} \hat{F}_{ij} \quad (2.46)$$

To find similar resolution for the two-particle operator the four-fold sum must be separated into sums over: all indices different, a pair of indices equal (6 possibilities), two pairs of indices equal (3 possibilities), three indices equal (4 possibilities) and all four indices equal. Representing i, j, k, l as four dots in the corners of a square we may symbolically write

$$\begin{aligned} \sum_{ijkl} = & \begin{array}{ccccccc} \cdot & \cdot & & & & & \\ \cdot & & \text{---} & & & & \\ & & \text{---} & & | & & | \\ & & & & | & & | \\ & & & & \diagdown & & \diagup \\ & & & & & & \end{array} \\ & + \begin{array}{ccccccc} \text{---} & & & & & & \\ | & & & & & & \\ | & & & & & & \\ \diagdown & & & & & & \\ \diagup & & & & & & \end{array} \\ & + \begin{array}{ccccccc} \text{---} & | & & & & & \\ | & | & & & & & \\ \diagdown & & \times & & & & \\ \diagup & & & & & & \\ \text{---} & \text{---} & & & & & \\ | & & & & & & \\ \diagdown & & & & & & \\ \diagup & & & & & & \\ & & & & & & \square \end{array} \quad (2.47) \end{aligned}$$

where equal indices are joined together. Separating further the sums into $i < j < k < l$ components we obtain

$$\begin{aligned}
\hat{\mathbf{B}} &= \frac{1}{2} \sum_{ijkl} \{ij|kl\} \hat{E}_{ijkl} \\
&= \sum_{i<j<k<l} \left[\{ij|kl\} (\hat{E}_{ij} \hat{E}_{kl} + \hat{E}_{ij} \hat{E}_{lk}) \right. \\
&\quad + \{il|jk\} (\hat{E}_{il} \hat{E}_{jk} + \hat{E}_{il} \hat{E}_{kj}) \\
&\quad \left. + \{ik|jl\} (\hat{E}_{ik} \hat{E}_{jl} + \hat{E}_{ik} \hat{E}_{lj}) \right] \\
&+ \sum_{i<j<k} \left[\{ii|jk\} \hat{n}_i \hat{E}_{jk} + \{ij|ik\} (\hat{E}_{ij} \hat{E}_{ik} + \hat{E}_{ij} \hat{E}_{ki}) \right. \\
&\quad + \{ik|jj\} \hat{n}_j \hat{E}_{ik} + \{ij|jk\} (\hat{E}_{jk} \hat{E}_{ij} + \hat{E}_{kj} \hat{E}_{ij}) \\
&\quad \left. + \{ij|kk\} \hat{n}_k \hat{E}_{ij} + \{ik|jk\} (\hat{E}_{jk} \hat{E}_{ik} + \hat{E}_{kj} \hat{E}_{ik}) \right] \\
&+ \sum_{i<j} \left[\{ii|jj\} \hat{n}_i \hat{n}_j + \{ij|ij\} \left(\frac{1}{2} \hat{E}_{ij} \hat{E}_{ij} + \hat{E}_{ij} \hat{E}_{ji} - \hat{n}_i \right) \right. \\
&\quad \left. + \{ii|ij\} \hat{E}_{ij} \hat{n}_i + \{ij|jj\} \hat{n}_j \hat{E}_{ij} \right] \\
&+ \frac{1}{2} \sum_i \{ii|ii\} \hat{n}_i (\hat{n}_i - 1) + \text{h.c.}
\end{aligned} \tag{2.48}$$

where h.c. designates the missing Hermitian conjugate operators contributing to the half of the $\hat{\mathbf{B}}$ operator. The shift operators above make the i -th level always more occupied in $\langle L|$ so if the two paths L, R start to diverge at this level and reversed lexical ordering is used L precedes R and the operator $\hat{\mathbf{B}}$ without the h.c. part may be converted to the lower half of the \mathbf{B} matrix, the upper being its Hermitian conjugate.

In spin-orbital case the two-particle operator has much simpler form. Using Eq (2.14) and defining $\{ij|kl\}_A = \{ij|kl\} - \{il|jk\}$ we find

$$\begin{aligned}
\hat{\mathbf{B}} &= \frac{1}{4} \sum_{i \neq j \neq k \neq l} \{ij|kl\}_A \hat{E}_{ij} \hat{E}_{kl} \\
&+ \sum_{i \neq j \neq k} \{ii|jk\}_A \hat{n}_i \hat{E}_{ik} + \sum_{i < j} \{ii|jj\}_A \hat{n}_i \hat{n}_j \\
&= \sum_{i < j < k < l} \left[\{ij|kl\}_A \hat{E}_{ij} \hat{E}_{kl} + \{ij|lk\}_A \hat{E}_{ij} \hat{E}_{lk} + \{ik|jl\}_A \hat{E}_{ik} \hat{E}_{jl} \right] \\
&+ \sum_{i < j < k} \left[\{ii|jk\}_A \hat{n}_i \hat{E}_{jk} + \{ik|jj\}_A \hat{n}_j \hat{E}_{ik} + \{ij|kk\}_A \hat{n}_k \hat{E}_{ij} \right] \\
&+ \sum_{i < j} \{ii|jj\}_A \hat{n}_i \hat{n}_j + \text{h.c.}
\end{aligned} \tag{2.49}$$

Summing up, this section has introduced standard formulas for matrix elements with some extensions in their interpretation. Now we are ready to set the rules for graphical calculation of matrix elements.

2.3

Matrix elements in the \hat{S}_z and \hat{L}_z -adapted spaces

Calculation of matrix elements in the \hat{S}_z -adapted space will serve as a simple application of the previous paragraph's general formalism. It will also serve as a preparation for more complex applications discussed in the next sections. In \hat{S}_z -adapted case $|L, \Sigma\rangle$ in Eq (2.37) represents a determinant, $|L\rangle$ designating the orbital product and $|\Sigma\rangle$ the product of α, β spin functions corresponding to these orbitals. The orbital configurations are represented by the three-slope graph (cf Fig 7, 8, 32) and the primitive spin functions by the M-diagram (Fig 9). Alternatively, the $|L, \Sigma\rangle$ states are represented by non-fagot graphs (cf Fig 4–8). The elements $\langle L\Sigma | \hat{O} | R\Theta \rangle$ may be obtained directly from these graphs (Duch 1985c) analyzing the paths corresponding to $|L, \Sigma\rangle$ and $|R, \Theta\rangle$. Let us start from analysis of the three-slope graph and the associated M-diagrams. Purely graphical method is presented first, with a more direct and computationally attractive approach evolving from it. The use of the four-slope and other non-fagot graphs is discussed later in this section. Because the \hat{L}_z and (\hat{L}_z, \hat{S}_z) -adapted spaces have also determinantal bases the same techniques as for \hat{S}_z eigenfunctions are applicable.

A. The three-slope graphs.

Our goal is to find the $\langle L : \hat{S}_z | \hat{O} | R : \hat{S}_z \rangle$ matrices of structure constants, Eq (2.39). In a way this task is trivial, because in determinantal spaces Slater rules are all that one needs. The most time-consuming part of calculations is then finding the pairs of interacting determinants and this is very efficiently done using graphical description of many-particle bases. Moreover, we would like to avoid all references to determinants, dealing rather with orbital configurations. For a given M value the dimension of structure constants matrices is $d(s_L, M) \times d(s_R, M)$, where

$$d(s_L, M) = \frac{s_L!}{(\frac{1}{2}s_L + M)!(\frac{1}{2}s_L - M)!} \quad (2.50)$$

is the number of different spin functions $|\Sigma\rangle$ associated with the orbital configuration $|L, \Sigma\rangle$. We would like to obtain the whole matrices simultaneously. It is enough to consider operators \hat{O} that are products of shift operators. The number of intermediate determinants in the matrix product

$$\begin{aligned} \langle L : \hat{S}_z | \hat{E}_{ij} \hat{E}_{kl} | R : \hat{S}_z \rangle &= \langle L : \hat{S}_z | \hat{E}_{ij} \sum_K (|K : \hat{S}_z\rangle \langle K : \hat{S}_z|) \hat{E}_{kl} | R : \hat{S}_z \rangle \\ &= \langle L : \hat{S}_z | \hat{E}_{ij} | I : \hat{S}_z \rangle \langle I : \hat{S}_z | \hat{E}_{kl} | R : \hat{S}_z \rangle \end{aligned} \quad (2.51)$$

is not $d(s_I, M)$ but at most 2. Once we know how to calculate the structure constants matrices for single operators the calculation for products of two or more operators is straightforward.

The general idea is as follows: in (2.39) the $\langle PL | \hat{E}_{ij} | R \rangle$ factor fixes the permutation P and is either zero or one. Because $D_{LR} = 0$ for determinants apart from the sign $(-1)^P$ elements of $U(P)$ matrix are equal to $\langle \Sigma | P | \Theta \rangle$. For a fixed P this matrix has only one non-zero element in each column. To find this element we may represent $|\Theta\rangle$ using M-diagram and perform the permutation P on its segments obtaining a path corresponding to $|\Sigma\rangle$; entry in column corresponding to $|\Theta\rangle$ is in the row $|\Sigma\rangle$, where the column and the row are identified by the lexical indices of the M-diagram paths. The permutation P depends on $|L\rangle$ and $|R\rangle$ and \hat{E}_{ij} . If the number of different permutations is rather small one may create a table, with P identifying the rows and with $d(s_R, M)$ columns, the table containing for each P non-zero values of $U(P)$. Calculation of matrix elements is then reduced to the identification of P and looking up the result in the table.

Before carrying out this general idea let's get graphical, as the saying goes, and develop a method of calculation that does not use any algebra. What corresponds to matrix element in the graphical terms? A pair of many-particle states or configurations is essential. Such a pair represented by two paths in a graph forms a loop. The concept of a *loop* is fundamental to our further considerations. I shall introduce some language to deal with the loops (cf Shavitt 1981; Duch and Karwowski 1981). Loops are composed of *segments* i.e. pairs of arcs of the two paths forming the loop. Parallel segments are made from two arcs of the same type. At each level of the graph the loop has certain *width* or a distance between the segments (counted in the number of particles for three-slope graphs). The loop starts at the first level counting from the top, where a nonparallel segment called the *top segment* is placed. The head of the graph is connected to the top segment by a fragment of the path called the *upper walk* that is identical in both paths forming the loop. The lowest nonparallel segment is called the *bottom segment* and the path below it the *lower walk*. The *loop range* or the *loop body* lies between its top and bottom segments. If the width of the loop inside the loop range is different from zero the loop is called *open*, otherwise it is called *closed*. The *value* of a loop is equal to the corresponding element (or a matrix) of structure constants. If this value is non-zero for some operator we say that the two configurations forming the loop are interacting.

B. Classification of loops in the three-slope graphs.

It is possible to reduce a loop to a more simple form. In Fig 40 first all parallel segments of empty and doubly occupied arcs are removed from the loop body, then the remaining parallel arcs are also removed, bringing the loop to its prototype or elementary shape. In this case two segments are left.

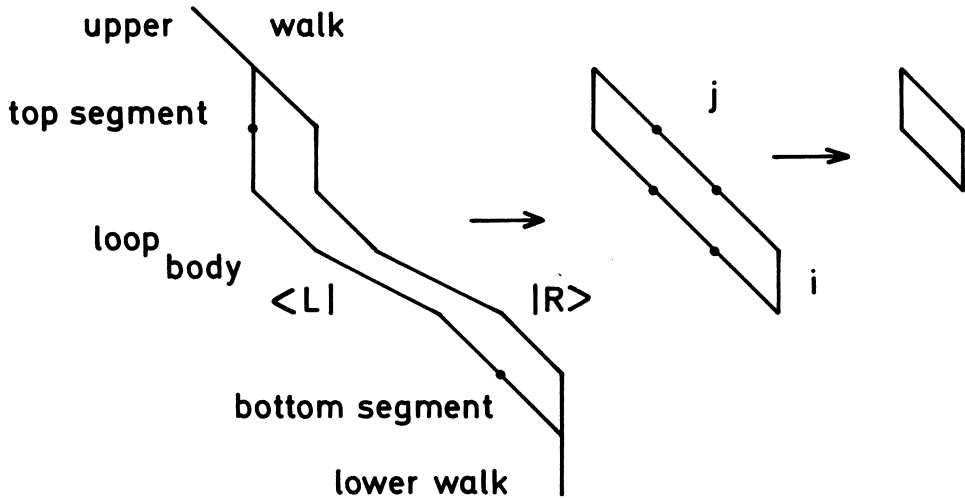


Fig 40. Reduction of a loop to the elementary shape.

I will classify the loops by their elementary forms. All loops that have p nonparallel segments may be reduced to p -segment elementary loops and therefore are called p -segment loops. The segments are designated in the text by their occupation numbers: $|01|$ is the top, $|10|$ the bottom segment in the reduced loop of Fig 40. Another useful way of referring to the segments is by giving their numbers in the ternary system, i.e. segment $|kl|$ has number $3k + l$. This convention gives a compact representation of the loops, for example the $|01|, |10|$ loop is designated now $[13]$. If we call the top segment level i and the bottom segment level j this loop has non-zero value only for \hat{E}_{ij} shift operator. Thus the loop automatically selects matrix elements.

The segment $|kl|$ either increases the width of the loop ($k < l$), decreases if ($k > l$), or if it is a parallel segment ($k = l$) it does not change the width. There are only two segments increasing the width on one particle, $|01|$ and $|12|$, and two adjoint segments decreasing the width on one, $|10|$ and $|21|$. The segment $|02|$ increases the width on two occupations. The sum of all increments of the loop's width (of course it must be equal to the sum of all decrements) is equal to the number of shift operators if the loop value has to be non-zero. Combining increasing segments with the decreasing ones

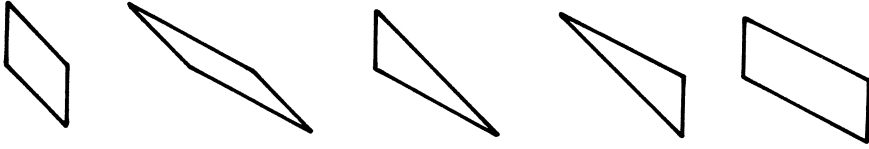
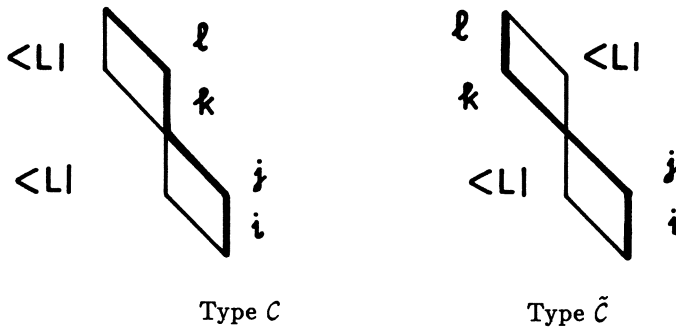


Fig 41. Elementary two-segment loops.

four elementary loops are obtained, [13], [57], [17] and [53], as shown in Fig 41. These loops are called simple; replacing their segments by the adjoint segments adjoint loops [31], [75], [35] and [71] are obtained. The fifth two-segment loop, [26], is composed of $|02\rangle$, $|20\rangle$ segments and has non-zero value only for $\hat{E}_{ij}\hat{E}_{ij}$ product of the shift operators.

The three-segment loops are obtained from one $|02\rangle$ (or $|20\rangle$) segment and two decreasing (or increasing) ones. There are 4 loops with $|02\rangle$ at the top: [233], [237], [273] and [277]. Moving $|02\rangle$ segment to the middle or to the bottom of a loop leads to additional 8 elements, as shown in Fig 42. Placing the $|02\rangle$ segment in the middle makes crossing of the two arcs of this segment unavoidable. If we choose the $|L\rangle$ path as the left one at the bottom segment in the reversed lexical ordering of the paths its lexical index is larger than that of $|R\rangle$ path, and the corresponding matrix element is in the lower triangle (to the left of diagonal) of the final matrix. The two shift operators $\hat{E}_{ij}\hat{E}_{kl}$ involved in this matrix element have either $j = l$ or $i = k$. The four-segment case may be partially combined from the two-segment loops. In this way 16 elementary shapes are obtained. Each of these closed loops (Fig 43) corresponds to two matrix elements depending on the way paths $|L\rangle$ and $|R\rangle$ are chosen. If the $|L\rangle$ path is always on the left side the loop is called the C type, otherwise it is called the \tilde{C} type loop.



Another elementary shapes are obtained if the two middle segments in closed loops are exchanged, giving 16 new loops of open type. All two, three and four-segment loops fit very well in a rather small part of a full graph shown in Fig 44.

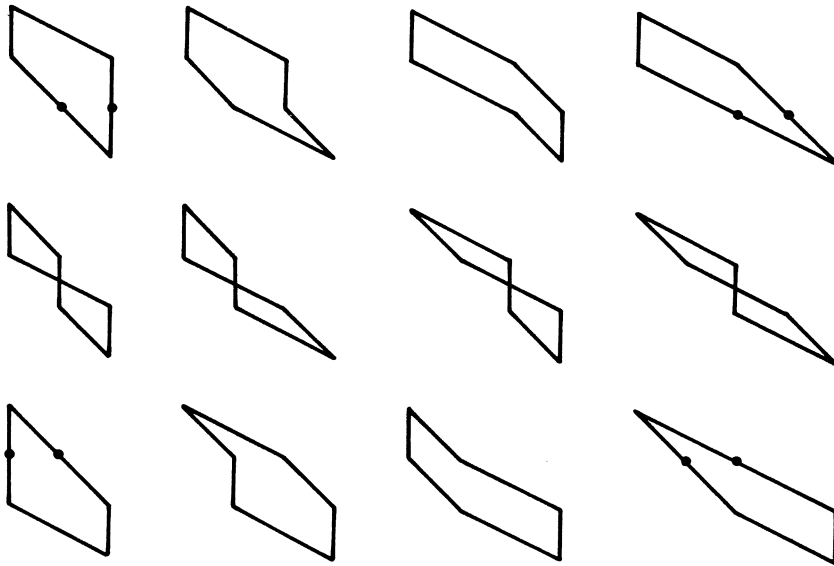


Fig 42. Elementary three-segment loops.

Instead of the usual weights the number of elementary loops is inscribed in the vertices at which the loops terminate. This picture also shows how many orbitals and particles are involved in each loop, for example, there are 12 elementary four-segment loops each involving 5 particles.

The analysis of the configuration space, as described by the three-slope graphs, is now complete. Fortunately separate analysis of all the loops is not necessary. In the \hat{S}^2 -adapted spaces two-segment loops are all we need.

C. Graphical rules for matrix elements.

Parallel segments with empty or doubly occupied arcs do not contribute to the loop value. It is obvious that dropping the empty segments no information is lost. Dropping a parallel segment with doubly occupied arcs amounts to removing a doubly occupied orbital from both configurations. Moving $\phi\alpha\phi\beta$ spinorbital pair has no influence on the determinant; once it occupies the same positions in both determinants partial integration may be performed to remove it. Calculation of lexical indices corresponding to $|\Sigma\rangle, |\Theta\rangle$ should be done using M-diagram that describes spin functions of the singly occupied orbitals only. Therefore the half-reduced loop in Fig 40 contains enough information to calculate matrix elements. We do not even need the labels of the parallel

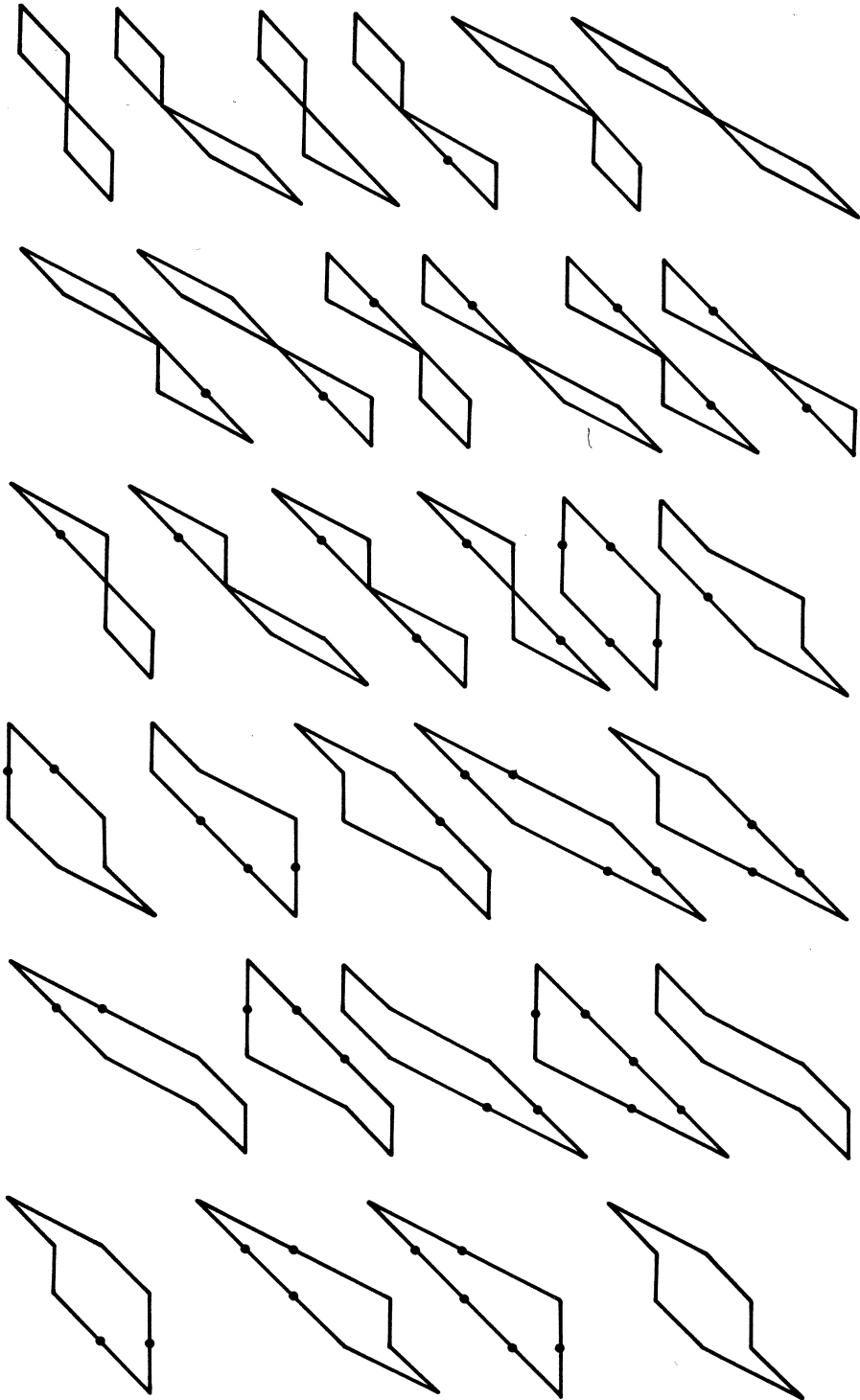


Fig 43. Elementary four-segment loops.

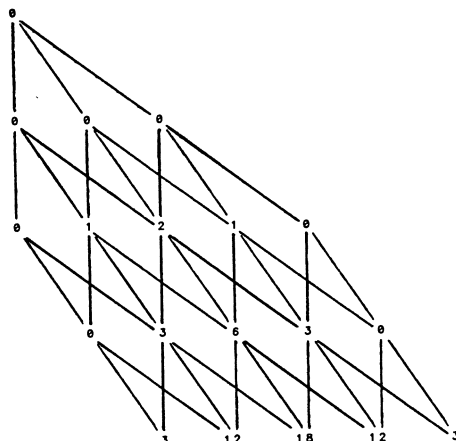
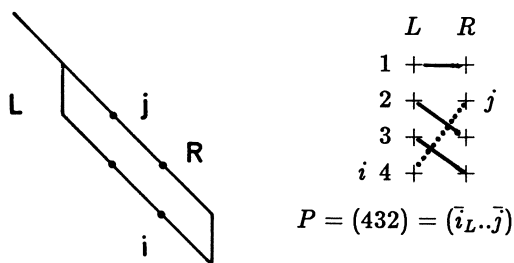


Fig 44. All two, three and four-segment elementary loops fit in this graph. Their number is inscribed in the vertices.

segments, just the number of singles in the upper and lower walks. The i and j labels of the top and bottom segments tell us that the loop has non-zero value for the $\hat{E}_{i,j}$ operator multiplied (Eq 2.8, 2.48) by an appropriate integral. Let us take the [13] loop of Fig 40 and find the structure constants, i.e. interacting $|\Sigma\rangle$ and $|\Theta\rangle$ paths in the corresponding M-diagram. This will be done in two steps. First, permutation P that puts the orbitals in $|L\rangle$ at the same positions they have in $\hat{E}_{i,j}|R\rangle$, thus making $\langle PL|\hat{E}_{i,j}|R\rangle$ factor in Eq (2.38) non-zero, is found. Second, P is applied to $|\Theta\rangle$ functions associated with $|R\rangle$, giving non-zero elements equal ± 1 of $U(P)$ structure constants matrix, $P|\Theta\rangle = |\Sigma\rangle$, with $(-1)^P$ giving the signs. In Fig 40 there is one single in the upper walk and 3 singles in the loop range. The permutation that moves the arc i , that is the 4-th singly occupied arc in $|L\rangle$, to the same position that j has in $|R\rangle$ or as i has in $|L'\rangle = \hat{E}_{i,j}|R\rangle$ is $P = (432)$, as is evident from the diagram below.



The orbitals are represented here by + symbols; those that are identical in L and R are joined together by solid lines, those that are identical in L and L' are joined together by dotted lines. These diagrams (cf Karwowski 1973) are very useful when orbital orderings in two configurations are compared.

Remark: Two basic interpretations of permutations are in use: active (cf Hamermesh 1962) and passive (cf Pauncz 1979). In the active interpretation permutations refer to places rather than objects, i.e. $(123)(\alpha(1)\beta(2)\alpha(3)) = (12)(\alpha(1)\beta(3)\alpha(2)) = \alpha(3)\beta(1)\alpha(2) = \beta\alpha\alpha$, transposition (12) always changing the objects in places 1, 2. In the passive interpretation permutations refer to the original objects,

as in $(123)(\alpha(1)\beta(2)\alpha(3))=(12)(\alpha(1)\beta(3)\alpha(2))=\alpha(2)\beta(3)\alpha(1)=\alpha\alpha\beta$. This may also be expressed as $(123)(\alpha\beta\alpha)=(12)(\alpha\alpha\beta)=\alpha\alpha\beta$, i.e. (123) acts as (12) applied to the result of (23). For this reason the passive interpretation is used throughout this work.

A permutation P may act on a function $|\Theta\rangle=\prod_{i=1}^N |\theta_{\lambda_i}(\sigma_i)\rangle$ in 3 ways: it may permute variables σ_i , or the indices λ_i or move the functions from their absolute positions i . The cyclic permutation $(p..q)=(234)=(23)(34)=(\begin{smallmatrix} 234 \\ 342 \end{smallmatrix})$ moves an object from position 4 to 3, 3 to 2 and 2 to 4, i.e. for $p < q$ it shifts to the left (or up in diagrams), placing an object from the p -th place at the q -th place. The inverse cyclic permutation $(q..p)=(432)$ shifts to the right (or down), placing an object from the q -th place at the p -th place. A permutation P acting on variables is equivalent to an inverse permutation P^{-1} acting on the indices of the functions, ex:

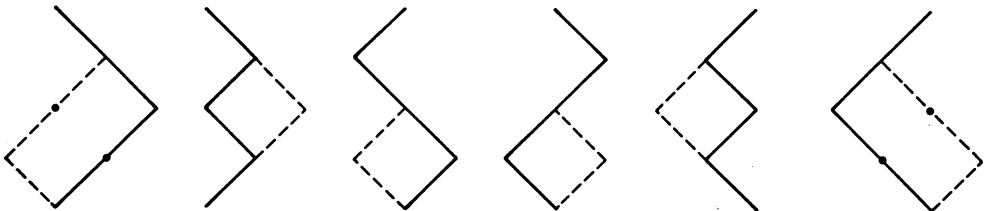
$$\begin{aligned} (234)|\theta_1(1)\theta_2(2)\theta_3(3)\theta_4(4)..> &= |\theta_1(1)\theta_2(3)\theta_3(4)\theta_4(2)..> \\ &= |\theta_1(1)\theta_4(2)\theta_2(3)\theta_3(4)..> = |(432)\theta_1(1)\theta_2(2)\theta_3(3)\theta_4(4)..> \end{aligned}$$

where (432) acts on the indices of the functions rather than on their variables. The same result is achieved when the $(p..q)$ permutation is applied to the functions at their 'absolute positions', i.e. each successive transposition ($k\ k+1$) exchanges functions standing at the positions k and $k+1$. In our example:

$$(234)|\Theta\rangle=(23)|\theta_1(1)\theta_2(2)\theta_4(3)\theta_3(4)..>=|\theta_1(1)\theta_4(2)\theta_2(3)\theta_3(4)..>$$

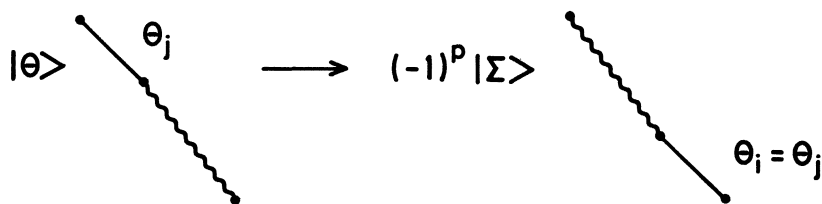
To specify the permutation in a general form let us introduce symbols \bar{i}_K, \bar{j}_K to designate the positions of i and j arcs among other singly occupied arcs (orbitals) in a configuration $|K\rangle$; for example $\bar{j}_R = 2$ in $|R\rangle$ and $\bar{i}_L = 4$ in $|L\rangle$. These positions refer directly to the levels at which the corresponding M-diagram arcs are placed. The position of i in $|R\rangle$ would have been $\bar{i}_R = 5$ if it had been present there. Doubly occupied and unoccupied arcs may have a position assigned too. This should be the position that these arcs would have had they been singly occupied. For example, if we characterize an orbital configuration by its occupation numbers and one of the configurations is $|R\rangle = |\phi_1\phi_2\dots\phi_7\rangle = |1120101\rangle$, the position of arcs (orbitals) $i = 1, 2..7$ are $\bar{i}_R = 1, 2, 3, 3, 4, 5, 5$. For simplicity I will omit index R if it refers to the right-hand configuration.

We are ready now to take the second step, i.e. to find $P|\Theta\rangle = |\Sigma\rangle$. Here $P = (432)$ acts on the spin variables, therefore we should apply the inverse permutation $P^{-1} = (234)$ to the M-path arcs, or we may exchange first arcs 2,3 and then in the resulting path arcs 3,4. Either way taking successive $|\Theta\rangle$ functions we obtain the $|\Sigma\rangle$ as the



drawings here show (solid lines represent $|\Theta\rangle$, dashed lines $|\Sigma\rangle$).

We may justify this purely graphical method of matrix element calculations in operational terms. The orbital j in $|R\rangle$ should be placed at the same position as i in $|L\rangle$, and this should be reflected in the M -diagram. Draw one of the $|\Theta\rangle$ path. Remove the arc corresponding to the unoccupied single in $|L\rangle$, in this case the second arc. Move the rest of the M -path arcs that correspond to the loop body upwards (to close the gap created by removing j -th arc). Put the j -th arc below the path's fragment that was moved upwards. This operation simply shifts the j -th arc to the position that it should have in $|L\rangle$, or assures that the θ_j function in $|\Theta\rangle$ is the same as θ_i in $|\Sigma\rangle$, forcing all other θ_k functions to be the same in both spin functions. The element $\langle L\Sigma|\hat{E}_{ij}|R\Theta\rangle = (-1)^p$, where p is the number of parallel segments in the reduced loop body, so in our example the elements are $+1$. Schematically this operational procedure is illustrated above.



A more practical way of obtaining these elements is as follows. Reverse lexical ordering is used for the M -diagram paths (Fig 9). For $s = 4, M = 0$ this ordering gives:

$$\begin{aligned} |1\rangle &= |++--\rangle; & |2\rangle &= |+-+-\rangle; & |3\rangle &= |-++-\rangle; \\ |4\rangle &= |+---\rangle; & |5\rangle &= |-+-+\rangle; & |6\rangle &= |--++\rangle \end{aligned}$$

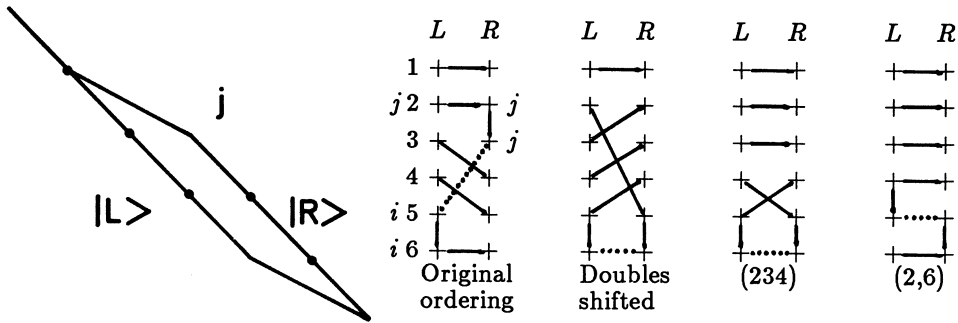
with the $+(-)$ symbols designating the arcs increasing (decreasing) M value. Let us write now the paths symbols in form of a matrix, representing all $|\Theta\rangle$ spin functions, and make the second column of this matrix the last one. The new path symbols correspond to the interacting $|\Sigma\rangle$ functions. Their lexical numbers are read off the M -diagram.

$$\begin{array}{c|c|c|c|c|c} 1 & & ++-- & & +--+ & 4 \\ 2 & & +-+- & & ++-- & 1 \\ 3 & = & -++- & \longrightarrow & -++- & = & 5 \\ 4 & & +--- & & +-+- & & 2 \\ 5 & & -+-+ & & --++ & & 6 \\ 6 & & --++ & & -++- & & 3 \end{array}$$

I will also use a symbol $\langle 4, 1, 5, 2, 6, 3 \rangle$ to specify that in $U(P)$ matrix elements $+1$ are located in row 4 of the first column, row 1 of the second ... row 3 of the sixth, all other elements being zero.

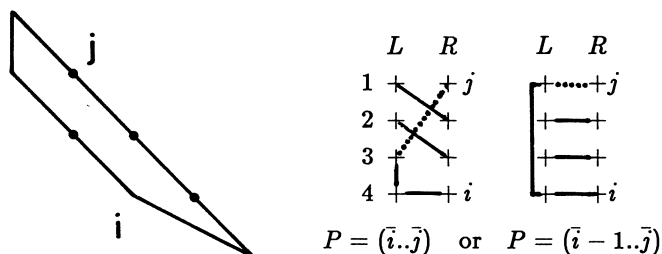
Analysis of the [13] loop is essentially complete now. We know how to find interacting configurations in a purely graphical way: two-segment loops for one-particle operators or two, three and four-segment loops for two-particle operators should be created in the three-slope graph. Once we have a loop we easily find non-zero elements in the structure constants matrices analyzing M-diagram. We have found that \hat{E}_{ij} operator for $\bar{i}_L = 4$ and $\bar{j}_R = 2$ gives $\langle 4, 1, 5, 2, 6, 3 \rangle$ matrix. The number of different positions \bar{i}_L and \bar{j} for $s = s_L = s_R$ singly occupied orbitals is s^2 . Because $\bar{i}_L = \bar{j}$ gives identity ($P = I$) and $\bar{i}_L = k, \bar{j} = k + 1$ is the same as $\bar{i}_L = k + 1, \bar{j} = k$ only $s^2 - s - (s - 1) = (s - 1)^2$ different positions should be considered. In each case we find the interacting $|\Sigma\rangle$ functions and put them in a table. An example for $s = 4$ is shown in Table 2.1. If we wish to use the positions of arcs or orbitals referring only to the configuration $|R\rangle$ we should take $\bar{i}_R = \bar{i}_L + 1$ if $i > j$ and $\bar{i}_R = \bar{i}_L$ if $i < j$.

Let us consider now loops of [57] type. The occupations of i and j in $|R\rangle$ are $n_i = 1, n_j = 2$, and in $|L\rangle$ are $n_i = 2, n_j = 1$. Placing the doubly occupied orbitals in both configurations after the singly occupied ones we notice that this case does not differ much from the previous one. A cyclic permutation $(\bar{j}_L..i)$ aligns all the singly occupied orbitals that are identical in both configurations, with the subsequent transposition $(\bar{j}_L, s_L + 1)$ or $(\bar{j}_L, s_L + 2)$ aligning i and j orbitals (see the illustration below).

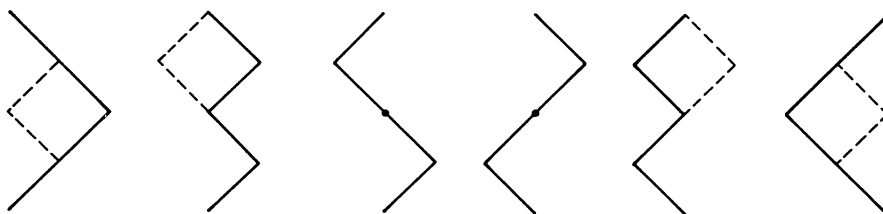


Therefore the ordering permutation $P = (\bar{j}_L, s_L + 1)(\bar{j}_L..i)$ or $P = (\bar{j}_L, s_L + 2)(\bar{j}_L..i)$. The spin functions corresponding to j in $|L\rangle$ and i in $|R\rangle$ have to be the same, therefore the last transposition is exchanging the same spin functions, and thus has no effect acting on $|\Theta\rangle$. It changes however the parity of the permutation, therefore I will write symbolically $P = -(\bar{j}_L..i)$ to remember of this change of sign. Table 2.1 constructed for [13] loop contains already the results for the present case. In the example used above we have $\bar{j}_L = 2, \bar{i} = 4$ and the non-zero elements are $\langle -2, -4, -6, -1, -3, -5 \rangle$. The same result may be obtained by a direct manipulation of M-diagram paths.

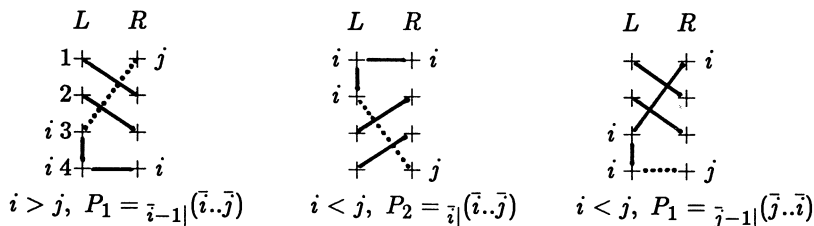
There are two more elementary loop types that we have to consider: loops [17] and [53]. Let us look at the first of these loops; it implies $n_i = n_j = 1$ in $|R\rangle$ configuration and $n_i = 2, n_j = 0$ in $|L\rangle$ configuration. Drawing the diagrams with orbital orderings we find that there are two permutations contributing in this case: $P_1 = (\bar{i}..j)$ and $P_2 = (\bar{i} - 1..j)$.



The arcs $\bar{i}-1, \bar{i}$ in $|\Sigma\rangle$ path correspond to the doubly occupied orbital i and therefore must be $+-$; these arcs are removed from the final $|\Sigma\rangle$ paths before their lexical indices are read off the M-diagram with $s_R - 2$ levels. Another way of looking at this is to use $P = (\bar{i} - 1.. \bar{j})$ permutation only: if the arcs $\bar{i} - 1, \bar{i}$ in $P|\Theta\rangle$ are $++$ or $--$ they do not match any $|\Sigma\rangle$ paths and all elements in the $|\Theta\rangle$ column of $U(P)$ are zero. If the two arcs are $+-$ then $|\Sigma\rangle = P|\Theta\rangle$ is a valid path and the element $\langle \Sigma|P|\Theta\rangle = (-1)^{\bar{i}-\bar{j}-1}$. If the two arcs are $-+$ then $P = (\bar{i}.. \bar{j})$ would make them $+-$, without changing the other arcs of $(\bar{i} - 1.. \bar{j})|\Theta\rangle$ path, but changing the sign of the element to $\langle \Sigma|P|\Theta\rangle = (-1)^{\bar{i}-\bar{j}}$. Therefore we may always use only one of the two permutations remembering to change the sign if the arcs $\bar{i} - 1, \bar{i}$ come as $-+$. In our example we obtain the matrix $\langle 1, 2, 0, 0, -1, -2 \rangle$, with the first two arcs of $P|\Theta\rangle$ path giving the lexical number of the path and the last two the value of the element, as illustrated below.

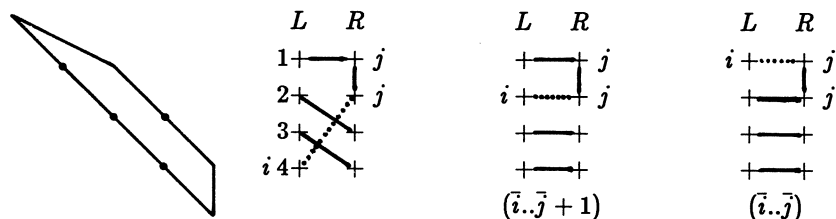


As for the previous loops let us make a table containing the results for all \bar{i}, \bar{j} values. The results for \bar{i}, \bar{j} are the same as for \bar{j}, \bar{i} . In the first case $P = (\bar{i}.. \bar{j})$ with doubly occupied pair in $|L\rangle$ at positions $\bar{i} - 1, \bar{i}$. I will use the symbol $P_1 = \bar{i}-1 |(\bar{i}.. \bar{j})$ to designate the presence of this pair in $\langle L|$ Taking \bar{j}, \bar{i} instead case $P_2 = \bar{i} |(\bar{i}.. \bar{j})$ is found. The two permutations differ only on a shift of the doubly occupied orbital i in $|L\rangle$ (see the diagram below).

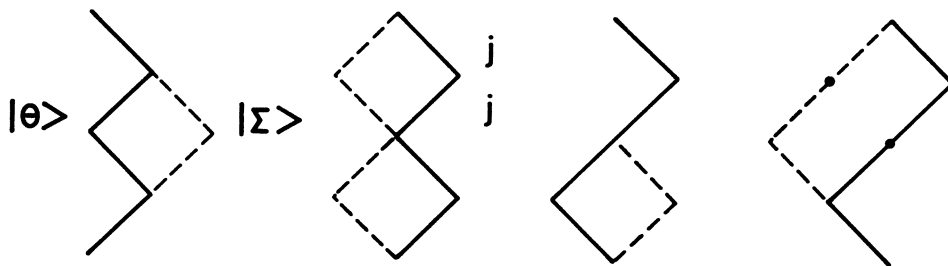


Moving the doubly occupied orbital i to position $\bar{i} - 1, \bar{i}$ we obtain the same permutation P_1 as before, hence the two cases are equivalent. Because of this symmetry only $\binom{s}{2}$ rows are necessary in the tables storing results for [17] loops (cf Table 2.2).

The last type of elementary loop, [53], differs only slightly from the previous cases. The two permutations, bringing orbitals in $|L\rangle$ to the same ordering as they have in $\hat{E}_{i,j}|R\rangle$ are $P_1 = (\bar{i}.. \bar{j} + 1)$ and $P = (\bar{i}.. \bar{j})$. Acting on $|\Theta\rangle$ they give two different functions $|\Sigma\rangle$. The $|\Theta\rangle$ paths are taken from the s_R -level M-diagram with $+-$ arcs added at the positions $\bar{j}, \bar{j} + 1$ to account for the doubly occupied orbital j . Applying P_1 and P_2 to the two paths for $s_R = 2$ we obtain 4 elements $\langle 1 - 5, 2 - 6 \rangle$, i.e. the first column of $U(P)$ matrix contains $+1$ in the first row and -1 in the 5-th, ect.



The results could as well be taken from the Table 2.1 if we notice that the first $|\Theta\rangle$ function, with $+-$ arcs added, becomes $|+--+ \rangle = |2\rangle$, and the second is $|+--- \rangle = |4\rangle$. In our example $\bar{i} = 4$ and $\bar{j} = 1$ or 2. Taking $\bar{i} = 4, \bar{j} = 1$ entries from column 2 and 4 we obtain $-5, -6$, and for $\bar{j} = 2$ we have 1, 2. In this way Table 2.3 is constructed. This table is also symmetric, i.e. the entries for \bar{j}, \bar{i} are the same as for \bar{i}, \bar{j} . The proof



is analogous as in the previous case. The result for all 4 elementary loops, giving the occupation of i, j orbitals in $|R\rangle$, entry to the Tables 2.1–2.3 in terms of \bar{i}, \bar{j} positions, and permutations P for lowering operators $\hat{E}_{i,j}, i > j$ and raising operators $\hat{E}_{i,j}, i < j$, are collected in Table 2.4. The minus signs in front of the cycles reminds that we should change sign using Table 2.1.

Table 2.1

Case: $n_i = 0, n_j = 1$, or [13] loop.

| k, l | 1 | 2 | 3 | 4 | 5 | 6 |
|--------|----|----|----|----|----|----|
| 12 | -1 | -3 | -2 | -5 | -4 | -6 |
| 13 | 3 | 1 | 2 | 5 | 6 | 4 |
| 14 | -3 | -5 | -6 | -1 | -2 | -4 |
| 23 | -2 | -1 | -3 | -4 | -6 | -5 |
| 24 | 2 | 4 | 6 | 1 | 3 | 5 |
| 34 | -1 | -4 | -5 | -2 | -3 | -6 |
| 31 | 2 | 3 | 1 | 6 | 4 | 5 |
| 41 | -4 | -5 | -1 | -6 | -2 | -3 |
| 42 | 4 | 1 | 5 | 2 | 6 | 3 |

Table 2.2

Case: $n_i = 1, n_j = 1$, or [17] loop.

| k, l | 1 | 2 | 3 | 4 | 5 | 6 |
|--------|----|----|----|----|----|----|
| 12 | 0 | 1 | -1 | 2 | -2 | 0 |
| 13 | -1 | 0 | 1 | -2 | 0 | 2 |
| 14 | 1 | 2 | 0 | 0 | -1 | -2 |
| 23 | 1 | -1 | 0 | 0 | 2 | -2 |
| 24 | -1 | 0 | -2 | 1 | 0 | 2 |
| 34 | 0 | 1 | 2 | -1 | -2 | 0 |

Table 2.3

Entries for [53] loop.

| k, l | 1 | 2 |
|--------|-----|-----|
| 11 | 2-3 | 4-5 |
| 12 | 3-1 | 6-4 |
| 13 | 1-5 | 2-6 |
| 22 | 1-2 | 5-6 |
| 23 | 4-1 | 6-3 |
| 33 | 2-4 | 3-5 |

Table 2.4

Permutations and entries to the Tables 2.1–2.3 for two-segment loops

| Loop | n_i, n_j | P for $i > j$ or lowering \hat{E}_{ij} | k, l |
|------|------------|---|----------------------|
| [13] | 0, 1 | $(\bar{i}_L \dots \bar{j}) = (\bar{i}-1 \dots \bar{j})$ | $\bar{i}-1, \bar{j}$ |
| [57] | 1, 2 | $(\bar{j}_L, s_L+1)(\bar{j}_L \dots \bar{i}) = -(\bar{j} \dots \bar{i})$ | \bar{j}, \bar{i} |
| [17] | 1, 1 | $\bar{i}_{-1} (\bar{i} \dots \bar{j}) = \bar{i}_{-1} (\bar{i}-1 \dots \bar{j})$ | \bar{i}, \bar{j} |
| [53] | 0, 2 | $(\bar{i}+1 \dots \bar{j})_{ \bar{j}}, (\bar{i}+1 \dots \bar{j}+1)_{ \bar{j}}$ | $\bar{i}+1, \bar{j}$ |
| Loop | n_i, n_j | P for $i < j$ or raising \hat{E}_{ij} | k, l |
| [31] | 0, 1 | $(\bar{i}_L \dots \bar{j}) = (\bar{i} \dots \bar{j})$ | \bar{i}, \bar{j} |
| [75] | 1, 2 | $(\bar{j}_L, s_L+1)(\bar{j}_L \dots \bar{i}) = -(\bar{j}-1 \dots \bar{i})$ | $\bar{j}-1, \bar{i}$ |
| [71] | 1, 1 | $\bar{i}_1 (\bar{i} \dots \bar{j}) = \bar{i}_1 (\bar{i}+1 \dots \bar{j})$ | \bar{i}, \bar{j} |
| [35] | 0, 2 | $(\bar{i} \dots \bar{j})_{ \bar{j}}, (\bar{i} \dots \bar{j}+1)_{ \bar{j}}$ | \bar{i}, \bar{j} |

D. Example.

Let us consider now a more complicated example: matrix elements of a Hamiltonian between two 6 orbital, 6 electron configurations. Let us take a path $|R\rangle = |112011\rangle$ and another path $|L\rangle = |011121\rangle$ that differs from $|R\rangle$ in 4 occupations. Drawing these paths in the three-slope graph (Fig 7) we find that the nonparallel segments (corresponding to the orbital mismatches) are at levels 1,3,4,5. Using expressions (2.45) or (2.48) for a two-particle operator we find:

$$\begin{aligned} \langle 011121 | \hat{H} | 112011 \rangle &= \langle 011121 | [\{43|51\} \hat{E}_{43} \hat{E}_{51} + \{41|53\} \hat{E}_{41} \hat{E}_{53}] | 112011 \rangle \\ &= \{43|51\} A_{LR}^{4351} + \{41|53\} A_{LR}^{4153} \end{aligned} \quad (2.52)$$

where A_{LR} matrices for $M = 0$ are 6-dimensional. They are calculated as easily as the matrices for single generators. The first operator product gives:

$$\hat{E}_{43} \hat{E}_{51} | 112011 \rangle = \hat{E}_{43} | 012021 \rangle = | 011121 \rangle$$

For \hat{E}_{51} we have $n_i = n_j = 1$ with $\bar{i} = 1, \bar{j} = 3$ and from the Table 2.2 we obtain $\langle -1, 0, 1, -2, 0, 2 \rangle$ as non-zero entries in the $U(P)$ matrix. For \hat{E}_{43} we have $n_i = 0, n_j = 2$ and $\bar{i} = 2, \bar{j} = 2$. Using the Table 2.3 we find that spin function $|1\rangle$ becomes now $|1\rangle - |2\rangle$, and $|2\rangle$ gives $|5\rangle - |6\rangle$, therefore the result is $\langle -1 + 2, 0, 1 - 2, -5 + 6, 0, 5 - 6 \rangle$, i.e. the matrix

$$A_{LR}^{4351} = \begin{pmatrix} -1 & 0 & 1 & 0 & 0 & 0 \\ 1 & 0 & -1 & 0 & 0 & 0 \\ 0 & 0 & 0 & 0 & 0 & 0 \\ 0 & 0 & 0 & 0 & 0 & 0 \\ 0 & 0 & 0 & -1 & 0 & 1 \\ 0 & 0 & 0 & 1 & 0 & -1 \end{pmatrix} \quad (2.53)$$

The second operator product gives:

$$\hat{E}_{41}\hat{E}_{53}|112011\rangle = \hat{E}_{41}|111021\rangle = |011121\rangle$$

For \hat{E}_{53} we have [57] loop with $\bar{i} = 3, \bar{j} = 3$. Using Table 2.1 we find -1 in columns $\langle -1, -2, -3, -4, -5, -6 \rangle$. For \hat{E}_{41} , $\bar{i} = 3$ ($i > j$, therefore $\bar{i} - 1$ is taken) and $\bar{j} = 1$ entries are in columns $\langle -2, -3, -1, -6, -4, -5 \rangle$, i.e. the matrix

$$A_{LR}^{4153} = - \begin{pmatrix} 0 & 0 & 1 & 0 & 0 & 0 \\ 1 & 0 & 0 & 0 & 0 & 0 \\ 0 & 1 & 0 & 0 & 0 & 0 \\ 0 & 0 & 0 & 0 & 1 & 0 \\ 0 & 0 & 0 & 0 & 0 & 1 \\ 0 & 0 & 0 & 1 & 0 & 0 \end{pmatrix} \quad (2.54)$$

Finding the entry to the table does not require analysis of the configuration pair, only the positions of orbitals in $|R\rangle$ have to be specified. These positions are easy to calculate while searching for the paths in the graph.

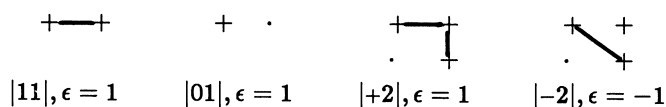
E. The four-slope graphs.

Non-fagot graphs, like the four-slope graphs, represent individual spin-orbital configurations or determinants. In most cases it is rather a disadvantage, because for each orbital configuration with s singly occupied orbitals all $d(M, s)$ paths are analyzed separately. In some methods however, when only a few determinants belonging to each configuration are accepted, it may be an advantage, because manipulation with individual determinants is easy. In the fagot graphs the classification of the final functions (determinants in this case) is hidden in separate diagrams. It is of course possible to keep the information on the determinants associated with each configuration. Calculation of matrix elements with the help of four-slope and other non-fagot graph is nevertheless worth investigating.

With the three type of arcs there were nine type of segments $|kl|$. The number of segments in the four-slope graphs is increased to 16. Classification of all elementary loops becomes therefore more tedious. Increasing segments $|01|$ are now in two versions, $|0+|$ and $|0-|$, where $+$ represents a singly occupied orbital multiplied by α spin function, and $-$ by β spin function. I will use the segment designations like $|01|$ whenever the type of the singly occupied arc does not matter. Segments $|12|$ are now $|+2|, |-2|$ and a new increasing segment is possible, $|+-|$. Segments $|0+|, |-2|$ combined with the decreasing segments $|+0|, |2-|$ give four types of loops, and segments $|0-|, |+2|$ combined with decreasing segments $|-0|, |2+|$ give another four loops. These eight type of loops have non-zero values for single shift operator $\hat{E}_{i\sigma, jr}$. As in the three-slope graph case, there is one more two-segment loop, with $|02|, |20|$ segments, that has non-zero value

The four-slope graph allows us to find the non-zero elements by forming loops in the graph. One and two-particle operators, expressed as combinations of the shift operators (Eq 2.43-2.49), lead to non-zero loop values for at most four-segment loops. The loop value for the shift operators or their products is ± 1 and depends on the reordering of arcs (spin orbitals) in the two paths $|L\rangle, |R\rangle$ (spin-orbital configurations) forming the loop (matrix element). The loop value may be computed by analyzing the influence each segment has on this reordering and thus on sign. The reordering is necessary only for arcs in the loop range.

Each vertex in the graph is characterized by the level, the number of particles and the M -value. Let us fix a level and take two vertices, v_L and v_R , one belonging to $|L\rangle$ and the other to $|R\rangle$ path. We define the width Δ_e of the segment connecting this level with the level below it as the number of particles corresponding to the vertex v_R minus the number of particles corresponding to the vertex v_L . Let us assign a phase factor $\epsilon_{|kl|}$ to each segment $|kl|$. If more than one reordering leads to non-zero matrix element we assume that the $|L\rangle$ spin-orbital configuration is reorder making the lowest number of transpositions. For $\Delta_e = 0$ all segments should have $\epsilon_{|kl|} = 1$ except for $|2-$ and $|-2|$; because doubly occupied arc corresponds to $\phi\alpha\phi\beta$ spin orbital order one transposition is necessary to put $\phi\beta$ in one spin-orbital configuration against $\phi\beta$ in the other. Diagrams below should help to illustrate this.



The phase factors of $|11|, |12|$ and $|21|$ segments are changed to the opposite each time Δ_e is changed by one, i.e for $\Delta_e = \pm 1$ we have -1 for $|11|, |+2|, |2+|$, and $+1$ for $|-2|, |2-|$. In general we may write:

$$\epsilon_{|kl|} = \epsilon_{|lk|}; \quad \epsilon_{|kl|} = \begin{cases} 1 & \text{for } |00|, |22|, |01|, |02|; \\ (-1)^{\Delta_e} & \text{for } |11|, |+2|; \\ (-1)^{\Delta_e+1} & \text{for } |-2| \end{cases} \quad (2.55)$$

The total phase factor for a loop is a product $\epsilon_{LR} = \prod_p \epsilon_p$ of segment's factors within the loop range. Taking a two-electron operator instead of pure shift operator products the following loop values are found:

1. Diagonal matrix elements - no loops.

$$\begin{aligned} \langle L|\hat{B}|L\rangle &= \sum_{i=1}^n n_i \{i|i\} + \sum_{ij=1}^n \delta_{n_i 2} (1 - \delta_{n_j 0}) (2J_{ij} - K_{ij}) \\ &+ \sum_{i < j}^n \delta_{n_i 1} \delta_{n_j 1} (J_{ij} - \delta_{i,t_j} K_{ij}) \end{aligned} \quad (2.56)$$

where $J_{ij} = \{i i | j j\}$, $K_{ij} = \{i j | i j\}$ and $\delta_{i,t_j} = 1$ only if arcs i and j in the path $|L\rangle$ are of the same type (i.e. both are + or both are - arcs), otherwise it is zero.

2. Two-segment loops: eight elementary loops.

$$\langle L|\hat{B}|R\rangle = \epsilon_{LR} \left(\{i|j\} + \sum_{k=1}^n \left[n_k \{ij|kk\} - (\delta_{n_k 2} + \delta_{n_k 1} \delta_{t_i t_k}) \{ik|jk\} \right] \right) \quad (2.57)$$

with $n_k = \min(n_k^L, n_k^R)$ and $\delta_{t_i t_k}$ for $n_i = 1$ defined as previously. For $n_i = 2$ it is clear that we can exchange spin orbitals k with this i that has no counterpart in the second configuration, thus if i -th segment is $|2+|$ then $t_i = -$, and if it is $|2-|$ then $t_i = +$ (this part is a contribution from $\hat{E}_{ik}\hat{E}_{kj}$ operator).

3. Two-segment loops: two special loops.

$$\langle L|\hat{B}|R\rangle = \epsilon_{LR} K_{ij} \quad (2.58)$$

4. Three-segment loops: 48 elementary loops.

$$\langle L|\hat{B}|R\rangle = \epsilon_{LR} \{ik|jk\} \quad (2.59)$$

5. Four-segment loops: 312 elementary loops. Let us assume that $i > k$ belongs to $|L\rangle$ (i.e. occupations at the levels i, k are $n_i^L > n_i^R, n_k^L > n_k^R$) and $j > l$ belongs to $|R\rangle$. The formula is:

$$\langle L|\hat{B}|R\rangle = \epsilon_{LR} \left[\{ij|kl\} \delta_{t_i t_j} \delta_{t_k t_l} - \{il|jk\} \delta_{t_i t_l} \delta_{t_j t_k} \right] \quad (2.60)$$

To illustrate how the last formula is applied in practice let us suppose that a loop was created corresponding to the following matrix element (same as one of the elements computed in the previous subsection):

$$\begin{aligned} \langle L|\hat{H}|R\rangle &= \langle 0+-+2-|\hat{H}|++20--\rangle \\ i &= 5, j = 3, k = 4, l = 1 \\ \text{segments: } & |0+| \quad |++| \quad |-2| \quad |+0| \quad |2-| \quad |--| \\ \Delta_e : & \quad 0 \quad 1 \quad 1 \quad 2 \quad 1 \quad 0 \\ \epsilon_p : & \quad + \quad - \quad - \quad + \quad - \quad + \\ \langle L|\hat{H}|R\rangle &= -\{ik|kl\} + \{il|jk\} = -\{53|41\} + \{51|43\} \end{aligned}$$

Actually it is easier to analyze this element examining a loop in a graph than looking at the paths written using 0, +, -, 2 symbols, because in the graph i, j, k, l levels, segments and Δ_e values are immediately visible.

F. Other non-fagot graphs.

The two-slope graphs $\mathcal{G}_{2,2}(2n : N, M_S)$ of Fig 5,6 and the two-slope graphs of Fig 4, with α and β parts separated, are also useful in representing the \hat{S}_z -adapted space.

The graphs of the last type are rather trivial to analyze; the formulas for matrix elements result directly from Slater rules (cf Slater 1968; Duch 1985c), with the phase factors equal to the number of $|11\rangle$ segments in the loop range. The use of $\mathcal{G}_{2,2}(2n : N, M_S)$ graphs doesn't introduce any new aspects to the problem of matrix element evaluation either. The same approach as was described above for the four-slope graphs is directly translated to these graphs. Doubly occupied arcs are replaced now by $+-$ pairs of arcs, two segment loops have non-zero values for one-particle operators, there are no special two segment loops and no three-segment loops, and the four-segment loops have non-zero values only for products of two operators. The same formulas are used as in the four-slope case, with the formula for the four-segment loops automatically taking care for the special two-segment and the three-segment cases. The arc types t_i appearing in δ_{t_i, t_j} are always those of the nonparallel arcs. The $\mathcal{G}_{2,2}(2n : N, M_S)$ graphs, because of their better legibility and the above mentioned simplifications, should be preferred over the four-slope ones. The only reason that I have described the use of the four-slope graph first is to facilitate a direct comparison with the results for the \hat{S}^2 -adapted GUGA graphs that are of the four-slope type.

G. Matrix elements in the \hat{L}_z and (\hat{L}_z, \hat{S}_z) -adapted spaces.

The \hat{L}_z and (\hat{L}_z, \hat{S}_z) -adapted graphs, described in sections 1.4, 1.5, seem to be much more complicated compared to \hat{S}_z -adapted graphs. However, this complication, arising from the fact that different slopes of arcs are used for different m_l values to assure the desired final M_L value, is completely inessential from the point of view of matrix element evaluation. We are still dealing with determinantal bases. Loops in the \hat{L}_z -adapted graphs are formed in the same way as in the \hat{S}_z -adapted ones. Disregarding m_l values the arcs may be classified according to their occupations and (for non-fagot graphs) singly occupied arcs are further divided into α and β types. Tables 2.1 – 2.4 may still be used for fagot graphs, and the segment values ϵ_p are computed as above for the non-fagot graphs. Similarly adaptation of \hat{S}^2 eigenfunctions to the \hat{L}_z operator will have no influence on the method of matrix element evaluation, as will be shown soon.

2.4

Reduction from \hat{S}_z to \hat{S}^2 eigenspace

Calculation of matrix elements between determinants is much easier than between spin eigenfunctions. It should be possible to use this simplicity and perform a direct reduction of structure constants matrices from \hat{S}_z to \hat{S}^2 -adapted space. The disadvantages of using determinants instead of spin eigenfunctions are twofold: first, the number of many-electron functions needed in calculation is greater than necessary. Second, it is not always clear which state was computed. One can reduce the number of functions needed in calculation retaining the simplicity of matrix element calculation by taking a simple combination of determinants, as it was done by Handy (1980), but still the number of functions is significantly larger than necessary. The method described in this section is equally simple, leads to rigorous coupling coefficients of \hat{S}^2 eigenfunctions, and may easily be extended to more complicated cases such as \hat{L}^2 eigenfunctions.

Results of the previous section on the three-slope graph are the starting point here. Determinants form the simplest basis of the subspace corresponding to a configuration $|L\rangle$. Another basis that can be introduced is the \hat{S}^2 -adapted basis, described by the S-diagram (branching diagram). In Fig 46 both M and S-diagrams are presented at the same picture, with the S-diagram weights inscribed above the vertices and the M-diagram weights inscribed below. A given $|L\rangle$ subspace of determinants of $d(s_L, M_S = S)$ dimensions may be decomposed into \hat{S}^2 eigenspaces: $d(s_L, S) = f(s_L, S) + f(s_L, S + 1) + \dots + f(s_L, N/2)$, i.e. the number $d(s_L, M)$ below a vertex in Fig 46 is a sum of all numbers above it, for example for $s_L=6$ we have $d(6,0)=5+9+5+1=20$. The ratio $d(s_L, S)/f(s_L, S)$ gives the number of determinants per one spin function and for $S=0$ is equal simply to $\frac{1}{2}s_L + 1$.

Let us turn now to the calculation of matrix elements. The matrices A_{LR}^{pq} of structure constants contain only a few non-zero elements that are immediately obtained

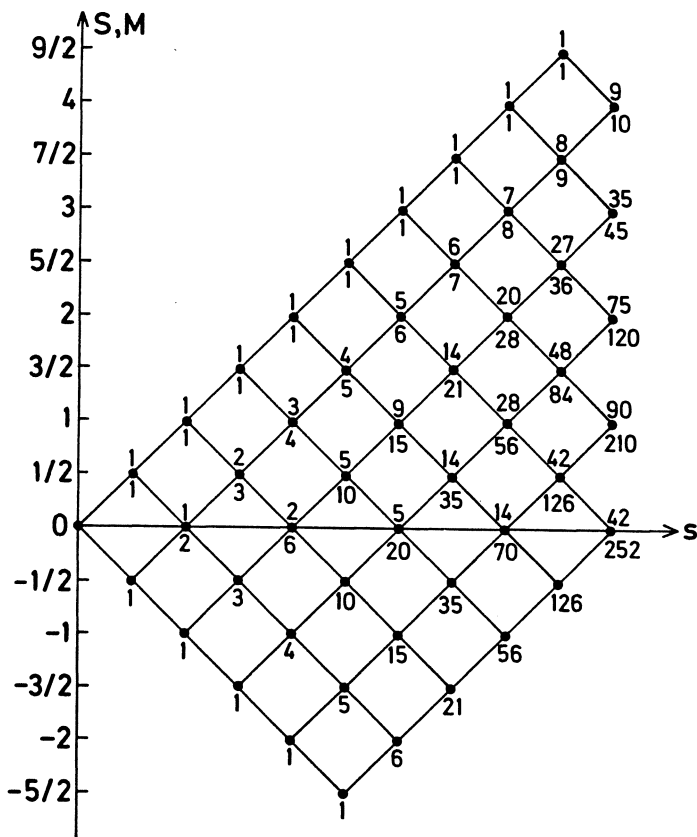


Fig 46. M and S-diagrams for up to 10 spins.

with the help of the tables given in the preceding section. The calculation of the two-electron coupling coefficients is usually rather tedious but, as we have seen, in case of determinants there is no essential difference between one operator or products of two or more operators. We would like to find now unitary matrices T_L, T_R that transform the structure constants matrices A_{LR} to a block-diagonal form \tilde{A}_{LR} corresponding to the elements calculated in the \hat{S}^2 basis

$$\tilde{A}_{LR} = T_L A_{LR} T_R^\dagger \tag{2.61}$$

This of course means that we have to find the matrix that transforms determinants into spin eigenfunctions. Because A_{LR} contains just a few non-zero elements equal to ± 1 this matrix multiplication may be carried out very efficiently. For $d(s_L, M)$ determinants and $f(s_L, S)$ spin functions only the rectangular part $f(s_L, S) \times d(s_L, M)$ of the full transformation matrix T is necessary to get the matrices in the spin-adapted basis. Each S-diagram path corresponds to a combination of determinants. Coefficients of a

given M–diagram path in this combination, i.e. elements of our matrix \mathbf{T} , are equal to products of C_{++}^{SM} , C_{+-}^{SM} , C_{-+}^{SM} and C_{--}^{SM} coefficients, where S and M values are taken at the vertices of the S and M–diagram paths, and

$$\begin{aligned} C_{++}^{SM} &= \sqrt{\frac{S+M}{2S}}; & C_{-+}^{SM} &= -\sqrt{\frac{S-M+1}{2S+2}} \\ C_{+-}^{SM} &= \sqrt{\frac{S-M}{2S}}; & C_{--}^{SM} &= \sqrt{\frac{S+M+1}{2S+2}} \end{aligned} \quad (2.62)$$

The values of these coefficients are given in Graebenstetter *et al* (1976) or Pauncz (1979). Using M and S–diagrams for classification of determinants and spin eigenfunctions makes calculation of the transformation matrix very efficient. One of the advantages of reduction of structure constants matrices versus their direct calculation is that in forming of the matrix elements where many integrals contribute, i.e. when $|R\rangle$ and $|L\rangle$ are the same or differ on one orbital, for two–particle operators (Eq 2.43–44), there is no multiplication of structure constant matrices by the integrals because the reduction Eq (2.61) is performed only after the element is constructed in the determinantal basis. Thus if K terms contribute to the matrix element $K \cdot d(s_L, S) \cdot d(s_R, S)$ multiplications are saved. Matrix A_{LR} has for a single shift operator usually only $d(s_R, S)$ non–zero elements equal to ± 1 , while \tilde{A}_{LR} , if it is not a large matrix, is rather dense. The square of the number above the vertex to the number below it (Fig 46) should therefore give an estimation of the number of non–zero elements in a matrix block in the spin–adapted versus determinantal basis.

When only one or two integrals contribute to the matrix element multiplications may be reduced to additions and matrices to vectors. Suppose that A_{LR} contains only one non–zero element in each row, in columns (k_1, k_2, \dots, k_d) . Then multiplication $A_{LR} \mathbf{T}_R^\dagger$ gives $\mathbf{T}_R^\dagger(k_1, k_2, \dots, k_d)$, i.e. transformation matrix \mathbf{T}_R^\dagger with reordered rows: k_1 as first, k_2 as second ect. Thus $\tilde{A}_{LR} = \mathbf{T}_L \mathbf{T}_R^\dagger(k_1, k_2, \dots, k_d)$ and precomputing all the products $T_{11}T_{11}, T_{11}T_{12}, \dots, T_{11}T_{1d}; T_{12}T_{11}, \dots, T_{12}T_{1d}, \dots, T_{1d}T_{11}, \dots$ and storing them in a vector we simply pick up $T_{11}T_{1k_1}$ from the first set of $d(s_L, M)$ elements, $T_{12}T_{1k_2}$ from the second set of elements, ect. If there are two elements in a row, $\mathbf{T}_R^\dagger(k_1, k_2, \dots, k_d; l_1, l_2, \dots, l_d)$, a sum $T_{11}T_{1k_1} + T_{11}T_{1l_1}$ is taken from the first set of elements, ect. The summation is always performed in a single loop through $T_{ij}T_{kl}$ elements, with a loop step of $d(s_L, M)$ elements at a time. The rows of transformation matrix \mathbf{T} , after a common factor is extracted, are small integers, and therefore matrix multiplication in Eq (2.61) is easy also in hand calculations.

As an example let us obtain the transformation matrix for $s_L = 4$. The coefficient of the first primitive spin function in the $S = 2, M = 0$ spin eigenfunction is:

$$\langle S : + + + + | M : + + - - \rangle = C_{++}^{\frac{1}{2}, \frac{1}{2}} C_{++}^{1, 1} C_{+-}^{\frac{3}{2}, \frac{1}{2}} C_{+-}^{2, 0} = \sqrt{\frac{1}{6}}$$

and similarly for all other M-diagram paths we get $\sqrt{\frac{1}{6}}$. The three spin functions for $S=1$ are

$$|1\rangle = |+-+ \rangle, \quad |2\rangle = |++- \rangle, \quad |3\rangle = |+++ \rangle$$

and the two functions for $S=0$ are $|1\rangle = |+-+ \rangle$, $|2\rangle = |++- \rangle$. The ordering of the spin paths assumed here corresponds to the reversed lexical ordering. The transformation matrix is:

$$\mathbf{T} = \begin{pmatrix} \sqrt{\frac{1}{6}} & \sqrt{\frac{1}{6}} & \sqrt{\frac{1}{6}} & \sqrt{\frac{1}{6}} & \sqrt{\frac{1}{6}} & \sqrt{\frac{1}{6}} \\ 0 & \frac{1}{2} & -\frac{1}{2} & \frac{1}{2} & -\frac{1}{2} & 0 \\ \sqrt{\frac{1}{3}} & -\sqrt{\frac{1}{12}} & -\sqrt{\frac{1}{12}} & \sqrt{\frac{1}{12}} & \sqrt{\frac{1}{12}} & -\sqrt{\frac{1}{3}} \\ \sqrt{\frac{1}{6}} & \sqrt{\frac{1}{6}} & \sqrt{\frac{1}{6}} & -\sqrt{\frac{1}{6}} & -\sqrt{\frac{1}{6}} & -\sqrt{\frac{1}{6}} \\ 0 & \frac{1}{2} & -\frac{1}{2} & -\frac{1}{2} & \frac{1}{2} & 0 \\ \sqrt{\frac{1}{3}} & -\sqrt{\frac{1}{12}} & -\sqrt{\frac{1}{12}} & -\sqrt{\frac{1}{12}} & -\sqrt{\frac{1}{12}} & \sqrt{\frac{1}{3}} \end{pmatrix} \quad (2.63)$$

It is interesting to notice that \mathbf{T} is the same matrix as the matrix giving the symmetry orbitals in benzene (cf Eyring *et al* 1949). This is not hard to understand because the determinants correspond here to a basis of the D_{6h} regular representation and \mathbf{T} is reducing this regular representation to the block-diagonal form. This transformation matrix covers all spin multiplicities for $s_L = 4$. If only the triplet states are of interest we can start from the M-diagram for $M=1$ and obtain a 4×4 matrix \mathbf{T} reducing the problem from a four-dimensional to a three-dimensional subspace of $|S = 1, M = 1\rangle$ spin functions.

Reducing the matrices obtained in the previous section we take the last 2 rows of \mathbf{T} , remove the common factor $\frac{1}{2}$ from the first and $\sqrt{\frac{1}{12}}$ from the second row, and multiply \mathbf{T} by the reordered \mathbf{T}^\dagger , obtaining

$$\tilde{A}_{LR}^{4351} = \begin{pmatrix} \frac{1}{2} & \frac{\sqrt{3}}{2} \\ -\frac{\sqrt{3}}{2} & -\frac{3}{2} \end{pmatrix} \quad \tilde{A}_{LR}^{4153} = \begin{pmatrix} \frac{1}{2} & -\frac{\sqrt{3}}{2} \\ \frac{\sqrt{3}}{2} & \frac{1}{2} \end{pmatrix} \quad (2.64)$$

The transformation method described above is more universal than group-theoretical approaches (cf Robb and Nazi 1984; Duch and Karwowski 1985). Connected with the graphical description of determinantal spaces it should be competitive, especially when matrix elements of more than two generator products are required, or when the number of integrals contributing to an element is larger than two. The number of operations per matrix element obtained in the unitary group approach depends on the length of a loop and so it is proportional to the number of (internal) orbitals. In the symmetric group approach it depends on the length and complication of the permutation cycles. Here the number of operations to get one matrix element depends on s_R and M and is equal to $\binom{s}{\frac{1}{2}s+M}$. However, for elements of a single shift operator the direct computation of structure constants matrices described in the next section seems to be more efficient.

2.5

Matrix elements in the \hat{S}^2 -adapted space.

Calculation of matrix elements in the spin eigenfunction basis has a long history (cf Pauncz 1979). The importance of this subject comes from the fact that for light molecules, where relativistic effects are negligible, the spin and the point group symmetries are the only symmetries of the system. Implementation of the abelian point group symmetry is rather trivial, being reduced to the choice of configurations of a proper symmetry. Non-abelian point group eigenfunctions on the other hand, are much harder to deal with than spin eigenfunctions, leaving the latter as the first non-trivial problem to attack. In recent years powerful group theoretical methods were applied to the problem of matrix element evaluation in \hat{S}^2 -adapted spaces (cf Hinze 1981; Sutcliffe 1983 or McWeeny and Sutcliffe 1985). The same techniques are applicable also to eigenfunctions of isospin operator \hat{T} in nuclear shell-model calculations (cf Bohr and Mottelson 1969). Graphical approach that I will present here uses much simpler concepts than group theoretical approaches giving the same results.

I will start from the three-slope graph and leave the four-slope graph for the next section, where comparison with the unitary group approach is done. General strategy will be as follows: Eq (2.8),(2.43–48) present one and two-particle operators as sums of the shift operators weighted by one and two-particle integrals. The shift operators, giving non-zero contributions to matrix elements, are automatically selected by forming a loop between the two configurations involved in matrix element. The loops in the three-slope graph were already analyzed in section 2.3. The spin-contracted shift operators \hat{E}_{ij} are used here, i.e. indices i, j refer always to orbitals. Structure constants matrices in Eq (2.38) are products of orbital factors $\langle PL|\hat{E}_{ij}|R\rangle$ and the spin integral matrices $U(P)$, Eq (2.39). The permutations for single shift operators are collected in Table 2.4. Only one permutation P_0 should be used if the coefficient $\sqrt{2}^{n_i+n_j-1}$ is taken. This will be proven shortly.

The orbital part being trivial, we are left with calculation of $U(P_0)$ matrix elements. Because P_0 is a simple cyclic permutation, or a product of two cyclic permutations for two-particle shift operator, one strategy is simply to store all $\binom{s}{2}$ matrices for cycles (where s is the maximum number of open shells allowed) and work out detailed formula for matrix elements (cf Wetmore and Segal 1975; Ruttink 1978; Duch 1985a). The formulas depend on the occupations of the orbitals the two configurations differ by, i.e. on the elementary loop shape (Duch and Karwowski 1982, 1985). While this may be in some cases an effective approach products of two or more matrices have to be computed to find structure constant matrices for two-particle shift operators. This time, however, the matrices are $f(s_L, S) \times f(s_R, S)$ dimensional, where

$$f(s, S) = \frac{2S+1}{s+1} \binom{s+1}{\frac{1}{2}s-S} \quad (2.65)$$

The number of intermediate states in the matrix product

$$\begin{aligned} \langle L : \hat{S}^2 | \hat{E}_{ij} \hat{E}_{kl} | R : \hat{S}^2 \rangle &= \langle L : \hat{S}^2 | \hat{E}_{ij} \sum_K (|K : \hat{S}^2 \rangle \langle K : \hat{S}^2|) \hat{E}_{kl} | R : \hat{S}^2 \rangle \\ &= \langle L : \hat{S}^2 | \hat{E}_{ij} | I : \hat{S}^2 \rangle \langle I : \hat{S}^2 | \hat{E}_{kl} | R : \hat{S}^2 \rangle \end{aligned} \quad (2.66)$$

is $f(s_I, S)$, and the whole operation is more costly than in the case of determinants. In some applications (see remarks in Siegbahn 1984) this product may be performed directly (cf Segal, Wetmore and Wolf 1978). At best the number of intermediate summations in the product of two shift operators may be reduced to two (cf Shavitt 1981).

A. Permutations in the spin space.

The operators that act in the \hat{S}^2 eigenspace are equivalent to combinations of permutations. The simplest possible permutation is a transposition of two consecutive objects $(k-1 \ k)$. Such elementary transpositions are so important, that I will use an abbreviation ET referring to them. To find the matrix $U((k-1 \ k))$ we have to know, how ET acts on a spin function. In every standard textbook on quantum mechanics (cf Weissbluth 1978) Clebsch-Gordan coefficients for addition of angular momentum $\frac{1}{2}$ may be found. Designating the k -particle eigenfunction of \hat{S}^2 and \hat{S}_z operators as $|k; S, M\rangle$ the addition and subtraction formulas may be written as

$$\begin{aligned} |k; S, M\rangle &= C_M^S |k-1; S-\frac{1}{2}, M-\frac{1}{2}\rangle |\alpha(k)\rangle - C_{-M}^S |k-1; S-\frac{1}{2}, M+\frac{1}{2}\rangle |\beta(k)\rangle \\ |k; S, M\rangle &= C_{-M}^{S+1} |k-1; S+\frac{1}{2}, M-\frac{1}{2}\rangle |\alpha(k)\rangle - C_M^{S+1} |k-1; S+\frac{1}{2}, M+\frac{1}{2}\rangle |\beta(k)\rangle \end{aligned} \quad (2.67)$$

$$C_M^S = -\sqrt{\frac{S+M}{2S}}$$

These coefficients depend on quantum number M . Matrix elements of spin-independent operators (in general of operators rotationally invariant in the spin space) should not

depend on M . Indeed, applying the addition and subtraction formula twice to obtain explicit dependence on $|\sigma(k-1)\tau(k)\rangle$ spin functions, and exchanging variables $k-1, k$, after tedious but straightforward calculation one finds (cf Kotani, Ohno and Kayama 1961) that in $(k-1 k)|k; S, M\rangle$ all dependence on M is canceled. Let us write explicitly the $k-1$ and k -th couplings, $+$ if spin $\frac{1}{2}$ is added, $-$ if subtracted. For example $|++\rangle = |k; S, M, ++\rangle = |k; S_1 \dots S_{k-2}, S-1, S-\frac{1}{2}, S, M\rangle$, where S_i is the result of coupling of the first i spins. The effect of the elementary transposition $(k-1 k)$ is

$$\begin{aligned} (k-1 k)|++\rangle &= |++\rangle \\ (k-1 k)|+-\rangle &= -a_k|+-\rangle + b_k|-\rangle \\ (k-1 k)|-+\rangle &= b_k|+-\rangle + a_k|-\rangle \\ (k-1 k)|--\rangle &= |--\rangle \end{aligned} \tag{2.68}$$

$$a_k = \frac{1}{2S_k + 1}, \quad b_k = \sqrt{1 - a_k^2} = \frac{2\sqrt{S_k(S_k + 1)}}{2S_k + 1}$$

These two coefficients, a_k and b_k , are all that is needed to calculate matrix elements in the \hat{S}^2 -adapted spaces. Elements of $U(P)$ matrices and segment values in the unitary group approach are just combinations of products of a_k, b_k . The above results appear in many disguises as a starting point of different approaches, for example, as matrix elements of elementary generators \hat{E}_{ii+1} in the unitary group approach or as elements of Young's orthogonal representation defined in terms of axial distances in Young tableaux (Rutherford 1948). Graphical interpretation is here quite obvious (cf Duch 1985a): the $+$ and $-$ couplings are shown in the S-diagram (cf Fig 19,46). We would like to obtain $U(P)$ matrix elements directly from this diagram. Let us set the graphical rules of their calculation in a way that will automatically incorporate the $\sqrt{2^{n_i+n_j-1}}(-1)^P$ factors of Eq (2.39). Elements of the $U((k-1 k))$ matrix are given by a_k, b_k coefficients with changed sign. The elements depend only on the $k-1$ and k -th arcs of the S-diagram path, and the position of these arcs in the diagram, i.e. S_k value. Drawing these arcs we have

$$\begin{aligned} (k-1 k) \left| \begin{array}{c} \diagup \\ \diagdown \end{array} \right\rangle &= (-1) \left| \begin{array}{c} \diagup \\ \diagdown \end{array} \right\rangle \\ (k-1 k) \left| \begin{array}{c} \diagup \\ \diagup \end{array} \right\rangle &= a_k \left| \begin{array}{c} \diagup \\ \diagup \end{array} \right\rangle - b_k \left| \begin{array}{c} \diagdown \\ \diagdown \end{array} \right\rangle \\ (k-1 k) \left| \begin{array}{c} \diagdown \\ \diagdown \end{array} \right\rangle &= -b_k \left| \begin{array}{c} \diagup \\ \diagup \end{array} \right\rangle - a_k \left| \begin{array}{c} \diagdown \\ \diagdown \end{array} \right\rangle \\ (k-1 k) \left| \begin{array}{c} \diagdown \\ \diagup \end{array} \right\rangle &= (-1) \left| \begin{array}{c} \diagdown \\ \diagup \end{array} \right\rangle \end{aligned} \tag{2.69}$$

The arcs shown here do not have to be the last two arcs. Doubly occupied orbitals are associated with singlet-coupled pairs (SCPs) of spins. Their presence requires slight

modification of the S–diagram. To get a SCP at the positions $k - 1, k$ we have to find a combination of $| + - \rangle$ and $| - + \rangle$ spin functions that is antisymmetric in $k - 1, k$ variables. This requires diagonalization of $U((k-1 k))$ matrix in $| + - \rangle, | - + \rangle$ basis. We obtain

$$\begin{aligned} & \begin{vmatrix} -a - \lambda & b \\ b & a - \lambda \end{vmatrix} = 0 \implies \lambda = \pm 1 \\ & \begin{pmatrix} | + & 0 & + \rangle \\ | + & 1 & + \rangle \end{pmatrix} = \begin{pmatrix} C^+ & -C^- \\ C^- & C^+ \end{pmatrix} \begin{pmatrix} | + - \rangle \\ | - + \rangle \end{pmatrix} \\ & C^+ = \sqrt{\frac{1}{2}}(1 + a); \quad C^- = \sqrt{\frac{1}{2}}(1 - a) \end{aligned} \tag{2.70}$$

The eigenvectors give coefficients of the symmetric (1, triplet) and antisymmetric (0, singlet) combinations of genealogical spin states. The presence of SCP is therefore easily accounted for by presenting the singlet pair as a combination of $| + - \rangle$ and $| - + \rangle$ states and applying graphical rules to this combination. Symbolically this transformation may be written

$$C^+ \begin{array}{c} \diamond \\ \oplus \\ \diamond \end{array} \quad -C^- \qquad C^- \begin{array}{c} \diamond \\ \ominus \\ \diamond \end{array} \quad C^+$$

Note that functions $| + - \rangle$ for $S_k = 0$ (i.e. corresponding to the path $S = 0, \frac{1}{2}, 0$) are already singlet coupled.

At this point we are able to calculate matrix elements of all shift operators using Table 2.4 to find the permutations and applying graphical rules to successive ETs acting on the branching diagram paths. There are some improvements worthwhile to make in the computational technique. First let us make an analogue of Tables 2.1–2.3 for the spin eigenfunctions.

B. Spin function transformation (SFT) graph and table.

Although S–diagrams are very useful is easier to deal with spin function numbers, and the best with all $f(s, S)$ simultaneously, similarly as was done with M–diagrams. To this aim another graph, showing how the spin functions are transformed among themselves under the action of an ET, is helpful. In the nodes of this graph, which I will call further ‘spin function transformations graph’ or SFT graph, numbers corresponding to the positions of spin functions in some ordering scheme are written. When an elementary transposition $(k-1 k)$ acting on the spin function $|m\rangle$ gives a combination of this function with some other function $|m'\rangle$ the two nodes in which the m and m' numbers are written are joined by an arc, labeled by $(k-1 k)$ and by the intermediate spin value S_k , directed to the function corresponding to the upper i.e $| + - \rangle$ path. Such a graph is very useful because one can immediately find all non-zero elements of a permutation expressed as a product of the ETs with a fixed spin state $|m\rangle$.

Consider, for example, the case of six spins coupled to a triplet. There are 9 independent spin functions which are shown in the reversed lexical order in Fig 47. This ordering has been chosen because matrices $U(P)$ for $s = 4$ and $s = 2$ are simply 3×3 and 1×1 submatrices of the 9×9 matrix for $s = 6$. The reason is simple: in the reversed lexical ordering functions are grouped according to the number of SCPs at the last positions, i.e. the first function has two SCPs, the next two have one SCP and the remaining six are coupled to triplet at the two last positions. The spin functions are coupled here starting from the last one to the first, i.e. first s with $s - 1$, therefore the spin coupling symbols $+$, $-$ in Fig 47 should be read from right to left when using Eq (2.68). There is no such ambiguity if the graphical rules are used: the arcs stay as they are, no matter if we list them from right to left or from left to right.

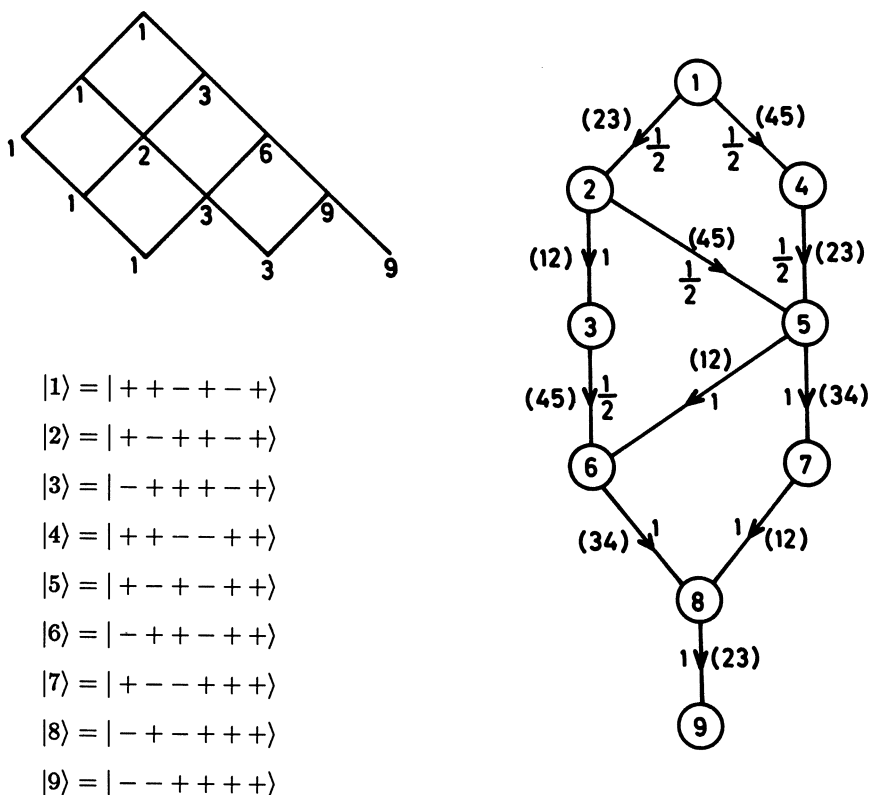


Fig 47. Reversed S-diagram and the SFT graph for $s = 6$, $S = 1$.

SFT graph corresponding to the S-diagram in the reversed lexical ordering is also shown in Fig 47. Computer representation of this graph (Table 2.5) contains additional information. For each spin path $|m\rangle$ result of $(k-1 k)|m\rangle$, as given by graphical rules in

Eq (2.69), is coded in the following way

$$(k-1 k)|m\rangle = \begin{cases} -|m\rangle & 0 \text{ is written} \\ |m\rangle & m \text{ is written} \\ a_k|m\rangle - b_k|m'\rangle & m' \text{ and } S_k \text{ is written} \\ -a_k|m\rangle - b_k|m'\rangle & -m' \text{ and } S_k \text{ is written} \end{cases} \quad (2.71)$$

Table 2.5
Representation of SFT graph for $s = 6, S = 1$

| $(k-1 k)$ | $ 1\rangle$ | $ 2\rangle$ | $ 3\rangle$ | $ 4\rangle$ | $ 5\rangle$ | $ 6\rangle$ | $ 7\rangle$ | $ 8\rangle$ | $ 9\rangle$ |
|-----------|------------------|------------------|------------------|------------------|-----------------|-----------------|-------------|-------------|-------------|
| (12) | 0 | -3 1 | 2 1 | 0 | -6 1 | 5 1 | -8 1 | 7 1 | 0 |
| (23) | $-2 \frac{1}{2}$ | $1 \frac{1}{2}$ | 0 | $-5 \frac{1}{2}$ | $4 \frac{1}{2}$ | 0 | 0 | -9 1 | 8 1 |
| (34) | 1 | 0 | 0 | 0 | -7 1 | -8 1 | 5 1 | 6 1 | 0 |
| (45) | $-4 \frac{1}{2}$ | $-5 \frac{1}{2}$ | $-6 \frac{1}{2}$ | $1 \frac{1}{2}$ | $2 \frac{1}{2}$ | $3 \frac{1}{2}$ | 0 | 0 | 0 |
| (56) | 1 | 2 | 3 | 0 | 0 | 0 | 0 | 0 | 0 |

As an example consider $P = (1234)$ for $s = 4, S = 1$. Using entries from Table 2.5 or SFT subgraph (Fig 47) for the first 3 functions we find

$$\begin{aligned} (1234) \begin{pmatrix} |1\rangle \\ |2\rangle \\ |3\rangle \end{pmatrix} &= (123) \begin{pmatrix} |1\rangle \\ -|2\rangle \\ -|3\rangle \end{pmatrix} = (12) \begin{pmatrix} -a_{\frac{1}{2}}|1\rangle - b_{\frac{1}{2}}|2\rangle \\ b_{\frac{1}{2}}|1\rangle - a_{\frac{1}{2}}|2\rangle \\ |3\rangle \end{pmatrix} \\ &= \begin{pmatrix} a_{\frac{1}{2}}|1\rangle + b_{\frac{1}{2}}a_1|2\rangle + b_{\frac{1}{2}}b_1|3\rangle \\ -b_{\frac{1}{2}}|1\rangle + a_{\frac{1}{2}}a_1|2\rangle + a_{\frac{1}{2}}b_1|3\rangle \\ -b_{\frac{1}{2}}|2\rangle + a_1|3\rangle \end{pmatrix} \end{aligned} \quad (2.72)$$

giving the matrix

$$U((1234)) = \begin{pmatrix} \frac{1}{2} & \frac{-\sqrt{3}}{2} & 0 \\ \sqrt{\frac{1}{12}} & \frac{1}{6} & \frac{-2\sqrt{2}}{3} \\ \sqrt{\frac{2}{3}} & \frac{\sqrt{2}}{3} & \frac{1}{3} \end{pmatrix} \quad (2.73)$$

The algorithm described here requires $|i - j| - 1$ operations (multiplications or sign changes) per matrix element of $(i..j)$ cyclic permutation obtained. Straightforward multiplication of ET matrices $(i..j) = (i i \pm 1)(i \pm 1 i \pm 2)...(j \mp 1..j)$ requires $2f^2$, $f = f(s, S)$ multiplications per one ET matrix, or $2(|i - j| - 1)$ multiplications per element of $(i..j)$. Using SFT table only non-zero elements are computed, while during matrix multiplication calculation of zeros is hard to avoid. Calculation of matrices for all cycles $(i..j)$, $i, j = 1, 2..s$ may be organized in such a way, that at most one multiplication is done to obtain new matrix element (Duch 1985a). This is obvious, because $(i + 1..j)|m\rangle$ is obtained from $(i..j)|m\rangle$ with the help of SFT table at a cost of no more than one operation per new element. It is hard to improve upon the efficiency of

this algorithm when matrices for all cycles are calculated (Duch 1986). For an arbitrary cycle a simple modification of the present algorithm reduces the number of operations per matrix element obtained to at most 3. If $(k-1 k)$ joins m, m' nodes in the SFT graph then

$$\langle m' | (i..j) | m \rangle = \langle m' | (i..k-1) | m' \rangle \langle m' | (k-1 k) | m \rangle \langle m | (k..j) | m \rangle \quad (2.74)$$

Diagonal matrix elements are easily calculated and stored

$$\langle m | (i..j) | m \rangle = (i..j)_{mm} = (i i \pm 1)_{mm} (i \pm 1 i \pm 2)_{mm} \dots (j \mp 1 j)_{mm} = \prod_k a_k \quad (2.75)$$

where the product of a_k is taken along the spin path $|m\rangle$. In practice the rows $(k-1 k)$ table containing diagonal elements (cf Table 2.6) are taken from SFT table or directly from S-diagram, and the other rows are obtained by recursive multiplication, eg. $(234) = (23)(34)$.

Table 2.6
Diagonal elements of $U((i..j))$
matrices for $s = 4, S = 1$

| $(i..j)$ | $ 1\rangle$ | $ 2\rangle$ | $ 3\rangle$ |
|----------|----------------|----------------|----------------|
| (12) | -1 | $-\frac{1}{3}$ | $\frac{1}{3}$ |
| (123) | $\frac{1}{2}$ | $-\frac{1}{6}$ | $-\frac{1}{3}$ |
| (1234) | $\frac{1}{2}$ | $\frac{1}{6}$ | $\frac{1}{3}$ |
| (23) | $-\frac{1}{2}$ | $\frac{1}{2}$ | -1 |
| (234) | $-\frac{1}{2}$ | $-\frac{1}{2}$ | 1 |
| (34) | 1 | -1 | -1 |

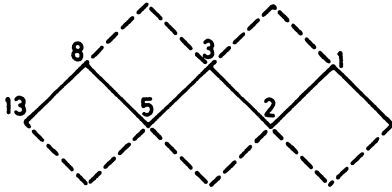
Calculation of $(i..j)$ elements is performed in the following way: the spin function $|m\rangle$ is chosen and diagonal element taken from the table of diagonal elements. The SFT table is scanned for function $|m\rangle$ and ETs of the $(i..j)$ cycle. If some $(k-1 k)$ couples $|m\rangle$ with $|m_1\rangle$ function coefficient $B_k = b_k(k..j)_{mm}$ is calculated and the element $(i..j)_{m_1 m} = (i..k-1)_{m_1 m_1} B_k$. The SFT table is now scanned for functions $|m\rangle, |m_1\rangle$ and ETs of the $(i..k-1)$ cycle. If $(l-1 l)$ couples $|m_1\rangle$ to $|m_2\rangle$ the element $(i..j)_{m_2 m} = (i..l-1)_{m_2 m_2} b_l B_l$, with $B_l = (l..k-1)_{m_1 m_1} B_k$ is calculated. Three multiplications are necessary to get this and further $(i..j)_{m' m}$ elements, provided that intermediate results B_k, B_l, \dots are stored. Using this method for (1234) cycle we obtain

$$(1234) \begin{pmatrix} |1\rangle \\ |2\rangle \\ |3\rangle \end{pmatrix} = \begin{pmatrix} (1..4)_{11}|1\rangle + (12)_{22} B_{\frac{1}{2}}|2\rangle + (-b_1) B_{\frac{1}{2}}|3\rangle \\ (12)_{11}(-b_{\frac{1}{2}})(34)_{22}|1\rangle + (1..4)_{22}|2\rangle + (-b_1)(234)_{22}|3\rangle \\ (-b_1)(234)_{33}|2\rangle + (1..4)_{33}|3\rangle \end{pmatrix} \quad (2.76)$$

with $B_{\frac{1}{2}} = (-b_{\frac{1}{2}})(34)_{11}$

It is interesting to note that the number of non-zero elements per column – let us call it r – depends on the length of the cycle and is independent of the $f(s, S)$ i.e. matrix size, except for an obvious inequality $r \leq f(s, S)$.

In fact, looking at the zig-zag spin path, coupled by a cyclic permutation to the largest number of other spin paths, drawn here with the dashed lines, we find, that the maximum number of non-zero elements in a cycle of length $|i - j|$, designed by $r_{max}(l)$ and fulfilling the relation $r_{max}(l) = r_{max}(l-1) + r_{max}(l-2)$, is one of the Fibonacci numbers (cf Schroeder 1984) with $r_{max}(1) = 2, r_{max}(2) = 3$.



For large s and some S values the dimension $f(s, S)$ grows faster than Fibonacci numbers. Then, even for the longest cycle $(1..s)$, each column of the corresponding matrix contains many zeros. Using branching diagram of Fig 46 we can set the following table

| | | | | | | | | | | | |
|-----------|---|---------------|---|---------------|----|---------------|----|---------------|----|---------------|-----|
| s | 2 | 3 | 4 | 5 | 6 | 7 | 8 | 9 | 10 | 11 | 12 |
| S | 0 | $\frac{1}{2}$ | 1 | $\frac{1}{2}$ | 1 | $\frac{1}{2}$ | 1 | $\frac{3}{2}$ | 1 | $\frac{3}{2}$ | 1 |
| $f(s, S)$ | 1 | 2 | 3 | 5 | 9 | 14 | 28 | 48 | 90 | 165 | 297 |
| r_{max} | 2 | 3 | 5 | 8 | 13 | 21 | 34 | 55 | 89 | 144 | 233 |
| max r | 1 | 2 | 3 | 5 | 8 | 13 | 21 | 21 | 34 | 34 | 55 |

For a given s that spin S is chosen which gives maximal $f(s, S)$. The maximal number of non-zero elements in a column, max r , is for all s lower than its estimation using Fibonacci numbers, and for $s \geq 6$ is also lower than the dimension $f(s, S)$. With their dimension growing the matrices tend to be more and more empty. The number of non-zero elements in all $\binom{s}{2}$ matrices for cycles $(i..j), i > j$ is given in Table 2.7. Dividing it by the total number of elements $\binom{s}{2} f(s, S)^2$ gives the percent of non-zero elements in all cycles.

Table 2.7
Non-zero elements in all $U((i..j))$ matrices

| s | S | $f(s, S)$ | No. elem. | % non-zero |
|-----|-----|-----------|-----------|------------|
| 6 | 0 | 5 | 185 | 49.3 |
| 6 | 1 | 9 | 381 | 31.4 |
| 8 | 0 | 14 | 1464 | 26.7 |
| 8 | 1 | 28 | 3364 | 15.3 |
| 10 | 0 | 42 | 11070 | 14.0 |
| 10 | 1 | 90 | 27359 | 7.5 |

It is worthwhile to note, that changing the spin couplings from the genealogical (called also Yamanouchi-Kotani) coupling scheme to some other coupling increases the

percent of non-zero elements in matrices for cycles. In Serber spin coupling scheme (Serber 1934; Fig 38), where pairs of spins are first coupled to a singlet or triplet, the pairs coupled later to the desired spin S , matrices for transpositions (12), (34), (56)... are diagonal. However, the number of non-zero elements in Serber's case, even when only one matrix among those related by a sign change is stored (cf Duch and Karwowski 1982), is still greater than the number of non-zero elements in genealogical coupling.

C. Manipulations with permutations.

Let us come back to the evaluation of spin integrals. To calculate elements of products of cyclic permutations we should become more familiar with products of cycles and transpositions. Although manipulation with cycles is very simple it is good to recall some of the rules. First, transposition $(a\ b)$ is symmetric, $(a\ b) = (b\ a)$, while a cycle $(a..b)$ is usually not. Two transpositions, sharing the same index, may be joined together. Inside the cycle we may rotate the indices clockwise or counterclockwise, and then break the cycle into smaller cycles or transpositions. The rules of commutation are easily found in this way.

$$(a\ b)(b\ c) = (a\ b\ c) = (b\ c\ a) = (b\ c)(a\ c) = (c\ a\ b) = (a\ c)(a\ b) \quad (2.77)$$

Multiplication of a transposition $(a\ b)$ by a cycle that contains the a, b indices gives

$$\begin{aligned} (a\ b)(a..b \pm 1\ b) &= (a\ b)(b\ a..b \pm 1) = (a..b \pm 1) \\ (a\ b)(i..a\ b..j) &= (i..b..j) \\ (i..a\ b..j)(a\ b) &= (i..a..j) \end{aligned} \quad (2.78)$$

Multiplication of $(a..b)$ by the reciprocal cycle $(b..a)$ gives a unit permutation. Therefore

$$\begin{aligned} (a\ b) &= (a..b \pm 1\ b)(b \pm 1..a) = (a..b \pm 1)(b..a) \\ &= (b..a \mp 1\ a)(a \mp 1..b) = (b..a \mp 1)(a..b) \end{aligned} \quad (2.79)$$

With these rules in mind we can bring products of arbitrary cycles to simplified form. In particular products of two cycles $(i..j)(k..l)$ are quite frequently not in the desired ordering. Because all possible relations between i, j, k, l indices appear when the four-segment loops in the three-slope graph are analyzed it is worthwhile to analyze the two cycle products carefully. There are 24 different relations between the four indices. Let us represent the cycle $(i..j)$ as an arrow $i \longrightarrow j$ if $i < j$ or $j \longleftarrow i$ if $j < i$, and the second cycle by a similar arrow placed above the first. The relative position of the two arrows shows the relations between the four indices and helps to write down systematically all

the cases (Table 2.8). To find $(k'..l')(i'..j') = (i..j)(k..l)$ the following four rules should be used

$$\begin{aligned} i \leq p < j, p' = p + 1; \quad j < p \leq i, p' = p - 1; \quad p = k, l \\ k < p \leq l, p' = p - 1; \quad l \leq p < k, p' = p + 1; \quad p = i, j \end{aligned} \quad (2.80)$$

These rules are written below the Table 2.8, with • representing one of the indices.

They result from consideration of the position p index is moved to after the permutation is done. Alternatively, one may easily prove each case in Table 2.8 by a direct calculation and derive general rules considering all cases in the Table. As an example let us calculate case No. 17, for $i < k < l < j$.

$$\begin{aligned} (i..j)(k..l) &= (i..k \ k + 1..l \ l + 1..j)(k..l) = (k + 1..l \ l + 1..j \ i..k)(k..l) \\ &= (k + 1..l + 1..j)(j \ i..k..l) = (k + 1..l + 1)(l + 1..j)(i..k..l)(l \ j) \\ &= (k + 1..l + 1)(i..l)(l + 1..j \ l) = (k + 1..l + 1)(i..j) \end{aligned} \quad (2.81)$$

D. Presence of the singlet-coupled pairs.

In Eq (2.70) we have already found a proper combination of $| + - \rangle, | - + \rangle$ states coupling the pairs of spins to a singlet. S-diagrams with such SCPs were presented and analyzed by Duch and Karwowski (1985). SCPs do not change the couplings in the S-diagram, they simply lead to renumbering of spins. Let us prove first that a SCP may be removed from a loop range. Spin eigenfunction with a SCP at positions $k, k + 1$ may be written as $|\Theta_1(1..k-1) \overset{+}{\underset{k \ k+1}{-}} \Theta_2(k+2..N)\rangle$. It is easy to see that

$$(N..k)^2 |\Theta_1(1..k-1) \overset{+}{\underset{k \ k+1}{-}} \Theta_2(k+2..N)\rangle = |\Theta_1(1..k-1) \Theta_2(k..N-2) \overset{+}{\underset{N \ N+1}{-}} \rangle \quad (2.82)$$

i.e. the cycle product $(N..k)^2$ simply shifts the SCP from position $k, k + 1$ to the last two positions $N - 1, N$. Calculating elements $\langle \Sigma | P | \Theta \rangle$ we may remove the SCPs common to both spin functions out of the permutation range. If in the range of a cycle $P = (i \ i + 1..k \ k + 1..j)$ indices $k, k + 1$ correspond to SCP in $|\Theta_k\rangle$ then the same SCP must be at positions $k + 1, k + 2$ in $\langle \Sigma |$. Designating by $\langle \Sigma_N |, |\Theta_N\rangle$ spin functions with SCP at the last positions we have

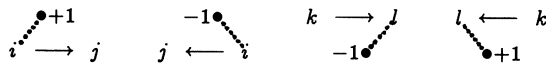
$$\begin{aligned} \langle \Sigma | (i \ i + 1..k \ k + 1..j) | \Theta \rangle &= \langle \Sigma_N | (N..k + 1)^2 (i..j)(k..N)^2 | \Theta_N \rangle \\ &= \langle \Sigma_N | (N..k + 1)^2 (k + 1..N)^2 (i..j - 2) | \Theta_N \rangle = \langle \Sigma_N | (i..j - 2) | \Theta_N \rangle \end{aligned} \quad (2.83)$$

where the cycles $(i..j)(k..N)$ were commuted as in case No 9, Table 2.8. Removing the SCPs out of the permutation range we simply have to renumber spins. The same is true not only for cyclic permutations, but also for an arbitrary permutation P , because

Table 2.8
 Products of two cycles: $(i..j)(k..l) = (k'..l')(i'..j')$

| No | Symbolic rep. | Index relations | $(k'..l')$ $(i'..j')$ |
|----|-------------------------------------|-----------------------|-----------------------|
| 1 | $i \xrightarrow{j} k \rightarrow l$ | $i \leq j < k \leq l$ | $(k..l)$ $(i..j)$ |
| 2 | $j \xleftarrow{i} k \rightarrow l$ | $j \leq i < k \leq l$ | $(k..l)$ $(i..j)$ |
| 3 | $i \xrightarrow{j} l \leftarrow k$ | $i \leq j < l \leq k$ | $(k..l)$ $(i..j)$ |
| 4 | $j \xleftarrow{i} l \leftarrow k$ | $j \leq i < l \leq k$ | $(k..l)$ $(i..j)$ |
| 5 | $k \rightarrow l \xrightarrow{i} j$ | $k \leq l < i \leq j$ | $(k..l)$ $(i..j)$ |
| 6 | $k \rightarrow l \xleftarrow{j} i$ | $k \leq l < j \leq i$ | $(k..l)$ $(i..j)$ |
| 7 | $l \leftarrow k \xrightarrow{i} j$ | $l \leq k < i \leq j$ | $(k..l)$ $(i..j)$ |
| 8 | $l \leftarrow k \xleftarrow{j} i$ | $l \leq k < j \leq i$ | $(k..l)$ $(i..j)$ |
| 9 | $k \rightarrow l \xrightarrow{i} j$ | $i \leq k < j \leq l$ | $(k+1..l)$ $(i..j-1)$ |
| 10 | $l \leftarrow k \xleftarrow{j} i$ | $l < j < k < i$ | $(k-1..l)$ $(i..j+1)$ |
| 11 | $k \rightarrow l \xrightarrow{i} j$ | $k < i \leq l < j$ | $(k..l+1)$ $(i-1..j)$ |
| 12 | $j \xleftarrow{i} l \leftarrow k$ | $j < l \leq i < k$ | $(k..l-1)$ $(i+1..j)$ |
| 13 | $j \xleftarrow{i} l \leftarrow k$ | $j < k \leq i \leq l$ | $(k-1..l)$ $(i-1..j)$ |
| 14 | $l \leftarrow k \xrightarrow{i} j$ | $l \leq i \leq k < j$ | $(k+1..l)$ $(i+1..j)$ |
| 15 | $i \xrightarrow{j} l \leftarrow k$ | $i \leq l \leq j < k$ | $(k..l+1)$ $(i..j+1)$ |
| 16 | $k \rightarrow l \xleftarrow{j} i$ | $k < j \leq l \leq i$ | $(k..l-1)$ $(i..j-1)$ |
| 17 | $i \xrightarrow{j} k \rightarrow l$ | $i \leq k \leq l < j$ | $(k+1..l+1)$ $(i..j)$ |
| 18 | $i \xrightarrow{j} k \rightarrow l$ | $i \leq l \leq k < j$ | $(k+1..l+1)$ $(i..j)$ |
| 19 | $k \rightarrow l \xrightarrow{i} j$ | $k < i \leq j \leq l$ | $(k..l)$ $(i-1..j-1)$ |
| 20 | $k \rightarrow l \xleftarrow{j} i$ | $k < j \leq i \leq l$ | $(k..l)$ $(i-1..j-1)$ |
| 21 | $l \leftarrow k \xrightarrow{i} j$ | $l \leq i \leq j < k$ | $(k..l)$ $(i+1..j+1)$ |
| 22 | $l \leftarrow k \xleftarrow{j} i$ | $l \leq j \leq i < k$ | $(k..l)$ $(i+1..j+1)$ |
| 23 | $j \xleftarrow{i} k \rightarrow l$ | $j < k \leq l \leq i$ | $(k-1..l-1)$ $(i..j)$ |
| 24 | $j \xleftarrow{i} k \rightarrow l$ | $j < l \leq k \leq i$ | $(k-1..l-1)$ $(i..j)$ |

Symbolic rules



The index \bullet lies between the indices attached to the arrow or is equal to an index joined by the dotted line.

the matrix $U(P)$ may always be computed as a product of the matrices for cycles. The equality above shows, that one may calculate the $U(P)$ matrices using positions of indices $\bar{i}, \bar{j} = 1..s$ as was done in the previous section.

What happens, if the two configurations differ on one SCP, so that $s_R = s_L - 2$ for example? Let the SCP follow all singles in $|R\rangle$, i.e. be at the positions $s - 1, s$. We should calculate $[U(P_{|s-1})]^{ff'}$ matrix, where only the rectangular part $f = f(s_L, S)$ by $f' = f(s_L - 2, S)$ should be calculated. This matrix is quite easy to obtain

$$[U(P_{|s-1})]^{ff'} = [U(P)]^{ff} [U(I_{|s-1})]^{ff'} = \sqrt{2} [U(P)]^{ff'} \tag{2.84}$$

The matrix $[U(I_{|s-1})]^{ff'}$ is diagonal, with the first $f(s - 2, S)$ elements equal to +1, because due to the reverse lexical ordering of the branching diagram paths (cf Fig 47), the first $f(s - 2, S)$ functions have SCP at position $s - 1, s$, thus giving +1 elements, with the normalization of an ‘unbalanced’ double contributing $\sqrt{2}$, as in Eq (2.39). The remaining $f(s, S) - f(s - 2, S)$ functions with triplet coupled pairs at these positions have no influence on f by f' matrix. Suppose now that the SCP is at some arbitrary position $k, k + 1$. Then

$$[U(P_{|k})]^{ff'} = [U(P)]^{ff} [U(I_{|k})]^{ff'} \tag{2.85}$$

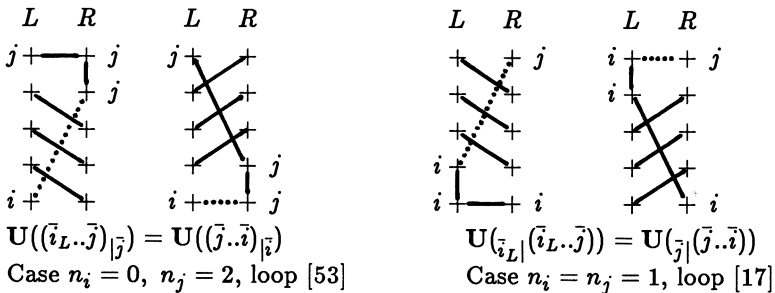
The $[U(I_{|k})]^{ff'}$ matrix is no longer diagonal. It has at most two non-zero elements per column, given by C^+ , C^- coefficients

$$U(I_{|k})_{\Sigma, \Theta} = U((k..s)_{|s-1})_{\Sigma, \Theta} = \begin{cases} \sqrt{2}C^+ & \text{for } |\Sigma\rangle = \langle \Theta_1 \text{---} \Theta_2 | \\ -\sqrt{2}C^- & \text{for } |\Sigma\rangle = \langle \Theta_1 \text{---} \Theta_2 | \\ 0 & \text{otherwise } k \ k + 1 \end{cases} \tag{2.86}$$

From Eq(2.82) it immediately results

$$\begin{aligned} U((i..j)_{|j}) &= U((i..j+1)_{|j}) = U((j..i)_{|i-1}) = U((j..i-1)_{|i-1}); \quad i > j \\ U(j_{|j}(j..i)) &= U(j_{|j}(j+1..i)) = U(i_{|i-1}(i..j)) = U(i_{|i-1}(i-1..j)) = U((i..j)_{|j})^\dagger \end{aligned} \tag{2.87}$$

The equalities above have a simple graphical explanation. They reflect how orbital ordering is changed when a SCP in one of the configurations is moved to another place.



As usually dotted lines join the orbitals equal in $|L\rangle$ and $|L'\rangle = \hat{E}_{ij}|R\rangle$ but different in $|L\rangle, |R\rangle$. Matrix elements of \hat{E}_{ij} for $n_i = 0, n_j = 2$ are therefore equal to $\mathbf{U}((\bar{i}_L \dots \bar{j})_{|\bar{j}})$ and for $n_i = n_j = 1$ to $\mathbf{U}((\bar{j} \dots \bar{i}_L)_{|\bar{i}_L})^\dagger$, i.e. they are combinations of columns of the full $\mathbf{U}((\bar{i} \dots \bar{j}))$ matrices, multiplied by $\sqrt{2}$ due to the scalar factor in Eq (2.39).

If the SCP at positions $k, k+1$ is within the range of a cycle $(i \dots j)$, for example $i > k > j$, then $\mathbf{I}_{|k}$ may be commuted with the cycle in the following way:

$$[\mathbf{U}((i \dots j)_{|k})]^{ff'} = [\mathbf{U}(\mathbf{I}_{|k-1})]^{ff'} [\mathbf{U}((i-2 \dots j))]^{f'f'} \quad (2.88)$$

and the matrix of a cycle is calculated in $f' = f(s-2, S)$ dimensional spin space.

There is one more case that should be covered, $n_i = 1, n_j = 2$. Similarly as in the previous section it may be reduced to the case $n_i = 0, n_j = 1$ with minus sign. In Table 2.4 the ordering permutation $P = (\bar{j}_L, s+1)(\bar{j} \dots \bar{i})$ is given, with $s+1$ corresponding to a SCP in both configurations. Moving these pairs to the positions $j+1, j+2$ direct calculation shows that

$$\mathbf{U}((j \ s+1)_{|s+1}) = \mathbf{U}((j \ j+1)_{|j+1}) = \mathbf{U}((j \ j+1 \ j+2)_{|j+1}) = -\frac{1}{2}\mathbf{I} \quad (2.89)$$

To prove it let us note that

$$a = \frac{1}{2S=1}; \quad a_{\pm} = \frac{1}{2(S \pm \frac{1}{2}) + 1} = \frac{1}{1/a \pm 1} = \frac{a}{1 \pm a} \quad (2.90)$$

Now draw S-diagram arcs joining vertices $j-1, j$ and $j+1$ and take the coefficients a, C^+, C^- for S_{j+1} intermediate spin value. Then

$$\begin{aligned} \left\langle \begin{array}{c} \text{---} \bullet \text{---} \bullet \\ \diagdown \quad \diagup \\ \bullet \text{---} \bullet \end{array} \middle| (j \ j+1) \middle| \begin{array}{c} \text{---} \bullet \text{---} \bullet \\ \diagdown \quad \diagup \\ \bullet \text{---} \bullet \end{array} \right\rangle &= -(C^+)^2 + (C^-)^2 a_- = -\frac{1}{2} \\ \left\langle \begin{array}{c} \text{---} \bullet \text{---} \bullet \\ \diagup \quad \diagdown \\ \bullet \text{---} \bullet \end{array} \middle| (j \ j+1) \middle| \begin{array}{c} \text{---} \bullet \text{---} \bullet \\ \diagdown \quad \diagup \\ \bullet \text{---} \bullet \end{array} \right\rangle &= -(C^+)^2 a_+ - (C^-)^2 = -\frac{1}{2} \end{aligned} \quad (2.91)$$

Off-diagonal elements are zero because $(j-1)$ -th arc is not affected by $(j \ j+1)$ transposition. The scalar factor $\sqrt{2}^{n_i+n_j-1} = 2$ makes the contribution of a transposition involving SCP the negative unit matrix. As a result $\mathbf{U}(P) = -\mathbf{U}((\bar{j} \dots \bar{i}))$ in this case. This concludes calculation of single shift operator matrix elements. Summing up, the elements corresponding to the two-segment loops are calculated in the following way

$$\langle L : \hat{S}^2 | \hat{E}_{ij} | R : \hat{S}^2 \rangle = \begin{cases} \mathbf{U}((\bar{i}_L \dots \bar{j})) & \text{for loop [13], [31]} \\ -\mathbf{U}((\bar{i} \dots \bar{j}_L))^\dagger & \text{for loop [57], [75]} \\ \mathbf{U}((\bar{i}_L \dots \bar{j})_{|\bar{j}}) & \text{for loop [53], [35]} \\ \mathbf{U}((\bar{j} \dots \bar{i}_L)_{|\bar{i}_L})^\dagger & \text{for loop [17], [71]} \end{cases} \quad (2.92)$$

Table 2.9
Total number of elements
in the unique $\langle L|\hat{E}_{ij}|R\rangle$ matrices.

| S | s | $U((\bar{i}..\bar{j})), i > j$ | $U((\bar{i}..\bar{j}) _{\bar{j}})$ | Total No |
|---------------|-----|--------------------------------|------------------------------------|----------|
| 0 | 6 | 375 | 360 | 735 |
| 0 | 8 | 5488 | 4480 | 9968 |
| 0 | 10 | 79380 | 58800 | 138180 |
| $\frac{1}{2}$ | 7 | 4116 | 3430 | 7546 |
| $\frac{1}{2}$ | 9 | 63504 | 47628 | 111132 |
| 1 | 6 | 1215 | 972 | 2187 |
| 1 | 8 | 21952 | 16128 | 38080 |
| 1 | 10 | 364500 | 252000 | 616500 |
| $\frac{3}{2}$ | 7 | 4116 | 2744 | 6860 |
| $\frac{3}{2}$ | 9 | 82944 | 54432 | 137376 |

For some applications (cf Siegbahn 1984; Duch 1986) this is the end of the story. Only two kinds of representation matrices appear in these formulas: cyclic $(i..j)$, $i > j$ (for $i < j$ transposed $(j..i)$ matrices should be taken) and $(i..j)|_j$ for all i, j . Although calculation of the matrices for cycles using the algorithm described here is very fast in large scale calculations it is advisable to precompute and store them. Elements of the $U((\bar{i}..\bar{j}))$ matrices for large number of open shells are mostly zero (cf Table 2.7), making the cases of $s \leq 10$ easily manageable on modern computers. Storage of $U((\bar{i}..\bar{j})|_j)$ matrices is not so important because using Eq (2.85-86,2.88) these matrices are calculated as combinations of columns or rows of $U((\bar{i}..\bar{j}))$ matrices. However, it is clear from the Table 2.9 that for very large number of open shells some ways of reducing the dimension of the spin space are necessary. Because such a reduction has no influence on the methods of matrix element calculation it is more appropriate to discuss it when dealing with applications (cf Duch 1985b; Duch and Karwowski 1985). In most methods matrix elements of the products of the shift operators are the most cumbersome.

E. Products of shift operators.

There are two approaches to evaluation of matrix elements of shift operators' products using three-slope graph. First, one can find the ordering permutation bringing orbitals in $\langle L|$ in maximal ordering with those in $|L'\rangle = \hat{E}_{ij}\hat{E}_{kl}\dots|R\rangle$. For two-particle operators detailed analysis of all four-segment loops shows (Duch and Karwowski 1985) that $U(P)$ is always expressible as a product of two matrices for cyclic permutations. The final formulas are very compact and involve matrices for arbitrary cycles $U((\bar{i}..\bar{j}))$, which may be precomputed and stored, and matrices with one or two SCPs in arbitrary

positions $U(\vec{i} \dots \vec{j})_{|\vec{k}, \vec{l}\rangle}$, which are calculated whenever required. Second approach, developed here, is based on factorization of products using Eq (2.66). It has an advantage of using only $U(\vec{i} \dots \vec{j})_{|\vec{j}\rangle}$ matrices that may be precomputed and stored. Moreover, the intermediate state $|I\rangle$ may always be chosen in such a way that $f(s_I, S) \leq f(s_R, S)$, thus saving some multiplications in product of matrices corresponding to the two elements $\langle L; \hat{S}^2 | \hat{E}_{ij} | I; \hat{S}^2 \rangle$, $\langle I; \hat{S}^2 | \hat{E}_{kl} | R; \hat{S}^2 \rangle$. Analysis of the four-segment loops gives the same formulas as before (Duch and Karwowski 1985) for a few loops involving only [13], [57] two-segment loops, and simplified formulas in all other cases. Computational methods presented below allow for derivation of formulas in both approaches.

Let us start from the same example as was considered in the previous sections, i.e. element $\langle 011121 | \hat{H} | 112011 \rangle$. Drawing the paths open loop [1537] with four nonparallel segments is found. Reduction of this loop to a product of two-segment loops may be done in two ways, giving two contributions to matrix element, as shown in Fig 48.

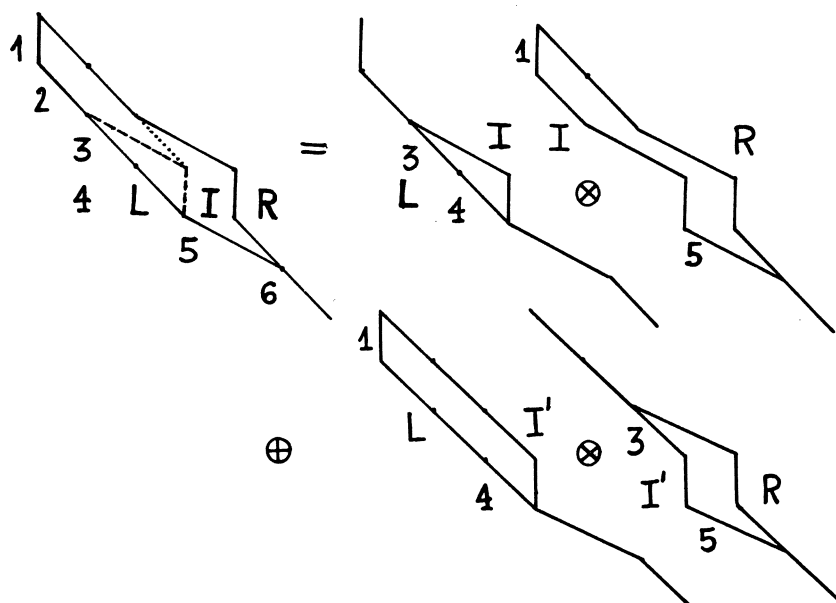
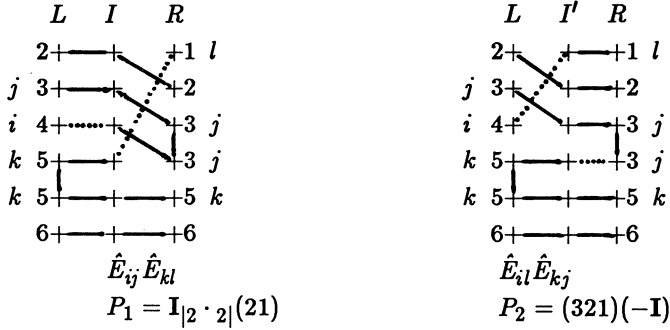


Fig 48. Factorization of the four-segment loop [1537] into a product of two-segment loops $[53] \otimes [17] \oplus [13] \otimes [57]$.

The intermediate path corresponding to the state $|I\rangle$ is parallel to the $|R\rangle$ path except for two arcs: one at the lowest non-parallel segment and the other either at the first, or at the second decreasing segment. In Fig 48 the first possibility corresponds to the integral $\{43|51\}$ and the operator product $\hat{E}_{43}\hat{E}_{51}$ and the second to the integral $\{41|53\}$ and the product $\hat{E}_{41}\hat{E}_{53}$. The loop is factorized into $[1537] = [53] \otimes [17] \oplus [13] \otimes [57]$. The orbitals of $|L\rangle$ that do not appear in $|R\rangle$ are designated i, j , $i > j$, and the orbitals of $|R\rangle$ that do not appear in $|L\rangle$ are designated k, l , $k > l$. In our example



$i = 5, j = 4, k = 3, l = 1$. The first operator product is thus $\hat{E}_{ij}\hat{E}_{kl}$ and the second $\hat{E}_{il}\hat{E}_{kj}$. To find the permutations let us draw the orbital orderings.

All four cases of Eq (2.91) appear in this example. Permutation P_1 puts orbital k in $|I\rangle$ against l in $|R\rangle$, with orbital j , doubly occupied in both configurations, being removed from the permutation range. Orbitals of $|L\rangle$ are already in a proper order contributing only $I|_2$. General form of the structure constant coefficients for this loop may be written as

$$\begin{aligned} \tilde{A}_{LR}^{ijkl} &= \tilde{A}_{LI}^{[53]}\tilde{A}_{IR}^{[17]} = \mathbf{U}((\bar{i}_L.. \bar{j}_I)_{|\bar{j}_I})[\mathbf{U}((\bar{l}.. \bar{k}_I)_{|\bar{k}_I})]^\dagger = \mathbf{U}((\bar{i}.. \bar{j}-1)_{|\bar{j}-1})[\mathbf{U}((\bar{l}.. \bar{k}-1)_{|\bar{k}-1})]^\dagger \\ \tilde{A}_{LR}^{ilkj} &= \tilde{A}_{LI'}^{[13]}\tilde{A}_{I'R}^{[57]} = \mathbf{U}((\bar{i}_L.. \bar{l}_{I'})_{|\bar{l}_{I'}})[-\mathbf{U}((\bar{j}_{I'}.. \bar{k})_{|\bar{k}})] = -\mathbf{U}((\bar{i}.. \bar{l})_{|\bar{l}})\mathbf{U}((\bar{j}.. \bar{k})_{|\bar{k}}) \end{aligned} \tag{2.93}$$

Using S-diagram for $s = 4, S = 0$ to calculate matrix elements of cycles we easily obtain

$$\begin{aligned} \tilde{A}_{LR}^{4351} &= \mathbf{U}(I|_2)\mathbf{U}(2|_2(21)) = \begin{pmatrix} -\sqrt{\frac{1}{2}} \\ \sqrt{\frac{3}{2}} \end{pmatrix} \begin{pmatrix} -\sqrt{\frac{1}{2}} & -\sqrt{\frac{3}{2}} \end{pmatrix} = \begin{pmatrix} \frac{1}{2} & \frac{\sqrt{3}}{2} \\ -\frac{\sqrt{3}}{2} & -\frac{3}{2} \end{pmatrix} \\ \tilde{A}_{LR}^{4153} &= -\mathbf{U}((321)) = \begin{pmatrix} \frac{1}{2} & -\frac{\sqrt{3}}{2} \\ \frac{\sqrt{3}}{2} & \frac{1}{2} \end{pmatrix} \end{aligned} \tag{2.94}$$

i.e. the same matrices as found in Eq (2.64). This time they were computed in a much easier way – no more than one multiplication per element obtained.

Quite another formula for \tilde{A}_{LR}^{ijkl} matrix is found if the intermediate state $|I\rangle$ is not introduced (Duch and Karwowski 1985). Drawing the orbital orderings for $|L\rangle$ and $|L'\rangle = \hat{E}_{ij}\hat{E}_{kl}|R\rangle$, with doubly occupied orbitals k and j shifted to positions $s + 1, s + 2$ we find that the ‘line-up’ permutation for this case is

$$P_1 = (\bar{i}_L, s + 1)(\bar{j}_L, s + 2)(\bar{i}_L.. \bar{l})(\bar{j}_L + 1.. \bar{k})$$

The transpositions between i, j and a SCP are expressed in a simpler way if we calculate, as in Eq (2.90), that

$$[(i\ s + 1) + (i\ s + 2)]|R; \hat{S}^2\rangle = -|R; \hat{S}^2\rangle \quad \text{if} \quad (s + 1\ s + 2)|R; \hat{S}^2\rangle = -|R; \hat{S}^2\rangle \tag{2.95}$$

i.e. if $s + 1$, $s + 2$ spins form a SCP. Then

$$\begin{aligned} I &= [(i\ s + 1) + (i\ s + 2)][(j\ s + 1) + (j\ s + 2)] \\ &= (i\ j)[(i\ s + 1) + (i\ s + 2)] + (i\ s + 1)(j\ s + 2) + (i\ s + 2)(j\ s + 1) \\ &= -(i\ j) + 2(i\ s + 1)(j\ s + 2) \end{aligned} \quad (2.96)$$

and hence $P_1 = \frac{1}{2}(I + (\bar{i}_L\ \bar{j}_L))(\bar{i}_L\dots\bar{l})(\bar{j}_L+1..\bar{k})$. Numerical factor in front of the matrix is equal $\sqrt{2^{n_i+n_j-1}} = 2$. One can express \tilde{A}_{LR}^{ijkl} matrix in three equivalent forms:

$$\begin{aligned} \tilde{A}_{LR}^{ijkl} &= \mathbf{U}((\bar{i}..\bar{j}-1)_{|\bar{j}-1})[\mathbf{U}((\bar{l}..\bar{k}-1)_{|\bar{k}-1})]^\dagger = [\mathbf{I} + \mathbf{U}((\bar{i}\ \bar{j}-1))] \mathbf{U}((\bar{i}..\bar{l})(\bar{j}..\bar{k})) \\ &= \mathbf{U}((\bar{i}..\bar{l})(\bar{j}..\bar{k})) + \mathbf{U}((\bar{j}-1..\bar{l})(\bar{i}..\bar{k})) \end{aligned} \quad (2.97)$$

If these formulas are used directly the first one is computationally the most attractive. However, if several four-segment loops in a graph are analysed at the same time matrices for products $(\bar{i}..\bar{l})(\bar{j}..\bar{k})$ and $(\bar{j}-1..\bar{l})(\bar{i}..\bar{k})$ may be used also for other loops and should anyway be computed. Relations between loop values and the unique matrices that have to be calculated are analysed in details in Part IV (compare also Duch and Karwowski 1985).

There are three types of the four-segment loops $[abcd]$: open type \mathcal{O} , and closed type \mathcal{C} and $\tilde{\mathcal{C}}$, as described in section 2.3. Factorization of the four-segment loops into two-segment ones depends only on a loop type

$$[abcd] = \begin{cases} [ab] \otimes [cd] \oplus [ad] \otimes [bc] & \text{for loops type } \mathcal{C} \\ [ab] \otimes [cd] \oplus [ac] \otimes [bd] & \text{for loops type } \tilde{\mathcal{C}} \\ [ac] \otimes [bd] \oplus [ad] \otimes [bc] & \text{for loops type } \mathcal{O} \end{cases} \quad (2.98)$$

Although the ordering of the two-segment loops is arbitrary, for example in Fig 48 it is $[bc] \otimes [ad]$, it has an influence on the permutations. The corresponding matrix element of a two-particle operator \hat{H} is

$$\hat{H}_{[abcd]} = \begin{cases} J_1 \mathbf{U}(P_{[ab]}P_{[cd]}) + J_2 \mathbf{U}(P_{[ad]}P_{[bc]}) & \text{loops type } \mathcal{C} \\ J_1 \mathbf{U}(P_{[ab]}P_{[cd]}) + J_3 \mathbf{U}(P_{[ac]}P_{[bd]}) & \text{loops type } \tilde{\mathcal{C}} \\ J_3 \mathbf{U}(P_{[ac]}P_{[bd]}) + J_2 \mathbf{U}(P_{[ad]}P_{[bc]}) & \text{loops type } \mathcal{O} \end{cases} \quad (2.99)$$

$$\text{with } J_1 = \{ab|cd\}; J_2 = \{ad|bc\}, J_3 = \{ac|bd\}; \quad a < b < c < d$$

In general $P_{[ab]}P_{[cd]} \neq P'_{[cd]}P'_{[ab]}$, where $P_{[ab]}$ is a cyclic 'line-up' permutation placing the 'extra' orbital (the one that has no counterpart in the other configuration) of the segment a against the 'extra' orbital of the segment b . Permutations P' are found with the help of the Table 2.8 or by examining the diagrams of orbital orderings.

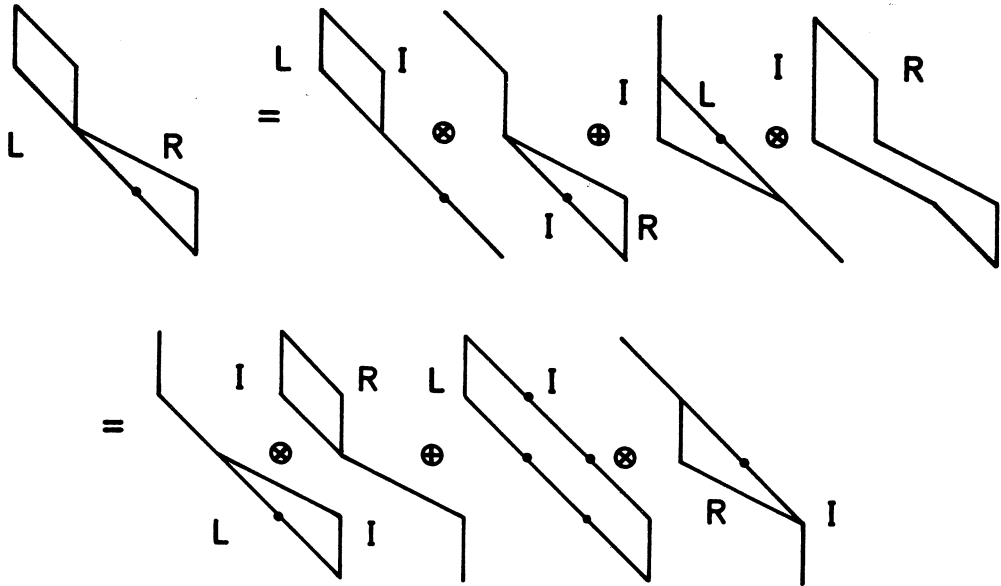


Fig 49. Factorization of the four-segment loop [1353] into a product of two-segment loops [13] ⊗ [53] ⊕ [35] ⊗ [13] = [53] ⊗ [13] ⊕ [13] ⊗ [35].

It is very easy to recognize the loop type. If $[ab]$ is one of the four simple two-segment loops shown in Fig 41, i.e. $[ab] = [13], [57], [17], [53]$, or one of the adjoint loops $[ba] = [31], [75], [35], [71]$, the loop $[abcd]$ is closed; otherwise it is of open type. Closed loop is of the \tilde{C} type if one of the two loops $[ab]$ or $[cd]$ is adjoint while the other is simple. If both two-segment loops are simple or both are adjoint the four-segment loop is of the C type. The assignment of the integrals to loops is thus automatical.

Let us apply the methods described so far to find a formula corresponding to the [1353] loop. The loop is obviously of the C type; its graphical decomposition and the intermediate states are shown in Fig 49. Drawing orbital ordering diagrams with different intermediate configurations or using the Table 2.8 and Eq (2.87) we easily find the permutations

$$\begin{aligned}
 P_{[ij]}P_{[kl]} &= (\bar{k}-1..l)(\bar{i}+1..\bar{j})_{|\bar{j}} = (\bar{k}-1..l)(\bar{j}..\bar{i})_{|\bar{i}} = (\bar{i}+1..\bar{j})_{|\bar{j}}(\bar{k}-1..l) \\
 P_{[il]}P_{[jk]} &= (\bar{i}+1..l)(\bar{k}..\bar{j})_{|\bar{j}} = (\bar{i}+1..l)(\bar{j}+1..\bar{k})_{|\bar{k}} = (\bar{k}-1..\bar{j}-1)_{|\bar{j}-1}(\bar{i}-1..l)
 \end{aligned}
 \tag{2.100}$$

where $i > j > k > l$ and as usually positions of orbitals in configuration $|R\rangle$ are used. The last two forms of the permutations are especially attractive because the matrices for $(\bar{k}-1..l)$, $(\bar{i}-1..l)$ cycles are calculated in $f' = f(s-2, S)$ dimensional spin space.

Three-segment loops are so simple that there is no reason to decompose them into the product of two-segment ones. Elementary three-segment loops with the same number of doubles in both paths (Fig 42, column 1 and 4) lead to $P = (\bar{i}..\bar{j})$ or transposed

permutation, where \bar{i} , \bar{j} are positions of the two singles involved in the configurations they belong to. If the two configurations differ on one double the permutation is $P = (\bar{i}.. \bar{j})_{\bar{j}}$ or transposed (Fig 42, column 2 and 3). The integral is always $J = \{ik|jk\}$ where k corresponds to the level at which segment $[2] = |02|$ or segment $[6] = |20|$ is placed (Duch and Karwowski 1985). If the decomposition into two-segment loops is performed segment $|02|$ is replaced by $|01|$ and $|12|$, and segment $|20|$ by $|21|$ and $|10|$. The loops in each row of Fig 42 are decomposed in a slightly different way

$$\begin{aligned} [2ab] &= [1a] \otimes [5b] = [5a] \otimes [1b] \\ [a2b] &= [a1] \otimes [5b] = [1b] \otimes [a5] \\ [ab6] &= [a7] \otimes [b3] = [b7] \otimes [a3] \end{aligned} \quad (2.101)$$

Of course the same formulas are obtained using this decomposition as by a direct ordering of $|L'\rangle = \hat{E}_{ik} \hat{E}_{jk} |R\rangle$ configuration. The same applies to other products of the shift operators, such as $\hat{E}_{ik} \hat{E}_{kj}$ for example. Decomposition into products of the two-segment loops is worthwhile only for the four-segment loops.

Matrix form of structure constants computation for products of shift operators is an advantage on modern computers. However, in many cases the number of operations to obtain the product of two representation matrices may be drastically reduced. Consider first a permutation P that can be written as the product of elementary transpositions that do not contain the same ET twice. Such a permutation will be called the nonoverlapping permutation. Products of two cycles without omissions that have at most one number in common are nonoverlapping permutations. An arbitrary permutation acting on a given spin function gives in general a linear combination of other functions. In the case of nonoverlapping permutations the coefficients in this combination are given by products of a_k and b_k values. On the SFT graph only the overlapping permutations lead to the routes that cross the same node twice, i.e. create closed loops. To prove it consider the permutation $(k-1 k)P_0$ acting on some function $|m_1\rangle$

$$(k-1 k)P_0|m_1\rangle = (k-1 k) \sum_i C_i |m_i\rangle \quad (2.102)$$

In a branching diagram the states $|m_i\rangle$ differ from $|m_1\rangle$ only in those arcs that were not affected by P_0 permutation. If $(k-1 k)$ did not appear in decomposition of P_0 into ETs there are no states among $|m_i\rangle$ differing only in these two arcs. Therefore the result of $(k-1 k)$ action is to add a_k factors to $C_i |m_i\rangle$ and contribute some new states with $C_i b_k$ coefficients. Applying the same argument over and over if P_0 is nonoverlapping all C_i must be simple products of appropriate a_k , b_k factors. Making a product of two matrices corresponding to $(a..b)$ and $(c..d)$ nonoverlapping cycles element $U((a..b)(c..d))_{kl}$ is equal to $U((a..b))_{ki} U((c..d))_{il}$ for some index i which is easy to determine with the help of SFT graph. If the matrices for the two cycles are stored the product matrix is thus determined at a very low cost of one multiplication per element.

What happens if the two cycles do overlap? Closed loops may appear then in the SFT graph for such permutations. Instead of being simple products matrix elements become linear combinations of such products. Although the elements may still be calculated in the same way a more efficient approach in case of strongly overlapping cycles would be to partition the shorter cycle into the ET or tricycles (three-element cycles). A transposition has at most one off-diagonal element while a tricycle at most two off-diagonal elements in a row. Multiplication of a full f -dimensional matrix by a transposition or a tricycle requires no more than $2f^2$ or $3f^2$ scalar multiplications respectively. A cycle $(i..j)$ contains $|i - j - 1|$ transpositions or $\frac{1}{2}|i - j|$ tricycles (plus one transposition if $|k - l|$ is odd. It is easy to check that already for $s = 6$, $S = 1$ direct multiplication by the tricycles is more efficient than multiplication of full matrices even for the longest cycles. Multiplication by ET matrices is also very efficient, as shown by Rettrup (1985). Another way of reducing the number of multiplications for overlapping permutations is described in the next section.

Summing up, single shift operators are involved in the four elementary two-segment loops Eq (2.91). Three and four segment loops are factorized into products of two-segment loops, Eq (2.98), (2.101). Permutations are obtained drawing the diagrams of orbital orderings and may always be presented as products of cycles without omissions. Matrices representing those cycles are calculated in a very efficient way using S-diagrams and SFT graphs. Matrices corresponding to products of two cycles are calculated either by taking matrix product or by multiplying a matrix corresponding to the longer cycle by ET or tricycle matrices. Cycles with SCPs should be placed to the left of cycles without SCPs to reduce the dimension of corresponding matrices. Computational techniques described in this section allow for straightforward derivation of matrix elements of many-particle operators in the \hat{S}^2 -adapted basis or alternatively for analysis of arbitrary loops in a three-slope graph.

F. Evaluation of matrix elements in the (\hat{L}_z, \hat{S}^2) eigenspace.

Fagot graph approach, described in this section, is ideal for extensions to (\hat{L}_z, \hat{S}^2) -adapted spaces. \hat{L}_z operator acts here as a selector of configurations with the desired M_L values. The three-slope graph has in this case the arc slopes dependent on m_i values; removing the m_S dependence from the graph of Fig 18 we obtain a very convenient graph of \hat{L}_z -adapted configurations. It forms a subgraph of the ordinary $\mathcal{G}_3(n : N)$ graph and should be used in the same way. Each loop formed in the new graph is identical with one of the loops in Fig 41–43 if the dependence of the arc slopes on m_i values is neglected. Adaptation of the three-slope graph to the abelian point group symmetries is formally equivalent to adaptation to \hat{L}_z operator: both cases have no effect on the spin part. Fagot graphs are most appropriate in such cases because they allow for selection of whole subspaces of a given symmetry.

Technically the use of other fagot graphs, like that of Fig 22, is somewhat different, but from the point of view of matrix element evaluation nothing new is added. The tools

presented in this section are directly applicable to all variants of the \hat{S}^2 -adapted graphs that do not influence the spin part. Moreover, once the permutations are determined genealogical S-diagrams may be replaced by Serber diagrams, by restricted S-diagrams (cf Duch and Karwowski 1985), or by any other description of spin space.

Let us see now how to calculate structure constants in \hat{S}^2 -adapted spaces with the help of a non-fagot graph.

2.6

Non-fagot graphs and the \hat{S}^2 -adapted space

S-diagrams are obtained from M-diagrams by removing the points with negative M values (cf Fig 9,19,46). Similarly the four-slope graphs $\mathcal{G}_4(n : N, S)$ and the two-slope graphs $\mathcal{G}_{2,2}(2n : N, S)$ representing \hat{S}^2 -adapted spaces are obtained from the corresponding graphs representing \hat{S}_z -adapted spaces removing points for negative M (cf Fig 5c,7c with Fig 20b,c). It is amazing how much this small change complicates segmentation rules derived in section 2.3 for \hat{S}_z -adapted four-slope graphs. For single shift operators segment values (called one-body segments) instead of ± 1 phase factors for determinants should be expressed using a_s, b_s coefficients of Eq (2.69) and C^+, C^- coefficients for segments [12] or [21] due to equation Eq (2.70). Therefore one-body segment values should be quite straightforward to obtain without graphical methods of spin algebras or general angular momentum theory. Products of many shift operators (many-body segments) in \hat{S}_z -adapted spaces are calculated using the same segmentation values, Eq (2.55). It is not so simple with the spin eigenfunction basis because the product (2.66) involves more than one intermediate state. One may artificially introduce these intermediate states and perform summations using one-body segment values (Shavitt 1978), but for products of two shift operators special tricks are possible reducing the number of intermediate summations to at most two (cf Drake and Schlessinger 1977; Paldus and Boyle 1980; Payne 1982).

Although the two-slope graphs $\mathcal{G}_{2,2}(2n : N, S)$ are simpler in this section I will use the four-slope graph $\mathcal{G}_4(n : N, S)$ to facilitate direct comparison with the unitary group approach results. Reading papers on UGA one finds a number of different notations – not only different authors use different notations, but also the same authors every few years change it. This fact encourages me to introduce yet another designation of loop segments, directly showing the situation in a graph, although Shavitt's typology (1981) will also be used. First let us compare S-diagrams and four-slope graphs.

A. One-body segments.

Let us forget for a moment about the doubly occupied orbitals and look at the paths of S-diagram and the corresponding paths of four-slope graph. Take one of the paths in \mathcal{G}_4 graph, for example $|0 + - - - + +\rangle$ drawn in Fig 50 with the thick line. Intermediate spin values are shown to the left of the path. In the reverse branching diagram this path looks very similar, the 'up' or + arcs (looking from right to left!) slightly less steep and the 'down' or - arcs going down instead of going slightly up as they do in the \mathcal{G}_4 graph. There is one important difference: S-diagrams do not contain empty arcs (nor doubly occupied).

Consider now a shift operator $\hat{E}_{ij} = \hat{E}_{18}$. How to find the combination of states (or, equivalently, matrix elements) this operator is producing when acting on the selected path in Fig 50 ? The operator removes 7-th singly occupied orbital and puts a new orbital, which should be the first singly occupied orbital, in its place, i.e. the shifting cycle in the spin space is (1234567) (to be more formal we could determine that the loop is of [31] type and use Eq (2.92) to find the cycle). In section 2.5A,B I have already described how a cycle acts in S-diagram: using graphical rules Eq (2.69) we easily find the 6 interacting paths. The coefficients introduced by each elementary transposition ($k-1 k$) are assigned to the k -th arc of the path at which the transposition is acting. In this way "a cycle generated subgraph" in the S-diagram is formed (Duch and Karwowski 1985). Matrix elements between the parent path (ket path, thick line in Fig 50) and daughter paths (bra paths, thin lines) are found taking a product of the coefficients along the daughter paths, for example diagonal element is equal to $(-a_1)^2(-1)(-1)a_1(-1)(-1) = -\sqrt{\frac{2}{3}}$.

In \mathcal{G}_4 graph the situation is very similar: a cycle generated subgraph of interacting paths is created. However, the empty arc present in this graph shifts the subgraph in respect to the ket or parent paths (Fig 50). To go back to S-diagram we have to shift the subgraph one level down. Two parallel arcs (a segment) in \mathcal{G}_4 correspond to two arcs in S-diagram, for example a segment $|++|$ becomes two arcs $++$. For the two arcs of the same type there are two possibilities: they either belong to the segment $++$ or $--$ in S-diagram, contributing always (-1) , or one arc belongs to $+-$ and the other to $-+$ segment, in which case they contribute $-b_S$. In the four-slope graph these two situations are recognized by looking at the values of the intermediate spin couplings S_k for the ket and S'_k for the bra arc. For $|++|$ segment $\Delta S_k = S_k - S'_k = \frac{1}{2}$ means that the lower end of the parent path has $S_{k-1} = S'_k$, i.e. it corresponds to $++$ arcs in the S-diagram, so the segment value is (-1) . If $\Delta S_k = -\frac{1}{2}$ the segment value has to be b_S . For $|--|$ segment $\Delta S_k = -\frac{1}{2}$ gives segment value (-1) while $\Delta S_k = +\frac{1}{2}$ gives $-b_S$. To differentiate between these two kinds of segments I will write $|++|, |--|$ for the segments that have value (-1) . Segments $|+-|$ or $|-+|$ have values $\mathcal{W}(|+-|) = a_S$, $\mathcal{W}(|-+|) = -a_S$. First symbol in the segment designation always refers to the bra path and the second to ket path.

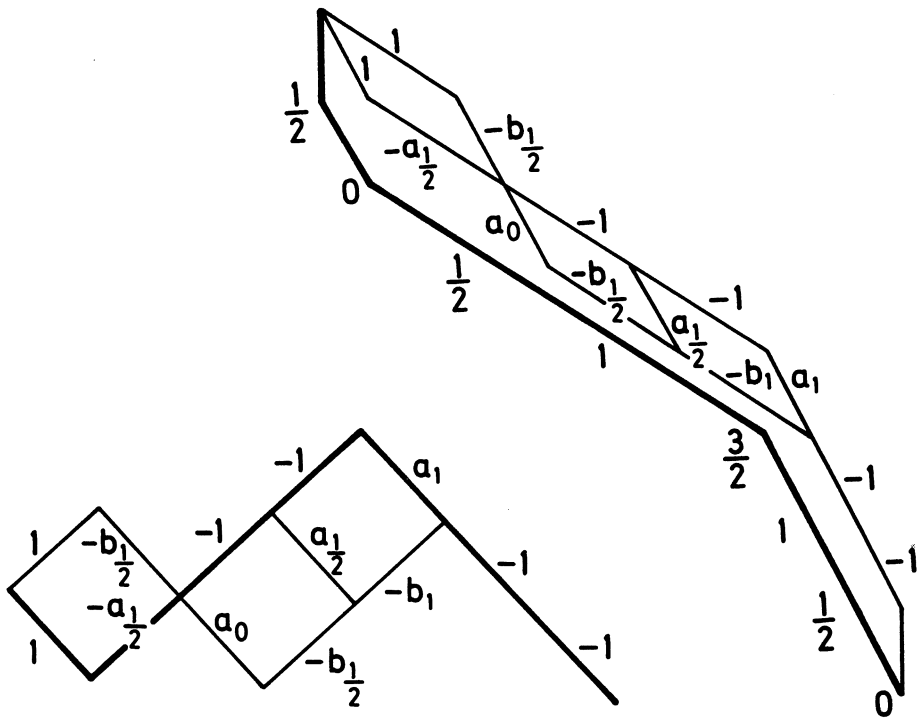


Fig 50. Cycle-generated subgraphs in the S -diagram and in the four-slope graph, for the cycle (1..7), raising operator \hat{E}_{18} . Parent (ket) path is drawn with the thick line. With top-down level numbering the loop is of R type.

The segment values found so far correspond to raising operators \hat{E}_{ij} , $i < j$, called by Shavitt (1981) "segments type R" and by Paldus and Boyle "segments of C' type". Not much different situation is encountered when the lowering operators are considered. Let us move an empty arc of the ket path of Fig 50 to the bottom and take \hat{E}_{81} operator. Reciprocal cycle (7..1) should be taken now, generating subgraph with 10 paths in the S -diagram (Fig 51). The segment values, as is clear from Fig 51, should be taken as $\mathcal{W}(|+-|) = -a_{s'}$, $\mathcal{W}(|-+|) = a_{s'}$, $\mathcal{W}(|++|)$ segments with $\Delta S = -\frac{1}{2}$ and $|--|$ segments with $\Delta S = +\frac{1}{2}$ the value is (-1) , otherwise the value of these segments is $-b_{s'}$. The value of $|00|$ and $|22|$ segments is of course always $+1$. The terminal segments $|01|$ and $|10|$ should also have value $+1$. In this way the value of each loop in the four-slope subgraphs of Fig 50, 51 may be computed as a product of the segment values.

The value of the segment depends on the loop type. In the last sections elementary loops that have bra path $\langle L|$ on the left side were called simple. They correspond to the lowering operators \hat{E}_{ij} and may be called 'L type'. The adjoint loops correspond

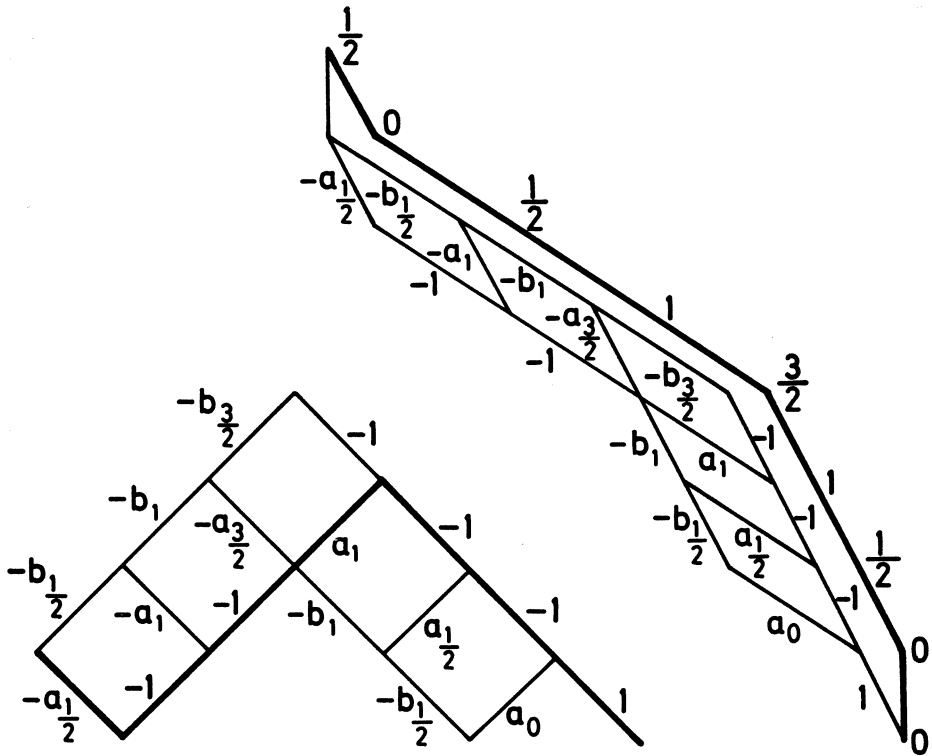


Fig 51. Cycle-generated subgraphs in the S -diagram and in the four-slope graph, for the cycle (7.1), lowering operator \hat{E}_{81} . With top-down level numbering the loop is of L type.

to the raising operators and are called 'R type'. In the four-slope graph the paths of a two-segment elementary loop may cross inside the loop range several times (in the three-slope graph only three-segment loops with $|02|$ segments in the middle could cross their paths) therefore the relative position of bra and ket arcs has little meaning. The values of the loop segments are the simplest if for loops of L -type (simple loops) the intermediate spin S'_k at the top of bra arc, and for the R -type loops (adjoint loops) value S_k at the top of ket arc is taken.

So far we have found non-trivial segment values for segments that are reduced to $|11|$ segment in three-slope graphs. Segment values, their shapes in S -diagram and in the four-slope graphs as well as the designations used by Shavitt (1981) to identify the segments are collected in Table 2.10. Shavitt's symbols dd' are the same as segment designations $|kl|$ used here, with $d = 0, 1, 2, 3$ for $k = 0, +, -, 2$, and his $\Delta b = 2\Delta S_k$. To

Table 2.10

One-body segment values for $|11\rangle$ segments. Ket arcs are drawn with thick lines.

| Segment | S-diagram loop | Four-slope loop | Value | Shavitt's symbols Type $\Delta b, d/d$ |
|-------------|----------------|-----------------|--------------|---|
| R, $ +- $ | | | a_s | L -1 12 |
| R, $ -+ $ | | | $-a_s$ | L +1 21 |
| R, $ ++ $ | | | $-b_s$ | L -1 11 |
| R, $ ++ _0$ | | | -1 | L +1 11 |
| R, $ -- $ | | | $-b_s$ | L +1 22 |
| R, $ -- _0$ | | | -1 | L +1 22 |
| L, $ +- $ | | | $-a_{s+1/2}$ | R -1 12 |
| L, $ -+ $ | | | $a_{s-1/2}$ | R +1 21 |
| L, $ ++ $ | | | $-b_{s-1/2}$ | R +1 11 |
| L, $ ++ _0$ | | | -1 | R -1 11 |
| L, $ -- $ | | | $-b_{s+1/2}$ | R -1 22 |
| L, $ -- _0$ | | | -1 | R +1 22 |

express the segment values given in Table 2.10 Shavitt is using auxiliary function

$$C(p) = \frac{\sqrt{(b+p-1)(b+p+1)}}{b+p} = b_{s+\frac{1}{2}(p-1)} \quad (2.102)$$

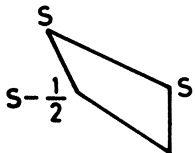
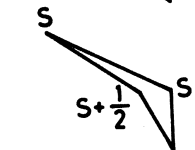
$$\frac{1}{b+p} = a_{s+\frac{1}{2}(p-1)}; \quad p = 0, \pm 1$$

Comparing the segment values given here with those of Shavitt (1981) a few sign differences are noticed. Phase conventions are discussed in detail by Paldus and Boyle (1980); for example, we have freedom of choosing signs of Clebsch-Gordan coefficients coupling two spins $\frac{1}{2}$ in Eq (2.67), influencing phases of the segments. Factorization into segment values is not unique (Shavitt 1978) – any adjustment of segment values that

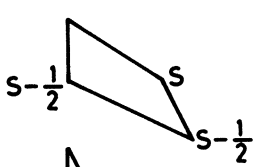
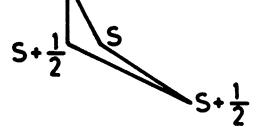
has no influence on the final loop value is allowed. The segment values given here are obtained from branching diagram as directly as possible and correspond to the 'symmetric' scheme with the phase factors $\epsilon = -1$, $\gamma = \gamma' = \phi = 1$, i.e. Yamanouchi-Kotani phase convention (Paldus and Boyle 1980).

In papers on unitary group approach graph's levels are always numbered from bottom up. For restricted spaces, when external part of the graph is separated, it is more convenient to number the levels from top down, as was consistently done in Part I. With the same definition of raising and lowering operators what is called R loop with bottom-top numbering of levels is L loop in top-bottom numbering and vice versa. Therefore comparing the segment values given here with those of UGA (cf Paldus and Boyle 1980; Shavitt 1981; Payne 1982; Robb and Niazi 1984) one should remember to exchange labels L and R.

It is time now to consider the remaining segments $|12\rangle$ and $|21\rangle$. Top segments $|12\rangle$ or $|+2\rangle$, $|-2\rangle$ and bottom segments $|2+\rangle$, $|2-\rangle$ belong to the L type loops, while the adjoint top segments $|2+\rangle$, $|2-\rangle$ and bottom segments $|+2\rangle$, $|-2\rangle$ belong to the R type loops. Following Shavitt top segments Q are designated \bar{Q} and bottom segments \underline{Q} . The easiest way to assign segment values to these segments is to complement them with $|10\rangle$, $|01\rangle$ segments and look at the value of the resulting matrix elements. This is done below: for top segments using Eq (2.70) we have

| | | |
|---|--|---|
|  | Segment \bar{L} , $ +2\rangle$ \bar{R} , $ 2+\rangle$ | $\left\langle \begin{array}{c} \text{V-shape} \\ \parallel \\ \text{+0+} \end{array} \right\rangle = -\sqrt{2}C_S^- = -C_S^V$ $S' = S$ |
|  | Segment \bar{L} , $ -2\rangle$ \bar{R} , $ 2-\rangle$ | $\left\langle \begin{array}{c} \text{^V-shape} \\ \parallel \\ \text{+0+} \end{array} \right\rangle = \sqrt{2}C_S^+ = C_S^\wedge$ $S' = S$ |

and for bottom segments

| | | |
|---|--|--|
|  | Segment \underline{L} , $ 2+\rangle$ \underline{R} , $ +2\rangle$ | $\left\langle \begin{array}{c} \text{+0+} \\ \parallel \\ \text{^V-shape} \end{array} \right\rangle = C_{S'}^\wedge = C_{S-\frac{1}{2}}^\wedge$ $\left\langle \begin{array}{c} \text{^V-shape} \\ \parallel \\ \text{+0+} \end{array} \right\rangle = C_S^\wedge$ |
|  | Segment \underline{L} , $ 2-\rangle$ \underline{R} , $ -2\rangle$ | $\left\langle \begin{array}{c} \text{+0+} \\ \parallel \\ \text{V-shape} \end{array} \right\rangle = -C_{S'}^V = -C_{S+\frac{1}{2}}^V$ $\left\langle \begin{array}{c} \text{V-shape} \\ \parallel \\ \text{+0+} \end{array} \right\rangle = -C_S^V$ |

The phase factors here are affected by the choice of signs in Eq (2.67) and (2.70). Coefficients C_S^\wedge , C_S^V are connected to auxiliary function $A(p, q)$ used by Shavitt

$$A(p, q) = \sqrt{\frac{b+p}{b+q}}; \quad C_{S+\frac{1}{2}p}^\wedge = A(p+2, p+1); \quad C_{S+\frac{1}{2}p}^V = A(p, p+1) \quad (2.103)$$

Collecting the values found so far we have

$$\begin{aligned}
 \text{L type } & \mathcal{W}(|+-|) = -a_{S'}; \quad \mathcal{W}(|-+|) = a_{S'}; \quad \mathcal{W}(|++|) = \mathcal{W}(|--|) = -b_{S'} \\
 & \mathcal{W}(|+2|) = \mathcal{W}(|2-|) = -C_{S'}^\vee; \quad \mathcal{W}(|2+|) = \mathcal{W}(|-2|) = C_{S'}^\wedge \\
 \text{R type } & \mathcal{W}(|+-|) = a_S; \quad \mathcal{W}(|-+|) = -a_S; \quad \mathcal{W}(|++|) = \mathcal{W}(|--|) = -b_S \\
 & \mathcal{W}(|+2|) = \mathcal{W}(|2-|) = C_S^\wedge; \quad \mathcal{W}(|2+|) = \mathcal{W}(|-2|) = -C_S^\vee \\
 \text{all loops } & \mathcal{W}(|00|) = \mathcal{W}(|01|) = \mathcal{W}(|10|) = \mathcal{W}(|22|) = +1 \\
 & \mathcal{W}(|++|_0) = \mathcal{W}(|--|_0) = -1
 \end{aligned} \tag{2.104}$$

One may check that the value of elementary loops [57], [75] is -1 as was found in the previous section. The four-slope segments may be numbered in quaternary counting system. The segments are conveniently arranged in a matrix

$$\begin{aligned}
 [0] &= |00| & [1] &= |0+| & [2] &= |0-| & [3] &= |02| \\
 [4] &= |+0| & [5] &= |++| & [6] &= |+-| & [7] &= |+2| \\
 [8] &= |-0| & [9] &= |-+| & [10] &= |--| & [11] &= |-2| \\
 [12] &= |20| & [13] &= |2+| & [14] &= |2-| & [15] &= |22|
 \end{aligned} \tag{2.105}$$

Segment $|kl|$ has the number $[4k + l]$. Mutually adjoint segments are at symmetric positions in this matrix. Except for $|02|$, $|20|$ all segments appear in one-body loops. Segments of the first row and first column have value $+1$. The values of other segments may be presented in form of a matrix

$$\begin{array}{ll}
 \text{L type loops} & [5] : -b; [5]_0 : -1 & [6] : -a & [7] : -C^\vee \\
 \text{bra values } S'_k & [9] : a & [10] : -b; [10]_0 : -1 & [11] : C^\wedge \\
 & [13] : C^\wedge & [14] : -C^\vee & [15] : +1
 \end{array} \tag{2.106}$$

and for the R type loops

$$\begin{array}{ll}
 \text{R type loops} & [5] : -b; [5]_0 : -1 & [6] : a & [7] : C^\wedge \\
 \text{ket values } S_k & [9] : -a & [10] : -b; [10]_0 : -1 & [11] : -C^\vee \\
 & [13] : -C^\vee & [14] : C^\wedge & [15] : +1
 \end{array} \tag{2.107}$$

The matrix form of segment values reveals complete symmetry between lowering and raising cases. The loops $|++|$, $|--|$ that come in two versions appear in the diagonal. All segments with $|\Delta S| \geq \frac{1}{2}$ have zero values. Analysis of one-body segments is complete now. Let us look at the loops corresponding to product of two operators.

B. Two-body segments.

The most straightforward approach to calculation of products of two shifts operators using graphical techniques was presented by Shavitt (1978). If the range of one operator does not overlap with the range of another two separate one-body loops are formed in the graph and the segment values given in the last section suffice for calculation. The problem is essentially the same as with overlapping and non-overlapping permutations. For the overlapping region Shavitt (1978) has advocated a simple recursive scheme that is in fact equivalent to multiplication of the representation matrices for the two cycles. Specification of permutations is replaced by analysis of segment shapes and intermediate paths that are necessary to perform the summation. The new segments have up to three values and are obtained as products of the old ones. I could repeat Shavitt's reasoning here without any modifications, because at this point it is just manipulation with paths and segment values, with no sign of unitary group theory left. However, some tricks are possible to reduce the number of intermediate summations in the overlap region. Drake and Schlessinger (1977) and later Paldus and Boyle (1980) used more sophisticated approach to show that double-valued segments (for singlet and triplet intermediate recoupling) are all that is needed to compute two-body loop values. Due to cumbersome nature of the derivations sketches rather than detail exposition are given in all (compare also Robb and Niazi 1984; Gould and Chandler 1984) except one (very long) paper (Payne 1982) on this subject. I will attempt to derive here the two-body segment values using the same technique as for the one-body values.

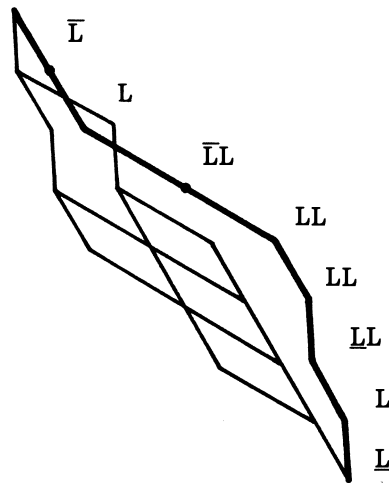


Fig 52. Example of a two-body loop. Numbering the levels from top down the loop is of $L, \bar{L}L$ type, from bottom up of R, RR type.

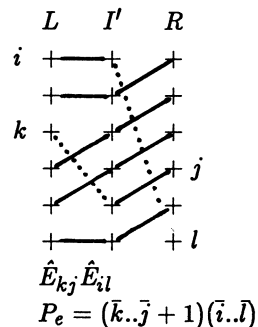
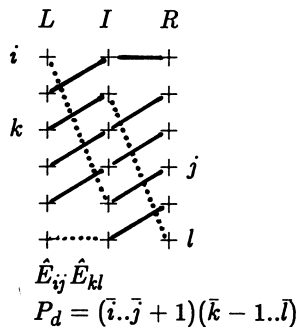
Let us look first at a typical two-body loop shown in Fig 52. At the top and at the bottom of the loop range it is a one-body loop of the type L. Inside the loop body new segments, with $\Delta S = 0, \pm\frac{1}{2}, \pm 1$, corresponding to the overlapping part of two cycles, are found. Following Shavitt (1981) they are classified adding another letter R or L to the one-body segment designation. The weight segments W being trivial we are left with six one-body segment types. Their multiplication table (Table 2.11) is symmetric because one can not differentiate segments XY and YX in the graph.

Table 2.11
Two-body segment types.

| | L | R | <u>L</u> | <u>R</u> | \bar{L} | \bar{R} |
|-----------|------------------|------------------|------------------|------------------|------------------|------------------|
| L | LL | RL | <u>LL</u> | <u>RL</u> | $\bar{L}\bar{L}$ | $\bar{R}\bar{L}$ |
| R | RL | RR | <u>LR</u> | <u>RR</u> | $\bar{L}\bar{R}$ | $\bar{R}\bar{R}$ |
| <u>L</u> | <u>LL</u> | <u>LR</u> | <u>LL</u> | <u>RL</u> | $\bar{L}\bar{L}$ | $\bar{R}\bar{L}$ |
| <u>R</u> | <u>RL</u> | <u>RR</u> | <u>RL</u> | <u>RR</u> | $\bar{L}\bar{R}$ | $\bar{R}\bar{R}$ |
| \bar{L} | $\bar{L}\bar{L}$ | $\bar{L}\bar{R}$ | $\bar{L}\bar{L}$ | $\bar{L}\bar{R}$ | $\bar{L}\bar{L}$ | $\bar{R}\bar{L}$ |
| \bar{R} | $\bar{R}\bar{L}$ | $\bar{R}\bar{R}$ | $\bar{R}\bar{L}$ | $\bar{R}\bar{R}$ | $\bar{R}\bar{L}$ | $\bar{R}\bar{R}$ |

Two-body loops with terminal segments at levels i, j, k, l correspond to the product of two shift operators: direct $\hat{E}_{ij}\hat{E}_{kl}$ and exchange $\hat{E}_{il}\hat{E}_{kj}$. Three-body loops with 6 terminal segments correspond to $3! = 6$ products of shift operators ect. In the expansion of a two-body operator Eq (2.48) each product is multiplied by appropriate integral. The value of some segments, out of 21 segment types in Table 2.11, is very easy to find using the technique of complementing a given segment with segments of known value to form a 'model loop'. For example $\mathcal{W}(|02\rangle) = \mathcal{W}(|20\rangle) = \sqrt{2}$ is assigned to $\bar{R}\bar{R}, \underline{R}\underline{R}, \bar{L}\bar{L}, \underline{L}\underline{L}$ segments. In more complicated cases one may use the same technique as for the one-body segments: first the permutation is determined, then acting on a parent path all interacting paths are determined and the segment values assigned. As an illustration of this technique all segment values for RR type of loops are derived below.

Consider the product of two raising shift operators $\hat{E}_{ij}\hat{E}_{kl}, i < k < j < l$, and the exchange product $\hat{E}_{kj}\hat{E}_{il}$. Permutations corresponding to these products are found from the diagrams below:



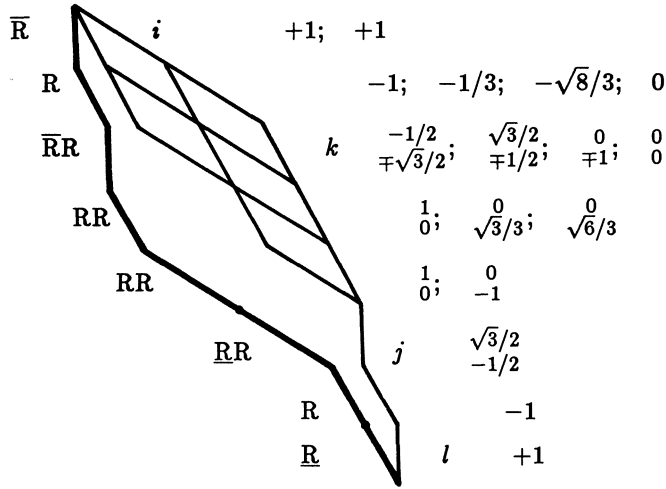


Fig 53. Example of loop value calculation for a two-body loop. Segment values are given to the right (see text for description).

where the positions $\bar{i} = \bar{i}_L$, $\bar{k} = \bar{k}_L$. Straightforward application of $P_e = (345)(1..6)$ to the triplet coupled parent state $|++--++\rangle$ shown in Fig 53 gives

$$\begin{aligned}
 (345)(1..6)|++--++\rangle &= (345) \left\{ \frac{\sqrt{3}}{4}|++--++\rangle + \frac{1}{4}|++--++\rangle + \right. \\
 &\quad \left. \frac{\sqrt{2}}{2}|+++++\rangle + \frac{1}{4}|++--++\rangle + \frac{\sqrt{3}}{12}|++--++\rangle + \frac{\sqrt{6}}{6}|+++++\rangle \right\} = \\
 &\quad -\frac{\sqrt{3}}{4}|+++++\rangle + \frac{1}{4}|++--++\rangle + \frac{\sqrt{2}}{2}|+++++\rangle + \frac{1}{4}|++--++\rangle + \\
 &\quad \frac{\sqrt{3}}{36}|+++++\rangle + \frac{\sqrt{6}}{18}|++--++\rangle + \frac{\sqrt{6}}{18}|+++++\rangle + \frac{2\sqrt{3}}{9}|+++++\rangle
 \end{aligned}
 \tag{2.108}$$

where application of the second cycle (345) demands some intermediate summations. These summations may be removed if we write the permutations in the following way

$$\begin{aligned}
 P_d &= (\bar{i}.. \bar{j} + 1)(\bar{k} - 1..l) = && i < k < j < l \\
 &(\bar{i}.. \bar{k})(\bar{k} - 1 \bar{k} \bar{k} + 1.. \bar{j} \bar{j} + 1)(\bar{k} - 1 \bar{k}.. \bar{j} \bar{j} + 1)(\bar{j} + 1.. \bar{l}) = \\
 &(\bar{i}.. \bar{k} - 1)(\bar{k} - 1 \bar{k})(\bar{k}.. \bar{j})_2 (\bar{j} \bar{j} + 1) (\bar{j} + 1.. \bar{l}) && (2.109) \\
 P_e &= (\bar{i}.. \bar{k} - 1) \quad \text{I} \quad (\bar{k}.. \bar{j})_2 (\bar{j} \bar{j} + 1) (\bar{j} + 1.. \bar{l}) \\
 &\quad \text{R} \quad \text{RR} \quad \text{RR} \quad \text{RR} \quad \text{R}
 \end{aligned}$$

The cycles are aligned here with the labels of segments they contribute to. The double cycle for RR segments, shifting on two positions, may be written as a product of tricycles

$$\begin{aligned}
 (\bar{k}.. \bar{j})_2 &= (\bar{k} \bar{k} + 1.. \bar{j} \bar{j} + 1)(\bar{k} - 1 \bar{k}.. \bar{j} - 1 \bar{j}) = \\
 &(\bar{k} + 1 \bar{k} \bar{k} - 1)(\bar{k} + 2 \bar{k} + 1 \bar{k})..(\bar{j} + 1 \bar{j} \bar{j} - 1) && (2.110)
 \end{aligned}$$

Direct and exchange terms differ only on one transposition $(\bar{k} - 1 \bar{k})$. To avoid intermediate summations we have to calculate matrix elements of the overlapping permutations in a retransformed basis. Let $|\Sigma_{k k+1}\rangle$ designate a basis of spin functions that have singlet and triplet pairs at positions $k, k + 1$, i.e. the spin functions are retransformed using Eq (2.70). The structure constant matrices corresponding to P_d, P_e permutations are then calculated in the following way

$$\begin{aligned} \langle \Sigma | P_d | \Sigma \rangle &= \langle \Sigma | (\bar{i} \dots \bar{k} - 1) | \Sigma \rangle \langle \Sigma | (\bar{k} - 1 \bar{k}) | \Sigma_{k-1 k} \rangle \times \\ &\langle \Sigma_{k-1 k} | (\bar{k} + 1 \bar{k} \bar{k} - 1) | \Sigma_{k k+1} \rangle \langle \Sigma_{k k+1} | (\bar{k} + 2 \bar{k} + 1 \bar{k}) | \Sigma_{k+2 k+1} \rangle \dots \\ &\langle \Sigma_{j j-1} | (\bar{j} + 1 \bar{j} \bar{j} - 1) | \Sigma_{j j+1} \rangle \langle \Sigma_{j j+1} | (\bar{j} \bar{j} + 1) | \Sigma \rangle \langle \Sigma | (\bar{j} + 1 \dots \bar{l}) | \Sigma \rangle \end{aligned} \quad (2.111)$$

Another way of expressing this equation is to introduce projection operators $T_{k k+1} = |\Sigma_{k k+1}\rangle \langle \Sigma|$ changing the basis $T_{k k+1} |\Sigma\rangle = |\Sigma_{k k+1}\rangle$. For the transpositions corresponding to the terminal segments $\langle \Sigma | (k - 1 k) | \Sigma_{k-1 k} \rangle$ and $\langle \Sigma_{j j+1} | (j j + 1) | \Sigma \rangle$ the result is the same as for the overlap integrals $\langle \Sigma | | \Sigma_{k-1 k} \rangle$ and $\langle \Sigma_{j j+1} | | \Sigma \rangle$ with the sign changed for the triplet pairs (the sign convention in the graphical rules of Eq (2.69) includes the sign change for each transposition to account for the parity of the permutation). Direct calculation in the $\langle S |, \langle T |$ basis taken as bra states and $| - + \rangle, | + - \rangle$ as ket states confirms that

$$\begin{aligned} \langle \Sigma | (k - 1 k) | \Sigma_{k-1 k} \rangle &= \\ \langle \Sigma | (k - 1 k) | \Sigma \rangle \langle \Sigma | | \Sigma_{k-1 k} \rangle &= \begin{pmatrix} a & -b \\ -b & -a \end{pmatrix} \begin{pmatrix} C^+ & C^- \\ -C^- & C^+ \end{pmatrix} = \\ \langle \Sigma | | \Sigma_{k-1 k} \rangle \langle \Sigma_{k-1 k} | (k - 1 k) | \Sigma_{k-1 k} \rangle &= \begin{pmatrix} C^+ & C^- \\ -C^- & C^+ \end{pmatrix} \begin{pmatrix} 1 & 0 \\ 0 & -1 \end{pmatrix} = \\ &\begin{pmatrix} C^+ & -C^- \\ -C^- & -C^+ \end{pmatrix} \end{aligned} \quad (2.112)$$

with identical result for $\langle \Sigma_{j j+1} | (j j + 1) | \Sigma \rangle$. In the example shown in Fig 53

$$\begin{aligned} P_d &= (12) (23) T_{23} (432)_{RR} (543)_{RR} T_{45}^\dagger (45) (56) \\ P_e &= (12) T_{23} (432)_{RR} (543)_{RR} T_{45}^\dagger (45) (56) \end{aligned} \quad (2.113)$$

where $(i + 1 i i - 1)_{RR} = T_{i-1 i}^\dagger (i + 1 i i - 1) T_{i i+1}$ are the retransformed tricycles.

These matrices contain the two-body segment values and correspond directly to the values stored in Shavitt's tables. The ket arc is the first one in $|k'\rangle$ basis, bra arc is the last drawn in $|k''\rangle$ basis, with the corresponding S, S' values taken at the left end of these arcs (the first arc in $|k''\rangle$ basis starts from S value). Designating the segments $|xy\rangle$ for $\Delta S = \pm 1$ as $|xy|_{\pm 1}$, where x, y are $+, -$ (or $d', d=1, 2$ using Shavitt's symbols) and adding a prime to the singlet-coupled segment values the following matrices show the correspondence of values in Eq (2.123) and Eq (2.125) with the segments:

$$\begin{pmatrix} \mathcal{W}(|--|_{-1}) & & & \\ & \mathcal{W}(|+-|_{-1}) & \mathcal{W}(|++|_{-1}) & \\ & \mathcal{W}'(|--|) & & \\ & & \mathcal{W}(|--|) & \mathcal{W}(|-+|) \end{pmatrix} \quad (2.126)$$

$$\begin{pmatrix} & & \mathcal{W}'(|++|) & \\ \mathcal{W}(|+-|) & & & \mathcal{W}(|++|) \\ \mathcal{W}(|--|_{+1}) & & \mathcal{W}(|-+|_{+1}) & \\ & & & \mathcal{W}(|++|_{+1}) \end{pmatrix} \quad (2.127)$$

The top segments \overline{RR} corresponding to $\langle \Sigma|(k-1 k)|\Sigma_{k-1} k \rangle$ for direct terms and $\langle \Sigma||\Sigma_{k-1} k \rangle$ for exchange terms are almost symmetric with \underline{RR} terms, except that now $\Delta S = \pm \frac{1}{2}$. For the direct term and $|10\rangle$ type segments the same matrix as in Eq (2.115) gives the values

$$\begin{aligned} \mathcal{W}_{-\frac{1}{2}}(|-0\rangle) &= \mp 1 \\ \mathcal{W}'_{-\frac{1}{2}}(|+0\rangle) &= C^+; \quad \mathcal{W}'_{+\frac{1}{2}}(|-0\rangle) = -C^- \\ \mathcal{W}_{-\frac{1}{2}}(|+0\rangle) &= \mp C^-; \quad \mathcal{W}'_{+\frac{1}{2}}(|-0\rangle) = \mp C^+ \\ \mathcal{W}_{+\frac{1}{2}}(|+0\rangle) &= \mp 1 \end{aligned} \quad (2.128)$$

where the top signs are for direct and the bottom signs for exchange terms. Segments of $|21\rangle$ type, due to the 'extra' particle in the doubly occupied orbital, demand calculation of $\langle \Sigma_{k k+1}^0|(k-1 k)|\Sigma_k k+1 \rangle$ and $\langle \Sigma_{k k+1}^0||\Sigma_k k+1 \rangle$ integrals. We may do the calculation in a matrix form, as in Eq (2.116), or we may calculate individual matrix elements (drawing the relevant spin path's fragments is always helpful). In Eq (2.91) we have already determined that $\langle +S|(k-1 k)|+S \rangle = \langle -S|(k-1 k)|-S \rangle = -\frac{1}{2}$, therefore \mathcal{W}' values are $-1/\sqrt{2}$. The remaining 4 non-zero elements are easy to find:

$$\begin{aligned} \mathcal{W}_{-\frac{1}{2}}(|2+\rangle) &= \langle +S|(k-1 k)|++-\rangle = C^\vee \\ \mathcal{W}'_{+\frac{1}{2}}(|2+\rangle) &= \langle +S|(k-1 k)|+S \rangle = -1/\sqrt{2} \\ \mathcal{W}_{+\frac{1}{2}}(|2+\rangle) &= \langle +S|(k-1 k)|+T \rangle = C^\vee C_-^- \\ \mathcal{W}_{+\frac{1}{2}}(|2-\rangle) &= \langle -S|(k-1 k)|---\rangle = -C^\wedge \\ \mathcal{W}'_{-\frac{1}{2}}(|2-\rangle) &= \langle -S|(k-1 k)|-S \rangle = -1/\sqrt{2} \\ \mathcal{W}_{-\frac{1}{2}}(|2-\rangle) &= \langle -S|(k-1 k)|-T \rangle = -\sqrt{2}C^+C_+^+ = -C^\wedge C_+^+ \end{aligned} \quad (2.129)$$

Table 2.12
 Values of two-body raising segments;
 upper signs for direct, lower for exchange elements.

| Segment | \mathcal{W}_{-1} | \mathcal{W}'_0 | \mathcal{W}_0 | \mathcal{W}_{+1} |
|---------|-------------------------------|------------------------------|------------------------------|-----------------------------|
| 0+ | | $-C^-$ | $-C^+$ | -1 |
| 0- | -1 | C^+ | $-C^-$ | |
| +2 | $-C^{\wedge}_+$ | $-\frac{1}{\sqrt{2}}$ | $-b(1+a_-)/\sqrt{2}$ | |
| -2 | | $-\frac{1}{\sqrt{2}}$ | $b(1-a_+)/\sqrt{2}$ | C^{\vee}_- |
| ++ | bb_+ | 1 | bb_- | 1 |
| +- | $-2a_+C^+$ | 0 | $-2a_-C^-$ | |
| -+ | | 0 | $2a_+C^+$ | $2a_-C^-$ |
| -- | 1 | 1 | bb_+ | bb_- |
| 20 | | $\sqrt{2}$ | 0 | |
| 02 | | $\sqrt{2}$ | 0 | |
| Segment | $\mathcal{W}'_{-\frac{1}{2}}$ | $\mathcal{W}_{-\frac{1}{2}}$ | $\mathcal{W}'_{\frac{1}{2}}$ | $\mathcal{W}_{\frac{1}{2}}$ |
| +0 | C^+ | $\mp C^-$ | 0 | ∓ 1 |
| -0 | 0 | ∓ 1 | $-C^-$ | $\mp C^+$ |
| 2+ | 0 | $\pm C^{\vee}$ | $-\frac{1}{\sqrt{2}}$ | $\pm C^{\vee}C^-$ |
| 2- | $-\frac{1}{\sqrt{2}}$ | $\mp C^{\wedge}C^+$ | 0 | $\mp C^{\wedge}$ |

with the signs of the \mathcal{W} segments (triplet coupled) changed for the exchange terms. The sign of ΔS and the ket arc symbol in the segment are the same as in the first arc (arc $k - 1$) of ket states. All segment values for the two-body raising loops are collected in the Table 2.12. Comparing this table with the tables of Shavitt (1981) and other authors one should remember that it corresponds to the LL segments with bottom-up numbering of graph's levels. In Eq (2.102) and (2.103) relations between b , C^{\vee} , C^{\wedge} coefficients and $C(p)$, $A(p, p + 1)$ auxiliary functions were presented. Other functions used by Shavitt are

$$\begin{aligned}
 A(p, p + 2) &= C^{\vee}_{S+\frac{1}{2}p} C^{\vee}_{S+\frac{1}{2}(p+1)}; & A(p + 2, p) &= C^{\wedge}_{S+\frac{1}{2}p} C^{\wedge}_{S+\frac{1}{2}(p-1)} \\
 B(p, p + 1) &= \sqrt{\frac{2}{(b+p)(b+p+1)}} = 2a_{S+\frac{1}{2}(p-1)} C^-_{S+\frac{1}{2}p} = 2a_S C^+_{S+\frac{1}{2}(p-1)} \\
 D(p) &= \sqrt{\frac{(b+p-1)(b+p+2)}{(b+p)(b+p+1)}} = b_{S+\frac{1}{2}p} b_{S+\frac{1}{2}(p-1)} \\
 D(0) &= bb_-; & D(1) &= bb_+
 \end{aligned}
 \tag{2.130}$$

Segment values for raising-lowering type of operator products are expressed using the same combinations of coefficients. One may find all loops in the graph, searching for pairs of paths, and compute loop values using segment values such as those in Table 2.12. An alternative strategy is to find a single path (parent path) and create the interacting paths (daughter paths) acting on it with appropriate P_d , P_e permutations. For example, matrix (2.123) tells us that

$$\begin{aligned} (k+1 \ k \ k-1)_{RR} | - S \rangle &= | S - \rangle \\ (k+1 \ k \ k-1)_{RR} | - T \rangle &= bb_+ | T - \rangle - 2a_+ C^+ | - - \rangle \\ (k+1 \ k \ k-1)_{RR} | + - \rangle &= bb_+ | - - \rangle + 2a_+ C^+ | T - \rangle \end{aligned} \quad (2.131)$$

Of course one may deduce the same information from Table 2.12 but not in such a straightforward way as from the segment values matrices.

C. Summary.

In this section GRMS techniques were applied to the non-fagot four-slope graph. No 'heavy' mathematics is involved in derivations, just the formula for addition of two $\frac{1}{2}$ spins Eq (2.67), graphical rules (2.69) and transformation to singlet and triplet coupled pairs Eq (2.70). In contrast, more sophisticated approaches use tensor operator recoupling techniques, graphical methods of spin algebras or unitary and symmetric group theory. I am aware that the word 'simple' means that something is simple only for the author, but if the reader does not find GRMS techniques simple, for example comparing to derivations in UGA framework by Gould and Chandler (1984), who claim several times that their approach is simple, then I have completely failed to present things clearly.

The results obtained here complement those of section 2.5E giving yet another method of computation of matrices corresponding to products of two cycles. Relationships Eq (2.114) between direct and exchange terms are here particularly interesting, allowing to replace a product of two long cycles for the exchange term by the product of shorter cycles corresponding to the direct term or vice versa. I will return to this in Part IV presenting detailed formulas resulting from application of the techniques described in this part. The use of other non-fagot graphs, including those adapted to the \hat{L}_z operator, does not introduce new aspects to the methods described here and therefore is not elaborated upon.

An interesting question arises: how far can one go with exploration of S-diagrams? Is it always possible to manipulate cycles and transpositions to obtain the same results as come from much more sophisticated mathematical techniques? Can one interpret all theorems of the graphical methods of spin algebra (cf El Baz and Castel 1972) in the language of S-diagrams? If not, when does the simple approach break? I leave it as open question - I have a feeling that, at least for electronic systems, everything can be easily obtained using S-diagrams because they give complete description of the spin space. However, some things are easy to express in one language but hard in all others. I have not devoted enough time to this subject but it should be interesting to pursue it further. Leaving this aside I will move now to the non-abelian point groups and more complicated problems.

REFERENCES

- Andrews GE (1976) The theory of partitions. Addison-Wesley, Reading MA
- Ahlrichs R (1981) A new MR-CI(SD) technique. In: Proceedings of 5th seminar on computational methods in quantum chemistry. van Duijen PTh, Nieuypoort WC (eds), Max-Planck-Institut, Garching b. München, p 254-272
- Armstrong L Jr, Judd BR (1970) *Proc Roy Soc* A315:27-37
Quasi-particles in atomic shell theory.
- Armstrong L Jr, Judd BR (1970) *Proc Roy Soc* A315:39-48
Atomic structure calculation in a factorized shell.
- Avery J (1976) Creation and annihilation operators. McGraw-Hill, New York
- Barut AO, Rączka R (1980) Theory of group representations and applications. PWN, Warsaw
- Beineke LW, Wilson RJ, eds (1978) Selected topics in graph theory. Academic Press, New York
- Biedenharn LC, Louck JD (1981) Angular momentum in quantum physics. Addison-Wesley, Reading MA
- Biedenharn LC, Van Dam H (1965) Quantum theory of angular momentum. Academic Press, New York
- Bohr A, Mottelson BR (1969) Nuclear structure, Vol 1. WA Benjamin Inc, New York
- Boyle MJ, Paldus J (1980) *Phys Rev A* 22:2316-2339
Particle-hole formulation of the unitary group approach to the many-electron correlation problem. II. Matrix element evaluation.
- Born G, Shavitt I (1982) *J Chem Phys* 76:558-567
A unitary group formulation of open-shell electron propagator theory.
- Brandow BH (1967) *Rev Mod Phys* 39:771-828
Linked-cluster expansion for nuclear many-body problem.
- Brooks BR, Schaefer HF (1979) *J Chem Phys* 70:5092-5106
The graphical unitary group approach to the electron correlation problem. Methods and preliminary applications.
- Brooks BR, Laidig WD, Saxe P, Handy NC, Schaefer HF (1980a)
Physica Scripta 21:312-332
The loop driven graphical unitary group approach: a powerful method for the variational description of the electron correlation.
- Brooks BR, Laidig WD, Saxe P, Goddard JD, Yamaguchi Y, Schaefer HF (1980b)
J Chem Phys 72:4652-4653
Analytic gradients from correlated wave functions via the two-particle density matrix and the unitary group approach.

- Brooks BR, Laidig WD, Saxe P, Schaefer HF (1980c) *J Chem Phys* 72:3837–3838
A multiconfigurational self-consistent-field formalism utilizing the two-particle density matrix and the unitary group approach.
- Brown FB, Shavitt I, Shepard R (1984) *Chem Phys Lett* 105:363–369
Multireference configuration interaction treatment of potential energy surfaces: symmetric dissociation of H_2O in a double-zeta basis.
- Brussaard PJ, Glaudemans PWM (1977) Shell-model applications in nuclear spectroscopy. North-Holland, Amsterdam
- Burton PG, Gray PD (1983) *Chem Phys Lett* 96:453–457
Full CI extrapolation compared to explicit full CI for H_2O in a double-zeta basis.
- Buenker RJ, Peyerimhoff SD (1968) *Theor Chim Acta(Berl.)* 12:183–199
CI method for the study of general molecular potentials.
- Buenker RJ, Peyerimhoff SD, Butscher W (1978) *Mol Phys* 35:771–791
Applicability of the multireference doubly excited CI (MRD-CI) method to the calculation of electronic wavefunctions and comparison with related techniques.
- Bunker P (1980) Molecular symmetry and spectroscopy. Academic Press, New York
- Condon EU, Odabaşı H (1980) Atomic structure. University Press, Cambridge
- Condon EU, Shortley GH (1935) The theory of atomic spectra. University Press, Cambridge
- Corson EM (1951) Perturbation methods in the quantum mechanics of N-electron systems. Blackie, London
- Cvitanović P (1984) Group theory, Part I. NORDITA, København
- Deo N (1974) Graph theory with application to engineering and computer science. Prentice Hall, Englewood Cliffs, New Jersey
- Diamond JJ, Segal GA, Wetmore RW (1984) *J Phys Chem* 88:3532–3538
A program for efficient perturbation configuration interaction.
- Downward M, Robb MA (1977) *Theor Chim Acta(Berl.)* 46:129–141
The computation of the representation matrices of the generators of the unitary group.
- Drake GWF, Schlesinger M (1977) *Phys Rev A* 15:1990–1999
Vector-coupling approach to the orbital and spin-dependent tableau matrix elements in the theory of complex spectra.
- Draayer JP, Valdes HT (1985) *Comp Phys Comm* 36:313–320
Model space dimensionalities for multiparticle fermion systems.
- Duch W (1985a) *Int J Quantum Chem* 27:59–70
Efficient method for computation of the representation matrices of the unitary group generators.

- Duch W (1985b) *Theor Chim Acta(Berl.)* 67:263-269
On the number of spin functions in the first order interaction space.
- Duch W (1985c) *J Phys A* 18:3283-3307
Graphical representation of Slater determinants.
- Duch W (1986) *Chem Phys Lett* 124:442-446
Calculation of the one-electron coupling coefficients in the configuration interaction method.
- Duch W (1986a) *Int J Quantum Chem* 29:xxx-xxx
From determinants to spin eigenfunctions - a simple algorithm.
- Duch W (1986b) *J Phys A* (submitted)
Visualization of many-particle model spaces, with application to shell-model calculations.
- Duch W, Karwowski J (1981) *Lecture Notes in Chem* 22:260-271
Symmetric group graphical approach to the configuration interaction method.
- Duch W, Karwowski J (1982) *Int J Quantum Chem* 22:783-824
Symmetric group graphical approach to the direct configuration interaction method.
- Duch W, Karwowski J (1985) *Comp Phys Rep* 2:92-170
Symmetric group approach to configuration interaction methods.
- Duch W, Karwowski J (1986) *Theor Chim Acta(Berl.)* (submitted)
Multireference direct CI program based on the symmetric group graphical approach.
- El Baz E, Castel B (1972) *Graphical methods of spin algebra*. Dekker, New York.
- Esser M (1984) *Int J Quantum Chem* 26:313-338
Direct MRCI method for calculation of relativistic many-electron wavefunctions. I. General formalism.
- Eyring H, Walter J, Kimball GE (1949) *Quantum chemistry*.
5th ed, Wiley, New York
- Garfinkel RS, Nemhauser GL (1972) *Integer Programming*. Wiley, New York
- Gelfand IM, Tsetlin ML (1950) *Dokl Akad Nauk SSSR* 71:825-828
Finite-dimensional representations of the group of unimodular matrices
(*in russian*).
- Gilmore R (1974) *Lie groups, Lie algebras, and some of their application*.
Wiley & Sons, New York
- Gołębiewski A, Broclawik E (1985) *Int J Quantum Chem* 27:613-623
New concepts in bonded functions theory I. Alternative way of matrix elements evaluation.
- Goscinsky O, Öhrn Y (1968) *Int J Quantum Chem* 2:845-856
Coupling of equivalent particles in a field of given symmetry.

- Gould MD, Chandler GS (1984) *Int J Quantum Chem* 25:553–601
Unitary group approach to many-electron problem. I. Matrix element evaluation and shift operators.
- Gould MD, Chandler GS (1984) *Int J Quantum Chem* 25:603–633
Unitary group approach to many-electron problem. II. Adjoint tensor operators for $U(n)$.
- Gould MD, Chandler GS (1984) *Int J Quantum Chem* 25:1089–1109
Unitary group approach to many-electron problem. III. Matrix elements of spin-dependent Hamiltonians.
- Graebestetter JE, Tseng TJ, Grein F (1976) *Int J Quantum Chem* 10:143–150
Generation of genealogical spin eigenfunctions.
- Hall M (1967) *Combinatorial Theory*. Blaisdel Publ Co, Waltham MA
- Hamermesh M (1962) *group theory and its application to physical problems*. Academic Press, New York
- Handy NC (1978) In: *Correlated wavefunctions, Daresbury Study Weekend Series No 10*. Saunders VR, Ed. Science Research Council, Daresbury
- Harary F (1969) *Graph Theory*. Addison-Wesley, Reading MA
- Harris FE (1967) *Molecular orbital theory*. *Adv Quantum Chem* 3:61–127
- Harrison RJ, Handy NC (1983) *Chem Phys Lett* 95:386–391
Full CI calculations on BH, H_2O , NH_3 and HF.
- Harter WG (1974) *Phys Rev A* 8:2819–2827
Alternative basis for the theory of complex spectra I.
- Harter WG, Patterson CW (1976a) *Phys Rev A* 13:1067–1082
Alternative basis for the theory of complex spectra II.
- Harter WG, Patterson CW (1976b) *Lecture Notes in Physics* 49
A Unitary Calculus for the Electronic Orbitals.
- Herzberg G (1966) *Molecular spectra and molecular structure Vol III*. D van Nostrand Co, Princeton NJ
- Hinze J(ed) (1981) *Lecture Notes in Chem* vol 22
The Unitary Group for the Evaluation of the Electronic Energy Matrix Elements. Proceedings of a workshop, Bielefeld 1979.
- Hinze J, Broad JT (1981) *Lecture Notes in Chem* 22:322–344
CI-energy expressions in terms of the reduced density matrices of a general reference.
- Hochstrasser RM (1966) *Molecular aspects of symmetry*. Benjamin, New York
- Jankowski K, Malinowski P (1980) *Phys Rev A* 22:51–60
Second-order correlation energies for F^{1-} , Na^{1+} , Mg^{2+} and Ar^{3+} :
Z dependence of irreducible pair energies.

- Jeziorski B, Monkhorst HJ, Szalewicz K, Zabolicki JG (1984)
Lecture Notes in Physics 198:279–288
Coupled cluster approach with explicitly correlated cluster functions.
- Judd BR (1979) *Lecture Notes in Chem* 12:164–177
The permutation group in atomic structure.
- Karayianis N (1965) *J Math Phys* 6:1204–1209
Atomic terms for equivalent electrons.
- Karwowski J (1973) *Theor Chim Acta(Berl.)* 29:151–166
Matrix elements of one- and two-electron operators.
- Karwowski J (1973a) *Chem Phys Lett* 19:279–283
Matrix elements of spin-dependent one- and two-electron operators.
- Karwowski J, Duch W, Valdemoro C (1986) *Phys Rev A* 33:2254–2261
Matrix elements of spin-adapted reduced Hamiltonian.
- Katriel J, Paldus J, Pauncz R (1985) *Int J Quantum Chem* 28:181–202
Generalized Dirac identities and explicit relations between the permutational symmetry and the spin operators for a system of identical particles.
- Kemble EC (1958) *The fundamental principles of quantum mechanics.*
Dover, New York
- Kent RD, Schlesinger M, Drake GWF (1981) *J Comp Phys* 40:430–439
Calculation of the atomic spin-orbit matrix elements in the unitary group approach.
- Kent RD, Schlesinger M (1981) *Phys Rev A* 23:979–990
Unitary group approach to the treatment of mixed-orbital configurations.
- Kent RD, Schlesinger M (1982) *Int J Quantum Chem* 22:223–239
Two-body operator matrix elements for pure and mixed configurations in the unitary group approach.
- Klein DJ, Carlisle CH, Matsen FA (1970) *Adv Quantum Chem* 5:219–260
Symmetry adaptation to sequences of finite groups.
- Knowles PJ, Handy NC (1984) *Chem Phys Lett* 111:315–321
A new determinant-based full configuration interaction method.
- Knowles PJ, Somasundram K, Handy NC, Hirao K (1985)
Chem Phys Lett 113:8–13
The calculation of higher-order energies in the many-body perturbation series.
- Kotani M, Amemiya A, Ishiguro E, Kimura T (1955)
Tables of molecular integrals. Maruzen, Tokyo.
- Kotani M, Ohno K, Kayama K (1961)
Encyclopedia of Physics, Vol XXXVII/2, p 1–172
Quantum mechanics of electronic structure of simple molecules.
- Knuth DE (1973) *Searching and sorting: the art of computer programming.* Vol 3.
Addison-Wesley, Reading MA

- Kutzelnigg W (1984) *J Chem Phys* 80:822–830
Quantum chemistry in Fock space III. Particle-hole formalism.
- Landau LD, Lifshitz EM (1974) *Quantum mechanics*, 3rd ed. Science Publ, Moscow
- Lipkin HJ (1965) *Lie groups for pedestrians*. North-Holland, Amsterdam
- Lischka H, Shepard R, Brown FB, Shavitt I (1981) *Int J Quantum Chem* S15:91–100
New implementation of the graphical unitary group approach for multireference direct CI calculations.
- Lischka H (1982) 183rd American Chemical Soc National Meeting, Las Vegas, Nevada
- Liu B, Yoshimine M (1981) *J Chem Phys* 74:612–616
The Alchemy configuration interaction method. I. The symbolic matrix method for determining elements of matrix operators.
- McGrory JB, Wildenthal BH (1980) *Ann Rev Nucl Part Sci* 30:383–436
Large-scale shell-model calculations.
- McLean AD, Liu B (1973) *J Chem Phys* 58:1066–1078
Classification of configurations and determination of interacting and noninteracting spaces in configuration interaction.
- McWeeny R, Pickup B (1980) *Rep Prog Phys* 43:1065–1144
Quantum theory of molecular electronic structure.
- McWeeny R, Sutcliffe BT (1979) *Methods of molecular quantum mechanics*. Academic Press, London
- McWeeny R, Sutcliffe BT (1985) *Comp Phys Rep* 2:217–278
Fundamentals of self-consistent-field (SCF), Hartree-Fock (HF), multi-configuration (MC) SCF and configuration interaction (CI) schemes.
- Matsen FA (1976) *Int J Quantum Chem* 10:525–544
Unitary group approach formulation of the many-electron problem.
- Mattuck RD (1976) *A guide to Feynman diagrams in the many-body problem*. 2nd ed, McGraw-Hill, New York
- Moshinsky M (1968) *Group theory and the many-body problem*. Gordon & Breach, New York
- Mordell LJ (1969) *Diophantine equations*. Academic Press, New York
- Nash-Williams C.St JA (1973) Unexplored and semi-explored territories in graph theory. In: *New directions in the theory of graphs*. Harary F, Ed. Academic Press, New York, pp 149–186
- Ore O (1962) *Theory of graphs*. *Am Mat Soc Coll Publ, Providence RI* Vol 38
- Paldus J (1976) Many-Electron Correlation Problem: A Group Theoretical Approach. In: *Eyring H and Henderson DJ (eds) Theoretical Chemistry: Advances and Perspectives*, vol 2. Academic Press, New York, pp 131–298

- Paldus J (1981) *Lecture Notes in Chem* 22:1-50
Unitary group approach to many-electron correlation problem.
- Paldus J, Boyle M (1980) *Physica Scripta* 21:295-311
Unitary group approach to many-electron correlation problem via graphical methods of spin algebras.
- Paldus J, Wormer PES (1986) Unitary group approach to many-electron correlation problem (to be published as a book)
- Parr RG (1964) *Quantum theory of molecular electronic systems*. Benjamin, New York
- Patterson CW, Harter WG (1977) *Phys Rev A* 15:2372-2379
Alternative basis for the theory of complex spectra III.
- Pauncz R (1979) *Spin functions: construction and use*. Plenum, New York
- Payne PW (1982) *Int J Quantum Chem* 22:1085-1152
Matrix element factorization in the unitary group approach for configuration interaction calculations.
- Pople JA, Beveridge DL (1970) *Approximate molecular orbital theory*. McGraw-Hill, New York
- Racah G (1949) *Phys Rev* 76:1352-1365
Theory of complex spectra IV.
- Redmond PJ (1954) *Proc Roy Soc A* 222:84-93
An explicit formula for the calculation of fractional parentage coefficients.
- Rettrup S, Sarma CR (1977) *Theor Chim Acta(Berl.)* 46:73-77
A new program for CI calculations in molecules.
- Rettrup S (1986) *Int J Quantum Chem* 29:119-128
Direct evaluation of spin representation matrices and ordering of permutation group elements.
- Riordan J (1958) *An Introduction to Combinatorial Analysis*. Wiley, New York
- Robb M, Hegarty D (1978) In: *Correlated wavefunctions, Daresbury Study Weekend Series No 10*. Saunders VR, Ed. Science Research Council, Daresbury
- Robb M, Niazi U (1984) *Comp Phys Rep* 1:127-236
The unitary group approach in configuration interaction (CI) methods.
- Roos BO, Taylor PR, Siegbahn PEM (1980) *Chem Phys* 48:157-173
A complete active space SCF method (CAS SCF) using a density matrix formulated super-CI approach.
- Roos BO (1980) *Int J Quantum Chem* S14:175-189
The complete active space SCF method in a Fock-matrix-based super-CI formulation.
- Roos BO, Nelin C, Agren H (1982) 183rd American Chemical Soc National Meeting, Las Vegas, Nevada

- Ruttink PCA (1978) *Theor Chim Acta(Berl.)* 49:223–239
On the evaluation of CI matrix elements for canonically ordered basis.
- Rutherford DE (1948) Substitutional analysis. Edinburg University Press, Edinburg
- Ruedenberg K, Poshusta RD (1972) *Adv Quantum Chem* 6:267–298
Matrix elements and density matrices for many-electron spin eigenstates built from orthonormal orbitals.
- Sahasrabudhe GG, Dinesha KV, Sarma CR (1980)
Theor Chim Acta(Berl.) 54:333–339
Some simplifications in the spin-free configuration interaction studies.
- Sarma CR, Rettrup S (1977) *Theor Chim Acta(Berl.)* 46:63–71
A programmable spin-free method for configuration interaction.
- Saunders VR, Van Lenthe JH (1983) *Mol Phys* 48:923–954
The direct CI method. A detailed analysis.
- Saxe P, Fox DJ, Schaefer HF, Handy NC (1982) *J Chem Phys* 77:5584–5592
The shape-driven graphical unitary group approach to the electron correlation problem. Application to ethylene molecule.
- Saxe P, Schaefer HF, Handy NC (1981) *Chem Phys Lett* 79:202–204
Exact solution (within a double-zeta basis set) of the Schrödinger electronic equation for water.
- Schroeder MR (1984) Number Theory in Science and Communication.
Springer, Berlin
- Segal GA, Wetmore RW, Wolf K (1978) *Chem Phys* 30:269–297
Efficient methods for configuration interaction calculations.
- Seligman TH (1981) *Lecture Notes in Chem* 12:178–192
Double cosets and the evaluation of matrix elements.
- Serber R (1934) *Phys Rev* 45:461–467
Extension of the Dirac vector model to include several configurations.
- Serber R (1934) *J Chem Phys* 2:697–710
The solution of problems involving permutational degeneracy.
- Shavitt I (1977a) *Int J Quantum Chem* S11:131–148
Graph theoretical concepts for the unitary group approach to the many-electron correlation problem.
- Shavitt I (1977b) The method of configuration interaction. In: Modern theoretical chemistry, Vol.3. Schaefer HF(ed), Plenum Press, New York
- Shavitt I (1978) *Int J Quantum Chem* S12:5–32
Matrix element evaluation in the unitary group approach to the electron correlation problem.
- Shavitt I (1979) *Chem Phys Lett* 63:421–427
The utilization of abelian point group symmetry in graphical unitary group approach to the calculation of correlated electronic wave functions.

- Shavitt I (1981) *Lecture Notes in Chem* 22:51-99
The graphical unitary group approach and its application to direct configuration interaction calculations.
- Shavitt I (1983) The unitary group and the electron correlation problem. In: Löwdin P-O, Pullman B (eds). *New Horizons in Quantum Chemistry*. D Reidel Pub Co, New York, p 279-293
- Shepard R, Simons J (1980) *Int J Quantum Chem* S14:211-228
Multiconfigurational wavefunction optimization using the unitary group method.
- Shudeman CLB (1937) *J Franklin Inst* 224:501
- Siegbahn PEM (1979) *J Chem Phys* 70:5391-5397
Generalization of the direct CI method based on the graphical unitary group approach. I. Single replacements from a complete CI root function of any spin, first order wave functions.
- Siegbahn PEM (1980) *J Chem Phys* 72:1647-1656
Generalization of the direct CI method based on the graphical unitary group approach. II. Single and double replacements from any set of reference functions.
- Siegbahn PEM (1984) *Chem Phys Lett* 109:417-423
A new direct configuration interaction method method for large CI expansions in a small orbitals space.
- Siegbahn PEM (1985) *Chem Phys Lett* 119:515-522
Multireference CCI calculations on the bond distance and dissociation energies of methane.
- Siegbahn PEM, Almlöf J, Heiberg A, Roos BO (1981) *J Chem Phys* 74:2384-2396
The complete active space SCF (CASSCF) method in a Newton-Raphson formulation with application to the *HNO* molecule.
- Siegbahn PEM, Heiberg A, Roos BO, Levy B (1980) *Physica Scripta* 21:323-327
A comparison of the super-CI and the Newton-Raphson scheme in the complete active space SCF method.
- Singer J (1970) *Bases in Banach spaces I*. Springer, Berlin
- Slansky R (1981) *Phys Rep* 79:1-128
Group theory for unified model building.
- Slater JC (1968) *Quantum theory of matter*. 2nd ed, McGraw-Hill, New York
- Sutcliffe BT (1983) Group theory applied to CI methods. In: *Methods in computational physics*. Diercksen GHF, Wilson S(eds), D.Reidel Publ Co, New York, pp 115-160
- Szabo A, Ostlund NS (1982) *Modern quantum chemistry: introduction to advanced electronic structure theory*. Macmillian, New York
- van Vleck JH (1932) *The theory of electric and magnetic susceptibilities*. Oxford University Press, London
- van Vleck JH, Sherman A (1935) *Rev Mod Phys* 7:167-228

- Wasilewski J (1986) *Mol Phys* (to be published)
- Watanabe H (1966) *Operator methods in ligand field theory*.
Prentice Hall, Englewood Cliffs, New Jersey
- Weissbluth M (1978) *Atoms and molecules*. Academic Press, New York
- Wetmore RW, Segal GA (1975) *Chem Phys Lett* 36:478–483
Efficient generation of configuration interaction matrix elements.
- Weyl H (1928) *Gruppentheorie and Quantenmechanik*. Hirzel, Leipzig
- Wilson EB, Decius JC, Cross PC (1955) *Molecular vibrations*. McGraw-Hill, London
- Wilson S (1984) *Electron correlation in molecules*. Clarendon Press, Oxford
- Wong SSM (1981) *Lecture Notes in Physics* 144:174–247
Nuclear shell model and statistical spectroscopy.
- Wormer PES (1975) *Intermolecular forces and the group theory of the many-body systems*. Stichting Studentenpers, Nijmegen
- Wormer PES, Paldus J (1979) *Int J Quantum Chem* 16:1307–1319
Configuration interaction matrix elements. I. Algebraic approach to the relationship between unitary group generators and permutations.
- Wybourne BG (1970) *Symmetry principles and atomic spectroscopy*.
Wiley, New York
- Wybourne BG (1974) *Classical groups for physicists*. Wiley, New York
- Zhenyi W (1983) *Int J Quantum Chem* 23:999–1009
Application of the unitary group approach to crystal field theory.

The index contains mainly references to the pages where the entries are defined.

adjoint (segment, loop), 120
atom(ic), 36, 57-63, 73, 99, 114, 134
annihilation operator, 105, 106, 110
basic symmetry operator, 104
branching diagram, 44
breadth search, 97

closed loop, 118, 156
combinatorial theory, 95
complete active space, 87
creation operator, 105, 106, 110
decreasing segment, 119
density operator, matrix, 107, 108
depth search, 97
double coset, 113
double indexing, 97
Diophantine equation, 94
distinct row table, 96

electronic Hamiltonian, 109
elementary loop, 119
elementary transposition (ET) 142, 143
fagot graph, 25
Fibonacci numbers, 147
Fock operator, 109
four-slope graph, 22, 47

Gelfand tableaux, row, 45, 50, 91
general linear group $GL(n)$, 91
generator of unitary group, 104, 142
graph theory, 90
increasing segment, 119, 120
isospin operator, 44, 140
integer programming, 95

loop, 118
 segment, range, body, value, 118
lexical ordering, number, 17, 127
lowering operator, 105
lower walk, 118
M-diagram, 23

model space, 5

node, 11
non-fagot graph, 25
nuclear 36, 64-66, 99, 140
open loop, 118
orbital configuration, 117
overlapping permutation, 158

particle number operator, 105
permutation, 123
point group, 67-73, 109, 140
position of an arc, 124
proper label, 5, 57
raising operator, 105
reference state, 74
replacement operator, 104
representation matrices, 113, 153
reverse lexical ordering, 15

S-diagram, 45
SCP (singlet-coupled pair), 143, 149
segment values, factors, 133, 142
Serber spin functions, 93, 94, 148
shift operator, 104
 two-particle, 106
 three-particle, 107
spin operators 109, 110
spin eigenfunctions, 136, 138, 149
tensor product space, 104
three-slope graphs, 21
three-particle operator, 107
two-slope graphs, 13
two-particle integrals, 107
 operator, 106, 107, 115, 116

upper walk, 118
unitary group, 7, 8, 9, 91, 140, 146
weight operator, 105
Weyl basis, 108
 tableaux, 49

Young tableaux, 45, 50
 \hat{O} -adapted (space, states), 7

Lecture Notes in Chemistry

- Vol. 1: G. H. Wagnière, Introduction to Elementary Molecular Orbital Theory and to Semiempirical Methods. V, 109 pages. 1976.
- Vol. 2: E. Clementi, Determination of Liquid Water Structure. VI, 107 pages. 1976.
- Vol. 3: S. R. Niketic and K. Rasmussen, The Consistent Force Field. IX, 212 pages. 1977.
- Vol. 4: A. Graovac, I. Gutman and N. Trinajstić, Topological Approach to the Chemistry of Conjugated Molecules. IX, 123 pages. 1977.
- Vol. 5: R. Carbo and J. M. Riera, A General SCF Theory. XII, 210 pages. 1978.
- Vol. 6: I. Hargittai, Sulphone Molecular Structures. VIII, 175 pages. 1978.
- Vol. 7: Ion Cyclotron Resonance Spectrometry. Edited by H. Hartmann and K.-P. Wanczek. VI, 326 pages. 1978.
- Vol. 8: E. E. Nikitin and L. Zülicke, Selected Topics of the Theory of Chemical Elementary Processes. X, 175 pages. 1978.
- Vol. 9: A. Julg, Crystals as Giant Molecules. VII, 135 pages. 1978.
- Vol. 10: J. Ulstrup, Charge Transfer Processes in Condensed Media. VII, 419 pages. 1979.
- Vol. 11: F. A. Gianturco, The Transfer of Molecular Energies by Collision: Recent Quantum Treatments. VIII, 328 pages. 1979.
- Vol. 12: The Permutation Group in Physics and Chemistry. Edited by J. Hinze. VI, 230 pages. 1979.
- Vol. 13: G. Del Re et al., Electronic States of Molecules and Atom Clusters. VIII, 177 pages. 1980.
- Vol. 14: E. W. Thulstrup, Aspects of the Linear and Magnetic Circular Dichroism of Planar Organic Molecules. VI, 100 pages. 1980.
- Vol. 15: A.T. Balaban et al, Steric Fit in Quantitative Structure-Activity Relations. VII, 178 pages. 1980.
- Vol. 16: P. Čársky and M. Urban, Ab Initio Calculations. VI, 247 pages. 1980.
- Vol. 17: H. G. Hertz, Electrochemistry. X, 254 pages. 1980.
- Vol. 18: S. G. Christov, Collision Theory and Statistical Theory of Chemical Reactions. XII, 322 pages. 1980.
- Vol. 19: E. Clementi, Computational Aspects for Large Chemical Systems. V, 184 pages. 1980.
- Vol. 20: B. Fain, Theory of Rate Processes in Condensed Media. VI, 166 pages. 1980.
- Vol. 21: K. Varmuza, Pattern Recognition in Chemistry. XI, 217 pages. 1980.
- Vol. 22: The Unitary Group for the Evaluation of Electronic Energy Matrix Elements. Edited by J. Hinze. VI, 371 pages. 1981.
- Vol. 23: D. Britz, Digital Simulation in Electrochemistry. X, 120 pages. 1981.
- Vol. 24: H. Primas, Chemistry, Quantum Mechanics and Reductionism. XII, 451 pages. 1981.
- Vol. 25: G. P. Arrighini, Intermolecular Forces and Their Evaluation by Perturbation Theory. IX, 243 pages. 1981.
- Vol. 26: S. Califano, V. Schettino and N. Neto, Lattice Dynamics of Molecular Crystals. VI, 309 pages. 1981.
- Vol. 27: W. Bruns, I. Motoc, and K. F. O'Driscoll, Monte Carlo Applications in Polymer Science. V, 179 pages. 1982.
- Vol. 28: G. S. Ezra, Symmetry Properties of Molecules. VIII, 202 pages. 1982.
- Vol. 29: N.D. Epiotis, Unified Valence Bond Theory of Electronic Structure. VIII, 305 pages. 1982.
- Vol. 30: R.D. Harcourt, Qualitative Valence-Bond Descriptions of Electron-Rich Molecules: Pauling "3-Electron Bonds" and "Increased-Valence" Theory. X, 260 pages. 1982.
- Vol. 31: H. Hartmann, K.-P. Wanczek, Ion Cyclotron Resonance Spectrometry II. XV, 538 pages. 1982.
- Vol. 32: H.F. Franzen, Second-Order Phase Transitions and the Irreducible Representation of Space Groups. VI, 98 pages. 1982.
- Vol. 33: G.A. Martynov, R.R. Salem, Electrical Double Layer at a Metal-dilute Electrolyte Solution Interface. VI, 170 pages. 1983.
- Vol. 34: N.D. Epiotis, Unified Valence Bond Theory of Electronic Structure - Applications. VIII, 585 pages. 1983.
- Vol. 35: Wavefunctions and Mechanisms from Electron Scattering Processes. Edited by F.A. Gianturco and G. Stefani. IX, 279 pages. 1984.
- Vol. 36: J. Ugi, J. Dugundji, R. Kopp and D. Marquarding, Perspectives in Theoretical Stereochemistry. XVII, 247 pages. 1984.
- Vol. 37: K. Rasmussen, Potential Energy Functions in Conformational Analysis. XIII, 231 pages. 1985.
- Vol. 38: E. Lindholm, L. Åsbrink, Molecular Orbitals and their Energies, Studied by the Semiempirical HAM Method. X, 288 pages. 1985.
- Vol. 39: P. Vanýsek, Electrochemistry on Liquid/Liquid Interfaces. 2, 3-106 pages. 1985.
- Vol. 40: A. Plonka, Time-Dependent Reactivity of Species in Condensed Media. V, 151 pages. 1986.
- Vol. 41: P. Pyykkö, Relativistic Theory of Atoms and Molecules. IX, 389 pages. 1986.
- Vol. 42: W. Duch, GRMS or Graphical Representation of Model Spaces. V, 189 pages. 1986.
-